0-315-05952-4

National Library of Canada — Bibliothèque nationale du Canada
Canadian Theses Division — Division des thèses canadiennes
Ottawa, Canada
K1A 0N4

53872

PERMISSION TO MICROFILM — AUTORISATION DE MICROFILMER

• Please print or type — Écrire en lettres moulées ou dactylographier

Full Name of Author — Nom complet de l'auteur

PAULO BRANCO JUNIOR

Date of Birth — Date de naissance

JUNE, 13, 1955

Country of Birth — Lieu de naissance

BRAZIL

Permanent Address — Résidence fixe

R. CONSOLACAO 2801 / 92
SAO PAULO - SP - BRAZIL
CEP 01410

Title of Thesis — Titre de la thèse

BEHAVIOUR OF A SHALLOW TUNNEL IN TILL

University — Université

UNIVERSITY OF ALBERTA

Degree for which thesis was presented — Grade pour lequel cette thèse fut présentée

MASTER OF SCIENCE

Year this degree conferred — Année d'obtention de ce grade

1981

Name of Supervisor — Nom du directeur de thèse

Z. EISENSTEIN

Date

SEPT 22, 1981

Signature

Paulo Branco Júnior

NL-91 (4/77)

THE UNIVERSITY OF ALBERTA

BEHAVIOUR OF A SHALLOW TUNNEL IN TILL

by

© PAULO BRANCO JR.

A THESIS

SUBMITTED TO THE FACULTY OF GRADUATE STUDIES AND RESEARCH

IN PARTIAL FULFILMENT OF THE REQUIREMENTS FOR THE DEGREE

OF MASTER OF SCIENCE

CIVIL ENGINEERING

EDMONTON, ALBERTA

FALL 1981

THE UNIVERSITY OF ALBERTA

RELEASE FORM

NAME OF AUTHOR PAULO BRANCO JR.

TITLE OF THESIS BEHAVIOUR OF A SHALLOW TUNNEL IN TILL

DEGREE FOR WHICH THESIS WAS PRESENTED MASTER OF SCIENCE

YEAR THIS DEGREE GRANTED FALL 1981

(SIGNED) Paulo Branco Junior

PERMANENT ADDRESS:

Rua da Consolacao 2801 / 92

Sao Paulo - SP - Brazil

CEP 01410

DATED Sept. 10, 1981

THE UNIVERSITY OF ALBERTA

FACULTY OF GRADUATE STUDIES AND RESEARCH

The undersigned certify that they have read, and recommend to the Faculty of Graduate Studies and Research, for acceptance, a thesis entitled BEHAVIOUR OF A SHALLOW TUNNEL IN TILL submitted by Paulo Branco Jr in partial fulfilment of the requirements for the degree of MASTER OF SCIENCE.

....
Supervisor

....

....

Date Sept. 10, 1981

TO LUCILA

ABSTRACT

The characteristic elements of the behaviour of a large diameter, shallow tunnel, constructed for the extension of the Light Rail Transit System in the City of Edmonton have been documented and analysed in this thesis.

A comprehensive monitoring program that included the measurement of the displacements of the soil and primary lining and the measurement of loads in the primary lining was used in the analysis of the factors that affect the behaviour of the tunnel lining and surrounding soil mass.

The monitoring of ground displacements indicated that most of the soil movements occurred immediately above the tunnel crown and that the tunnel construction did not affect the nearby structures.

The measurement of loads on the primary lining system showed that the steel ribs, at the tunnel crown, carried loads from 9% to 26% of the overburden and that these loads are 85% to 213% higher than the average loads carried by the timber lagging.

The coupled analysis of the soil and lining behaviour of the tunnel reported herein and of other tunnels constructed in Edmonton indicated that there is no simple theoretical design method, such as Closed Form Solutions or Convergence-Confinement Method, applicable to the study of shallow tunnels.

ACKNOWLEDGEMENTS

I would like to express my deepest appreciation and profound thanks to Lucila, my wife, for her immense contribution over the past two years. Lucila unselfishly stopped her studies and left her family and friends to come with me to Canada. Without her love and overwhelmingly enthusiastic support many of the frustrations and difficulties could not have been overcome. To her I dedicate this degree.

To my daughters, Patricia and Renata, I owe the happiest moments during the past couple of years. With their love and happiness, they contributed to make our stay in Canada unforgetable.

I wish to thank my research supervisor and friend, Prof. Z. E. Eisenstein, for his guidance and enthusiastic encouragement during the period we worked together. To him I am grateful.

The financial support provided by the City of Edmonton and the Department of Civil Engineering of the University of Alberta is gratefully acknowledged.

My thanks are extended to the staff within the Department of Civil Engineering, in particular to G. Cyre and A. Muir. They worked on the manufacturing of most equipments used in the monitoring program. G. Cyre provided invaluable help during all phases of the field investigation.

Prof. S. Thomson, C. Mackay, F. El-Nahhas and D. Hutchinson edit this thesis and provided many valuable comments and suggestions. Their contribution is greatly appreciated.

I owe special thanks to A. Negro and D. Hutchinson for the many hours they spent at the site installing instruments, taking readings and pictures for me. Their contribution through stimulating discussions on topics related to tunneling, played an important role in the development of this research.

I also wish to thank the academic staff in the Dept. of Civil Engineering, in special Prof. P. K. Kaiser with whom I have had fruitful discussions on tunneling.

My thanks are extended to the members of my examining committee who provided interesting comments during the final oral examination.

The help provided by Sergio and Helena, who helped us to settle in Edmonton and get adjusted to the new life, will never be forgotten.

To my friends Jose Roberto and Claudia I owe the best of my feelings. Their warm friendship taught me many things about life and made my stay in Canada very pleasant. I hope they go back home soon so we can spend more time together. To them I extend my utmost appreciation and thanks.

I wish to thank my brother, Luiz, and sisters, Helena and Cristina, for the moral support and love they have dedicated to me.

In closing, I would like to express profound thanks to my parents, Paulo and Maria Helena, who gave me the desire and opportunity to undertake this work. I hope I can reflect to my daughters all the love and care they have dedicated to me.

I am extremely happy that now I will be able to spend more time together with my lovely family.

Table of Contents

List of Tables

Table		Page

List of Figures

Figure Page

Figure | Page

Figure		Page

Figure		Page

Figure		Page
5.7	CHARACTERISTIC CURVES FOR THE LRT AND EXPERIMENTAL TUNNELS	242
B.1	ME5 MP#1 D=2.35m	279
B.2	ME5 MP#2 D=4.88m	280
B.3	ME5 MP#3 D=6.85m	281
B.4	ME5 MP#4 D=8.13m	282
B.5	ME5 MP#5 D=10.86m	283
B.6	ME5 MP#6 D=12.91m	284
B.7	ME5 MP#7 D=14.81m	285
B.8	ME5 MP#8 D=16.78m	286
B.9	ME5 MP#9 D=18.08m	287
B.10	ME9 MP#1 D=1.43m	288
B.11	ME9 MP#2 D=2.93m	289
B.12	ME9 MP#3 D=4.89m	290
B.13	ME9 MP#4 D=7.01m	291
B.14	ME9 MP#5 D=8.93m	292
B.15	ME9 MP#6 D=11.16m	293
B.16	ME9 MP#7 D=13.89m	294
B.17	ME9 MP#8 D=15.61m	295
B.18	ME9 MP#9 D=16.92m	296
B.19	ME9 MP#10 D=18.36m	297
B.20	ME10 MP#1 D=2.53m	298
B.21	ME10 MP#2 D=4.58m	299
B.22	ME10 MP#3 D=6.38m	300
B.23	ME10 MP#4 D=8.40m	301
B.24	ME10 MP#5 D=10.22m	302

Figure		Page

List of Plates

1. INTRODUCTION

1.1 General

The need for tunnels for transportation, drainage and sanitary purposes has increased in the last decade due to the growth of the cities. The increase in tunneling activities is not proportional to the improvement in the understanding of the complex phenomena involved in the transfer of load from the excavated ground to the support during and after the tunnel construction. The need for a better understanding of the factors affecting the development of lining loads and displacements and ground displacements is reflected by the fact that the available tunnel design methods do not take into account factors that directly affect the lining and ground behaviour, such as minor construction details. The need for a better knowledge of factors affecting the interaction between tunnel support system and the surrounding soil mass enhances the importance of full scale field observations.

The City of Edmonton is presently constructing the extension of its Light Rail Transit System. This extension crosses the city core with two parallel, large diameter tunnels, bored close to the ground surface. The lack of detailed, full-scale, field observations on large diameter tunnels excavated in the Edmonton till led to a comprehensive monitoring program.

In this thesis, the monitoring program that involved measurements of soil displacements and primary lining loads and deformations carried out during the construction of the north tunnel of the South Extension of the L.R.T. System of Edmonton is documented and interpreted.

1.2 Aim of this Thesis

The field data presented in this study should enable the analysis of the influence of the construction procedure, the effect of the soil and lining strength and deformation properties on the magnitude and distribution of loads on the lining and on the displacement field in the soil mass surrounding the instrumented tunnel. The analysis of the factors affecting the lining and ground behaviour should provide an insight into the interaction between the elements of the lining system and the surrounding soil mass and the effect of soil movements on the structures near the tunnel.

The comparison of the field data documented here with the data collected from another monitoring program carried out in Edmonton, in a deeper, small diameter tunnel (El-Nahhas, 1980) should enable the analysis of the influence of the depth ratio (depth of the tunnel axis/tunnel diameter) on the mode of deformation and plastic behaviour of the soil and how these affect the lining behaviour.

1.3 Scope of this Thesis

A brief outline of the Light Railway Transit System (LRT) presently being extended in the City of Edmonton is presented in Chapter 2. This chapter gives an overview of the geology of the Edmonton area, a description of the subsurface soil profile close to the instrumented section and the construction procedure employed in the tunnel construction.

Chapter 3 summarizes the ground displacement measurement techniques. It presents a detailed description of the design, installation and measurement procedure of the instruments chosen for the measurement of ground movements used in the monitoring program carried out during the construction of the north tunnel of the LRT South Extension. The measured soil displacements are presented and interpreted in this Chapter.

In Chapter 4, the methods available to obtain the magnitude and distribution of ground loads on linings are presented and discussed. A detailed description of the design, installation and measurement procedure of the instruments used in the study of the LRT primary lining behaviour is presented. The results obtained from the lining instrumentations are presented and discussed in this Chapter.

Chapter 5 presents an analysis of the interaction between the soil and the tunnel support system based on the data presented in Chapter 3 and Chapter 4. In this chapter, the applicability of Closed Form Solutions and the Convergence-Confinement Method for the evaluation of the soil and structure behaviour in shallow-tunnels is analysed. This analysis enables insights into the factors affecting the ground and lining interaction to be discussed.

Finally, conclusions are offered in Chapter 6.

2. THE L.R.T. SOUTH EXTENSION

2.1 The L.R.T. System

The City of Edmonton is presently building the South Extension of the Light Rail Transit System - LRT. The South Extension completes the connection of the southern region of the City with the City core.

The North-East line, already built, connects the LRT Central Station, located in the downtown core, with the north-eastern suburbs while the "South Extension", under construction, will connect the Central Station with the Canadian Pacific Railway right-of-way, south of 100th avenue, parallel to 109th street.

A schematic representation of the LRT South Extension is shown on Figure 2.1.

2.2 LRT South Extension Construction Procedure

The construction of the South Extension is divided into three different sections:

- The tunnel section
- The stations
- The portal section

Each of these sections is described in the following section.

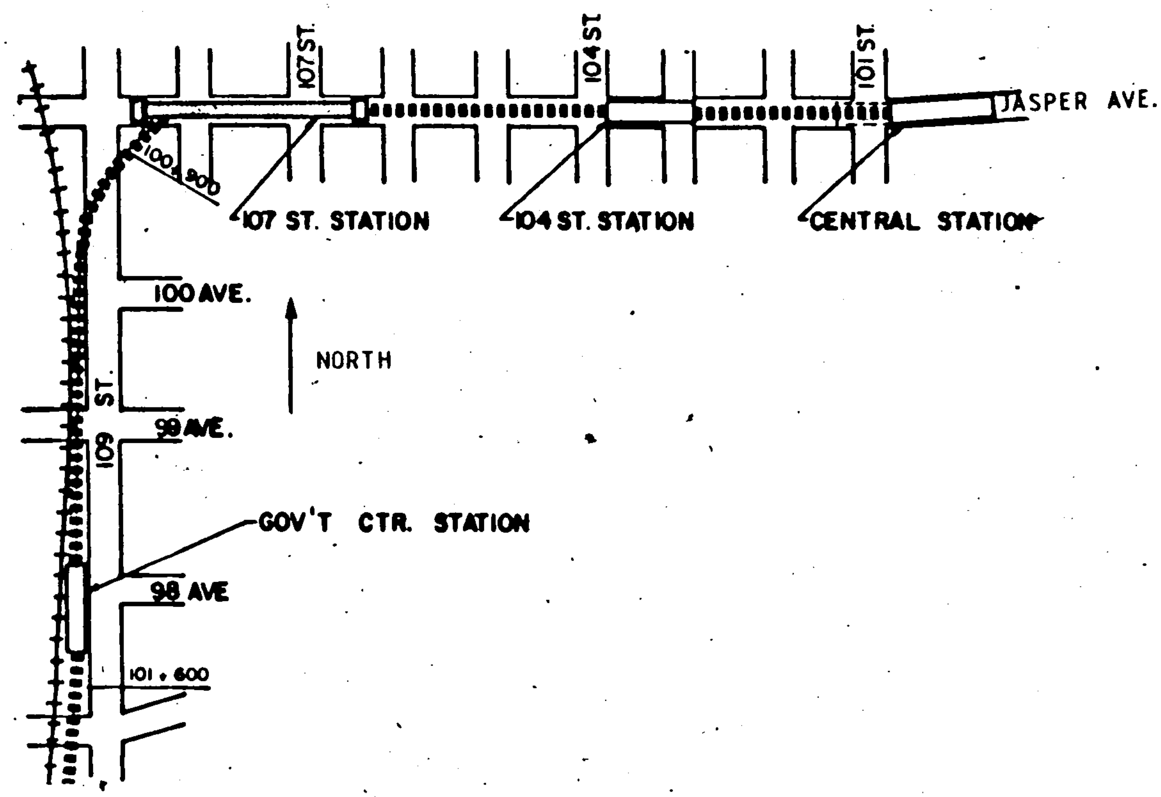

Figure 2.1 THE L.R.T. SOUTH EXTENSION - PLAN VIEW

2.2.1 The Tunnel Section.

Due to the fact that the construction area is intensively developed and that the obstruction of the traffic would lead to serious problems, it was decided that the LRT Central Station, the 104th St and 107th St Stations (Fig. 2.1) were to be connected by two parallel tunnels, employing the same construction procedure as that used for the construction of the underground portions of the North-East line.

The north tunnel excavation was planned to begin from the LRT Central Station and proceed westwards under Jasper Avenue. This procedure would facilitate the disposal of spoil material that would be transported in rail cars to the north-eastern region of Edmonton, using the existing LRT line.

The tunnelling boring machine (TBM), later described in this chapter, was planned to proceed to 106th Street where an access shaft is to be constructed. The TBM will be dismantled in this shaft and taken back through the existing tunnel to the Central Station, to begin the excavation of the second tunnel (south tunnel).

Section 2.4 specifically, deals with the tunnel section since the north tunnel construction between Central Station and 104th Street Station is the major focus of this thesis.

2.2.2 Stations

Three stations will be built between the LRT Central Station and the river crossing:

104th St Station

107th St Station

Government Station

The 104th St and the 107th St Stations will be built using a cut and cover method. The walls of the excavation will consist of cast in place concrete tangent piles.

The concrete piles will be installed to a depth of about 18 metres below the existing grade (street level) and will carry the lateral earth pressure from the soil, as well as the vertical loads from the station and street above. Permanent horizontal struts will be provided at the street level, the mezzanine level, and at the base of the station.

The first of the LRT tunnels (North tunnel) will be bored through the 104th St Station after installation of the tangent pile walls. The excavation of the station itself will be finished after the first one of the two tunnels has been completed.

The Government Station will be constructed near 98th Avenue on the existing CP rail right of way. The LRT tracks at this station will be near the existing CP rail track level.

2.2.3 The Portal Section

The Portal Section will consist of twin tunnels which curve southwards from the 107th St Station and pass under 109th Street (Fig 2.1). In this section, the tunnels rise to emerge on the existing CP rail right of way south of 100th Avenue where , at the location of the proposed tunnel portals, the LRT tracks will be approximately 5 metres below the existing CP rail track level.

From the tunnel portals the LRT tracks rise at a constant grade and merge with the existing CP rail track level, between 98th and 99th Avenues, immediately north of the proposed Government Station.

2.3 Geological and Geotechnical Description in the Edmonton and the LRT System Area

Experience has shown that a knowledge of the geologic origin of glacial deposits can provide a framework for an analysis and interpretation of geotechnical data (May and Thomson, 1978).

Based on this experience, a summary of the geology of the Edmonton area is presented in this section. The geotechnical properties of the soil deposits in the vicinity of the ground and lining instrument installation are also presented in this section.

2.3.1 Geology of the Edmonton Area

The City of Edmonton is located in an area of low relief, with elevations ranging from 700 metres to 830 metres.The surficial material is a glacial lake sediment that caps a succession of Pleistocene deposits that infilled a preglacial valley system. The present North Saskatchewan river has eroded through the Pleistocene deposits and into the bedrock.

The pre-glacial channels were eroded into the Horseshoe Canyon Formation of the Edmonton Formation. The material composing this Formation is of the Upper Cretaceous age (140 to 190 metres thick) and consists of mudstones, clayshales and sandstones, deposited in brackish to fresh water of a shallow inland sea. The presence of bentonite in form of seams and admixtures in this Formation is ascribed to volcanic ash deposition.

After the uplift early in the Cenozoic, the bedrock surface was eroded by a well integrated river system (Kathol and McPherson, 1975). Portions of these pre-glacial channels were filled with late Tertiary sands and gravels termed Saskatchewan Sands and Gravels the thickness of which varies from 4 metres to 20 metres in the Edmonton area.

The advance of ice into the Edmonton area during the late Pleistocene laid down two till sheets. The lower unit, up to 6 metres thick, rests directly on the Saskatchewan Sands and Gravels. It was laid down by an ice lobe moving from somewhat west of north. The ice advance direction can be evaluated from elongated pebbles with the longer axis oriented in the NW-SE direction. The lower till is characterized by its greyish colour and rectangular joint system. The upper till was derived from an ice lobe advancing from east of north. The ice reworked the upper metre of the lower till. The upper till, of brownish colour and with a columnar system of joints, is in some areas separated from the lower till by stratified sand lenses, called Tofield Sands. These lenses vary in size and shape, varying from contorted inclusions, less than 10cm in size, to more lenticular shaped bodies, continuous over distances in excess of 50 metres (May and Thomson, 1978). These sand lenses often are water bearing and might be a source of problems during tunneling activities. The two till layers have similar geotechnical properties the lower one being slightly stiffer than the upper one. Dejong and Morgenstern (1973) reported blow counts (SPT) higher in the lower till.

Above the upper till are silty clays, deposited in glacial Lake Edmonton. Within these sediments, large pieces of till-like material are found and have been termed diamicton by Westgate (1969) or lacustro-till by Kathol and McPherson (1975).

The lake deposits are covered in some areas by fill material, generally consisting of clay, mixed topsoil, sand and occasionally rubble.

Figure 2.2 presents a summary of the Quaternary geology of the Edmonton area.

Cenozoic	Quarternary	Holocene	Alluvium, Organic deposits, recent lake deposits.
		Pleistocne	Lacustrine sand, silt and clay, organic deposits, aeolian sand and silt, river Alluvium
			Till
			Sand and sandy gravel, some silt and clay
			Till
	Tertiary (undivided)		Saskatchewan gravels and sands

Figure 2.2 QUARTERNARY GEOLOGY OF EDMONTON AREA (AFTER MAY AND THOMSON, 1978)

A generalized east-west section through central Edmonton is shown on Figure 2.3.

2.3.2 Stratigraphy Along the LRT Track Centreline in the Area of the Present Study

The stratigraphy along the LRT track centreline, close to the region where the ground and lining instruments were installed is presented in Figure 2.4.

The boreholes indicated in Fig 2.4 have been reported by Thurber Consultants Ltd.(1980).

2.3.3 Geotechnical Properties of the Soil Surrounding the Tunnel

The results from laboratory tests carried out on undisturbed samples extracted from the boreholes drilled along the LRT South Extension are presented in Tables A1 to A6 in Appendix A. The location of the boreholes from which the samples were removed is given in drawing no. 14-31-1-6 in the report by Thurber Consultants Ltd.(opt. cit.)

The geotechnical properties of the Edmonton till have been extensively studied and a summary of some properties is presented in Table 2.1. The lab tests results presented in Tables A1 to A6 are summarized in the last column of Table 2.1.

Reference	Morgenstern and Thomson (1970)	Dejong and Harris (1971)	Thomson and Yacyshyn (1977)	El-Nahhas (1977)	Eisenstein and Thomson (1978)	LRT South Extension
Density (kN/m³)	-	19-22	-	22	20.6-21.2	19.7-23.3
Natural Moisture Content %	12-22	11-19	15	12	12-20	10.1-28.7
Liquid Limit %	28-48	22-42	40	31	20-40	26.8-66.8
Plastic Limit %	12-22	9-20	20	15	12-20	13.6-22.7
% Clay	20-30	20	20-30	42	20-30	7.5-55
% Sand	-	42	40-50	27	40-50	9.0-47.5
Void Ratio	-	0.35-0.4	-	0.36	-	-
Degree of Saturation %	-	75-95	-	89	-	-
Undrained Strength (kPA)	345-828	140-240	140-245	-	140-245	94-662
Peak Angle of Shearing Resistance	-	-	37	-	-	-
Peak Cohesion (kPa)	-	28	-	-	-	-
Standard Penetration (blows/0.3 m)	-	60-150	-	-	40-60 some over 100	-

TABLE 2.1 - GEOTECHNICAL PROPERTIES OF EDMONTON TILL (AFTER THOMSON AND EL-NAHHAS, 1980)

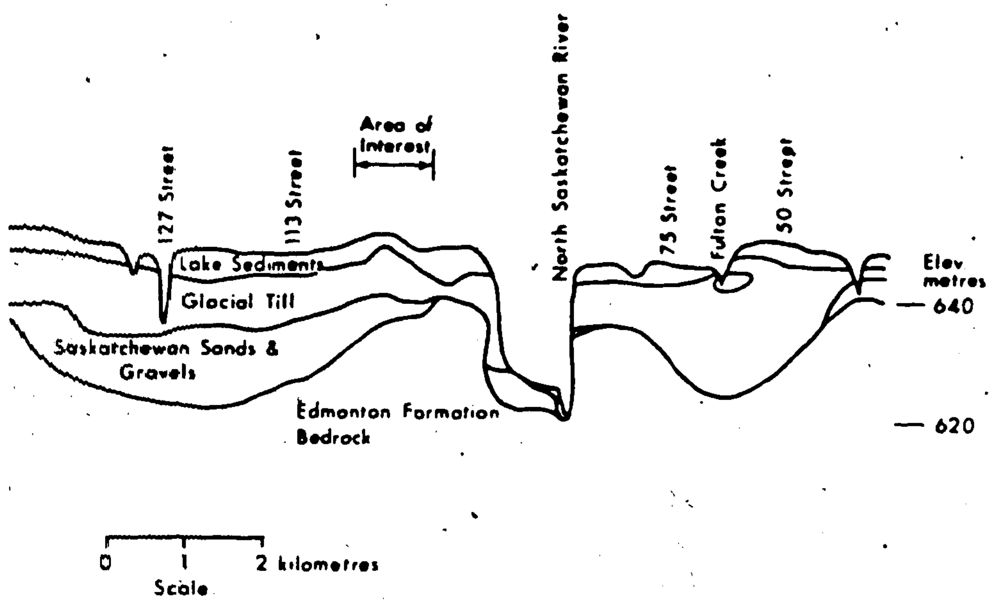

Figure 2.3 GENERALIZED GEOLOGIC EAST-WEST CROSS SECTION THROUGH EDMONTON (AFTER KATHOL AND McPHERSON, 1975)

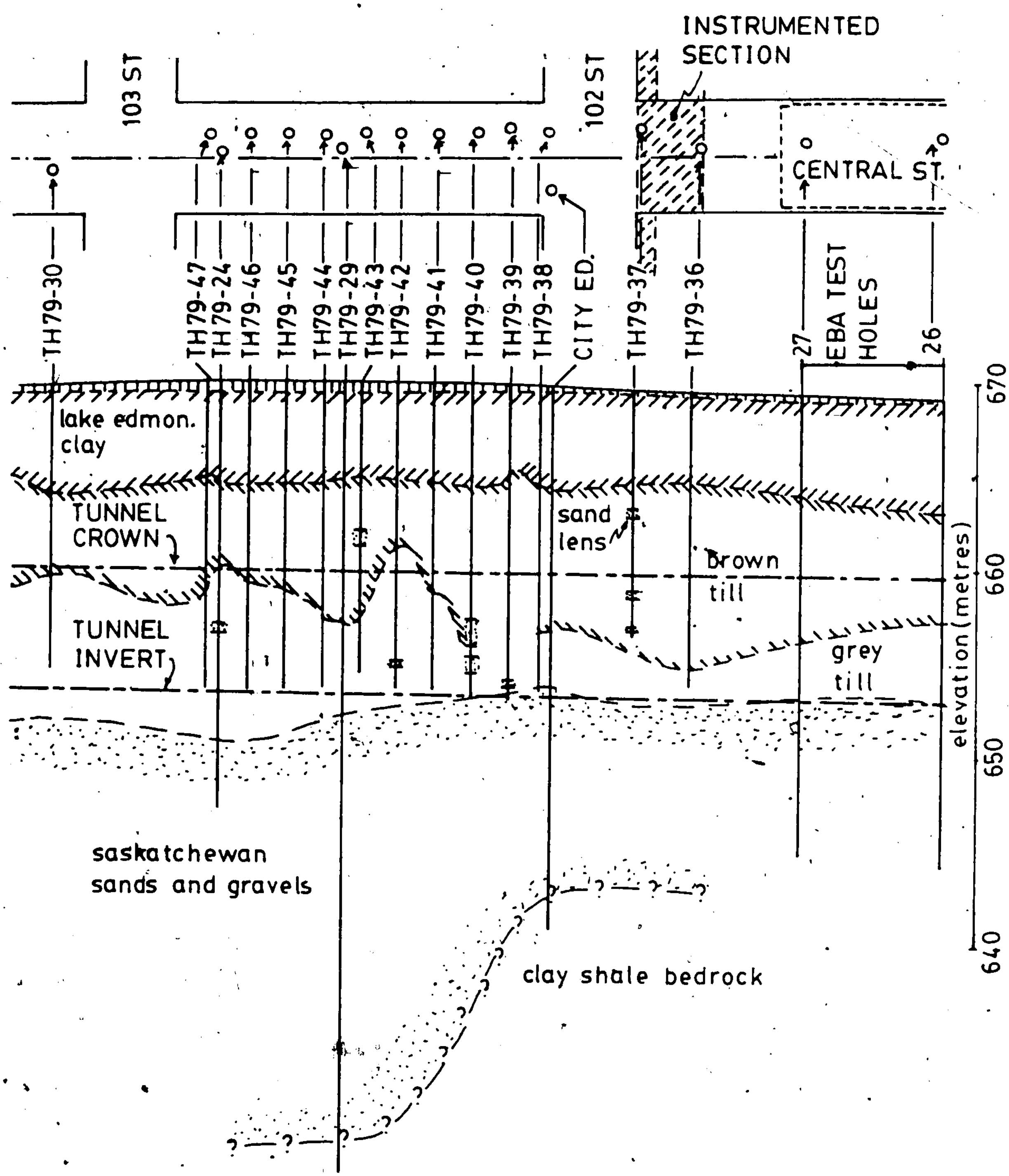

Figure 2.4 PLAN AND PROFILE FROM CENTRAL STATION TO 103 STREET (AFTER THURBER, 1980)

2.4 Detailed Description of the Construction of the Tunnel Sections

2.4.1 Tunnel Boring Machine

The tunnel sections of the existing north east line of the LRT System were excavated with the tunnelling boring machine (TBM) built by Lovat Tunnel Equipment Inc., Ontario, Toronto (Model M-246 Series 2100). The machine is owned by the City of Edmonton and a section illustrating its operation is presented in Figure 2.5.

The decision to use this TBM in the construction of the LRT South Extension was based on the convenience of using an equipment already owned by the City (inital investment, experienced operating crew) and on the successful construction of the existing tunnels of the subway system of the City of Edmonton.

The specifications of the TBM are given in Table 2.2 and more details will be given in the construction method description, later in this section.

2.4.2 The Lining System

The system chosen for the LRT South Extension tunnel is the same as that previously used in the construction of the tunnels of the existing lines. The system is a two-phase lining that comprises a primary, or temporary, and a secondary, or final, lining. As shown in Figure 2.6, the primary lining is composed of segmented steel ribs W6x25

BORE	: 6.27 m
CUTTING HEAD TORQUE	: 2412.5 KN.m
PROPULSION THRUST	: 22.24 MN
FRONT UNITIZED CONVEYOR	: 1.2m wide x 7.5m long
POWER	: 995 HP
ROTATIONAL SPEED	: 7 RPM
LENGTH	: 5.5m
MAXIMUM ADVANCE PER THRUST	: 1.68m
TOTAL WEIGHT	: 1174 KN

TABLE 2.2 - . SPECIFICATIONS OF THE TUNNEL BORING MACHINE (LOVAT MODEL M-246 SERIES 2100)

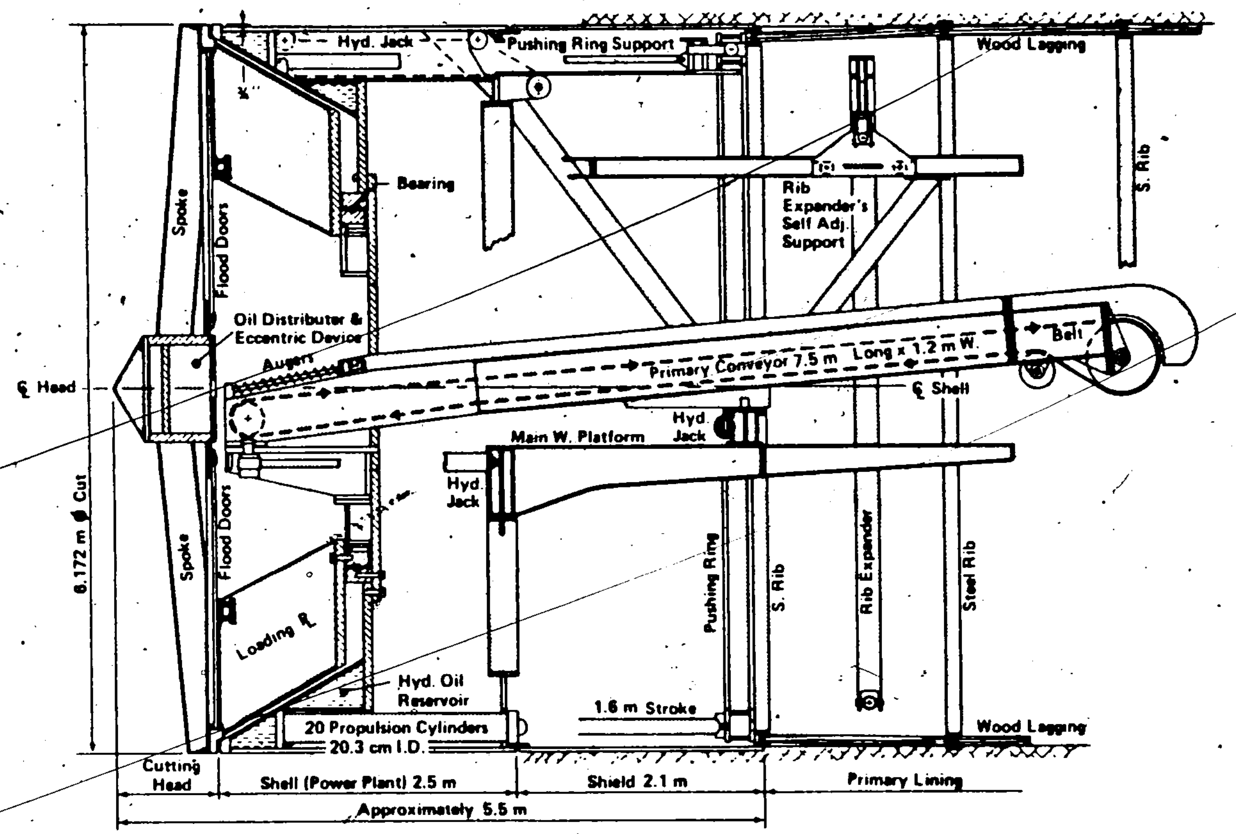

Figure 2.5 SECTION THROUGH THE SHIELDED MOLE (AFTER LOVAT TUNNELING EQUIPMENT INC.)

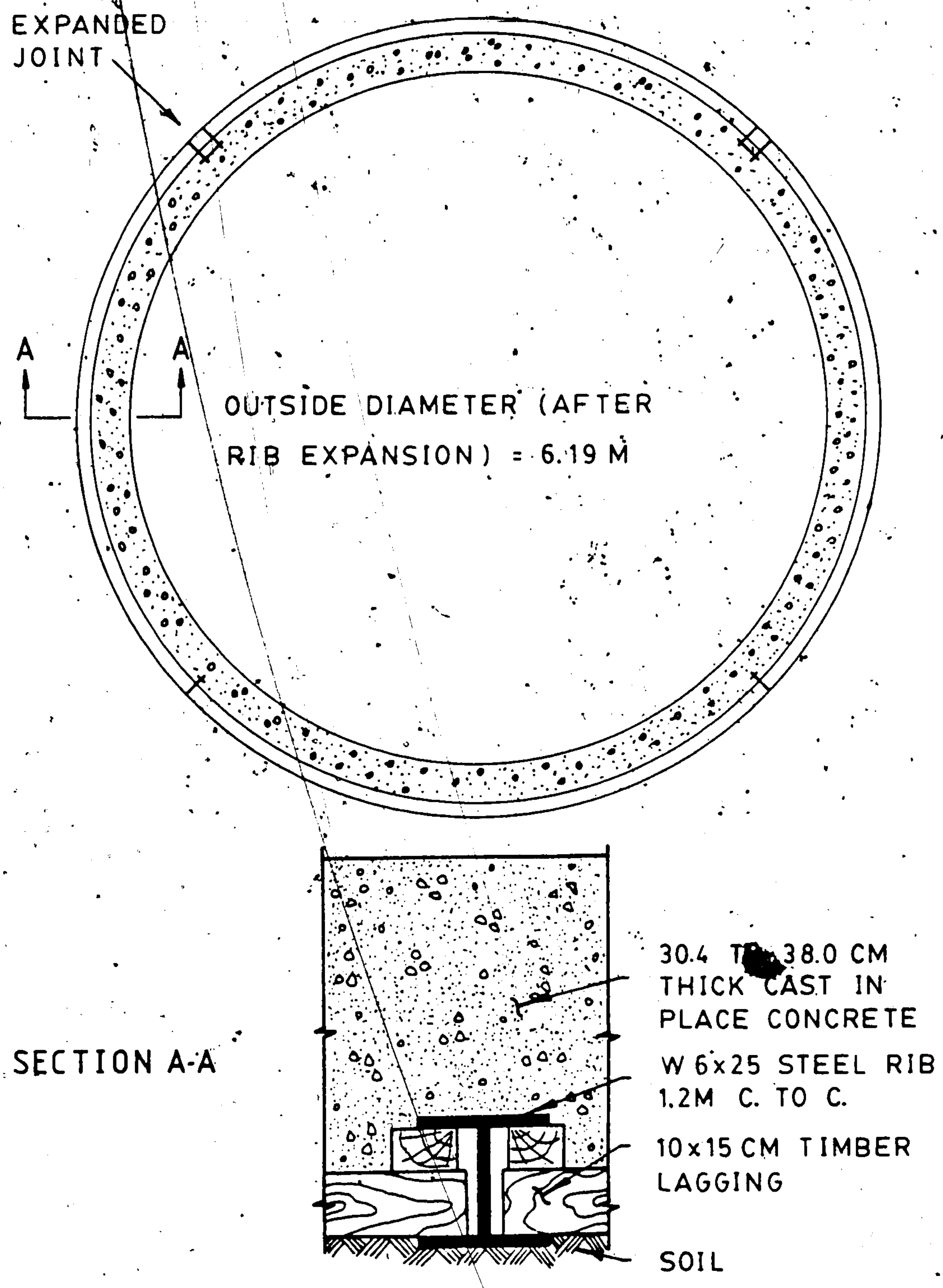

Figure 2.6 L.R.T. TUNNEL LINING SYSTEM

(yield point 300MPa), 1.22m centre to centre and 10x15cm timber lagging placed between the webs of successive ribs. The secondary lining consists of cast in place reinforced concrete and is planned to be installed after the construction of the second (south) tunnel.

Since, throughout this thesis, the measured ground and lining displacements and loads on the lining are taken before installation of the secondary lining installation, detailed description of lining installation will only refer to the primary lining.

2.4.3 Construction Procedure

The first phase of the tunnel construction (i.e. before the installation of the final lining) is discussed in detail, in the following paragraphs because its role in the tunnel lining and ground behaviour is of utmost importance.

The tunnel construction procedure basically consists of:

1. Ground excavation
2. Excavated material disposal
3. Material supply
4. Primary lining erection
5. Parallel activities

Each of these activities is described below:

Ground Excavation

The ground is excavated by the TBM described in Section 2.4.1. The cutting head of the TBM (Plate 2.1) is furnished

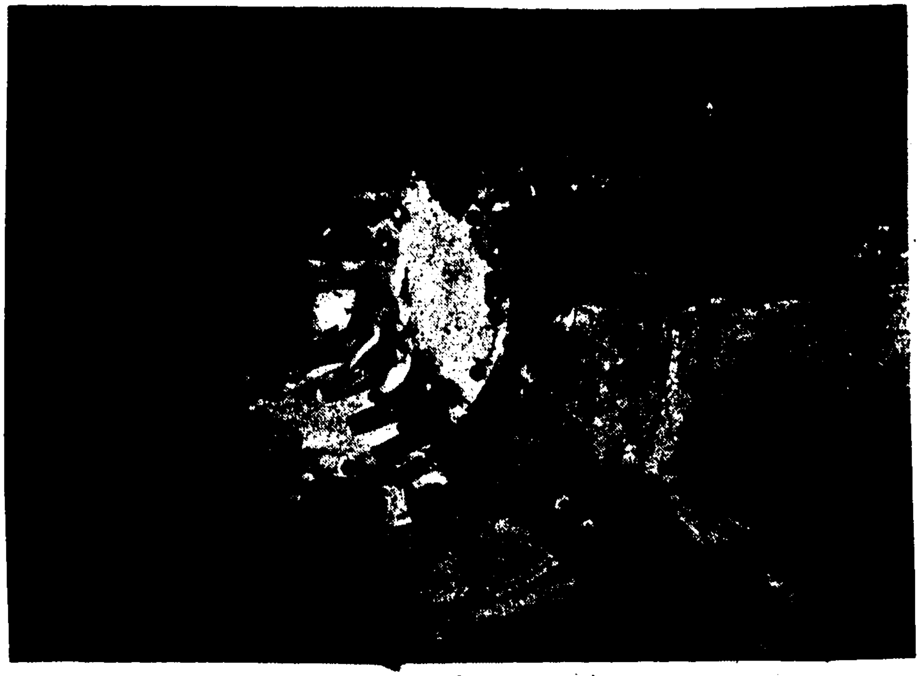

Plate 2.1 T.B.M. - CUTTING HEAD

Plate 2.2 EXPANDED LONGITUDINAL JACKS

with six spokes that give support to the slide gates. These doors are hydraulically operated and are designed to prevent any major flow of soil towards the face of the tunnel.

The advance of the mole is provided by a set of 20 hydraulic propulsion jacks located circumferentially around the perimeter of the mole. These jacks have an internal diameter of 20.32cm (8") and a maximum working pressure of 17237.5 KN/m^2 (2500 psi). The distance travelled by the mole, after one push is controlled by the depth of the jack pistons that goes up to 167.64cm (Plate 2.2).

The individual control of each jack makes possible the steering of the mole. The mole alignment is guided by a laser installed in the mezzanine level of the Central Station.

To reduce drag friction, the cutting profile of the mole is 19mm (in straight portions of the tunnel) larger than the diameter of the shield.

All the hydraulic systems and electric motors are controlled by the mole operator from the control panel shown in Plate 2.3. Individual controls open the front doors, turn the front wheel, advance the mole, activate the conveyor belt and expand or retract the rib expansion ring.

During the excavation, there is one person in charge of the face control. This person is responsible for stopping excavation whenever the behaviour of the soil at the face departs from normal.

Excavated Material Disposal

Plate 2.3 GENERAL VIEW INSIDE THE MOLE

Plate 2.4 CONVEYOR BELT STRUCTURE

The rotating cutting head delivers the soil to a conveyor belt system composed of two independent conveyor belts: the primary and the secondary. The primary conveyor is supported by the structure of the mole and delivers the soil cuttings to the secondary belt which is supported by a heavy steel structure pulled by the mole (Plate 2.4).

From the conveyor belt system, the excavated material falls into track mounted hopper cars that are pulled back to the Central Station by a small electric tractor.

The loading of the cars is a three man operation: the mole operator, controlling the conveyor belt system; the tractor driver who advances the car when a portion of it is filled and the third man stationed at the end of the secondary conveyor belt controlling the muck level inside the cars.

Material Supply

The basic material necessary for the first phase of the tunnel construction is the material for the primary lining erection (steel ribs and lagging) and for the tracks, used by the muck cars. This material comes from the eastern end of the North-East line, together with the empty muck cars, pushed by the subway trains. This material is brought to the face of the tunnel and unloaded by four men.

Lining Erection

After the mole advances a distance slightly longer than the required spacing between ribs, the longitudinal hydraulic propulsion cylinders are retracted and so is the mounting ring that remains between the propulsion jacks and the last installed steel ribs. This ring is provided with a chain that runs around its circumference and is connected to an electric motor that rotates the chain.

The first steel rib section is placed at the invert of the shield and its ends are attached to the chain in the mounting ring. The chain is rotated by 90° and the second steel section is placed at the invert, attached to the chain in the mounting ring and has one of the ends connected to the first rib section. This procedure is repeated until the fourth rib section is installed. Sometimes it is necessary to cut a few inches off the fourth rib in order to make it fit within the space left between the first and the third rib sections. The four ribs are connected to one another through end plates with two sets of bolts and nuts for each joint.

After the four ribs are installed, the pieces of wood lagging are placed between the webs of the successive ribs as shown in Plate 2.5. The spacing left between the last two installed steel ribs rings is slightly larger than the timber length (121.9cm) to facilitate its installation in between the ribs. The lagging installation starts from the invert and proceeds to the crown and is done by four men.

After all pieces of lagging are installed the longitudinal jacks are activated to close the additional space initially left between the last two steel rings to facilitate the lagging installation.

Plate 2.5 LAGGING INSTALLATION

Plate 2.6 RIB EXPANSION

The expansion of the steel ribs follows the lagging installation. The rib expansion is done immediately after these are exposed to the ground with the help of the rib expansion ring. The rib expansion ring has its diameter increased by the expansion of four jacks that can be individually activated (Plate 2.6). Each expansion jack has an internal diameter of 15.24cm and a maximum working pressure of 10343 kN/m². In the north tunnel of the LRT South Extension, the two upper joints were expanded and a 15.24cm spacer was placed in each of them.

After the rib expansion, the excavation proceeds with the mole jacking against the lining, repeating the cycle described in this section.

Parallel Activities

Several activities occur simultaneously with those previously described in this section. Some of these parallel activities are listed below:

1. Extension of the power supply and telephone cable
2 Verification of the laser alignment
3. Installation of the steel clamps that provide guidance for the conveyor belt structure
4. Installation of the tracks for the muck cars
5. Extension of the ventilation plastic pipe to the head of excavation.

The activities related to the tunnel construction are in the flow chart presented in Figure 2.7.

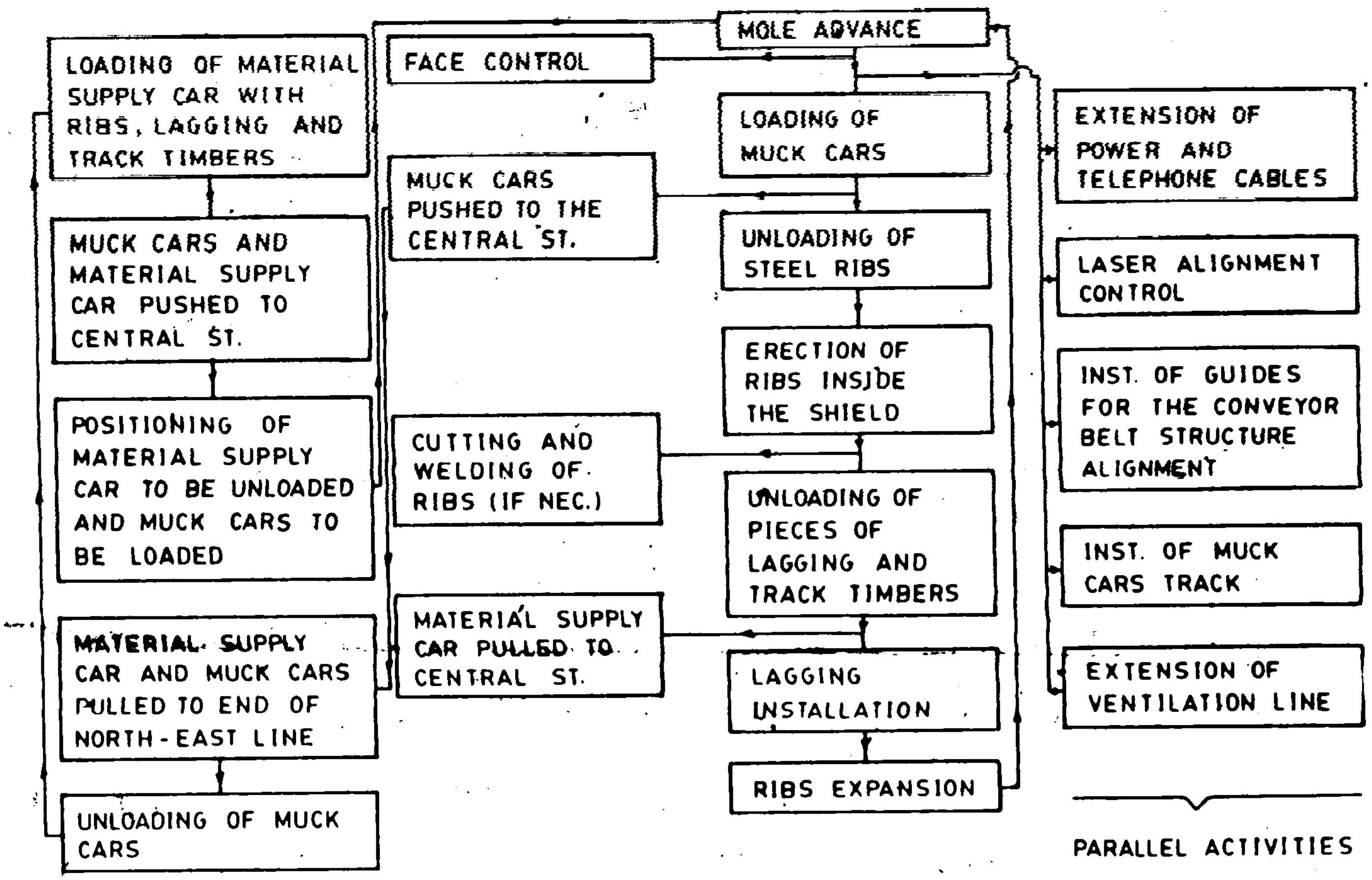

Figure 2.7 SIMPLIFIED FLOW CHART OF THE TUNNEL CONSTRUCTION PROCEDURE

2.4.4 Rates of Excavation

As explained in Section 2.2.1, the excavation of the north tunnel, LRT South Extension, was planned to start from the west end of the Central Station and proceed to the 104th St Station. The excavation beyond the east end of the 104th St Station would depend on the end of the construction of the tangent pile walls, later incorporated to the structure of that station. The critical path on the construction flow chart of the first stages of the south extension construction was determined by the work done in the 104th St Station since, well before the beginning of the construction of this station, the mole was in position to start digging. The beginning of the tangent pile construction occurred in early March, 1981, whereas the mole was ready to start digging in late November, 1980. The distance to be excavated before the mole reached the 104th St Station is 166 metres. This distance could be excavated in approximately 10 days if the excavation proceeded with three shifts of eight hours per day. The choice of excavating at a slower rate of advance in this first stage of the tunnel construction was encouraging because it would benefit all parts involved in the tunnel construction. As far as the monitoring program was concerned, the decrease in the mole advance rate would permit a greater number of readings and give more time, if necessary, to solve eventual problems with instruments.

The beginning of excavation was January 19, 1981, with one crew working eight hours a day, and the 104th St Station was reached on March 16, 1981. The tunnel construction was shut down until the completion of the tangent pile walls of this station.

The rates of excavation measured in the construction of the first stage of the tunnel construction described in this section can be obtained from Figure 2.8 where the position of the mole is plotted versus time.

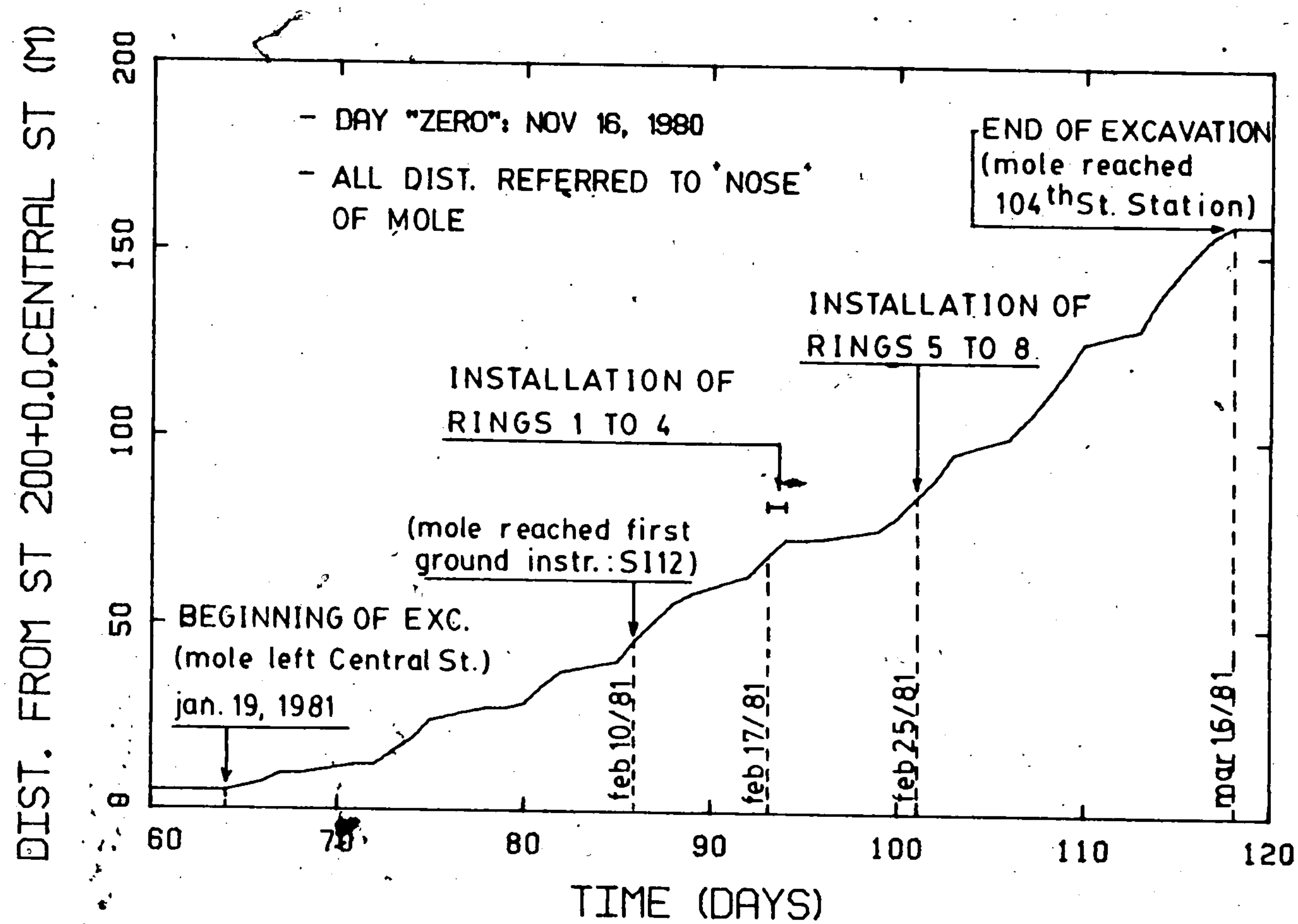

Figure 2.8 MOLE POSITION VERSUS TIME

3. SOIL DISPLACEMENTS DUE TO TUNNELING

3.1 Introduction

Observational and instrumentation programs on tunneling are extremely helpful for an understanding of the ground response, for the evaluation of the stability of the opening of the adequacy of design and in the determination of the sources of eventual problems related to the tunnel construction.

Studies of the prediction of ground behaviour before and after tunnel construction have enhanced the importance of full scale field observations. Field observations have shown that uncharted ground conditions are common and the effects of the construction procedure on the surrounding soil is not easily predicted.

The monitoring of soil movements around tunnels in the City of Edmonton is relatively modest when compared to the tunneling activity in this area. El-Nahhas (1980) carried out a comprehensive observational program to measure soil movements in a small diameter, deep tunnel dug in the lower till of Edmonton. Eisenstein and Thomson (1978) monitored surface settlements at the construction of the North-East section of the LRT System. Thomson and El-Nahhas (1980) presented surface settlements due to the construction of a small diameter tunnel in the Horseshoe Canyon Formation, in Edmonton. The few data available on the ground displacement around large and shallow tunnels in Edmonton and the necessity to accurately predict the effects of tunneling on the nearby structures along Jasper Avenue (Fig 2.1) made the ground instrumentation in the early stages of the construction of the LRT South Extension, north tunnel, of utmost value.

This chapter presents a brief description of ground displacement measurement techniques and a more detailed description of the instruments utilized in the LRT South Extension ground displacement monitoring program are presented.

3.2 Currently Available Ground Displacement Measurement Techniques

The movement of a point in the soil mass can be described by a displacement vector. This vector can be resolved into three perpendicular vectors: one vertical and two horizontal, parallel and perpendicular to the tunnel axis.

The knowledge of the displacement vectors within the soil mass during tunneling enables the construction of a spatial displacement field that is the main tool for interpreting the ground behaviour. Vertical and horizontal ground movements recorded in different stages of the tunnel construction provide data for the calculation of the three displacement vectors mentioned above.

3.2.1 Vertical Displacements

3.2.1.1 Surface Vertical Displacements

- Settlement Points

Vertical movements at the surface are obtained by comparing the elevation of a measuring point, anchored to the soil surface, to the elevation of a bench mark. The bench mark must not be affected by the tunnel excavation, must be installed outside the range of the construction influence and isolated from the overlying strata by casing.

The measuring points (settlement points) should be robust, well protected from damage, isolated from movements associated with other phenomena other than tunnel construction ones and solidly anchored to the soil in order to yield accurate and repeatable results.

There are many different designs of surface settlement points. Some of these designs are described by Burland and Moore (1973), USBR Earth Manual (1963) and Cording et al. (1975).

The accuracy of the elevation measurements is affected by the optical levelling. The surveying techniques can be improved by limiting the sight distances, balancing sights, carefully plumbing the rod, using a clearly marked staff as well as selecting stable turning points. Further improvements in accuracy can be obtained by locating the bench mark so that it is directly visible, by using invar rods and self levelling levels.

3.2.1.2 Subsurface Vertical Displacements

- Single-Point Extensometer

Simple deep settlement points are used in the measurement of settlements at various depths below the ground surface.

The requirements for the Single Point Extensometer are the same for the Surface Settlement Point, cited in the previous section. Special care should be taken to prevent the interference of the soil layer above the anchored tip in the readings.

Detailed description of the installation and design details of Single Point extensometers is given by Cording et al. (1975), El-Nahhas (1980), Hanna (1973) and Burland and Moore (1973).

Terzaghi (1938) introduced the "hose level" manometer to be used in locations where the installation of the "traditional" Single Point Extensometer, composed of a steel rod anchored to the soil, is not possible. The shortcomings and further developments of "hose level" settlement point are discussed in Hanna (opt.cit.).

- Multi-Point Extensometers

The same principle, proposed by Terzaghi in the "hose level" settlement points, can be applied to the measurement of settlements at several depths and positions by adding several cells to the manometer tube (Ward et al. 1968).

The commonest multi-point extensometers are those installed in a vertical borehole, called borehole extensometers, where displacements related to the top of the borehole can be obtained at different depths of a vertical line.

According to Cording et al. (1975) borehole extensometers are basically divided in three types:

- Rod type
- Wire type
- Probe type

There are many drawbacks of the Wire type extensometers and most of them were reported by Hedley (1969) and Hansmire (1975). The inaccuracy of the wire type extensometer is ascribed to the friction existing between its components (wires, casing, anchors). Hansmire (1975) reported inaccuracy of up to 10mm in the Wire type extensometer.

The friction between the components is minimized in the rod type extensometer by individually encasing the rods with oil filled tubes (Cording et al., opt. cit.).

The friction problem present in the Wire and Rod extensometers does not exist in the Probe type extensometers. In the Probe extensometers there is no connection between anchored points in the borehole. Instead, a probe, that transmits signals to the surface when an anchor point is passed, is lowered down the hole. The depth of the probe, related to a reference point at the top of the borehole, is read from a calibrated cable connected to its top.

Three are the most commonly used Probe extensometers:

- the Radio transmitter probe extensometer
- the Impedance coil probe extensometer
- the Magnetic reed switch probe extensometer

In the first two types of extensometers the intensity of signals transmitted to the surface changes when the probe goes through a circular plate.

In the magnetic extensometer, the reed switch closes when in the presence of the axial magnetic field existing around the circular magnets anchored to the borehole walls and activates an indicator light or buzzer at the surface.

The use of magnetic extensometers has increased since it was first developed in the Building Research Station (Burland et al. 1972)).

The success of the magnetic extensometer for ground displacement measurements is ascribed to the simplicity of its construction and use, to its reliability and low cost.

More details concerning the Magnetic extensometer are given in Section 3.3.2.3.

3.2.2 Horizontal Displacements

3.2.2.1 Surface Horizontal Displacements

Cording et al. (1975) recognize four principal methods of measuring surficial horizontal movements.

1. offsets from a transit line
2. direct chaining with a steel tape or a portable

extensometer

3. electronic distance measuring
4. triangulation

Hanna (1973) also describes the photogrammetric method which can be used when an accuracy not better than 5mm is required.

All the methods mentioned above are described by Cording et al. (opt.cit.) and Hanna (opt.cit.).

The major use for measurements of surficial horizontal movements is to check the results obtained from slope indicators, described later in this chapter.

3.2.2.2 Subsurface Horizontal Displacements

- Extensometers

The Wire, Rod and Magnetic extensometers discussed in Section 3.2.1.2 can be used in the measurement of horizontal displacements provided an horizontal borehole can be drilled within the soil mass.

In tunneling, the installation of horizontal extensometers is often made from inside the tunnel which limits its utility because displacements ahead of the tunnel are difficult to obtain.

For the measurement of horizontal movements within the soil ahead of the tunnel face, the inclinometers or slope indicators, described in the next section are more commonly used.

- Inclinometers

Inclinometers or slope indicators are installed in the ground or structure to measure inclinations and change in inclinations at several levels which, when integrated over the length of the vertical line defined by the casing, yield horizontal displacements.

Inclinometers are divided into two major types:

- Portable borehole inclinometers
- Fixed borehole inclinometers

[illegible]ive of the inclinometer type, the bottom of th[illegible] or guide, must be anchored in the ground well below [illegible] area affected by the construction, thus ensuring that the bottom is fixed.

- *Portable Borehole Inclinometers*

Portable borehole inclinometers have been extensively used due to their relatively low cost, good quality results, easy installation and reading procedure.

It is basically composed of three units:

- casing
- sensing unit and cable
- electrical readout

The aluminium or plastic casings are provided with four vertical slots which are positioned at the quarter points of its inside circumference and serve as guide for the torpedo or sensing unit.

The sensing unit is usually provided with four wheels, two of which are spring-loaded which track within opposite grooves of the casing and align the sensing unit in stable and repeatable positions.

The electrical readout supplies voltage to the sensing unit and displays the measured inclinations as numerical readings. A multi-wired, reinforced cable connects the readout unit to the sensing unit and provides an indication of depth through its colored neoprene markers, usually attached at 30.5cm spacings.

The various systems used in the sensing unit transducers differentiate the types of portable borehole inclinometers.

Cording et al. (1975) cited five different kinds of transducers:

1. pendulum actuated resistors
2. vibrating wire strain gauges
3. differential transformers
4. servo-accelerometers
5. photographic cameras

The commonest of these are the pendulum actuated resistors and, more recently, the servo-accelerometers that are less vulnerable to temperature effects and zero drift.

The inclinometers that use the pendulum actuated resistors, known as Wilson Slope Indicator (Wilson, 1962), convert inclinations into electrical measurements with the help of a conventional Wheatstone bridge circuit. A precision-wound resistance coil is subdivided into two resistances by a pendulum, that remains vertical, making up one half of the bridge. The remainder of the bridge and associated circuitry is contained in the control box. The precision of this device is reported (Savigny, 1980) to vary between $1.7x10^{4}$ to $8.3x10^{4}$ (Precision given in units of shear strain or simply metres of deflection per metre of depth, defined by Gould and Dunnicliff, 1971).

A more accurate type of transducer is the servo-accelerometer. A servo-accelerometer is composed of a "proof mass" that is free to swing within a magnetic field. The proof mass is provided with a coil or torquer that allows a lineal force to be applied to the "proof mass" in response to a current passed through the coil (Savigny, opt.cit.). The sensor is energized by an applied voltage and quickly stabilized in response to tilt by a change of current flow. The resulting voltage output is proportional to the sine of the angle of inclination. Precision between $0.4x10^{4}$ to $1.3x10^{4}$ has been reported in cases where the servo-accelerometer inclinometer has been used.

Savigny (opt.cit.) performed extensive lab and field tests with the Digitilt (servo-accelerometer type, made by Slope Indicator Co.) and reported the internal and external factors affecting its accuracy. Sensor axis rotation, casing spiral and temperature are some of the internal factors whereas recovery of equilibrium conditions around the casing, changing the degree of non parallelism of grooves are defined as external factors. More details concerning the Servo-accelerometer Inclinometer is given in Section 3.3.3.1.

- Fixed Borehole Inclinometers

As opposed to the portable borehole inclinometers, the fixed borehole inclinometers remain in place in the borehole in order to continually monitor inclination at discrete points along the borehole.

The sensing units used in the torpedo of the portable inclinometers are also used in the fixed inclinometers.

The major advantage of the fixed borehole inclinometers is that the inaccuracy coming from "tracking" and repeatable positioning is eliminated. In most cases, the fixed sensors can be removed and re-used.

Some of the potential problems are the loss of accuracy if the sensor units are removed from the borehole for repairs and danger of buckling of the elements in the case of settlement of the casing.

3.3 Ground Displacement Monitoring in the LRT South Extension

3.3.1 Instruments Location

The importance of observational and instrumentation programs in tunneling is mentioned in the introduction of this chapter. The effectiveness of the ground instrumentation on the study of the effects of construction of the LRT South Extension, north tunnel, on the buildings situated nearby the excavation was favoured by the scheduled

LRT South Extension construction sequence. The construction sequence described in Chapter 2 states that the tangent pile walls of the 104th Street Station should be completed before the mole excavates through this station. As the critical path on the early stages of the LRT South Extension construction was governed by the end of the construction of the tangent pile walls of the 104th Street Station, there was a choice of either starting the tunnel excavation as soon as possible from the Central Station (Sta.200 + 0.0) and stopping the mole at the east wall of the 104th St Station (Sta.200 + 164.0) until wall construction finished or to time the beginning of excavation with the end of construction in order not to stop the mole.

The first alternative was chosen because the anticipation of the tunnel excavation would present time to analyse the data collected from ground displacement measuring devices and to verify whether special care would be necessary in the construction of the remaining portions of the tunnel west of the 104th St Station.

The ground instruments were located at the east side of the intersection of 102nd Street and Jasper Avenue (Fig 3.1). This intersection is situated approximately 60 metres away from the west wall of the Central Station and tunneling in this area is considered not to be affected by the proximity of the Station.

As shown in Fig 3.1, ground instruments were installed between Sta.200 + 43.6 and Sta.200 + 57.1, and has been

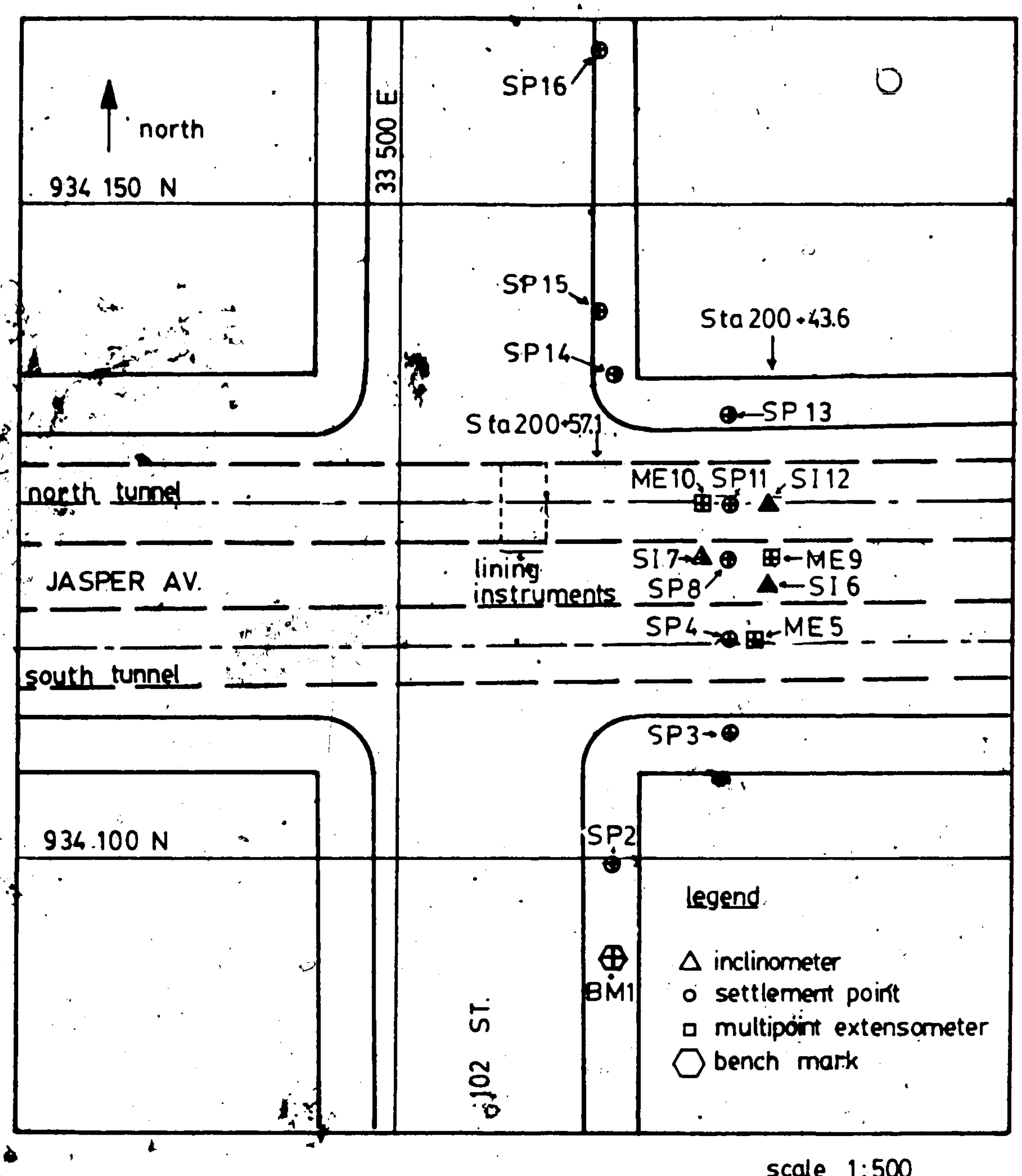

Figure 3.1 INSTRUMENTS LOCATION - PLAN VIEW

termed the "Instrumented Section".

The ground instruments, discussed later in this chapter, were located in positions that would enable the analysis of the strain field at the south side of the north tunnel, during and after its construction, to be carried out.

Figure 3.2 depicts a transverse section of the "Instrumented Section".

Detailed description of the design, installation, measurement procedure and field data related to the ground instruments used in the LRT South Extension program are presented in the following sections.

3.3.2 Vertical Displacements

Vertical displacements were measured close to the surface, at 3 metres depth, using settlement points and at several other depths with magnetic multipoint extensometers.

All readings presented in this section are referred to a bench mark, described below.

3.3.2.1 Bench Mark

Several Bench Marks (BM) were available at the site (Alberta Survey Control Monuments) but they were shallow and close to the excavated area or too far from the "Instrumented Section".

An ideal BM should be installed close to the "Instrumented Section", in order to minimize the number of

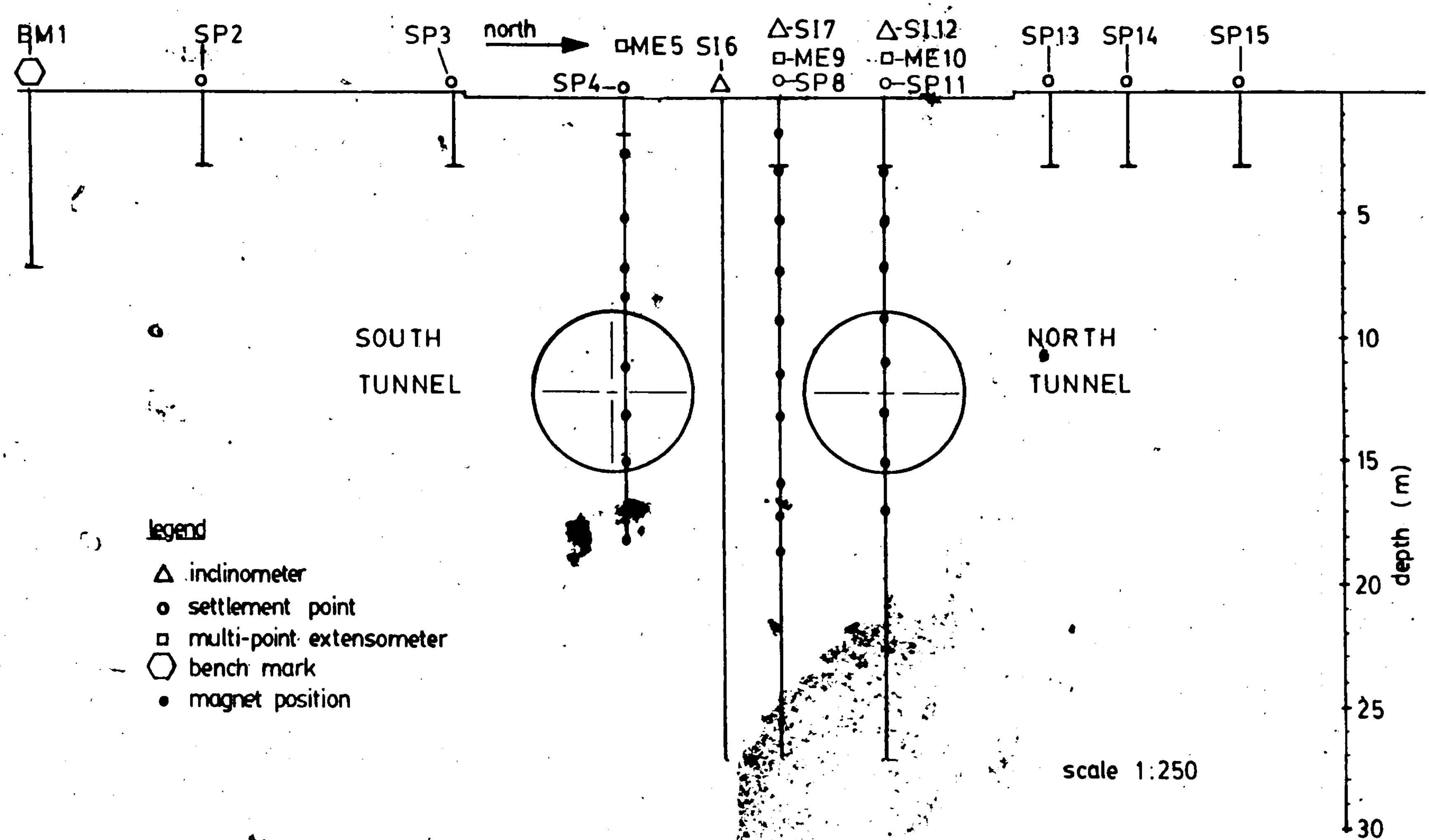

Figure 3.2 INSTRUMENTS LOCATION - TRANSVERSE SECTION

turning points and to keep the sight distance short (during levelling), and anchored in a region not affected by tunneling.

The depth and location of the BM installed for the LRT South-Extension ground monitoring program, indicated in Figures 3.1 and 3.2, fulfill the requirements mentioned.

Bench Mark Design Details

The details of the BM installed at 35m from the axis of the north tunnel are presented in Fig 3.3.

The BM is basically composed of a 7.93 metres long steel pipe (3.34cm O.D.) which has on its lower end a 15cm long nail, to provide good anchorage in the bottom of the hole. A pvc pipe (5.85cm I.D.) surrounds the steel inner pipe to prevent the interference of the soil layers above the anchored tip.

Bench Mark Installation

A 10.2cm diameter borehole was drilled with a solid auger to a depth of approximately 8 metres. The auger was retrieved and the steel pipe (3.34cm O.D.) lowered into the borehole. No sloughing of the borehole walls had occurred. By slowly applying downward forces to the top of the steel pipe, with the help of the drilling rig, the bottom of the steel pipe was pushed 15cm into the bottom of the borehole, ensuring a good anchorage.

The pvc casing was inserted into the borehole, surrounding the steel pipe. The void between the borehole walls and the pvc pipe was filled with clean sand.

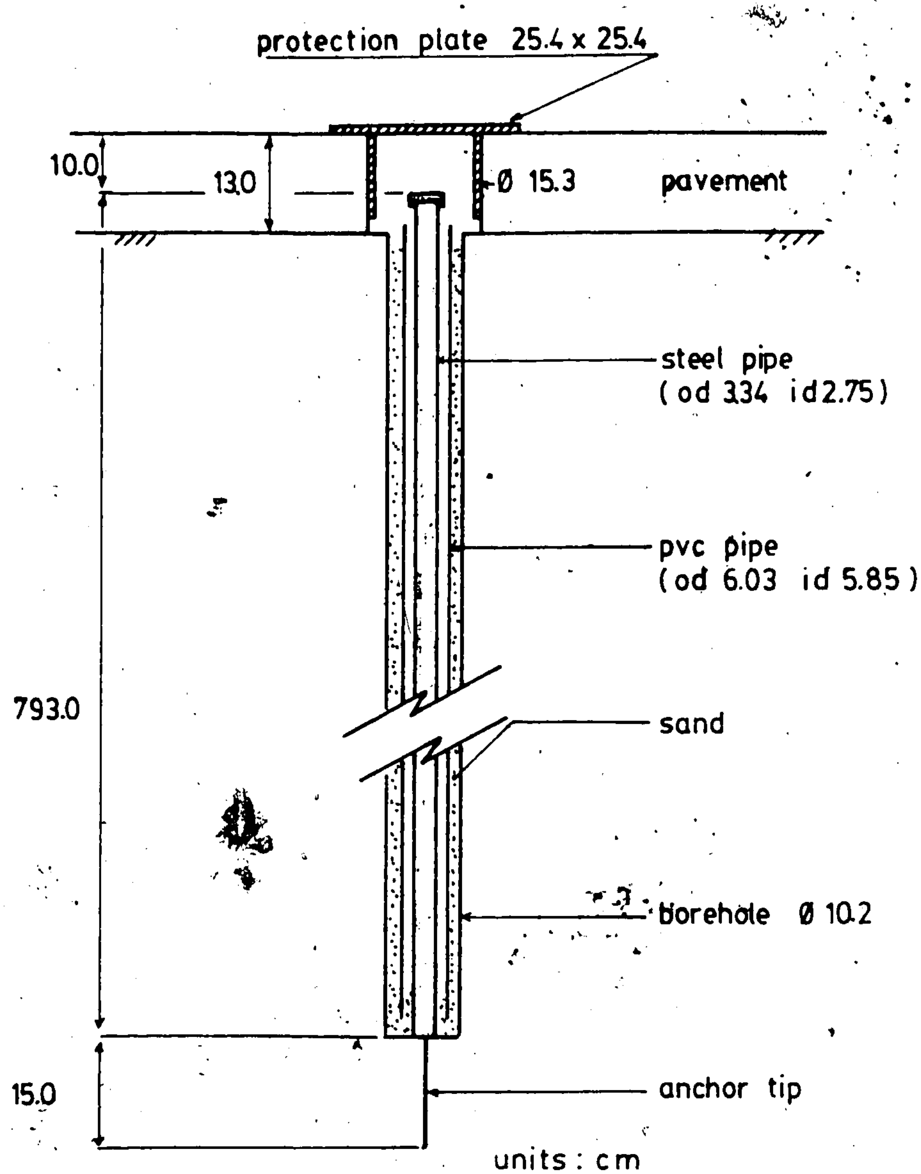

Figure 3.3 BENCH MARK BM1 - DESIGN DETAILS

The protection of the bench mark after installation was provided by a square steel plate (25.4cm x 25.4cm) fixed to the pavement.

3.3.2.2 Settlement Point

Nine settlement points (SP) were installed at different distances from the tunnel axis according to Table 3.1. These distances were chosen in order to obtain the complete shape of the settlement trought at surface due to tunneling.

As mentioned in Section 3.2.1.1, settlement points should be well protected from damage, isolated from movements associated with phenomena other than tunneling and solidly anchored to the soil.

Protection from damage was successfully provided by a steel plate cover. Movements associated with phenomena not related to tunneling might be the effects of the traffic and the frost penetration into the soil. Traffic problems were believed not to be of significant importance due to the good quality of the pavement but the frost penetration recorded in several locations in the City of Edmonton showed depths up to 2.4 metres where the snow drift had been removed due to traffic operations. This value (2.4m) was used as an upper boundary of frost penetration because most of the data analysed showed frost penetration no deeper than 1.8 metres.

By the time the decision to anchor the settlement points at 3.0 metres below surface was made, the settlement point SP4 had already been installed at 1.5 metre of depth.

SETTLEMENT POINT NO	DISTANCE FROM TUNNEL AXIS (m)	ANCHORAGE DEPTH (m)	INSULATION
SP2	27.7	3.0	PG
SP3	17.6 SOUTH	3.0	PG
SP4	10.4	1.5	N.I.
SP8	4.37	3.0	Z.
SP11	0.00	3.0	PG
SP13	6.80	3.0	PG
SP14	9.80 NORTH	3.0	PG
SP15	14.5	3.0	PG
SP16	34.7	3.0	PG

PG = Polystyrene foam guides
Z = Zonalite
NI = No insulation

TABLE 3.1 - SETTLEMENT POINTS - DETAILS OF INSTALLATION

Low temperatures inside the borehole where settlement points were installed, were prevented by the installation of polystyrene foam guides inside the pvc pipe (Fig 3.4) and by filling the void left under the protective plate with zonalite insulation.

Settlement Point Design Details

Figure 3.4 depicts the design details of the settlement points used to monitor surface vertical displacements.

The settlement points are basically composed of a steel rod (1.0cm diameter and 305cm long), and a pvc pipe (5.1cm I.D.). The steel rod has an end plate welded to it at 14.5cm from the lower end (Fig 3.4) and an aluminium cap attached to the upper end. This cap is provided with a cone shaped depression that fits the lower end of the levelling rod. The pvc pipe is installed around the steel rod to prevent the contact between the ground and the steel rod.

The protection of the settlement points against damage was accomplished with the installation of a square steel plate at the surface.

Settlement Point Installation

A 10.2cm diameter, 320cm long borehole was drilled and the inner steel rod inserted into the hole. The anchorage of the steel rod to the borehole bottom was accomplished by hammering its end plate (Fig 3.4) from the surface with a heavy steel pipe. The use of the heavy steel pipe enabled the application of the pushing force from the surface without touching the inner steel rod.

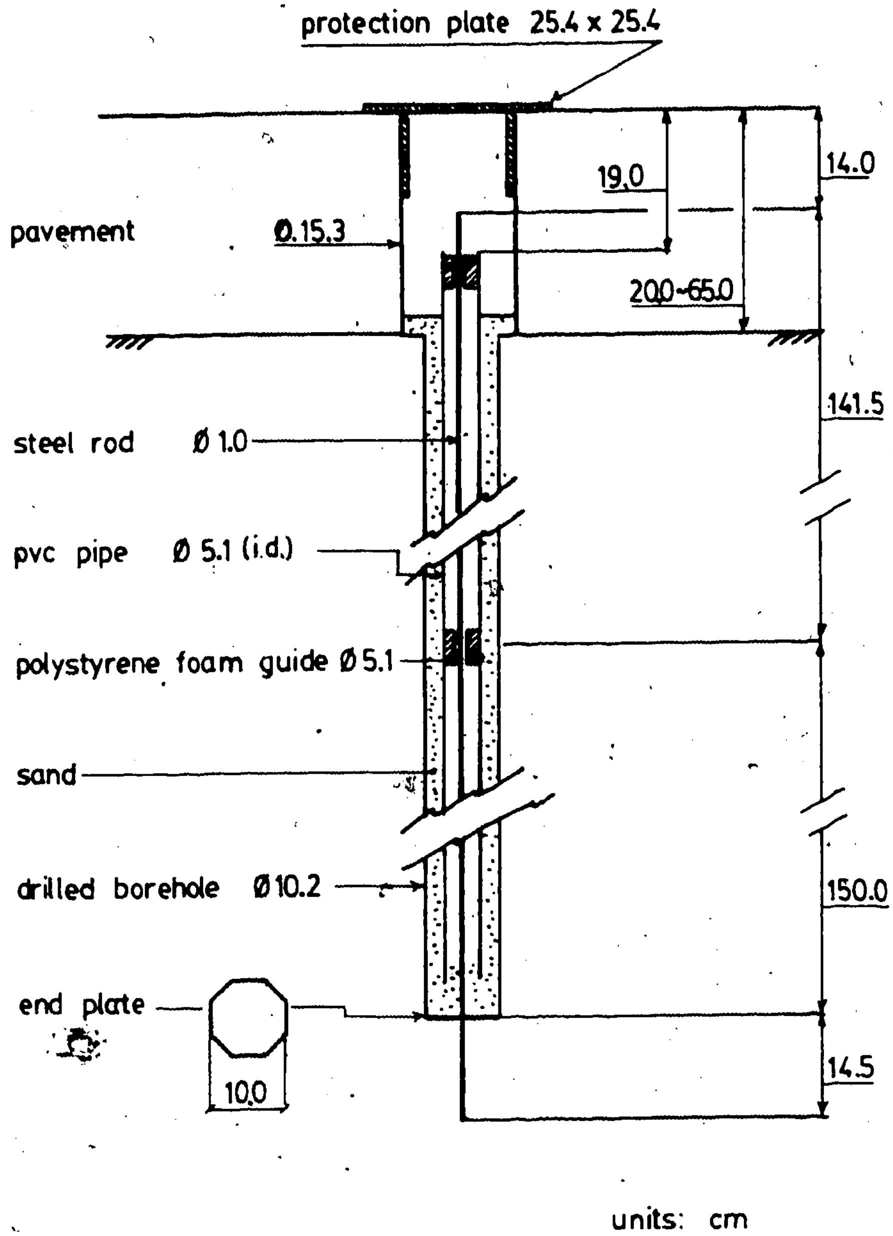

Figure 3.4 SETTLEMENT POINT - DESIGN DETAILS

The pvc pipe was inserted in the borehole, surrounding the inner steel rod and the void between the pvc pipe and the borehole walls filled with clean sand. Two cylindrical polystyrene foam guides (5.1cm diameter and 5.0cm long) were pushed into the pvc pipe with the inner steel rod passing through its centre (Fig 3.4) due to reasons discussed previously in this chapter. The middle hole passing through the polystyrene guides were slightly larger than the diameter of the inner steel rod and were carefully greased before insertion in order to avoid interference between the steel rod and the surrounding pvc pipe.

SP8 had the void between the steel rod and the pvc pipe filled with zonalite. Zonalite is a very light and deformable insulating material.

Settlement Point Measurement Procedure

The settlement points (SP) had their elevations compared to the elevation of the bench mark (BM1) through a very careful levelling technique. To ensure accuracy and repeatability of level measurements, sight distances were less than 10 metres. A special surveying rod, provided with a level bubble and 1mm divisions, and a self leveling optical level were used.

Gould and Dunnicliff (1971) suggest a maximum error of closure of 0.6mm for leveling procedures similar to the ones followed in the present study. Mendes et al. (1970) suggested a permissable error in elevation measurements, in Manicouagan 5 Dam of $0.01\sqrt{N}$ feet, where N is the number of instrument set-ups. The limitation of the sight distance (between the level and surveying rod) results in an increase in the number of instruments set-ups. To level the settlement points of the LRT South Extension, north tunnel, four level set-ups were necessary:

1st set up: between SP2 and SP3

2nd set up: between SP8 and SP4

3rd set up: between SP13 and SP14

4th set up: between SP15 and Sp16

Level readings were recorded on the field data sheet presented in Figure 3.5. This field sheet is provided with columns that enabled the level calculations to be made immediately after the readings were taken.

Settlement Point Field Data

The ground instruments (settlement points, multipoint extensometers and slope indicators) were levelled three times before the beginning of the tunnel excavation. These readings were taken in November 29, and December 14, 1980 and January 18, 1981. Most of the SP elevations obtained from the zero readings had to be disregarded due to reasons discussed later in this chapter. The SP elevations, related to the bench mark BM1, obtained on February 01, 1981 were then taken as reference. At this date, the nose of the mole was 19.1 metres away from the closest ground instrument is believed that, at this distance from the face o mole, no ground deformation due to tunneling had occurred

SETTLEMENT POINT FIELD SHEET

RECORDED BY:

DATE: TIME: TEMP: TUNNEL FACE AT:

		READINGS FOWARD RUN				READINGS BACKWARDS RUN				FORWARD	BACKWARD	FORWARD	BACKWARD	
BASE	S.P.	M	T	B	AV.	M	T	B	AV	δ_{1-i}				δ_{1-i} ADJ
P_1	1													
	2													
	3													

BASE	S.P.	M	T	B	AV.	M	T	B	AV.	δ_{3-i}		$\delta_{1-i} = \delta_{3-i} + \delta_{1-3}$		δ_{1-i} ADJ
P_2	3													
	4													
	5													
	6													
	7													
	8													
	9													
	10													
	12													
	11													

BASE	S.P.	M	T	B	AV.	M	T	B	AV	δ_{11-i}		$\delta_{1-i} = \delta_{11-i} + \delta_{1-11}$		δ_{1-i} ADJ
P_3	11													
	13													
	14													
	15													

BASE	S.P.	M	T	B	AV.	M	T	B	AV	δ_{15-i}		$\delta_{1-i} = \delta_{15-i} + \delta_{1-15}$		δ_{1-i} ADJ
P_4	15													
	16													

NOTE: $\delta_{i-j} \begin{cases} + & \text{IF } i \text{ BELOW } j \\ - & \text{IF } i \text{ ABOVE } j \end{cases}$

Figure 3 5 SETTLEMENT POINT FIELD SHEET

Table 3.2 depicts the difference in elevation between the settlement points and the bench mark BM1. The settlement point elevation data presented in Table 3.2 were obtained in sets of readings where the error of closure was always less than 1mm except those obtained in February 11, 1981 when the error of closure was 1.6mm. This increase in error of closure is probably due to the proximity of the mole to the "Instrumented Section"; settlements were probably taking place while settlement points were being levelled.

There were occasions that levelling had to be carried out during the evening. When this happened the levelling accuracy was found to be poorer than that obtained during daylight.

Figures 3.6 and 3.7 present the settlement point elevations plotted versus time and versus distance from the face of the mole, respectively. Individual settlement points elevations versus distance from nose of mole are plotted in Figures 3.8 to 3.16.

The combination of the data from Table 3.2 and Tables B1 to B4 (in Appendix B) made possible the construction of graphs where elevations were plotted versus distance from tunnel face.

Figures 3.17 and 3.18 present contour lines and settlement through transverse sections, respectively.

Discussions of the results presented in this section are presented in section 3.4.1.

VERTICAL DISPLACEMENTS (mm)

DATE (1981)	REF. DATE*	SP2	SP3	SP4	SP8	SP11	SP13	SP14	SP15	SP16
FEB 01	76	0.0	0.0	0.0	0.0	0.0	0.0	0.0	**	**
03	78	+0.55	+0.15	+0.20	+0.20	-0.10	+0.15	+0.35	+0.00	+0.00
05	80	+0.25	+0.00	+0.30	+0.30	+0.15	+0.40	+0.80	+0.55	+0.10
06	81	+0.30	+0.15	+0.25	+0.45	+0.70	+0.95	+1.40	+1.25	-
08	83	+0.05	-0.30	-0.45	+0.30	-0.25	-0.15	+0.20	+0.00	-0.05
09	84	+0.10	-0.30	-0.45	+0.25	-0.10	+0.30	+0.70	+0.35	+0.15
10	85	-0.05	-0.75	-1.15	+0.25	-0.55	+0.40	+1.15	+1.05	+1.10
10	85	-0.35	-1.05	-1.40	-1.10	-1.90	-0.85	-0.15	-0.35	-0.95
11	86	-0.40	-0.80	-1.35	-0.80	-1.60	+0.00	+0.70	+0.45	+0.65
11	86	+0.20	-0.45	-1.10	-1.45	-3.15	-0.45	+1.20	+1.00	+1.90
12	87	-0.75	-1.10	-2.10	-3.90	-5.35	-1.35	+0.30	+0.35	+0.10
13	88	-0.80	-1.05	-2.40	-4.[illegible]	-6.05	-0.90	-0.70	+1.05	+1.35
13	88	-0.80	-1.75	-3.30	[illegible]	-8.25	-2.90	-	-0.55	-1.00
16	91	-1.10	-1.15	-2.10	-5.20	-7.75	-1.70	-0.25	+0.45	[illegible].40
17	92	-0.90	-1.35	-2.30	-6.10	-8.65	-2.0[illegible]	-0.45	+0.05	+0.20
18	93	-0.75	-1.10	-1.80	-5.60	-8.40	-1.85	-0.40	+0.20	+0.70
19	94	-0.95	-1.05	-1.80	-6.00	-8.55	-1.90	-0.60	-0.05	-0.05
23	98	-0.80	-1.10	-1.50	-6.35	-8.95	-2.00	-0.65	+0.25	+0.65
26	101	-0.75	-1.45	-2.1[illegible]	-7.20	-9.65	-2.90	-1.25	-0.50	+0.95
MAR 19	122	+0.30	-0.40	-1.40	-7.65	-10.0	-3.55	-1.60	-0.55	-

* Day Zero = NOV 16, 1980

** Readings disregarded FEB 03 = Zero reading for this point

TABLE 3.2 - SETTLEMENT POINTS - CHANGE IN ELEVATION

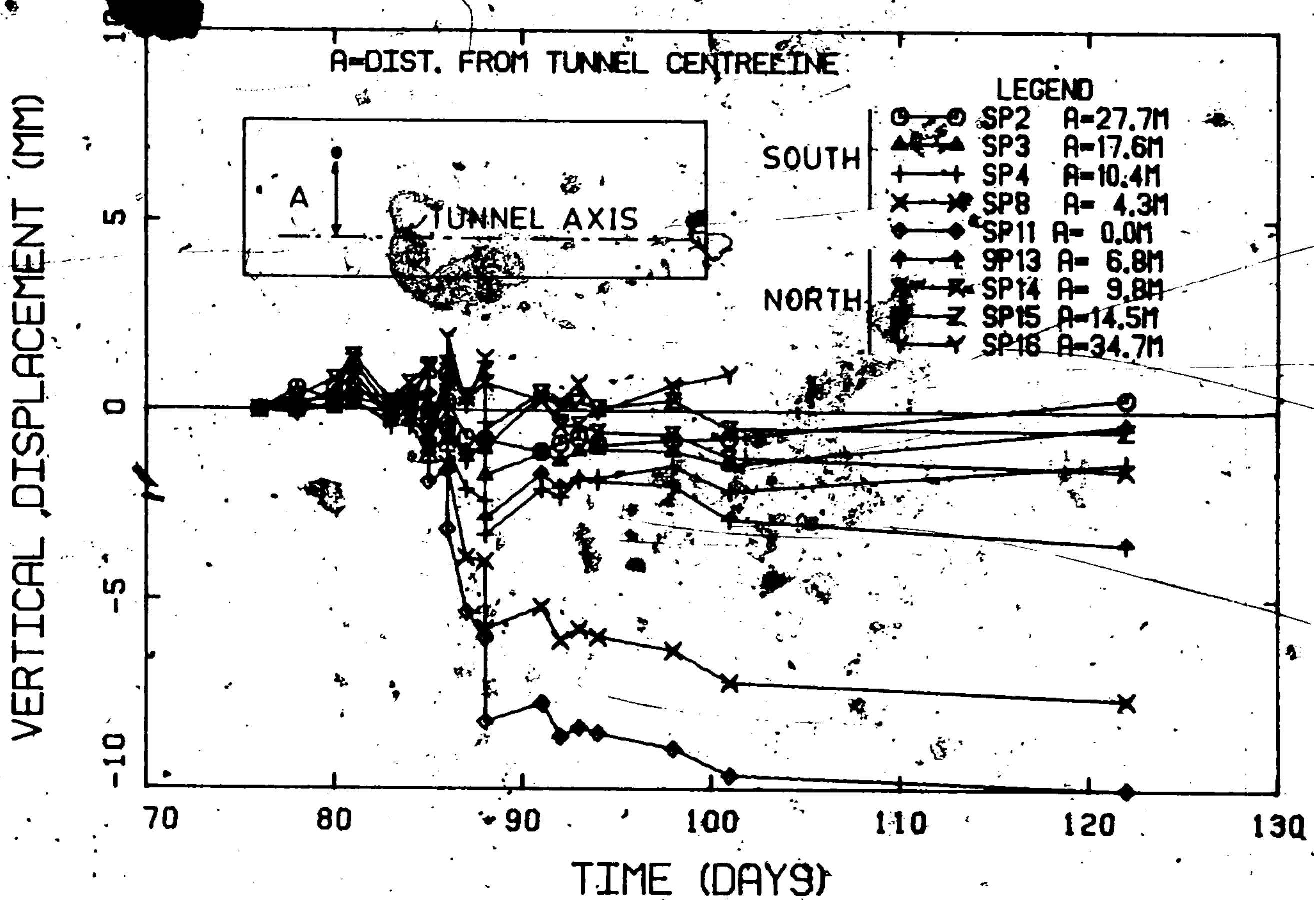

Figure 3.6 SURFACE SETTLEMENT VERSUS TIME

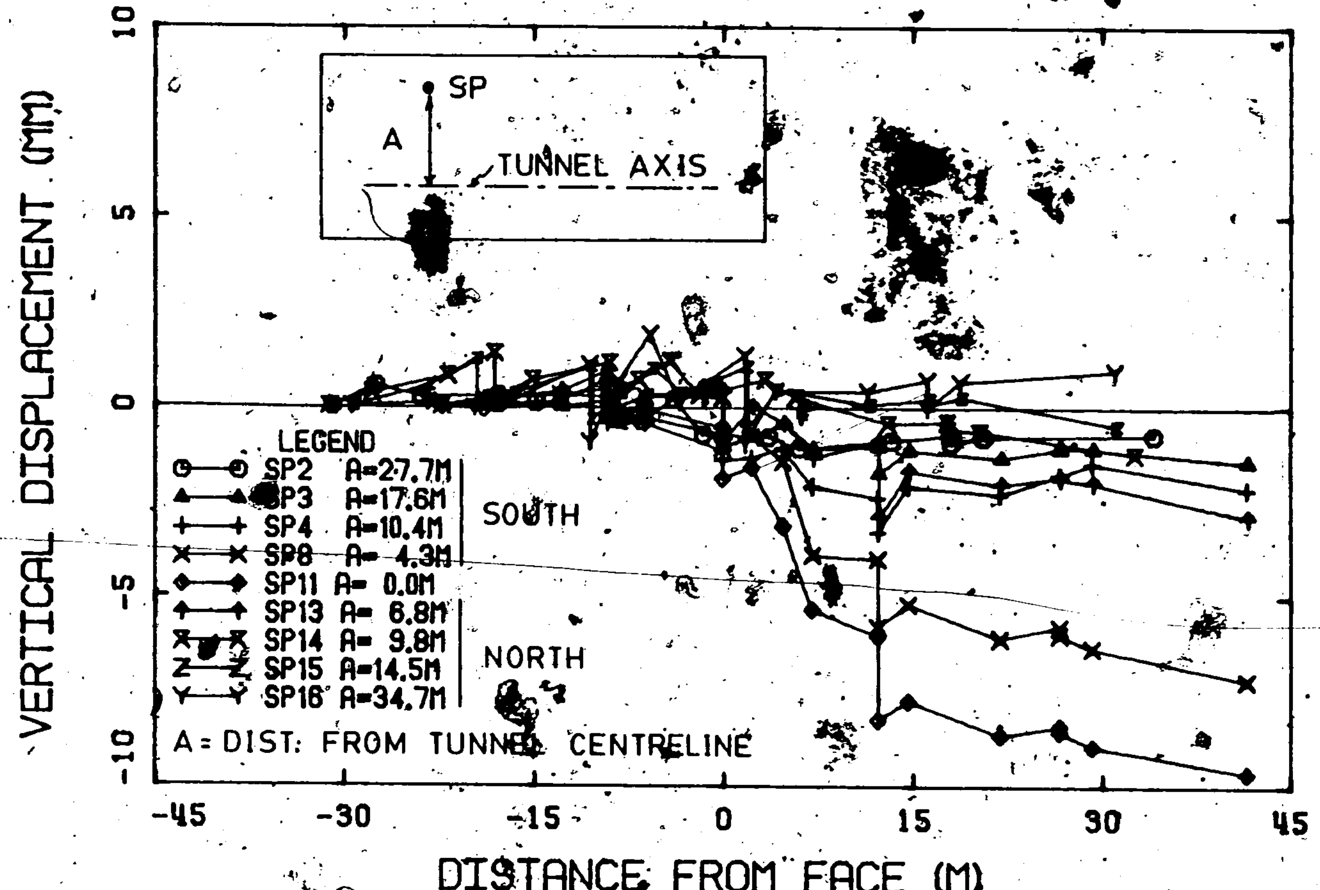

Figure 3.7 SURFACE SETTLEMENT VS DIST FROM FACE OF MOLE

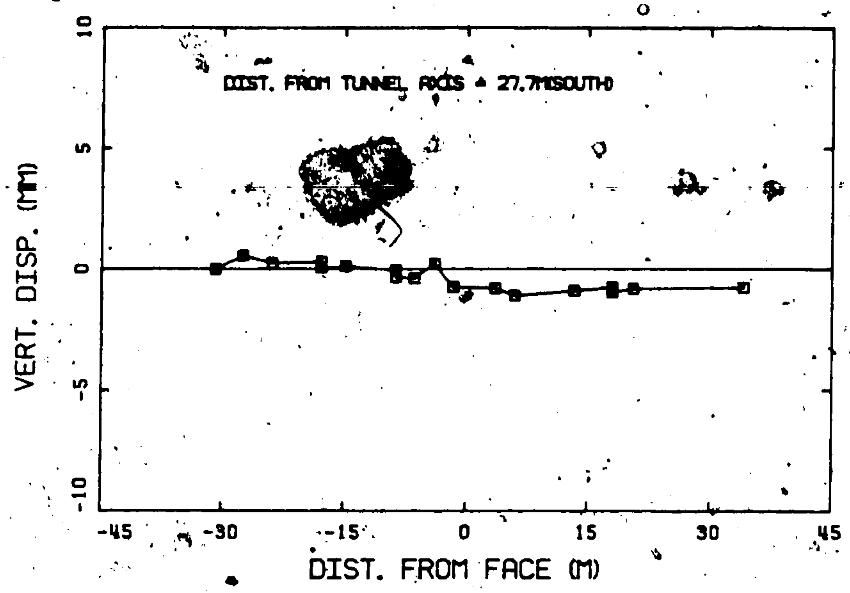

Figure 3.8 SETTLEMENT POINT SP2

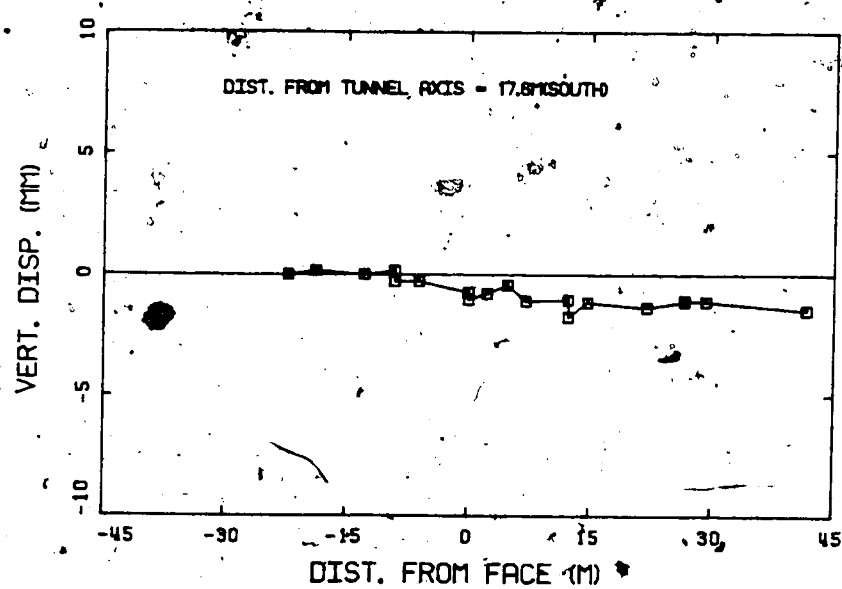

Figure 3.9 SETTLEMENT POINT SP3

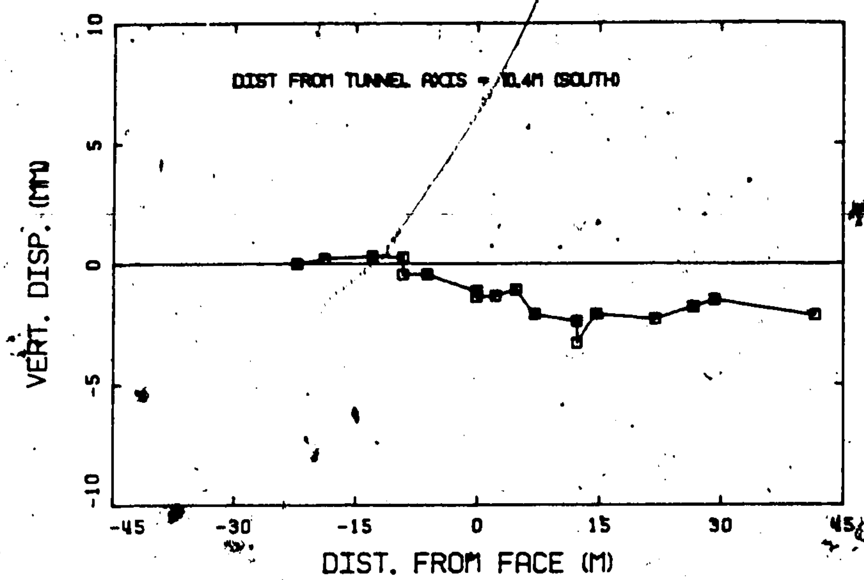

Figure 3.10 SETTLEMENT POINT SP4

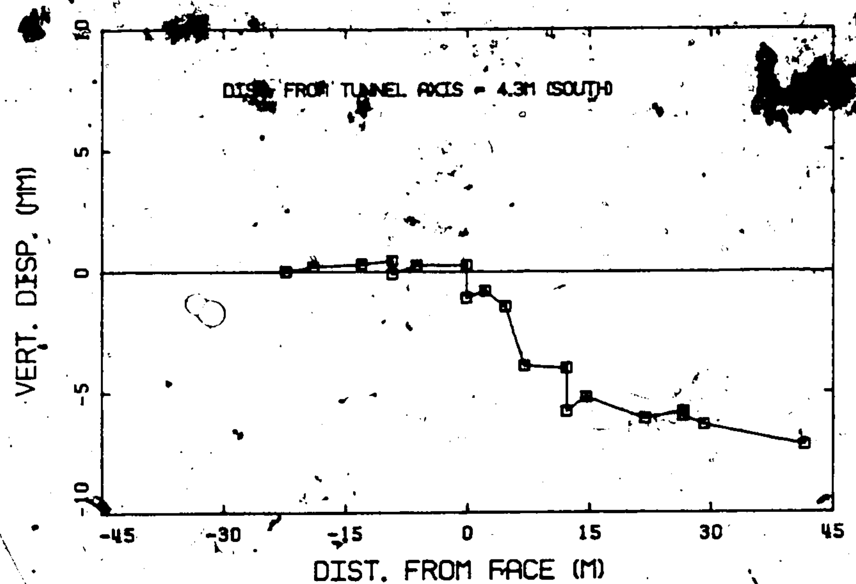

Figure 3.11 SETTLEMENT POINT SP8

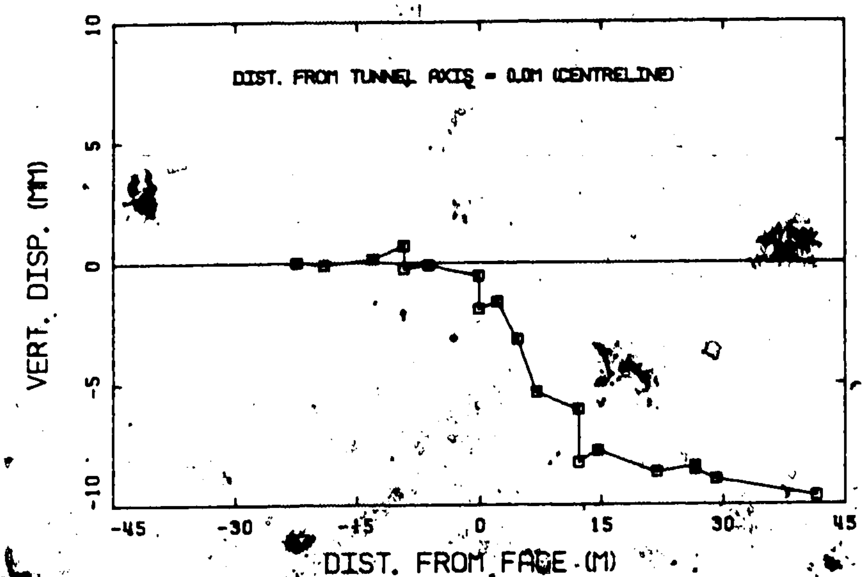

Figure 3.12 SETTLEMENT POINT SP11

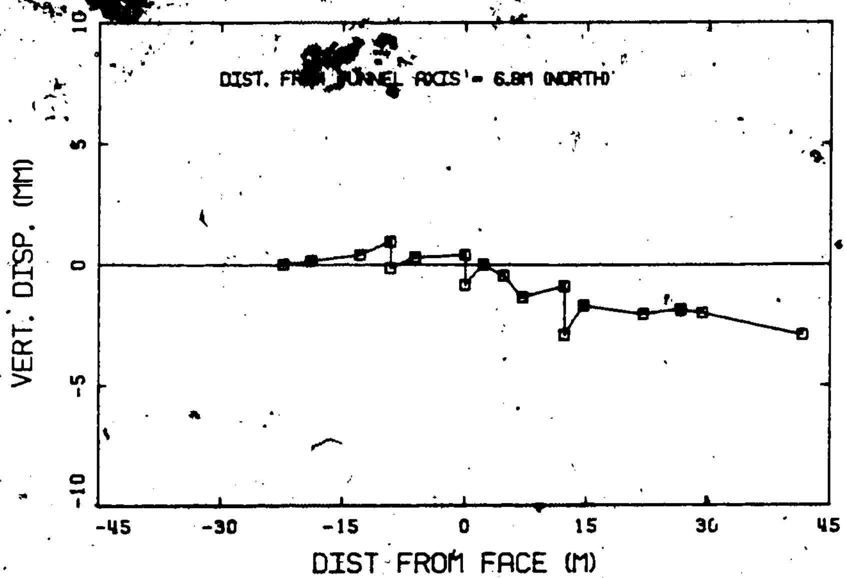

Figure 3.13 SETTLEMENT POINT SP13

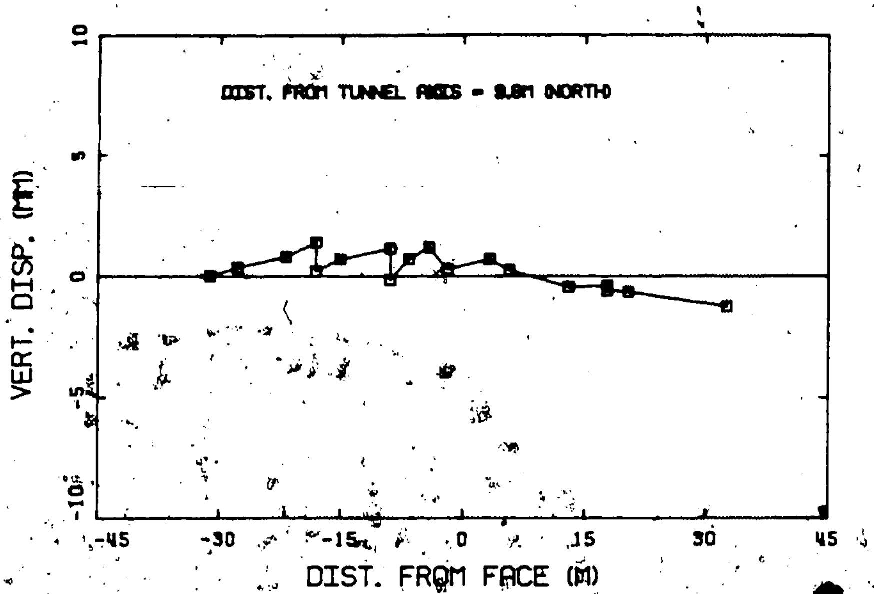

Figure 3.14 SETTLEMENT POINT SP14

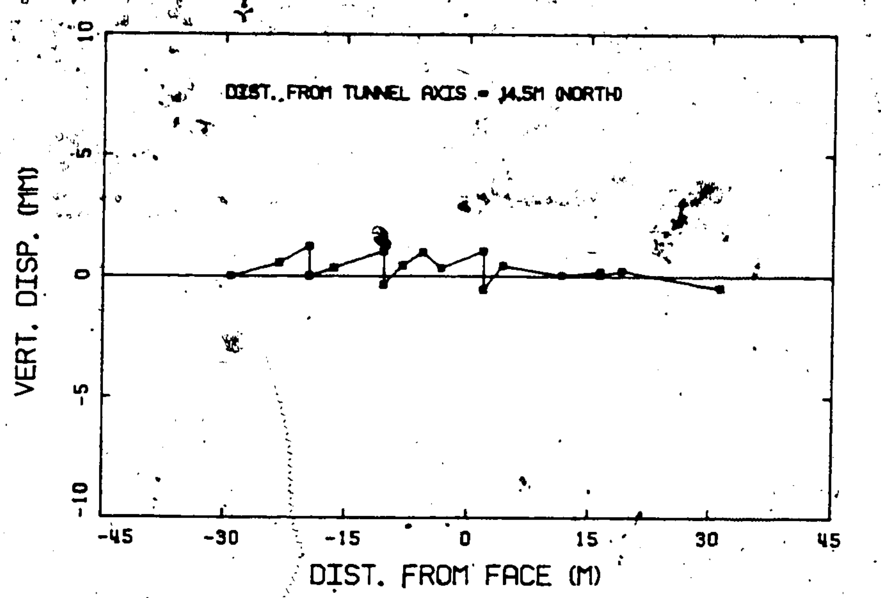

Figure 3.15 SETTLEMENT POINT SP15

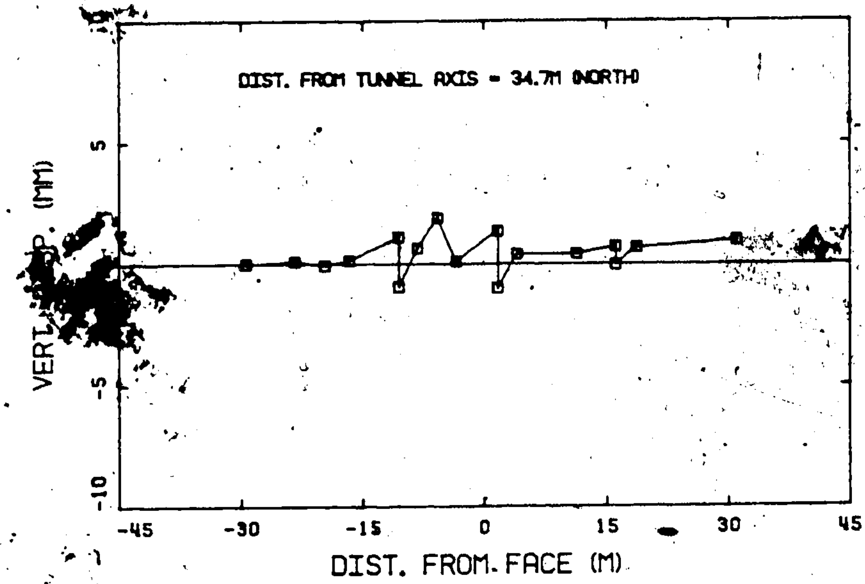

Figure 3.16 SETTLEMENT POINT SP16

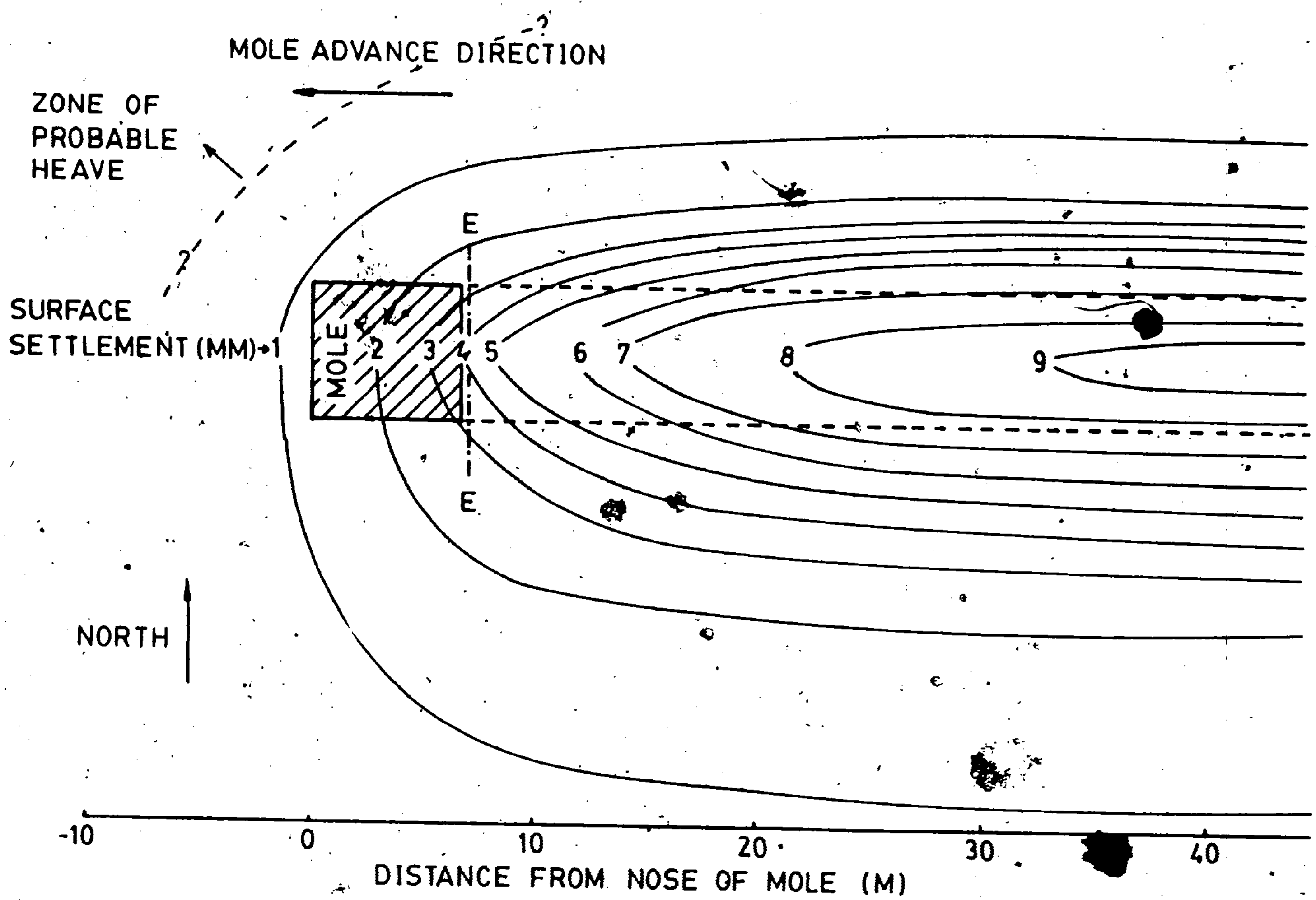

Figure 3.17 SETTLEMENT TROUGH — CONTOUR LINES

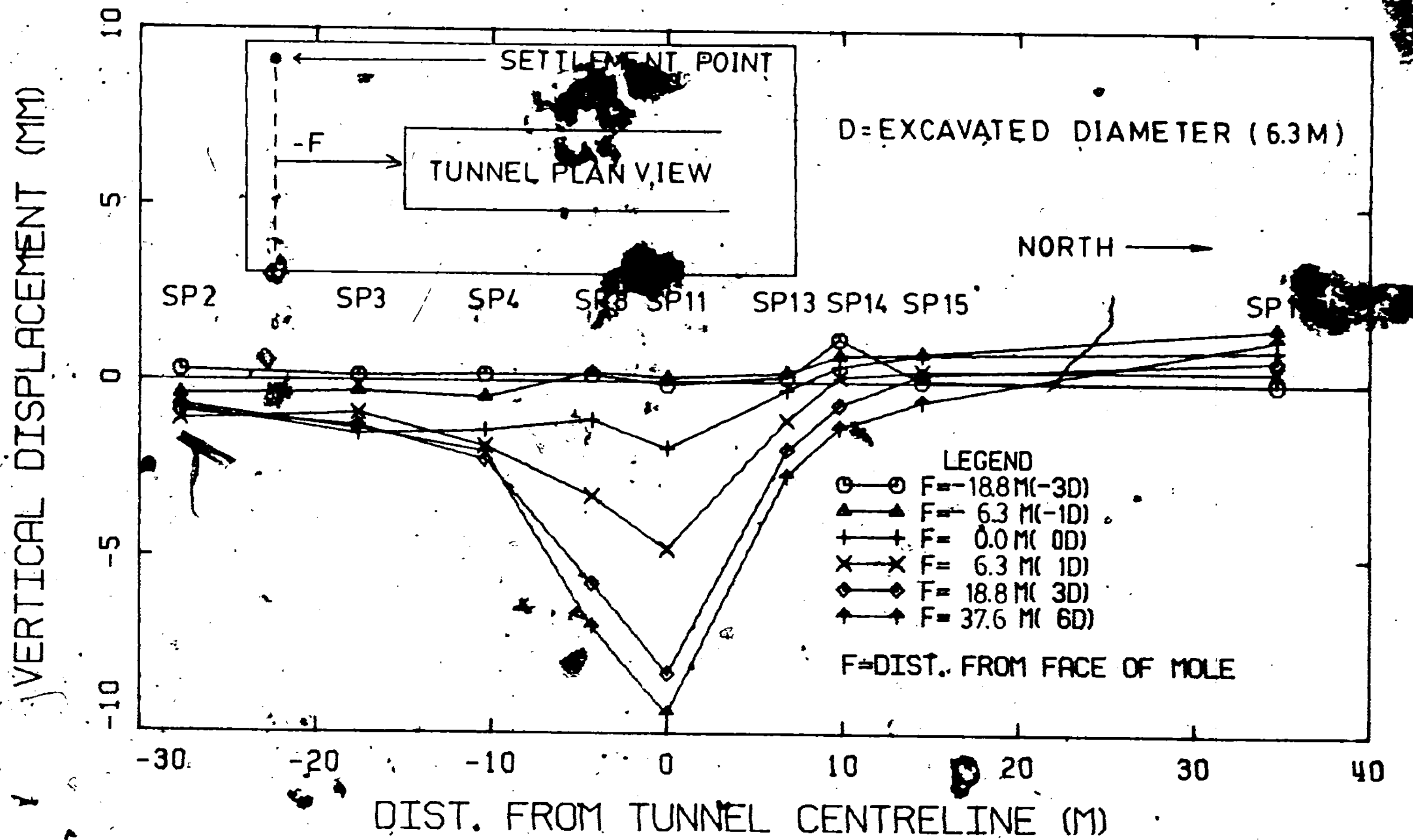

Figure 3.18 SURFACE SETTLEMENT TROUGH - TRANSVERSE SECTIONS

3.3.2.3 Magnetic Multipoint-Extensometer

Three magnetic multipoint extensometers (ME) were initially installed to measure vertical displacements at several depths. Their location and the magnets positions are shown in Figures 3.1 and 3.2. They were installed on the south side of the north tunnel to measure ground deformations in locations not affected by the building to the north of the tunnel.

Another multipoint extensometer (ME17) was later installed further west, at the tunnel centreline due to reasons explained later in this section.

Multipoint Extensometer design details

The successful use of the magnetic multipoint extensometer in Edmonton was reported by El-Nahhas (1980).

The magnetic extensometer (ME) is a probe type extensometer basically composed of four components:

1. anchor points (magnet points)
2. guide casing(access tube)
3. probe (reed switch)
4. buzzer or light indicator

The anchor points (Plate 3.1) have a ring of magnets in the lower end and move with the material (soil or rock) they are embedded in, independent of other assemblies and the probe guide pipe (Figure 3.19). The guide pipe, a flush jointed pvc pipe, enables the reed switch probe to be lowered through each of the magnet ring assemblies. As the probe reaches the magnet field the reed switch, carried by

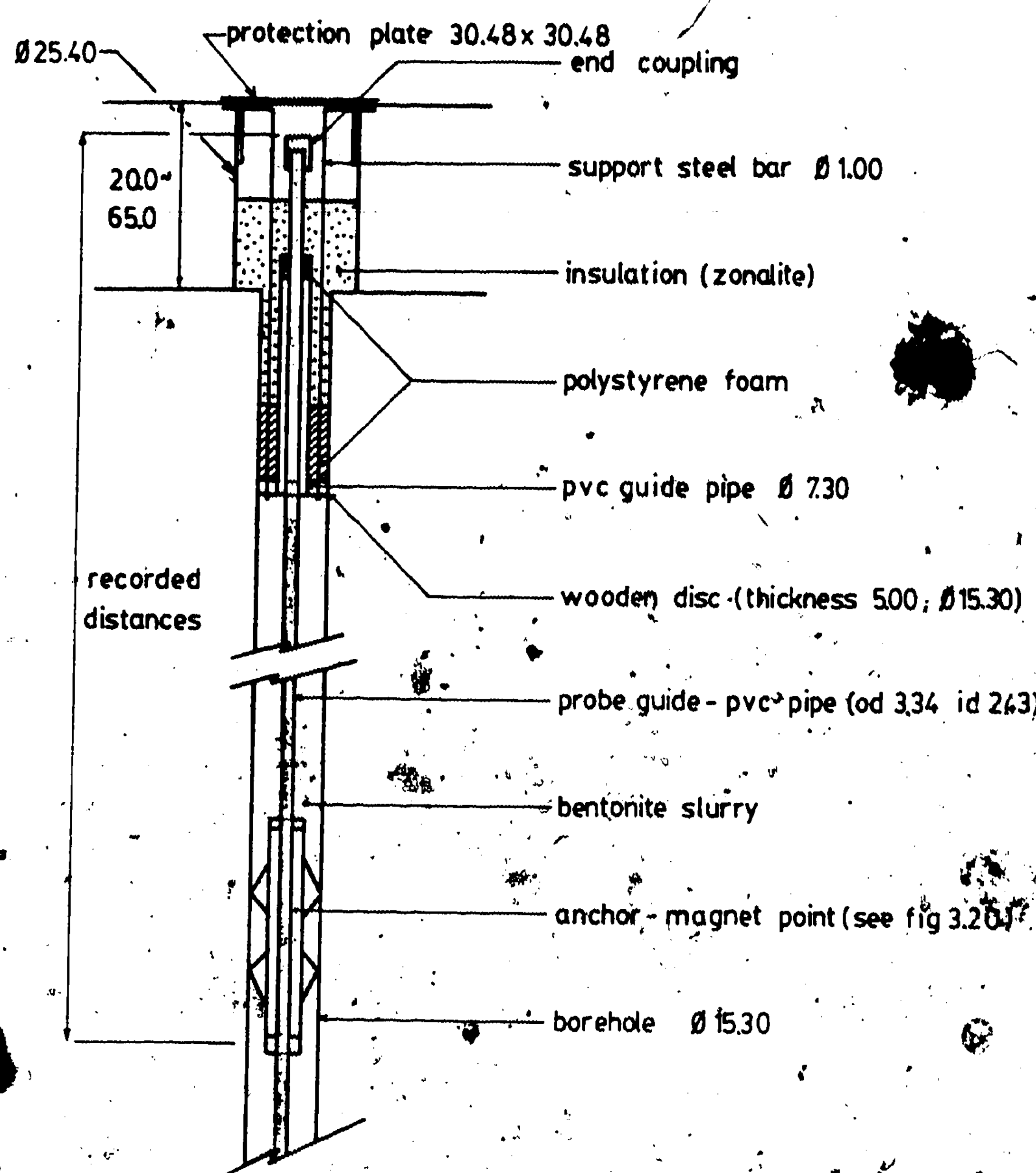

Figure 3.19 MAGNETIC MULTIPOINT EXTENSOMETER - DESIGN DETAILS

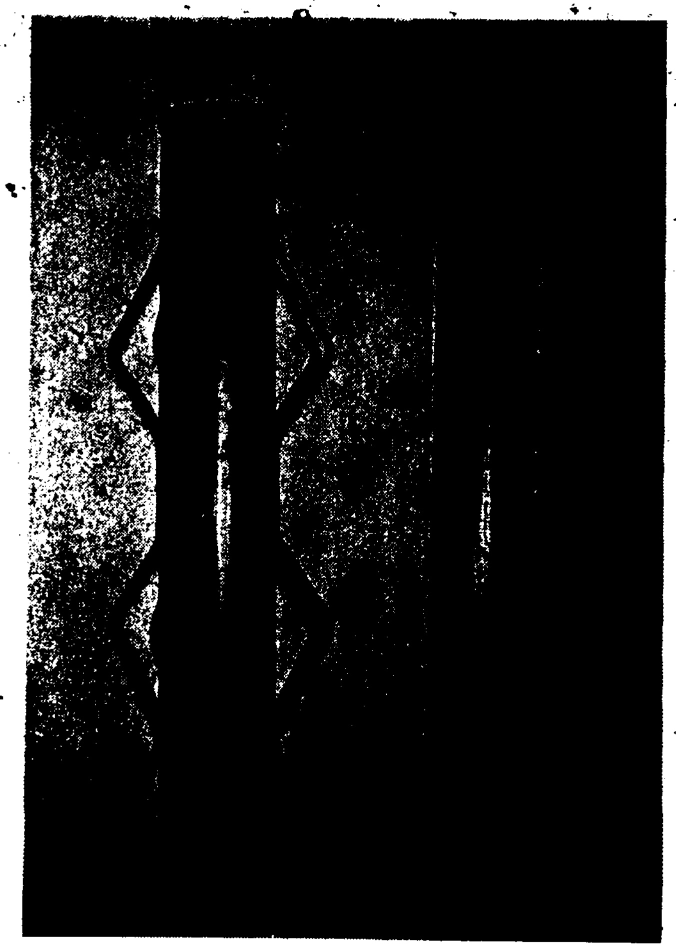

Plate 3.1 MULTIPOINT EXTENSOMETER ANCHOR POINT

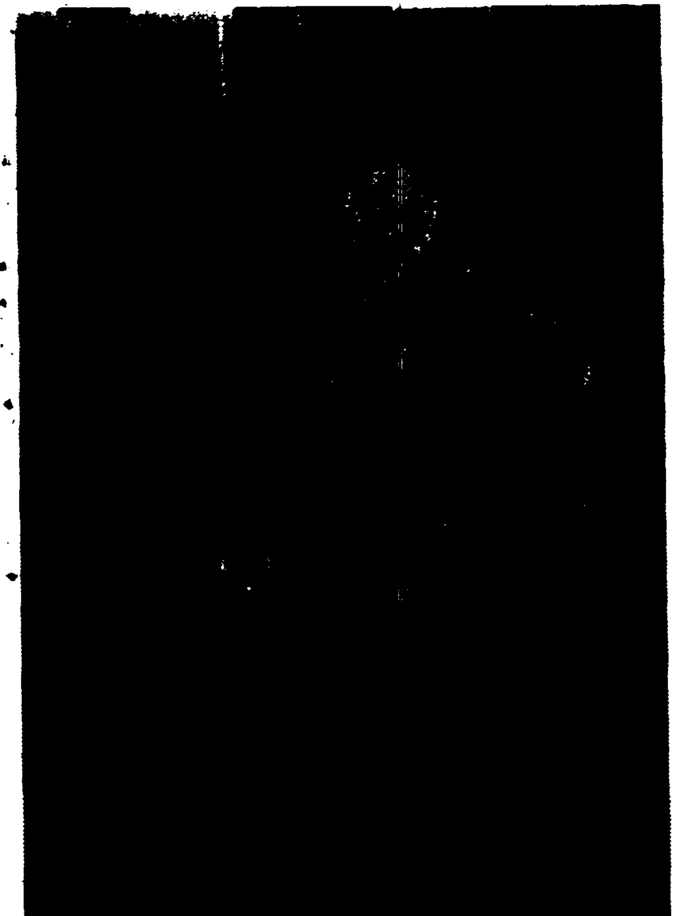

Plate 3.2 MULTIPOINT EXTENSOMETER INSTALLATION

the probe, closes and activates a buzzer or a light at surface. With a tape measure attached to the probe, the location of the magnet ring assemblies can be determined.

The anchor points are fixed to the borehole walls with four steel springs equally spaced around its perimeter (Figure 3.20).

The magnet rings, carried by the anchor points are composed of 14 ceramic magnets inserted between split steel washers (Figure 3.21). These washers concentrate and better define the magnetic fields of the magnet rings. Figure 3.22 illustrates the magnetic fields set up by the magnet rings. The buzzer (or light) is activated when the reed switch passes through any of the 3 magnetic fields. The absence of any of these fields indicates that at least two of the ceramic magnets were placed upside down (El-Nahhas, 1980). Ryzwk (1977) reported that the magnetic field is not altered with changes in temperature, with time, with mechanical action or when placed in any liquid short of a strong acidic solution.

The reed switch that sensed the magnetic field is encased in silicone and is carried inside a torpedo shaped weight, made of non-magnetic material (brass) and is heavy enough to ensure that the tape measure attached to it is kept taut during measurements.

Multipoint Extensometer Installation

Figure 3.23 illustrates the multipoint extensometer installation procedure.

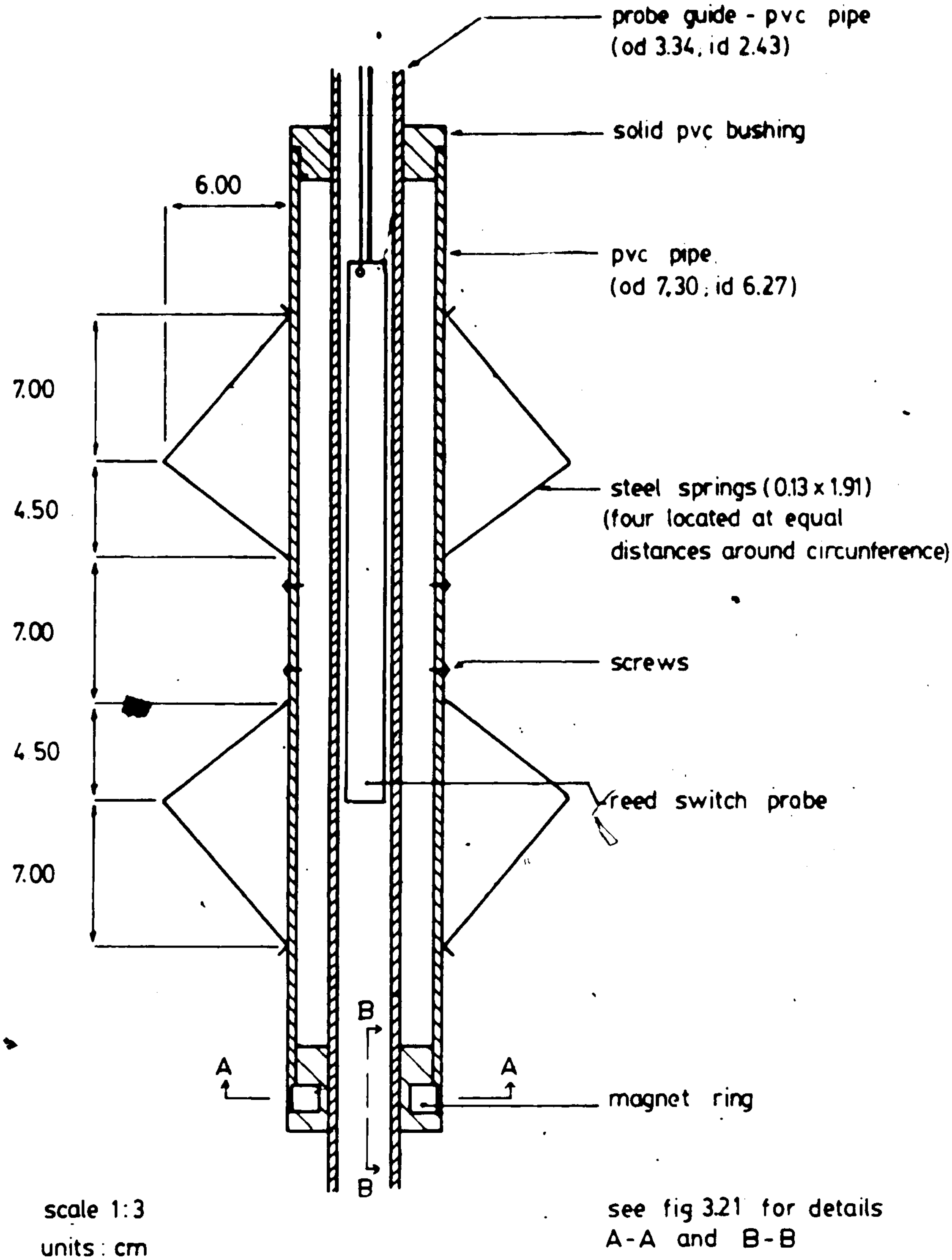

Figure 3.20 MAGNETIC MULTIPOINT EXTENSOMETER - ANCHOR POINT

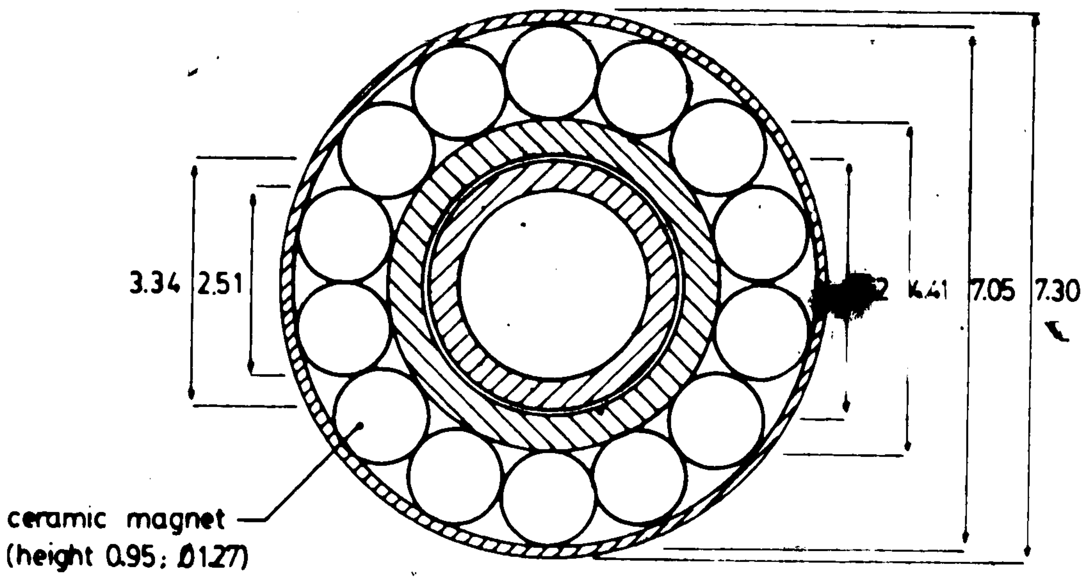

section A - A (fig 3.20)

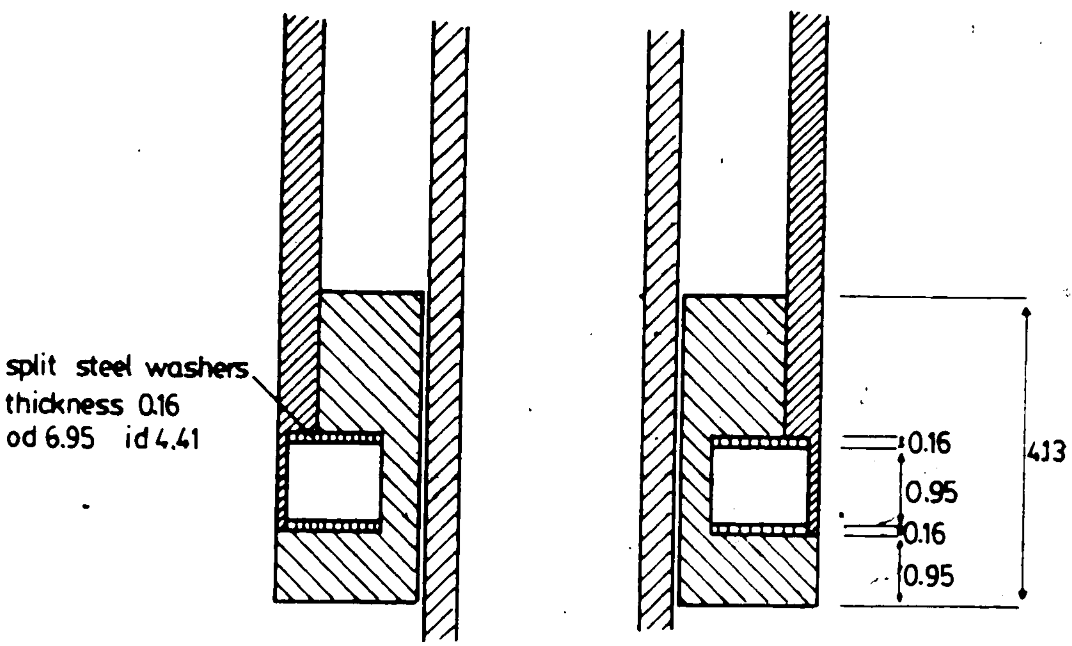

scale 1 : 1

section B - B (fig 3.20) units : cm

Figure 3.21 MAGNETIC MULTIPOINT EXTENSOMETER - MAGNETIC RING DETAIL

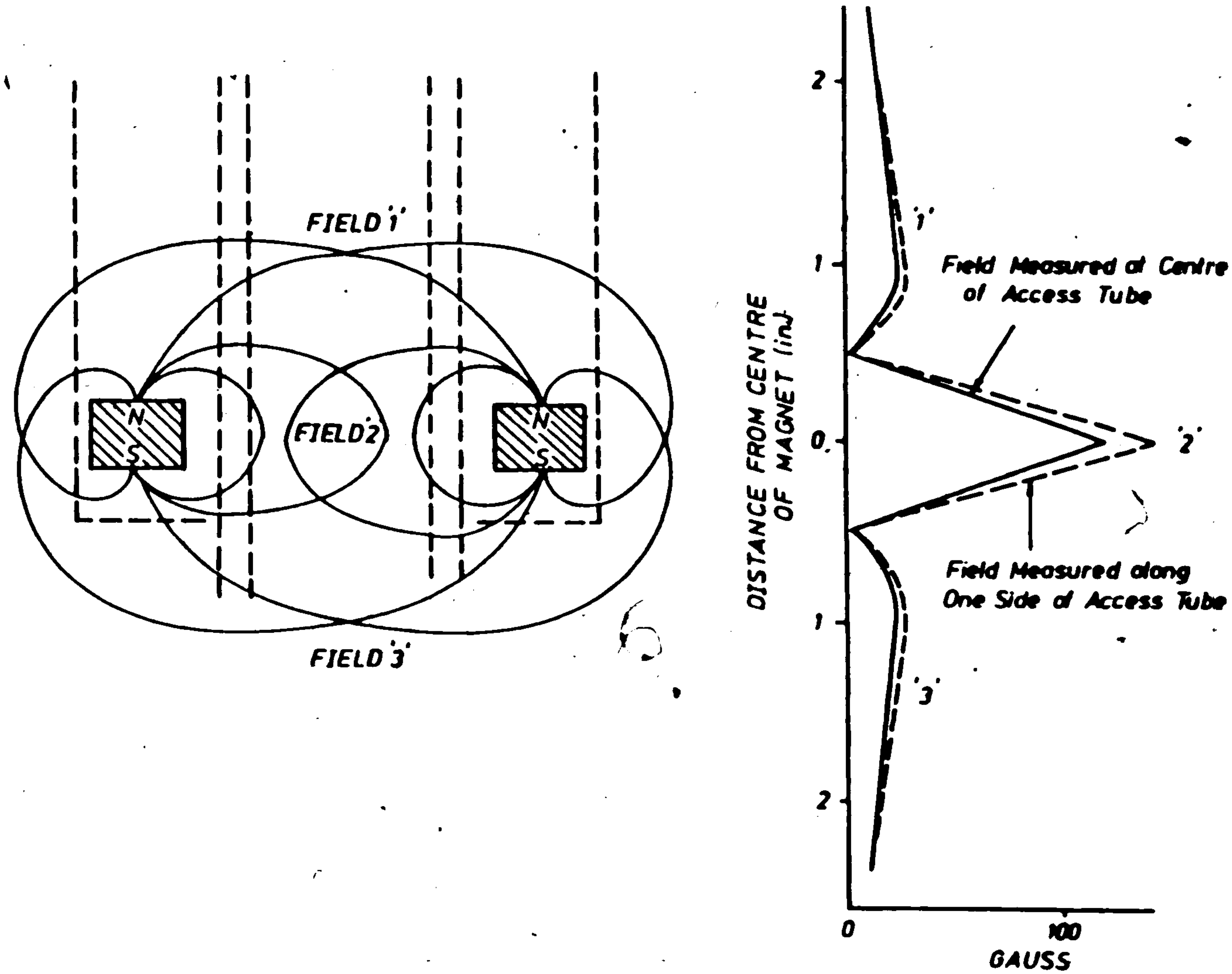

Figure 3.22 MAGNETIC FIELDS AROUND THE RING (AFTER EL-NAHHAS, 1980)

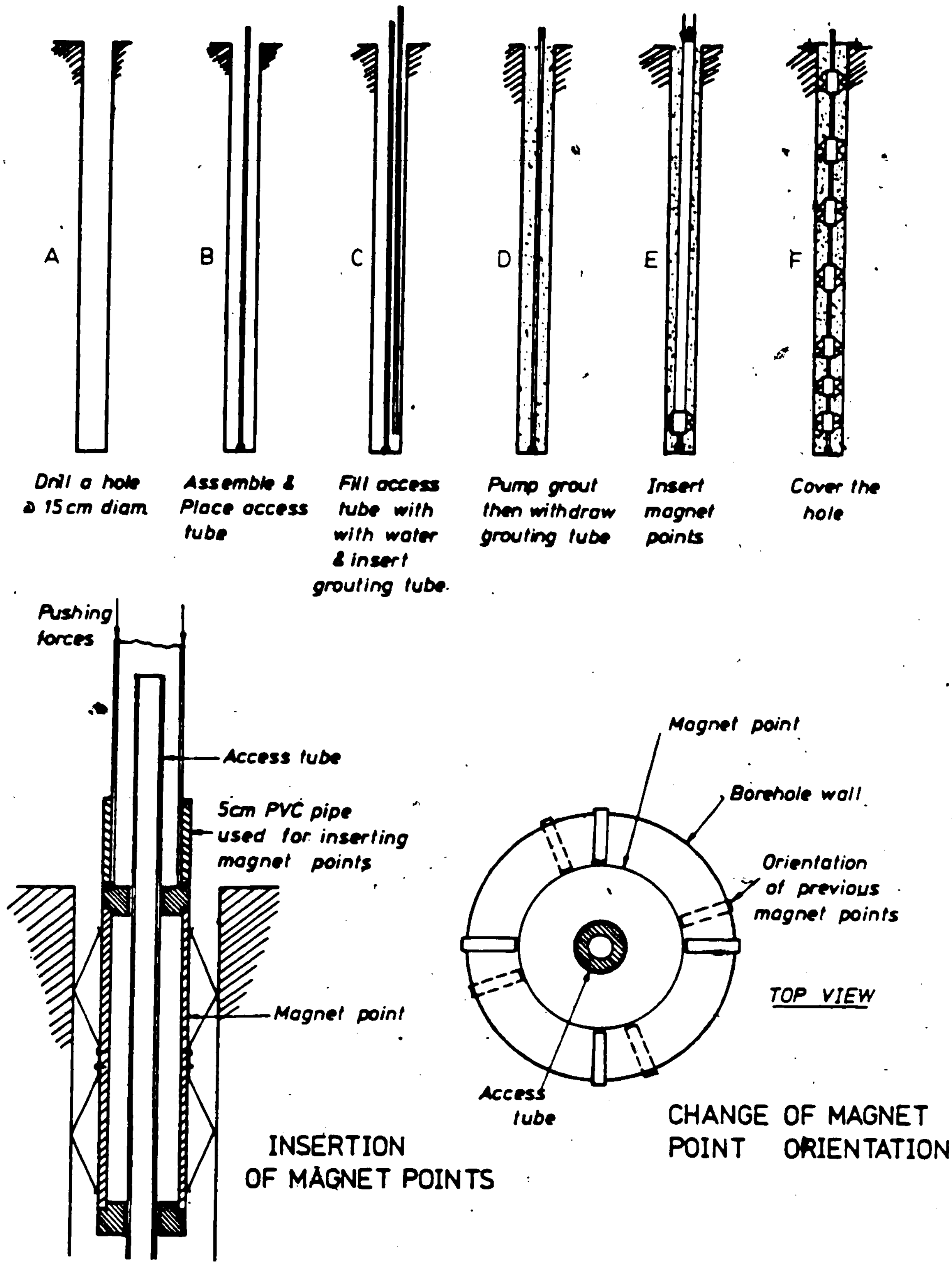

Figure 3.23 INSTALLATION OF MULTIPOINT EXTENSOMETERS (AFTER EL-NAHHAS, 1980)

For the three multipoint extensometers installations, ME5, ME9 and ME10, 15.2cm diameter boreholes, 20 metres deep, were drilled. The continuous flight solid auger was withdrawn and the boreholes were filled with bentonite grout before or after the insertion of the access tubes (Fig 3.23). The joints of the access tubes (guide pipe) were cemented with water tight fast setting adhesive and sealed at the bottom with an end cap so no material would get into it. The bentonite grout, a mixture of 36kg of bentonite and 0.3m³ of water, used to fill the borehole was thick in order to prevent sloughing of the borehole walls.

Once the access pipe was in place and the borehole filled with bentonite grout the magnet assemblies (magnetic points) were individually pushed down the hole to the required depth with the help of a 5cm diameter pvc pipe (Plate 3.2).

After inserting the first magnetic point in ME9 it was realized that the steel springs were not wide enough to provide good anchorage. The diameter of the steel springs were increased the insertion of 2cm thick pieces of wood between the body of the magnetic points and the steel springs. After this modification, the magnetic points anchored tight in the borehole walls.

During the installation, most of the magnetic points had to be hammered down to force them through very tight portions of the borehole. When these tight portions were found to be close to the planned depth of installation the magnets were left there, hence a good anchorage was ensured. The orientation of the steel springs of each magnet was changed in cases where the installation of the previous magnetic points in the same vertical resulted in a considerable increase in the borehole diameter (Fig 3.23)

For the multipoint extensometers, a special protection system was installed at the surface in order to protect the borehole from low temperatures and damage (Fig 3.19).

ME17 was installed at the tunnel centreline at Sta.200 + 133.5, west of the Instrumented Section, because ME10 had been damaged by the mole, no readings were taken in extensometer ME10. Extensometer ME17 was drilled to a depth approximately 1 metre above the tunnel crown to avoid damage.

The details of installation of the multipoint extensometers are depicted in Table 3.3.

Multipoint Extensometers Measurement Procedure

Readings of the multipoint extensometers are taken in two separate stages:

1. Levelling to the top of the access pipe to establish its elevation
2. Measurement of the depth of the magnetic points related to the top of the access pipe.

To improve the levelling accuracy, a special pvc cap, with a cone shaped depression machined in the middle, was installed on the top of the access pipe. The levelling of the access pipe was run simultaneously with the levelling of

ME	NO. OF MAGNETS	LOCATION	LOCATION FROM ℄ (m)	DATE OF INST.	DATE THE MOLE PASSED BY	MAGNETS DEPTH OF INSTALLATION (m)									
						MP1	MP2	MP3	MP4	MP5	MP6	MP7	MP8	MP9	MP10
5	9	ST200 +44.6	10.4	17-10-80	10-02-81	2.35	4.88	6.86	8.12	10.86	12.91	14.85	16.77	18.08	-
9	10	ST200 +43.4	4.3	16-10-80	10-02-81	1.44	2.93	4.89	7.01	8.93	11.16	12.89	15.61	16.92	18.37
10	8	ST200 +48.7	0	19-10-80	11-02-81	2.53	4.58	6.38	8.40	10.22	12.28	14.29	16.25	-	- -
17	5	ST200 +133.5	0	03-03-81	10-03-81	3.01	4.20	5.24	6.69	7.59	-	- -	-	-	-

TABLE 3.3 - DETAILS OF MULTIPOINT EXTENSOMETERS

the settlement points and slope indicators. Details of the levelling are described in Section 3.3.2.2.

The depth of each magnet point was measured with a tape measure connected to the reed switch probe. The probe was lowered into the access pipe and the depth of the upper and lower limits of the magnetic field 2 (Fig 3.22) of each magnetic point recorded in the field sheet presented in Figure 3.24. The difference between the depths of the upper and lower limits of the magnetic field 2 should be approximately constant for all magnetic points. This constancy in the difference between limits of the magnetic field 2 was used as a check of the quality of the readings.

Multipoint Extensometer Field Data

The data collected in the field was reduced by a computer program written by El-Nahhas (1980) and modified by the author.

Four sets of readings were taken for ME5, ME9 and ME10 before the beginning of the tunnel excavation. These readings were taken on November 16 and 29, December 14 and 22, 1980. The analysis of the data collected on these days allowed the verification of the repeatability of readings. The repeatability of the measurements of elevation of the top of the access tube was 1mm and the repeatability of the magnet points depth measurements was 0.5mm for the shallower magnets (less than 7 metres deep) and 1.5mm for the deeper ones. However the repeatability of readings in ME17 was 3mm which is worse than those mentioned above. ME17 was

MULTIPOINT EXTENSOMETER

FIELD SHEET

PROJECT : LRT TUNNEL

DATE :

READ BY RECORDED BY:

GENERAL COMMENTS :

MAGNET NO.	M.E. # HOLE : TIME : TO TEMPERATURE :				M.E. # HOLE TIME : TO TEMPERATURE				ME # HOLE TIME : TO TEMPERATURE			
	READINGS		CENTRE	✓	READINGS		CENTRE	✓	READINGS		CENTRE	✓
	TOP	BOTTOM			TOP	BOTTOM			TOP	BOTTOM		
1												
2												
3												
4												
5												
6												
7												
8												
9												
10												
	SURVEYING CORREC : (cm)				SURVEYING CORREC : (cm)				SURVEYING CORREC (cm)			

Figure 3.24 MULTIPOINT EXTENSOMETER FIELD SHEET

installed at approximately 80 metres from bench mark BM1 resulting in a poorer repeatability in the measurement of the elevation of the top of the access tube.

Chatterji et al. (1979) reported reproducibility of magnetic extensometer readings varying between 2mm and 10mm. El-Nahhas (1980) reported an accuracy of 1mm for magnetic multipoint extensometers installed in Edmonton.

The major source of errors in the magnetic point depth measurements is the presence of two components attached to the reed switch probe namely, the tape measure and the lead connected to the buzzer or light at the surface. At greater depths these two components may get entwined yielding unrealistic depths measurements. Differences as great as 50mm in depth measurements, at depth greater than 30 meters, have been observed (Figueiredo and Negro, 1981) and ascribed to the reasons noted. Figueiredo and Negro (opt.cit.) proposed a new sensing system in which the presence of the lead connecting the sensing probe to the buzzer is eliminated. This elimination is possible by using a coupled oscillator that is activated by the reed switch and generates waves that are conducted through the steel tape measure to the surface.

The reduced data obtained from multipoint extensometers are presented in Figures 3.25 to 3.28 and in Figures B1 to B32 in the Appendix B. Figures 3.29 and 3.30 depict the transverse section of the settlement troughs at different depths.

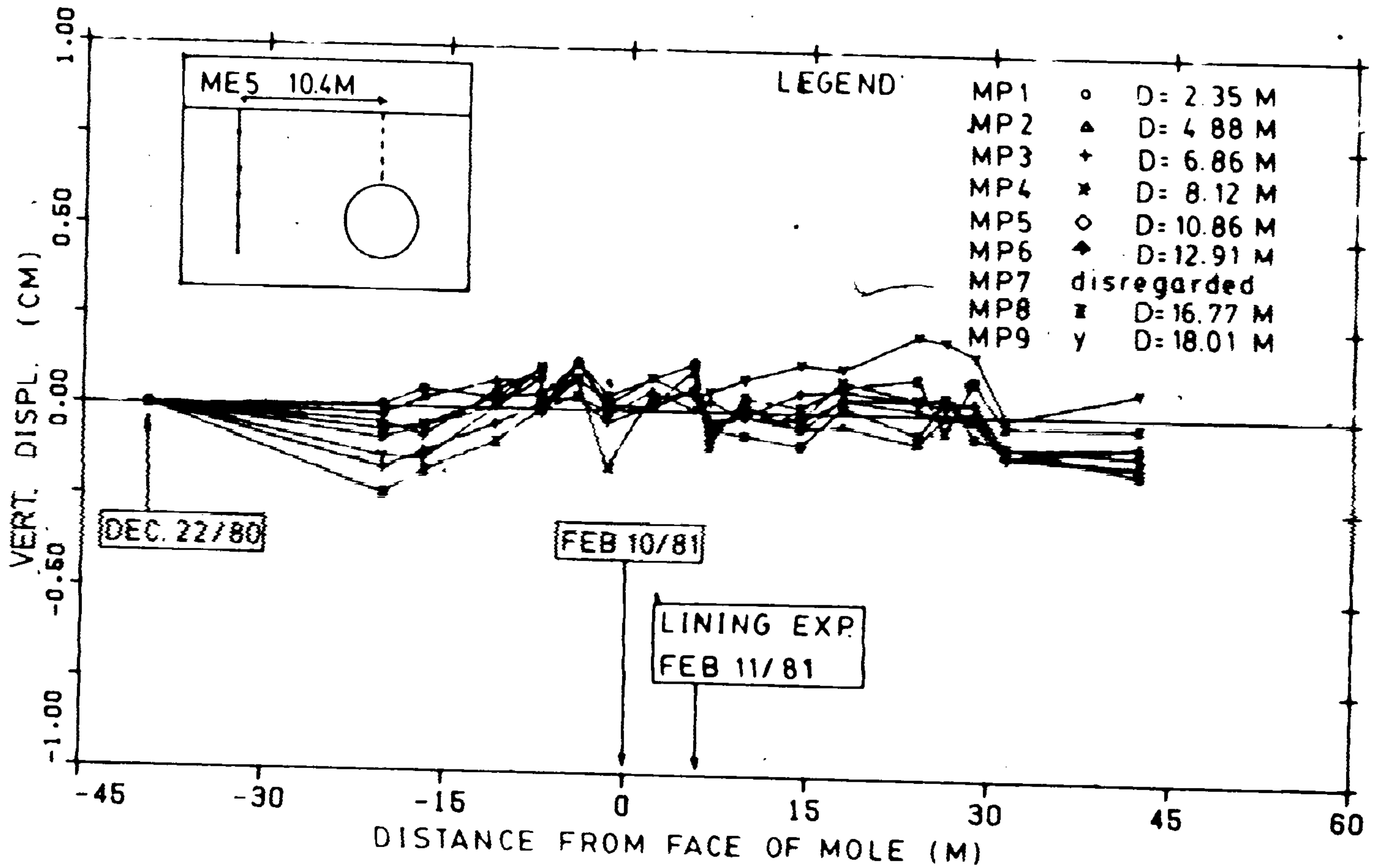

Figure 3.25 MULTIPOINT EXTENSOMETER ME5 - VERT. DISPL. X DIST. FROM FACE OF MOLE

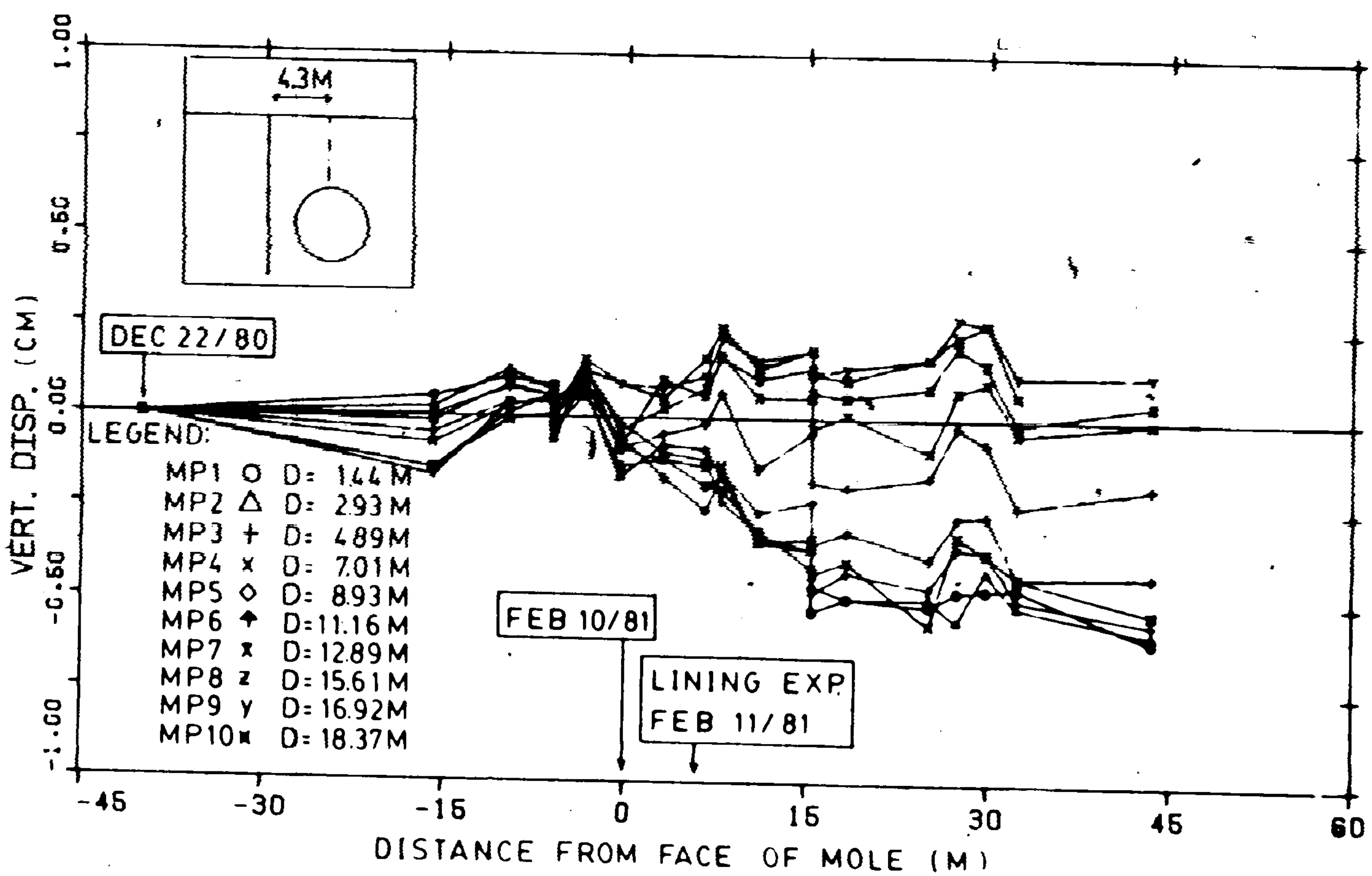

Figure 3.26. MULTIPOINT EXTENSOMETER ME9 - VERT. DISPL. X DIST. FROM FACE OF MOLE

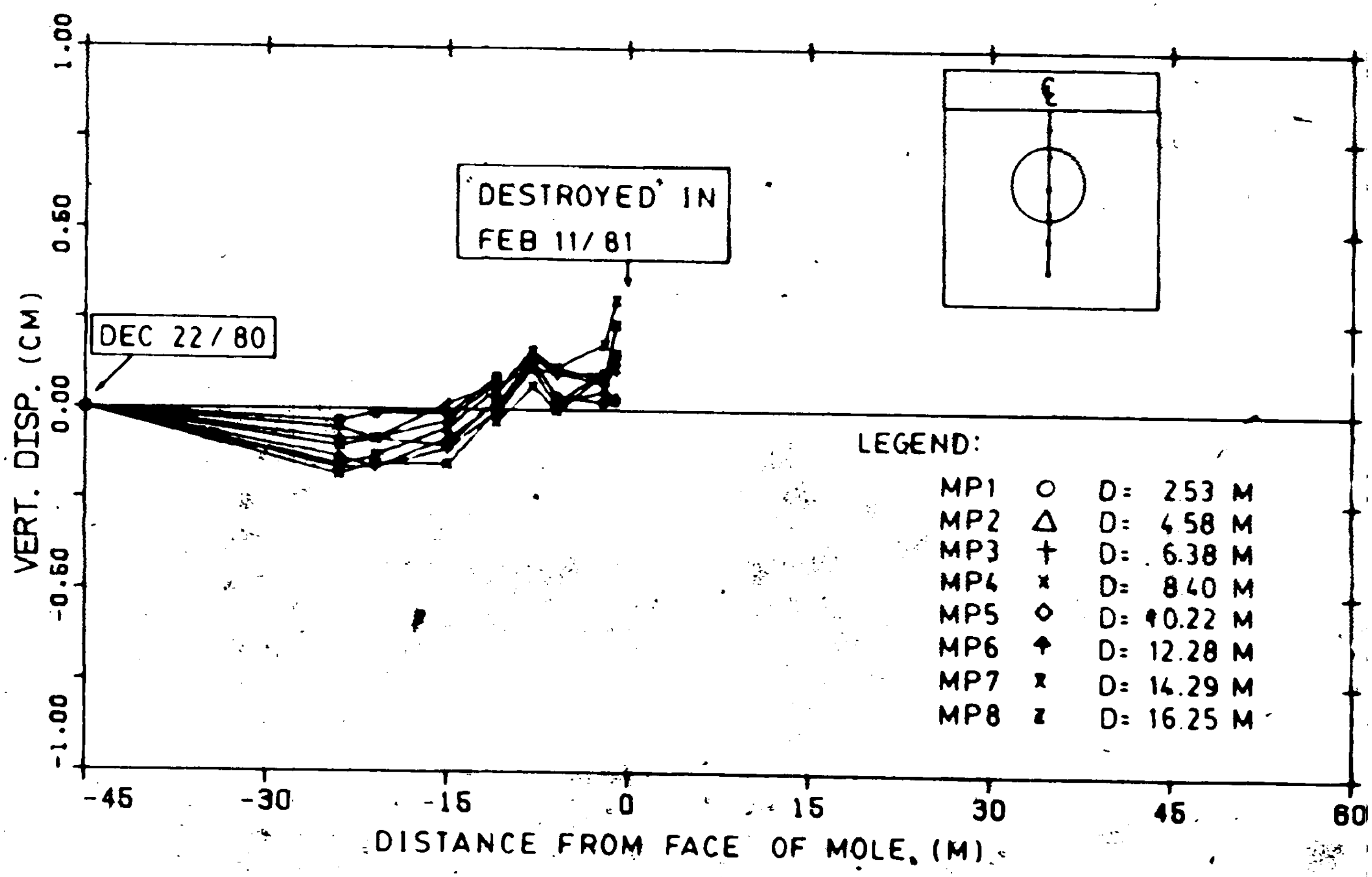

Figure 3.27 MULTIPOINT EXTENSOMETER ME10 - VERT. DISPL. X DIST. FROM FACE OF MOLE

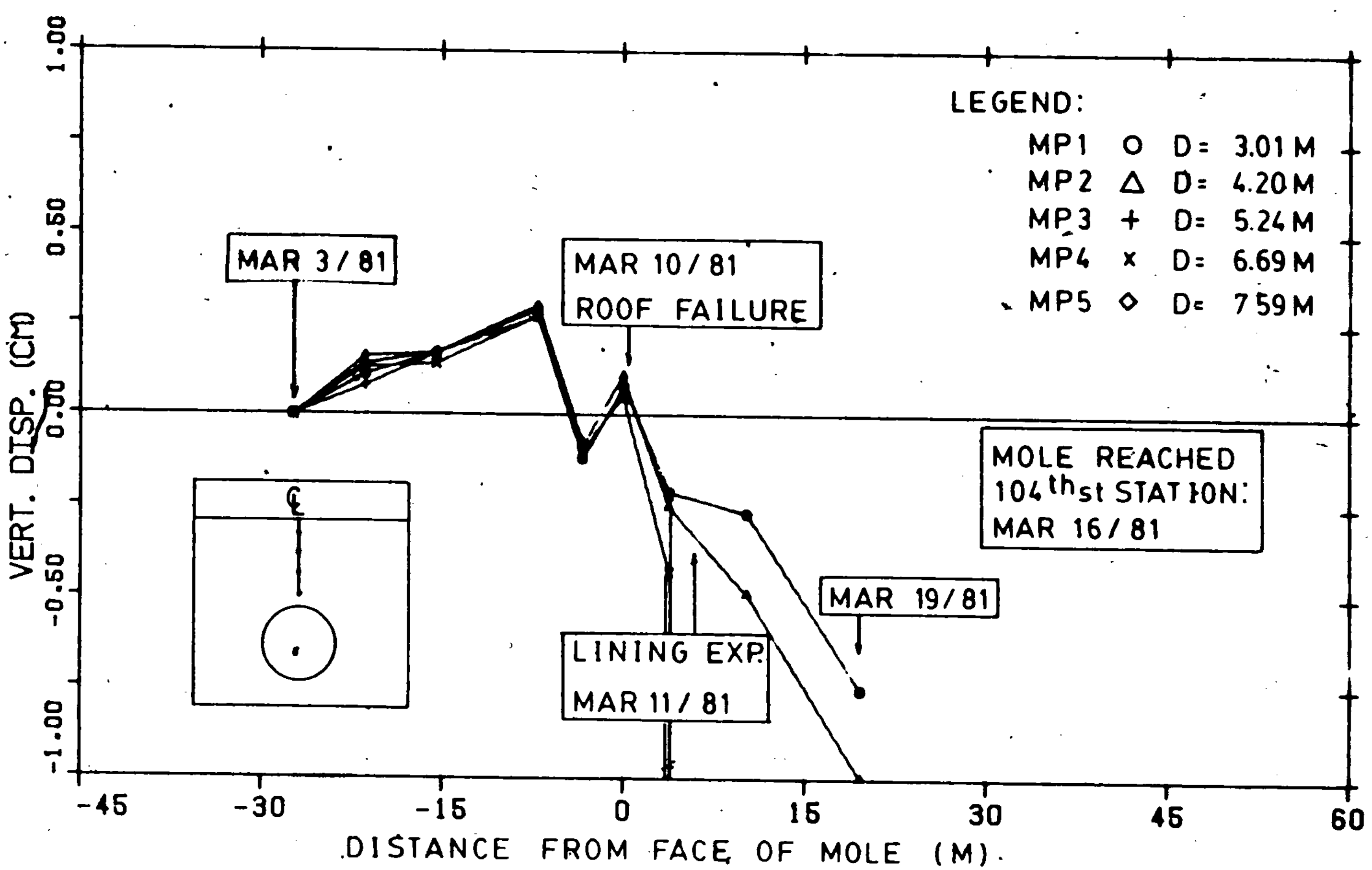

Figure 3.28 MULTIPOINT EXTENSOMETER ME17 - VERT. DISPL. X DIST. FROM FACE OF MOLE

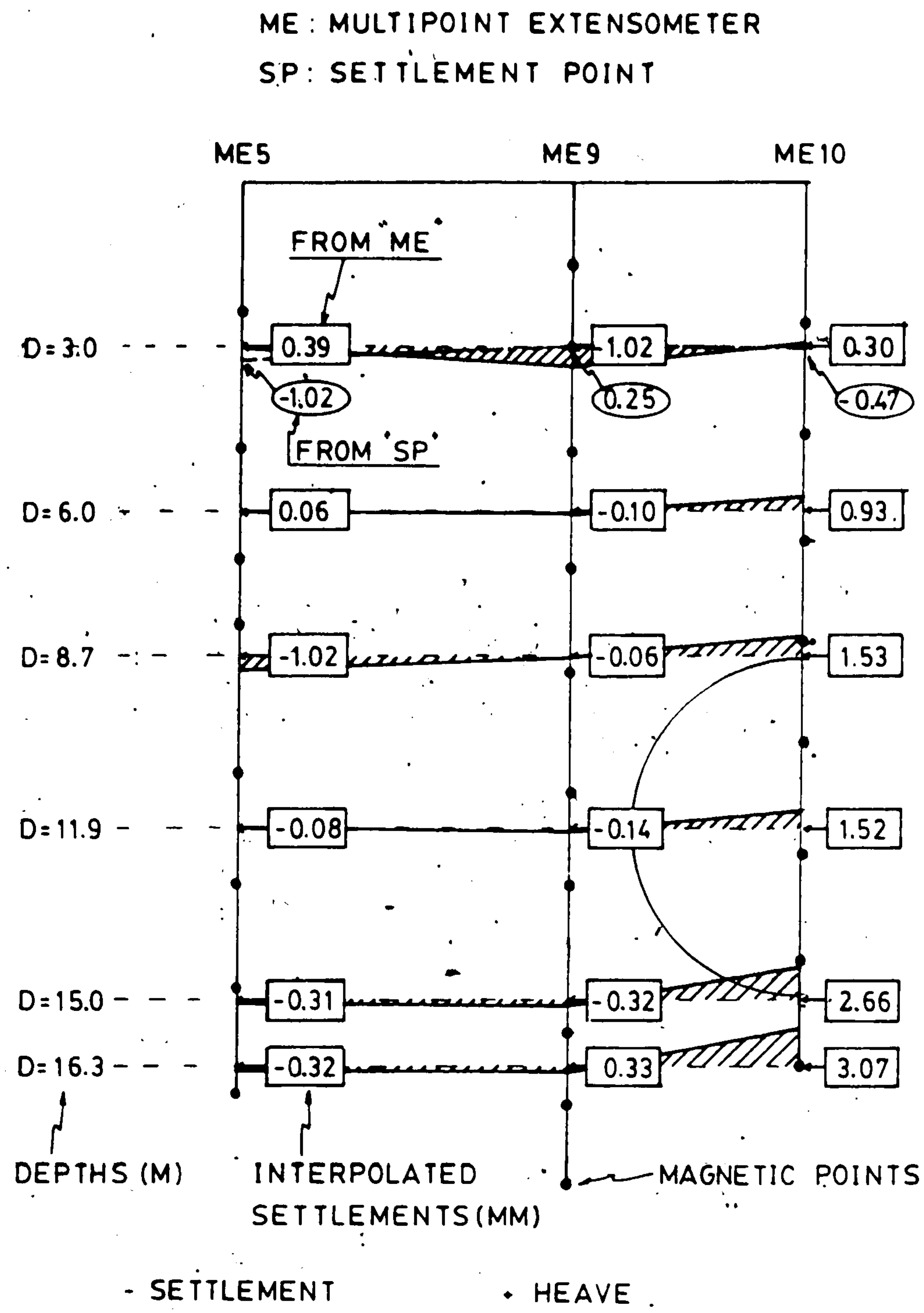

Figure 3.29 SETTLEMENT AT 1.2M AHEAD OF THE FACE OF THE MOLE

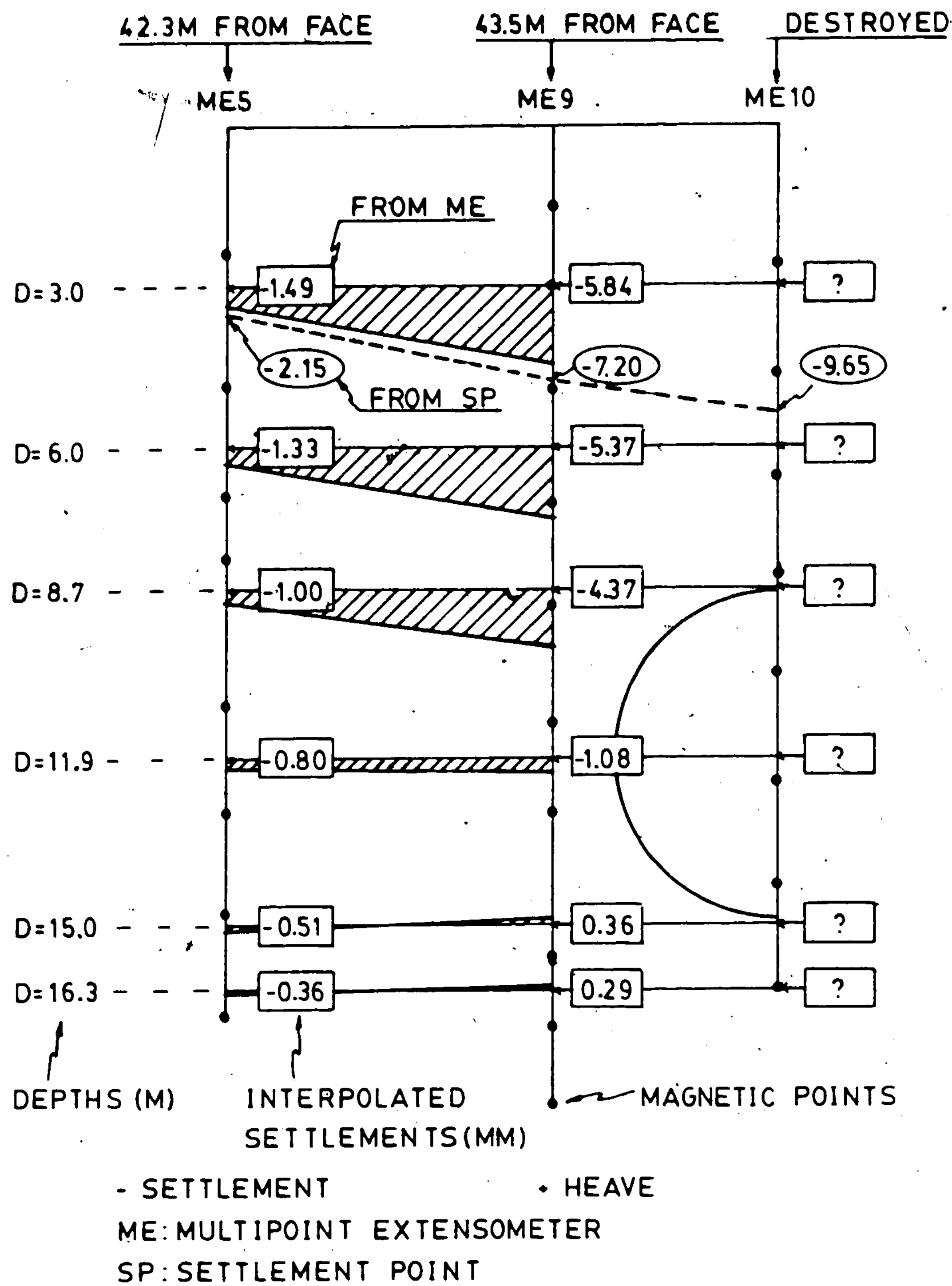

Figure 3.30 SETTLEMENT AT 43M BEHIND THE FACE OF MOLE

Comments on the data presented in this section are made in Section 3.4.2 of this thesis.

3.3.3 Horizontal Displacements

3.3.3.1 Inclinometer

Three inclinometers, or slope indicators were installed at three different distances from the tunnel axis as shown in Figures 3.1 and 3.2.

A SINCO Digitilt inclinometer, Model 50320, was used due to its adequate accuracy, precision and proven reliability (Savigny 1980).

Digitilt Inclinometer - Specification

Two servo-accelerometer sensing elements, mounted at 90° to one another, are housed in a 92.7cm long probe. This probe (torpedo) has two pairs of wheels, 61cm apart. Each pair consists of one fixed wheel and one spring-loaded wheel located in diametrically opposite directions. The torpedo is connected to the readout unit by a 0.95cm (O.D.) neoprene-coated six-strand cable. This cable has coloured neoprene markers spaced at 30.5cm intervals.

The readout device, SINCO model 50306, contains a 6 volt rechargeable battery which operates continuously for up to eight hours at room temperature and supplies voltage to the sensor elements.

ABS-plastic casings (70mm O.D.x50mm I.D.) with four longitudinal grooves equally spaced were assembled in 3 metre long sections. The casing sections were joined by special SINCO couplings, Model 57512, which do not require cement and rivets for their installation. Water tightness is provided by two "O" rings located on the inner walls of the couplings. Two nylon strings run simultaneously through grooves machined in the inside wall of the couplings and outside wall of the casing to prevent the separation of the casings due to traction. The lower end of the deepest casing section was provided with a SINCO grout shoe. This grout shoe has a check valve that enables the grounting of the borehole from within the casing.

Specifications for the inclinometer mentioned above are shown in Table 3.4.

Inclinometer Installation

The 20.3cm diameter boreholes were drilled with a hollow stem auger, to a depth of 28 metres. The 3.0 metre long casing sections were assembled and inserted in the borehole through the hollow stem (Plate 3.3). No special care was taken to position the grooves in directions perpendicular and parallel to the tunnel axis. After the whole casing was installed the auger was withdrawn and the void between the borehole walls and the casing was grouted.

The boreholes were grouted through a pipe inserted beside the inclinometer casing. The grouting started from the bottom of the boreholes and the grout pipe was slowly withdrawn to ensure that its tip was always immersed in grout. The grout shoe was not used to avoid the risk of

SENSOR: Slope Indicator Company Model 50320

Sensitivity:	± 0.0015 m per 30 m casing
Total System Accuracy:	± 0.0076 m per 30 m casing
Wheel Base:	61 cm
Overall Length:	93 cm
Outside Diameter (not including wheels):	4.3 cm
Sensors:	Two 0.5 g closed loop force-balanced servo accelerometers
Operating Range:	0° to 30° (from vertical)

CABLE: Slope Indicator Company 1.07 cm O.D., six conductor with 0.16 cm stranded-steel core; waterproof neoprene cover with external marks at 0.31 m intervals.

INDICATOR: Slope Indicator Company Model 50306

Dimensions:	14.3 x 6.0 x 22.9 cm
Weight:	2.27 kg
Internal Power:	6V, 6 Ah
Charger:	External; 6 VDC
Operating Time on Batteries:	8 hours
Digital Display:	4 digits
Recording:	Manual

CASING: Slope Indicator Company ABS Plastic Casing & Couplings

Casing Length:	3.05 m
O.D.:	7.0 cm
I.D.:	5.9 cm
Coupling Length:	0.15 m
O.D.:	7.0 cm
I.D.:	6.5 cm

Table 3.4 INCLINOMETER SPECIFICATIONS (AFTER SAVIGNY 1980)

Plate 3.3 INCLINOMETER - INSTALLATION

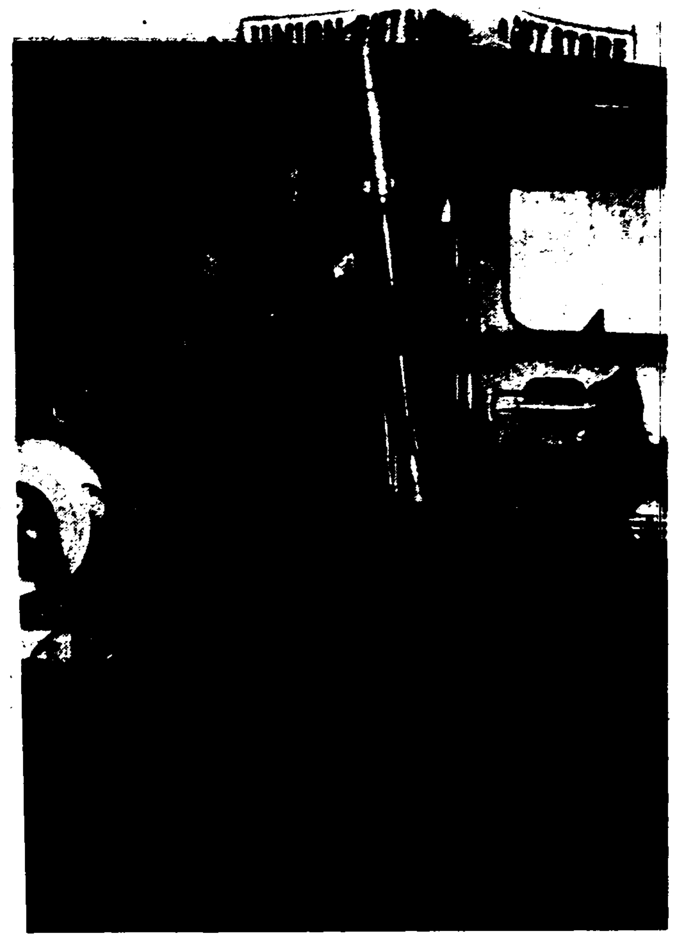

Plate 3.4 INCLINOMETER - READINGS

discharging of grout inside the casing in the case of malfunctioning of the check valve. The grout was mixed on the site with a bentonite/cement ratio equal to 0.1 and a water/cement ratio equal to 1.4 (weight ratios). These weight ratios were chosen based on local experience.

The angle between the groove directions and the tunnel axis (angular rotation θ) shown in Figure 3.31(d) was measured at the surface with the aid of a compass. The spiral distortion of the grooves along the casing (Fig 3.31(c)) with respect to the groove alignment at the surface was obtained at 1.5 metre intervals with a SINCO spiral checking device. The "SPIRAL CORRECTION" column in Table 3.5 is the average angle between the "A" groove direction and the tunnel axis, measured anticlockwise from "A" to the tunnel axis. The "A" direction is the direction defined by the four wheels of the torpedo, parallel to the tunnel axis, and the "B" direction is perpendicular to the "A" direction.

The inclinometer casings were protected at the surface with a square (25.4cm x 25.4cm) steel plate.

More details of the three inclinometers are presented in Table 3.5.

Inclinometer Measurement Procedure

No readings were taken until 30 days after the inclinometers were grouted in order to allow a complete setting of the grout.

To facilitate cable maneuvering, a 0.6 metre long casing extension was assembled to the shallower casing

INCLINO-METER	LOCATION	LOCATION FROM TUNNEL ℄ (m)	DATE OF INSTALLATION	DATE THE MOLE PASSED BY	DEPTH OF DEEPEST READING (m)	NO. OF READING POINTS	SPIRAL CORRECTION	NOTES
SI6	ST200 + 43.4	6.4	16-10-80	10-02-81	26.8	44	21.90°	
SI7	ST200 + 48.7	4.3	17-10-80	11-02-81	26.8	44	3.18°	
SI12	ST200 + 43.6	0.0	19-10-80	10-02-81	26.8	44	2.32°	(DAMAGED 10-02-81)

TABLE 3.5 - INCLINOMETERS - DETAILS OF INSTALLATION

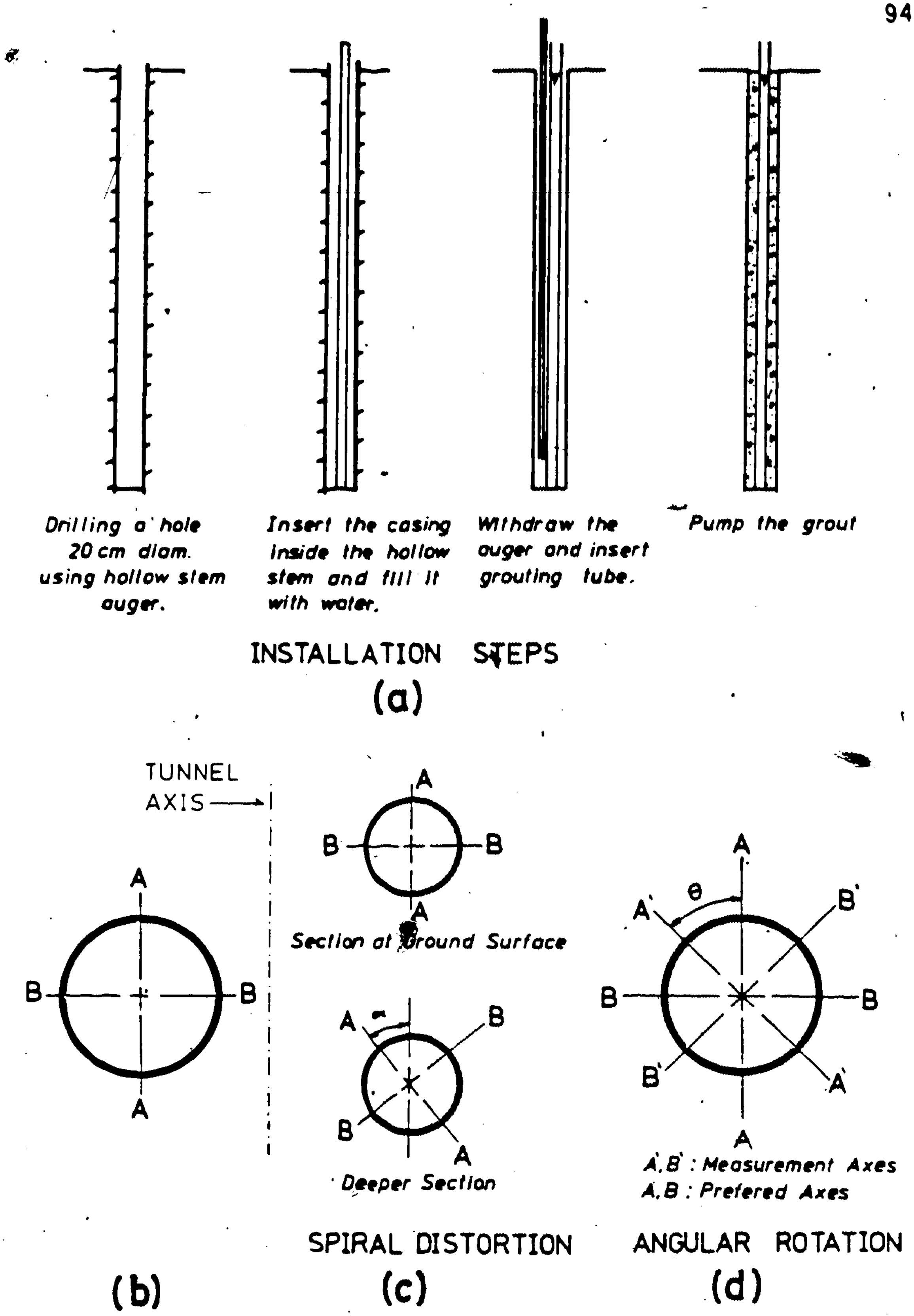

Figure 3.31 INSTALLATION OF SLOPE INDICATORS (AFTER EL-NAHHAS, 1980)

section. A removable pulley and clamp system was attached to the upper end of this casing extension and the probe inserted in the casing with the spring-loaded wheels facing west (Plate 3.4). The probe was initially lowered to a depth of 27.4 metres measured from the clamp, and left at this position for approximately 5 minutes to allow the sensors to achive temperature stabilization. The probe was then lifted and readings taken in intervals equal to the distance between the upper and lower wheels (0.6 metre). The depth of readings were chosen to ensure that during readings, the wheels were never placed on couplings. Once the probe reached the surface it was rotated 180° (spring loaded wheels facing east) and the whole procedure just described was repeated to minimize the errors due to irregularities in the casing and instrument calibration.

The readout unit remained switched on during the entire operation and was kept at temperatures above 10° Celsius.

The readings were recorded on the field sheet presented in Figure 3.32.

Inclinometer Field Data

The data obtained from the inclinometers were reduced with the help of a computer program written by Savigny (1980). The program provides plots of horizontal displacements versus depth in any two desired perpendicular directions, and produces tables with the reduced displacements and the sums of the readings taken at each depth in both, "A" and "B" directions. These values, SUM A

SLOPE INDICATOR FIELD SHEET

PROJECT : L RT TUNNEL

DATE :

SI NO :

READ BY : CABLE CONTROL :

TEMP :

TIME : SENSOR INS. : START READ END :

(+ 180°) SENSOR INS : START READ END.

DEPTH (FT)	A		B		DEPTH (FT)	A		B	
	[illegible] W	[illegible] E	[illegible] W	[illegible] E		[illegible] W	[illegible] E	[illegible] W	[illegible] E
93					33				
91					31				
89					29				
87					27				
85					25				
83					23				
81					21				
79					19				
77					17				
75					15				
73					13				
71					11				
69					9				
67					7				
65									
63									
61									
59									
57									
55									
53									
51									
49									
47									
45									
43									
41									
39									
37									
35									

Figure 3.32 SLOPE INDICATOR FIELD SHEET

and SUM B, are helpful in the verification of the input data. A statistical analysis may be carried out with the "SUM" values and a standard deviation of the "SUM" values obtained in different sets of readings might reflect a change in the degree of non-parallelism of grooves or any malfunction of the instruments.

For the three slope indicators, three zero readings were taken before the tunnel excavation began. These zero readings are presented in Figures 3.33, 3.34 and 3.35. The repeatability of the inclinometers readings can be calculated from the zero readings. The rate, defined by Gould and Dunnicliff (1971), metres of deflection per metre of depth, can be used to check the repeatability. The repeatabilities calculated to points at the springline level (11.8 metres deep) are:

INCLINOMETER	CHANNEL A	CHANNEL B
SI 6	1.19×10^{4}	1.3×10^{4}
SI 7	2.79×10^{4}	1.9×10^{4}
SI 12	2.73×10^{4}	4.5×10^{4}

The inclinometer repeatabilities are within the range of repeatabilities specified by SINCO, 5.06×10^{4} or ±7.6mm per 30 metres of casing. The Digitilt Model 50320 had been previously used by El-Nahhas (1980) and Savigny (opt.cit.). They reported repeatability of $\pm 0.67 \times 10^{4}$.

Figures 3.33 to 3.35 indicate that the three inclinometers used in the present study present erratic movements of points located close to the bottom of the

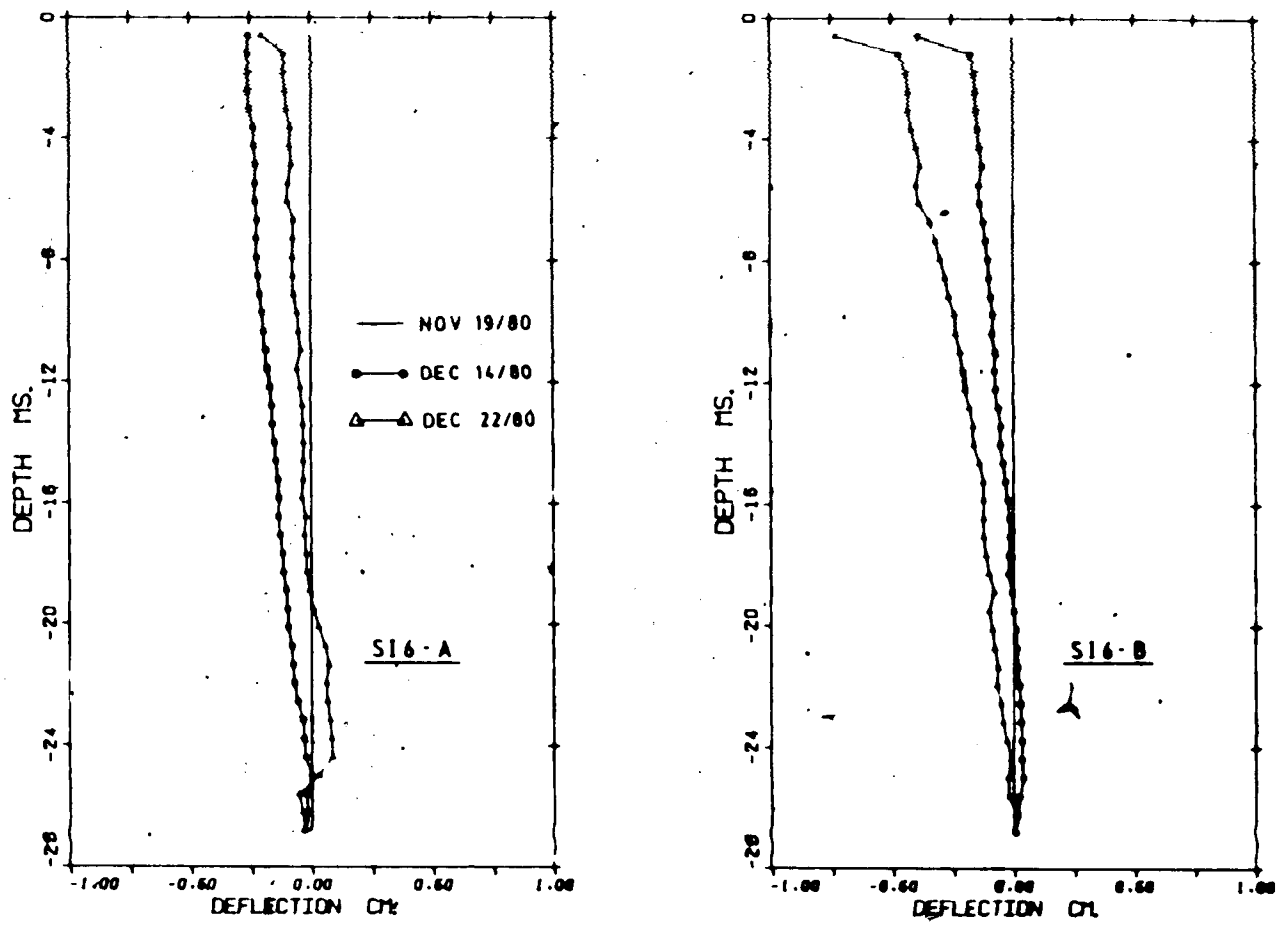

Figure 3.33 ZERO READINGS: SI6 (6.4M FROM TUNNEL AXIS)

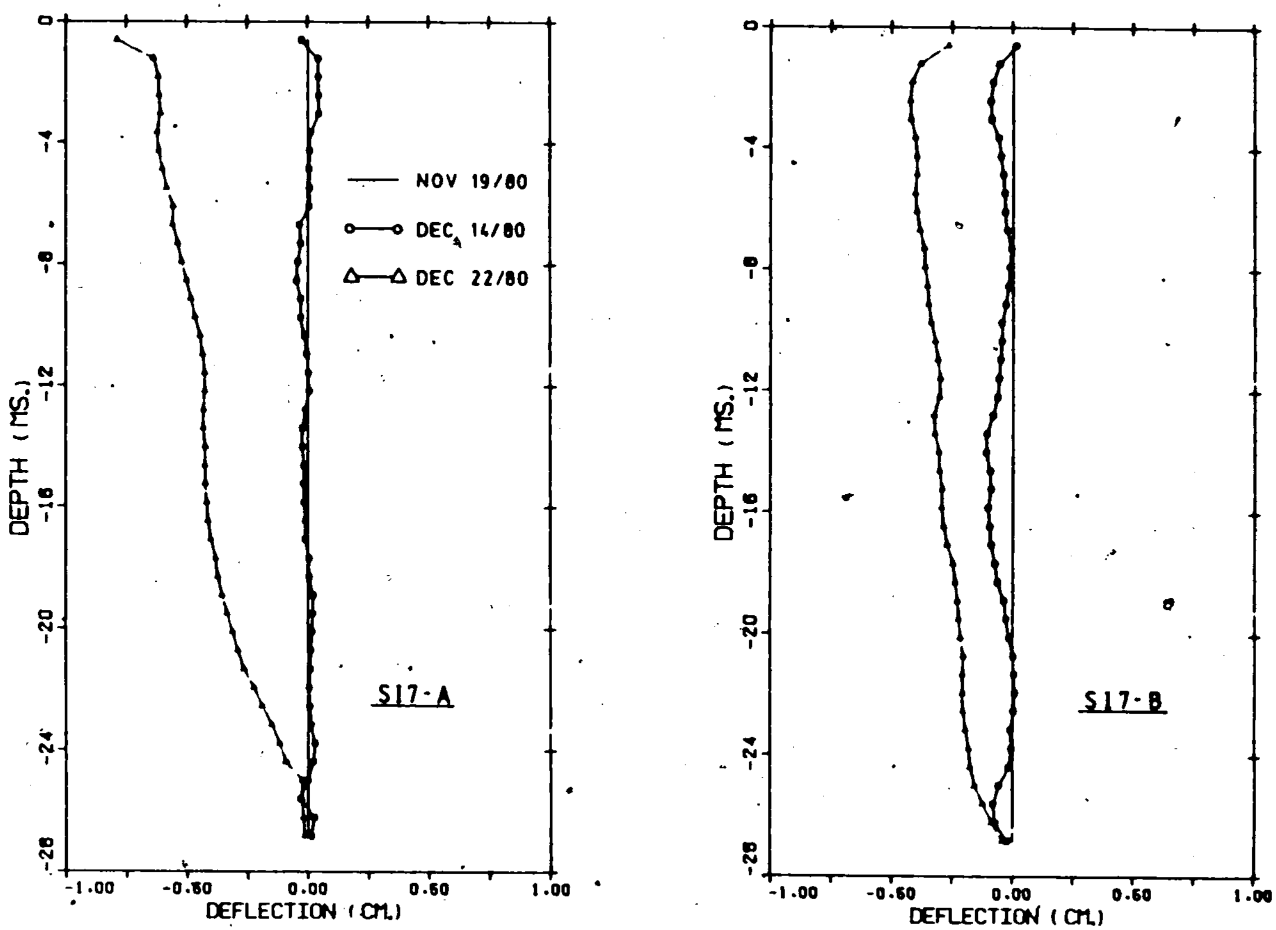

Figure 3.34 ZERO READINGS: SI7 (4.3M FROM TUNNEL AXIS)

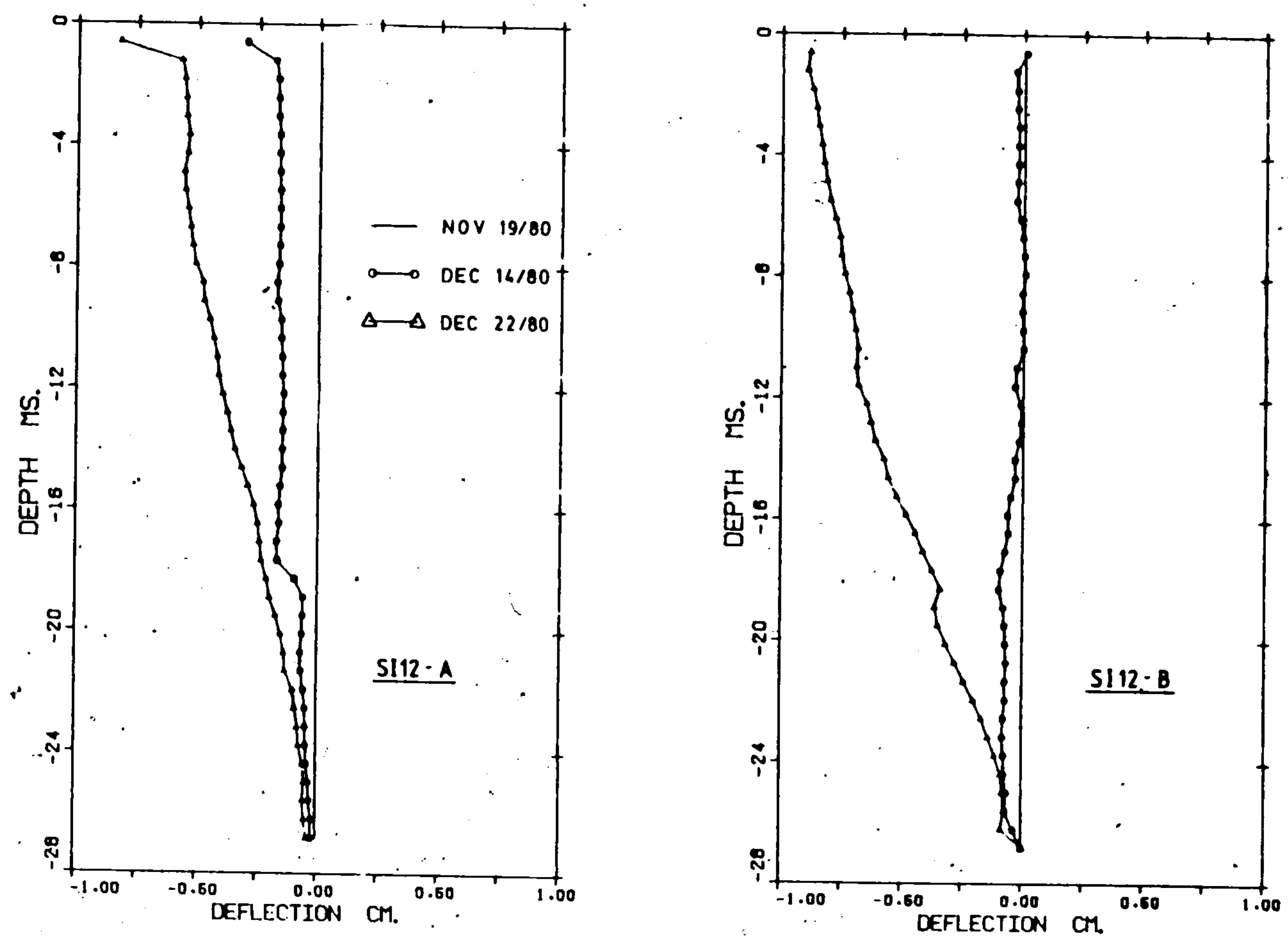

Figure 3.35 ZERO READINGS: SI12 (TUNNEL CENTRELINE)

casing which might be a major source of error. The statistical analysis carried out with the values of SUM A and SUM B, explained earlier in this section, indicated no major change in the standard deviation values, reflecting the good performance of the inclinometers throughout the monitoring period. Figures 3.36, 3.37 and 3.38 depict the position of an initially vertical line, at different phases of the tunnel construction, for SI6, SI7 and SI12, respectively, when the readings taken on December 22, 1980, are used as reference.

Figures 3.39 and 3.40 depict the horizontal displacements, perpendicular and parallel to the tunnel axis, of points located at 11.58 metres below surface (approximately at the springline level).

Tables B33 to B44 in Appendix B present the inclinometer readings and reduced data.

Comments on the inclinometers data are presented in Section 3.4.2 of this thesis.

3.4 Discussion of Soil Movements

3.4.1 Surface Vertical Displacements

The settlement point elevations obtained on November 29, December 14, 1980 and January 18, 1981 were disregarded due to erratic movements of SP11, used as a "turning point" between the second and third set-ups (Section 3.3.2.2 -

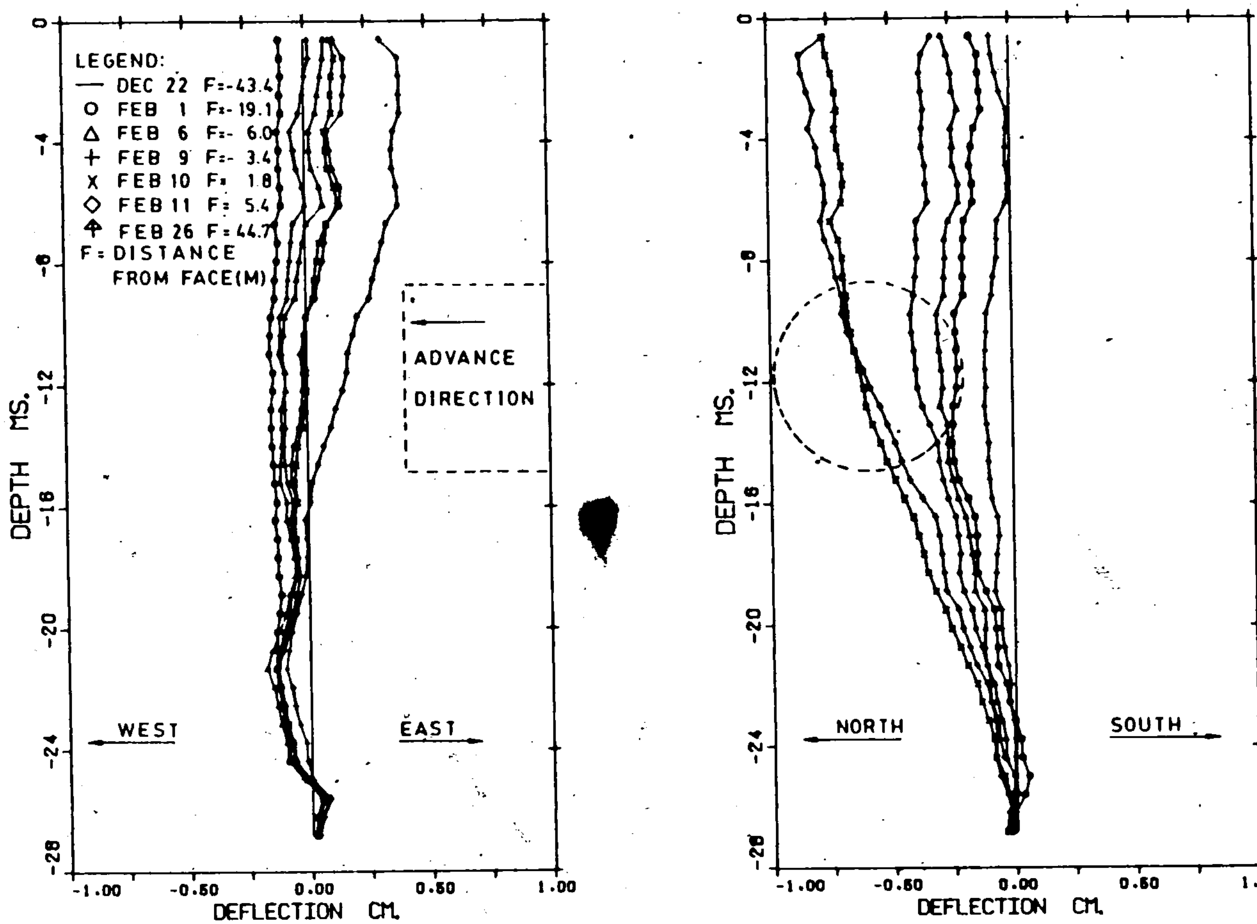

Figure 3.36 SLOPE INDICATOR SI6 (6.4M FROM TUNNEL AXIS)

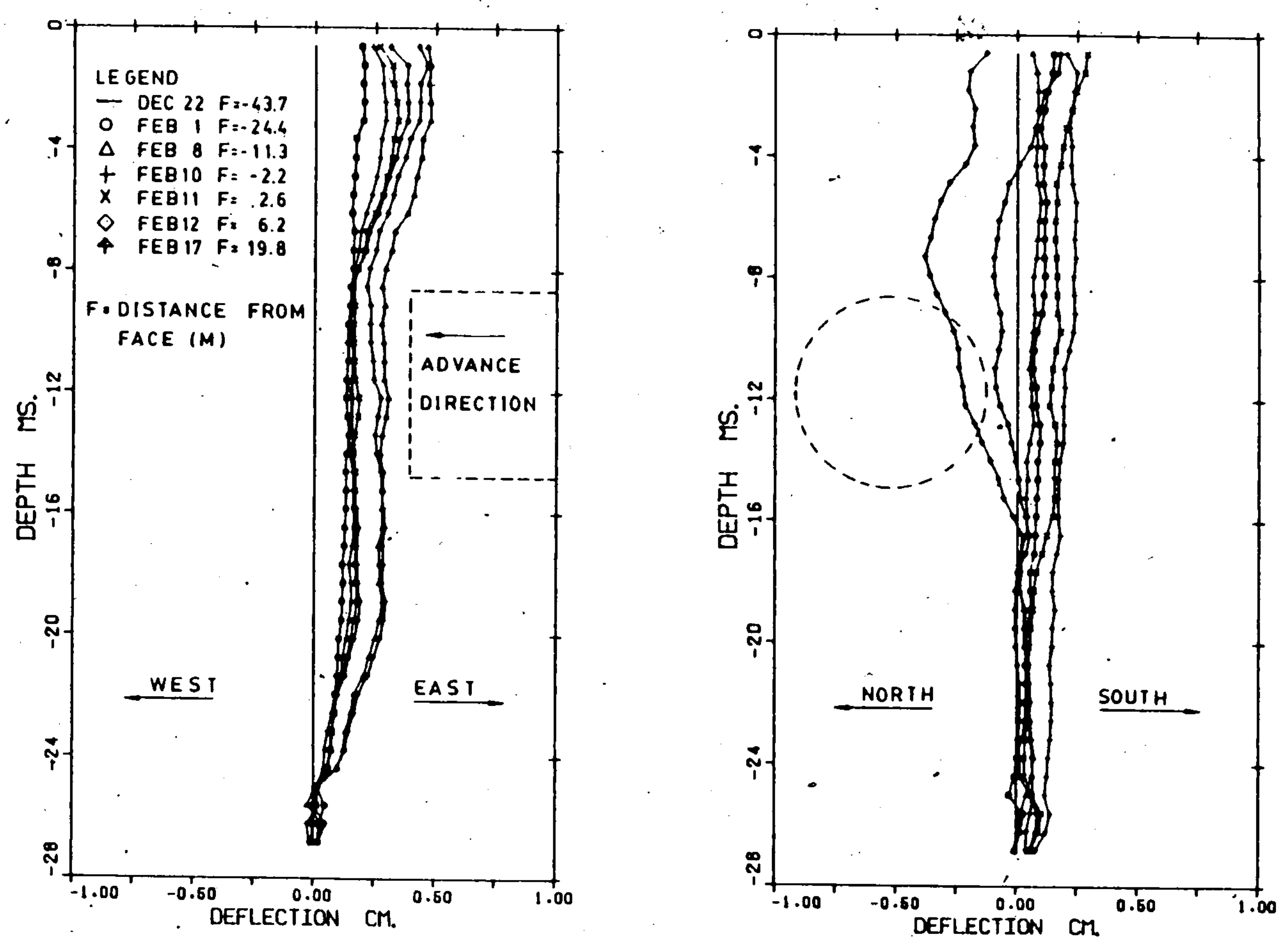

Figure 3.37 SLOPE INDICATOR SI7 (4.3M FROM TUNNEL AXIS)

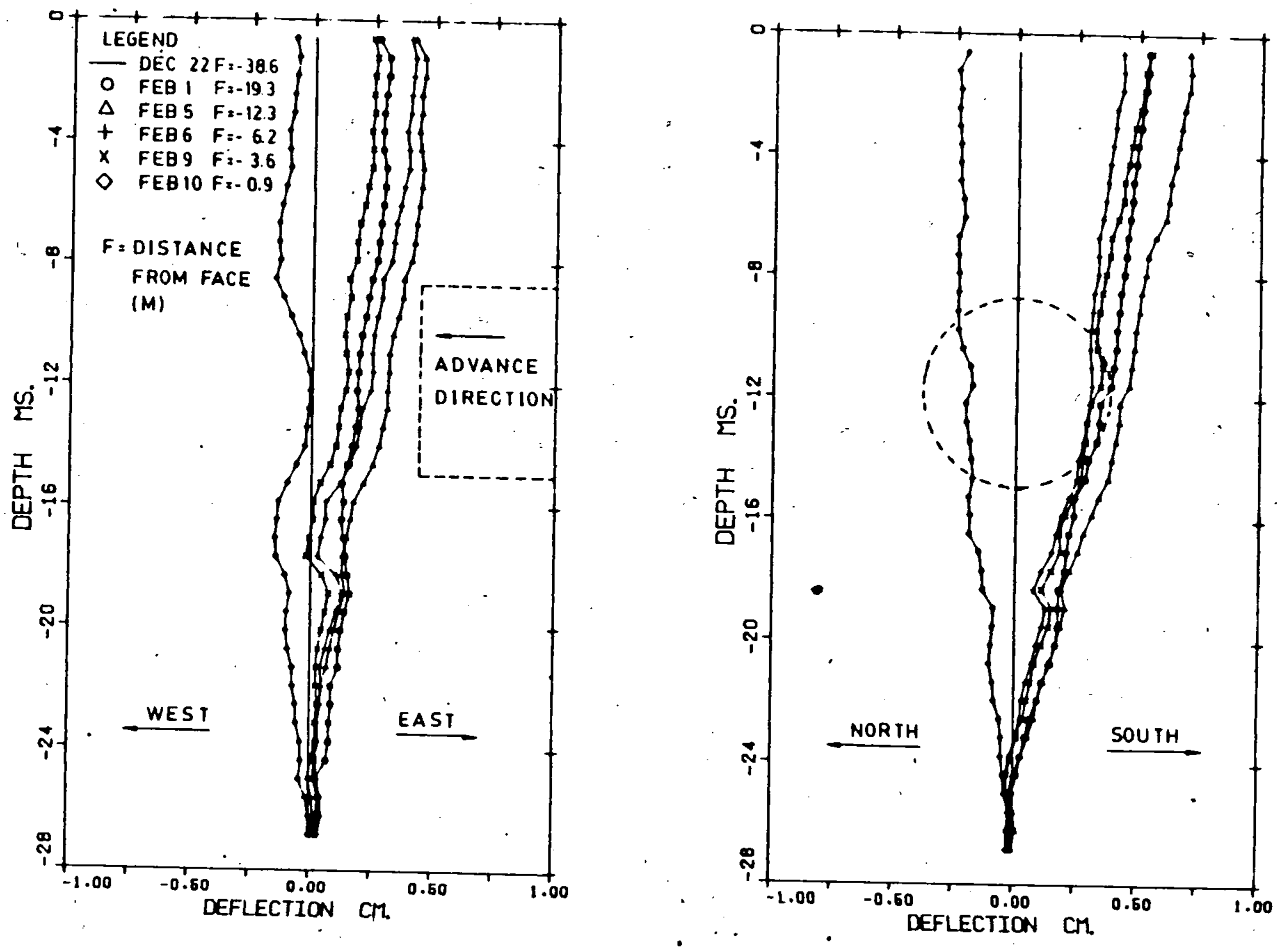

Figure 3.38 SLOPE INDICATOR SI12 (TUNNEL CENTRELINE)

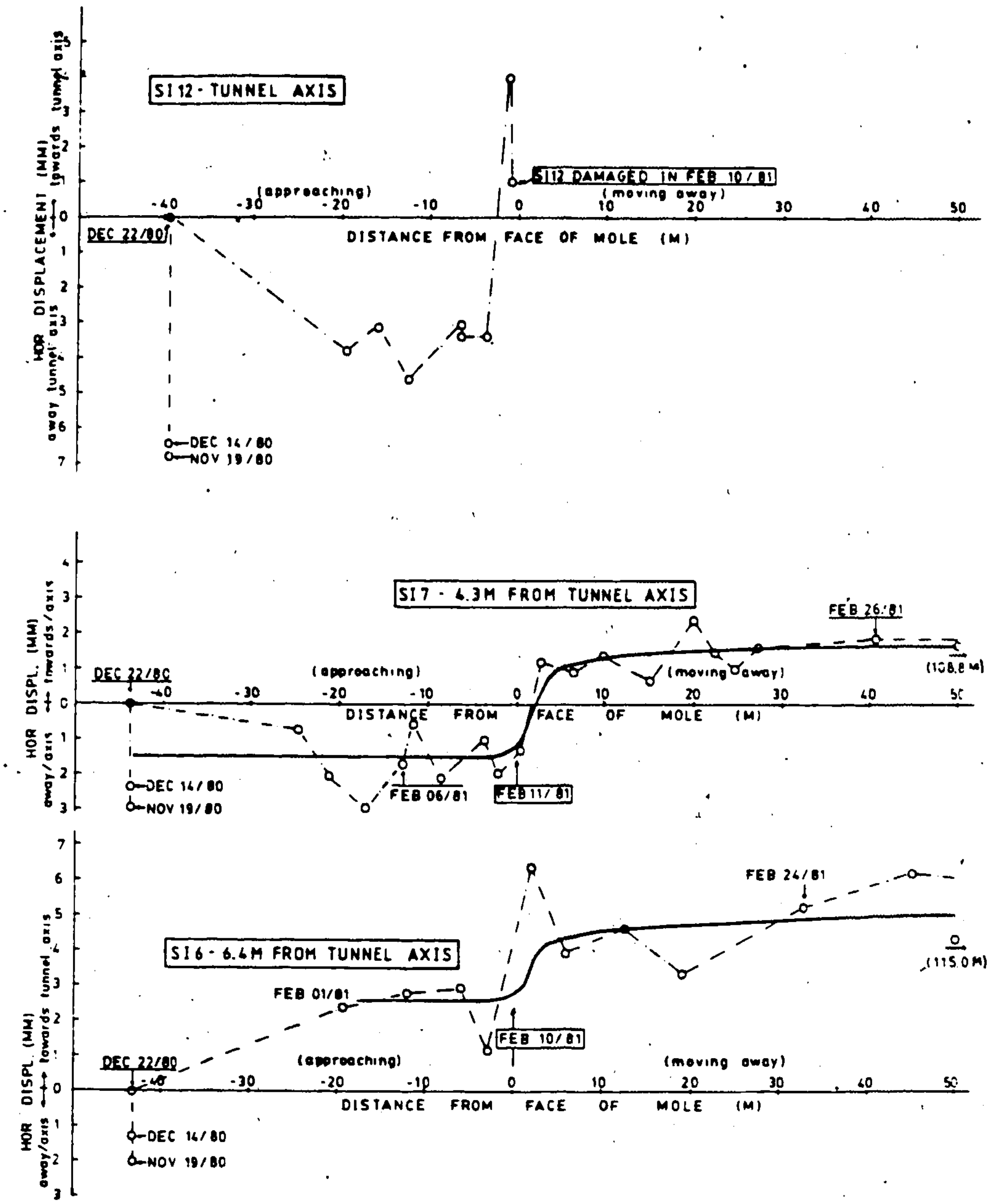

Figure 3.39 HORIZONTAL DISPLACEMENTS - PERPENDICULAR TO TUNNEL AXIS AT 11.58M BELOW SURFACE FOR SLOPE INDICATORS SI6, SI7 AND SI12

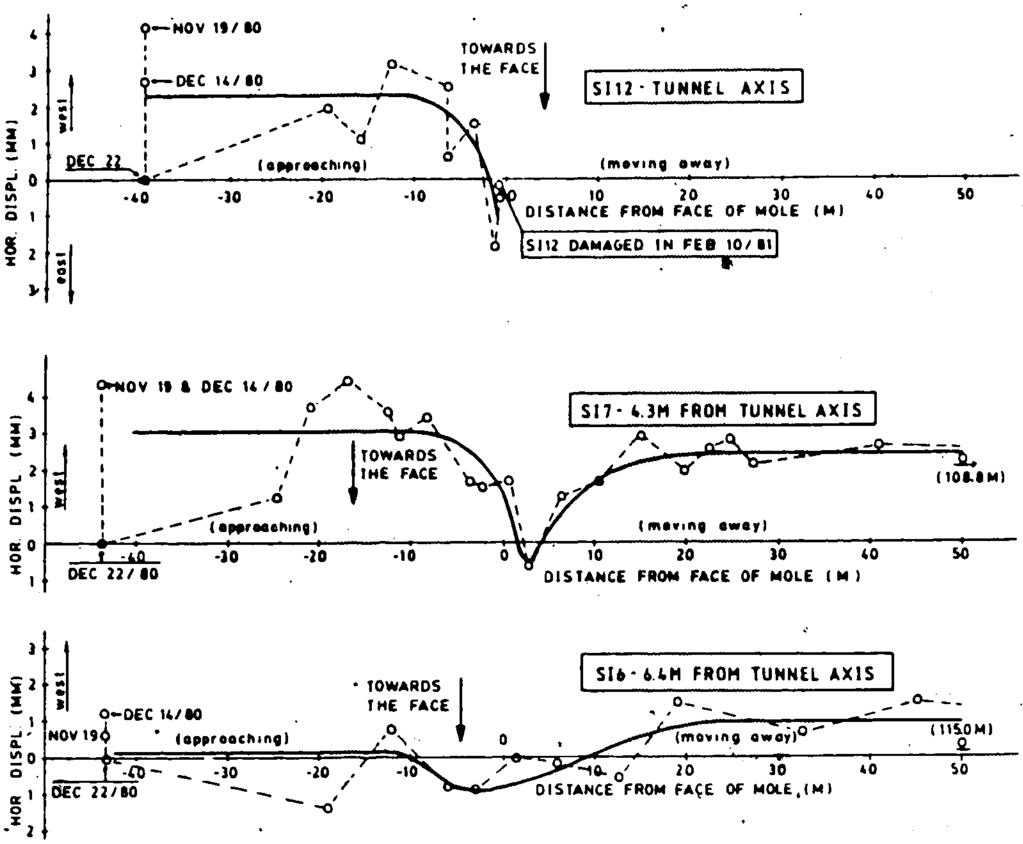

Figure 3.40 HORIZONTAL DISPLACEMENTS - PARALLEL TO TUNNEL AXIS AT 11.58M BELOW SURFACE FOR SLOPE INDICATORS SI6, SI7 AND SI12

Settlement Point Measurement Procedure). The erratic movements observed in SP11 were probably due to the presence of ice between the pvc pipe and the inner rod. The ice was probably restricting the free movement of the inner rod. In order to avoid the presence of ice inside the settlement points, they were filled with anti-freeze solution. It was noticed that the erratic movements ceased after this measure was taken.

The "loss" of the zero readings made the calculation of the repeatability of elevation difficult. The fluctuation of ±1mm in the elevations of SP2, SP15 and SP16 might be an indication of the repeatability of the elevation readings because negligible change in elevation was expected to occur at these points. The heavy traffic and adverse climatic conditions during levelling of settlement points probably affected to a great degree the repeatability of elevation. Figure 3.18 shows that the construction of the north tunnel of the LRT South Extension should not affect the buildings located at 10 meters north of the tunnel axis.

The analysis of Figures 3.17 and 3.18 indicate that the surface settlement trough is not symmetric to the tunnel axis. This asymmetry might be due to the presence of inter-till sand pockets, non-symmetric to the tunnel axis or due to the presence of the buildings at the north side of the tunnel axis as opposed to open area to the south. The shallow foundations of these buildings (2.8 metres deep) might locally increase the soil stiffness resulting in smaller settlements. The asymmetry observed in the surface settlement troughs indicates that these troughs do not fit the Gaussian distribution of surface settlements proposed by Litviniszyn (1956) and Peck (1969).

Hansmire (1975) reported that the surface settlement data obtained in the Washington D.C. Metro construction did not fit the probabilistic curve but would better fit a curve composed of two superimposed normal probabilistic curves.

The association of the shape of the settlement with a Gaussian curve is criticized by Mello (1981). The Gaussian distribution of surface settlements was obtained from a stochastic model proposed by Litviniszyn (opt.cit.) to simulate the subsidence in a loess due to local underground collapse. Mello (opt.cit.) states that Litviniszyn's model has no direct association with the change in the state of stress in the ground and corresponding strains and displacements associated with tunnel construction. Figure 13 of Mello's paper (opt.cit.) depicts several theoretical surface settlement distributions obtained from stress relief at a given depth. These settlement distributions are different from that proposed by Litviniszyn (opt.cit.).

The author believes that Peck's proposal for studying surface settlements based on Gaussian distribution is only justified as a first estimate of settlement distributions in the early stages of tunnel design where the detailed stratigraphy, the effects of construction procedure on the ground and the stress-strain behaviour of the soil under different stress paths are not well known.

The longitudinal section of the surface settlement trough, along the tunnel axis, presented in Figure 3.12, indicates that negligible surface vertical displacements occurred ahead of the face of the mole and that the stabilization of these settlements occurred at approximately 15 metres from the face of the mole. The decrease in the rate of surface settlements at 15 metres from the face of the mole, 9 metres from the position where the lining is expanded, indicates that the effects of the lining expansion are not immediately noticed at the surface.

3.4.2 Deep Vertical Displacements

The analysis of the surface settlement data obtained from settlement points and surficial magnet points indicated that the difference in settlement obtained from the two instruments (settlement point and multipoint extensometer) is always less than 2mm.

Figures B1 to B32 in Appendix B indicate that deep vertical displacements stabilize at approximately 15 metres from the tunnel face. This had been also observed in the settlement point data.

Extensometer ME5 situated at 10.4m from the tunnel axis did not detect significant soil movements due to tunneling.

Figure 3.26 shows that, in ME9, the magnetic points anchored below the springline level did not move significantly throughout the tunnel construction whereas the points located above the springline , detected uniform settlement after the tunnel passed by. The vertical straining detected by the magnetic points in ME9 was less than 0.1 per cent.

Figures 3.27 and 3.29 indicate that in ME10, the magnetic points installed close to the tunnel liner detected heave when they were within one tunnel diameter ahead of the mole. The measurements of lining deformation, Section 4.5.4.3, indicate that heave also occurred after the lining installation. No downward movement ahead of the mole was noticed in magnet points anchored above the tunnel crown which indicates that negligible loss of ground, defined in Section 3.4.4, occurs ahead of the tunnel face.

As discussed in Section 3.3.2.3, Multipoint Extensometer Installation, ME17 was installed approximately 80 metres from the Instrumented Section because, due to the damage of ME10, no ground movements were available above the tunnel crown after the mole passed a given section. The excavation of the tunnel through the section where ME17 was installed induced a roof failure. The upper portion of a sand pocket excavated by the mole caved in and left a void above the tunnel crown of approximately 1.5 cubic metre and 1.5 metre high. The magnetic point MP5 in ME17 was anchored in the sand pocket that caved into the tunnel.

The data recorded from ME17, presented in Tables B28 to B32 in Appendix B indicate that large vertical extension due to roof failure propagated up to 3.4 metres to 4.5 metres above the tunnel crown. The last reading in ME17 was taken three days after the mole stopped digging, close to the east wall of 104th St Station. This occurred when the face of the mole was 24.9 metres from ME17. At this distance from the mole the magnetic point located 3.0 metres from surface, in ME17, had settled 11.4mm whereas SP11, in the Instrumented Section, at the same distance from the face of the mole, had settled 8.4mm. This difference in surface settlements measured at the tunnel centreline in SP11 and M17 is probably due to the roof failure that occurred at ME17 and did not occur in the Instrumented Section.

The data obtained from ME17 cannot be analysed together with the data gathered in the Instrumented Section because, due to the failure of the roof, ME17 did not reflect the standard behaviour of the ground surrounding the tunnel.

3.4.3 Deep Horizontal Displacements

The difficulty in analysing the data presented in Figures 3.36 to 3.38 led to the plots presented in Figures 3.39 and 3.40. No trend of horizontal movements can be noticed in Figures 3.36 to 3.38 because the measured movements were small compared to the accuracy of the inclinometer. Figures 3.39 and 3.40 depict the soil displacements in a horizontal plane located at 11.58 metres below surface, approximately at the tunnel springline level.

The plots of horizontal displacements perpendicular to the tunnel axis at the springline level, in Figure 3.39, indicate that points located at 1.2 metre and 3.3 metres from the liner moved approximately 3.0mm and 2.0mm, respectively, towards the tunnel axis. These movements started to occur at 3.0 metres ahead of the face of the mole and stabilized at approximately 6.0 metres from it, where the primary lining was expanded against the ground.

The plots of horizontal displacements parallel to the tunnel axis, at the springline level, in Figure 3.40, indicate that a point located at the tunnel axis and at 4.3 metres from it moved 3.5mm towards the face of the mole before it passed by the inclinometers. This movement was only 1.0mm for a point at 6.4 metres from the tunnel axis. After the mole passed by the inclinometers, the points that were initially moving eastwards, against the tunnel advance direction, started to move westwards, in the tunnel advance direction, going back to their initial position. The soil movements in the direction parallel to the tunnel axis indicate that analytical studies of tunnel behaviour based on plane strain conditions do not reflect reality. The fact that the points in the ground move in the direction parallel to the tunnel axis during tunneling and go back to their initial position after the mole passes by enhances the fact that a study of the final displacements about the tunnel without taking into account the "strain history" of the soil is not acceptable.

3.4.4 Loss of Ground Around Tunnels

Hansmire (1975) defined loss of ground as the sum of the soil displacements normal to, and over a unit area of, the tunnel perimeter.

The loss of ground takes place at three different positions along the tunnel excavation:

a) Ahead of the face of excavation (face loss)

The face loss is the volume of soil excavated at the tunnel face in excess of the theoretical excavation volume.

b) Along the digging machine (shield loss)

The shield loss is the sum of soil displacements, perpendicular to the tunnel profile, immediately about the shield from the time the leading edge of the shield passes a section until the shield tail passes that section. Loss of ground due to the shield results from plowing and yawing of the shield and any displacement created by changes in the cross-sectional area of the shield.

c) Behind the tail of the shield (tail loss)

The tail loss happens because the tunnel lining insufficiently replaces the cross sectional area of the tail of the shield. The losses due to the flexibility of the lining are considered tail losses and are usually negligible.

A comprehensive study of ground movements around tunnels developed by Hansmire (opt.cit.) is based on the model presented in Figure 3.41. Hansmire (opt.cit.) proposed the following equation in his study:

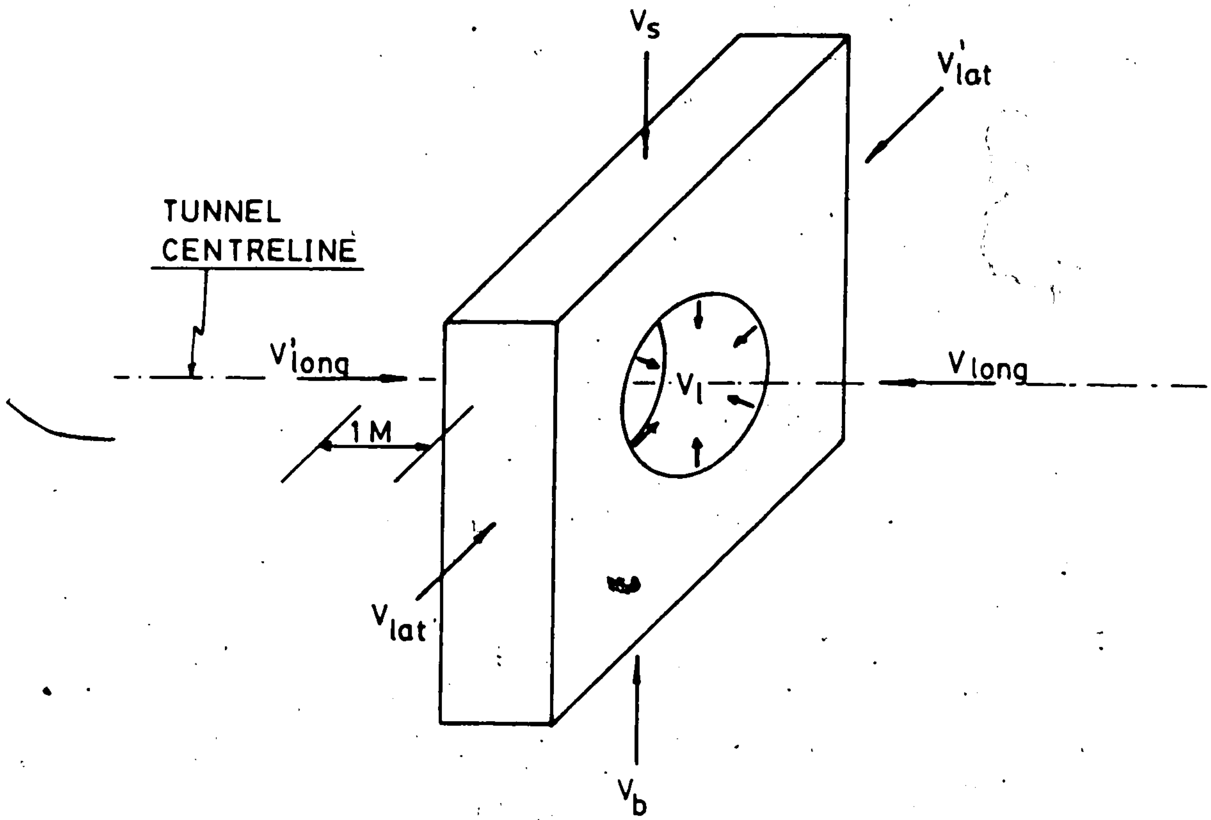

DEFINITION OF SYMBOLS AND UNITS

V_s	VOLUME OF SURFACE SETTLEMENT (M^3/M OF TUNNEL)
V_b	VOLUME OF BOTTOM DISPLACEMENT (M^3/M OF TUNNEL)
$V_{lat}^{(')}$	VOLUME OF LATERAL DISPLACEMENT (M^3/M OF TUNNEL)
V_l	VOLUME OF LOST GROUND (M^3/M OF TUNNEL)
$V_{long}^{(')}$	VOLUME OF LONGITUDINAL DISPLACEMENT (M^3)

Figure 3.41 THREE DIMENSIONAL GROUND MOVEMENTS ABOUT TUNNELS (HANSMIRE, 1975)

$$\Delta V = V_s + V_{lat} + V'_{lat} + V_{long} + V'_{long} + V_b - V_1 \quad 3.1$$

where

ΔV = soil volume change. ΔV is the sum of the volumetric change of the elements located outside the nominal limits of the tunnel excavation. It takes place due to stress-strain-volume changes in the presence of stress changes in the soil mass due to tunneling.

Vs, Vlat, V'lat, Vlong, V'long, Vb and Vl are defined in Figure 3.41.

The model proposed by Hansmire (opt.cit.) enables an analysis of the development of ground volume changes at several stages of tunnel construction based on soil instrumentation data to be carried out.

For the north tunnel of the LRT South Extension, the detailed study of the ground volume changes at different stages of the tunnel construction was not possible because no ground movement data was available in the region between SI7 (1.2 metre from the springline) and the tunnel axis after the mole passed a section. However, the ground volume changes can be calculated for the final displacement situation if the following assumptions are considered:

a) The lateral and lower boundaries in Figure 3.41 are considered far from the tunnel. In this case, Vlat = V'lat =

$V_b = 0$.

b) For the final displacement situation, the volume of longitudinal displacements, V_{long} and V'_{long}, are considered zero. Actually, there are volume changes in the longitudinal direction but they are expected to be small. In the tunnel excavated for the Washington D.C. Metro, the maximum longitudinal volume changes were less than 5% of the volume of lost ground.

With these assumptions, equation 3.1 becomes:

$$\Delta V = V_s - V_l \qquad 3.2$$

For the north tunnel, LRT South Extension, the volume of the surface settlement (V_s) calculated at 37.6 metres away from the face of the mole is $0.14 m^3/m$ or 0.46% of the nominal tunnel area.

The volume of lost ground (V_l) is assumed to be the difference between the volume defined by the cross-sectional area of the excavated face and the cross-sectional area of the expanded primary lining. It is assumed, then, that there is negligible loss of ground ahead of the mole, there is no shield loss due to plowing and yawing of the shield and the soil fills the voids around the lining. With these assumptions, V_l can be calculated: $V_l = 0.73 m^3/m$ or 2.42% of the nominal tunnel area. The values of V_s and V_l are substituted in Equation 3.2 and $\Delta V = 0.59 m^3/m$ or 1.96% of the tunnel nominal area. This value of ΔV indicated that an average increase in ground volume occurred around the LRT South Extension tunnel. This increase in volume of ground is similar to those measured by Hansmire (1975), in dense cohesionless soil: $0.32 m^3/m$ to $0.77 m^3/m$. In shallow tunnels, once the zone of disturbance, or the zone where ground plasticity occurs, reaches the ground surface, no further significant volume change takes place and the further increase of volume of lost ground is directly related to the downward movement of the block of soil above the tunnel. The verification of whether or not the "zones of disturbance" reached the surface is not possible with the data presented in this chapter. However, the data from load cells and steel lagging presented in Chapter 4 of this thesis indicate that only a small fraction of the overburden was being supported by the lining. This might be an indication that the "zone of disturbance" did not propagate to the surface.

The change of volume that takes place in the soil mass beside the tunnel can be evaluated through the relationship between Vlat and Vs, indicated in Figure 3.42. Vlat can be computed from the soil displacements measured by an inclinometer (SI6 or SI7). For no volume change in the soil, the lateral volume of soil displaced along a vertical plane, as shown in Figure 3.42, would produce an equal settlement volume at the ground surface.

Figure 3.43 depicts the values of Vlat and Vs, indicated in Figure 3.42, calculated with the data obtained

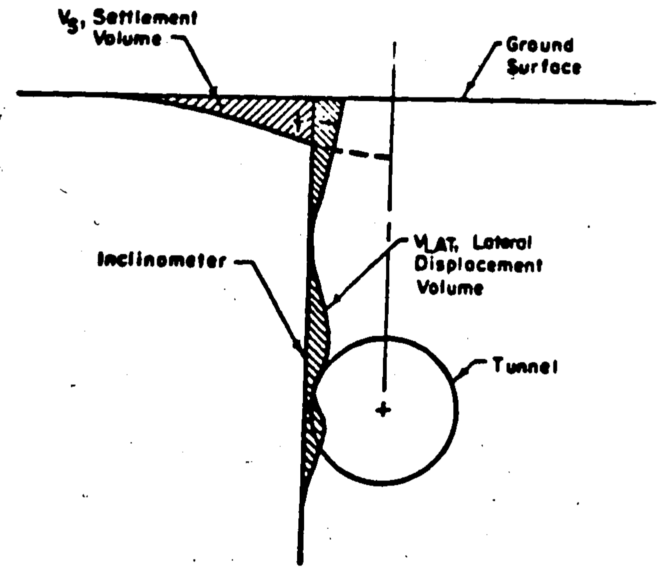

Figure 3.42 RELATIONSHIP OF SURFACE SETTLEMENT VOLUME TO LATERAL DISPLACEMENT VOLUME (AFTER HANSMIRE, 1975)

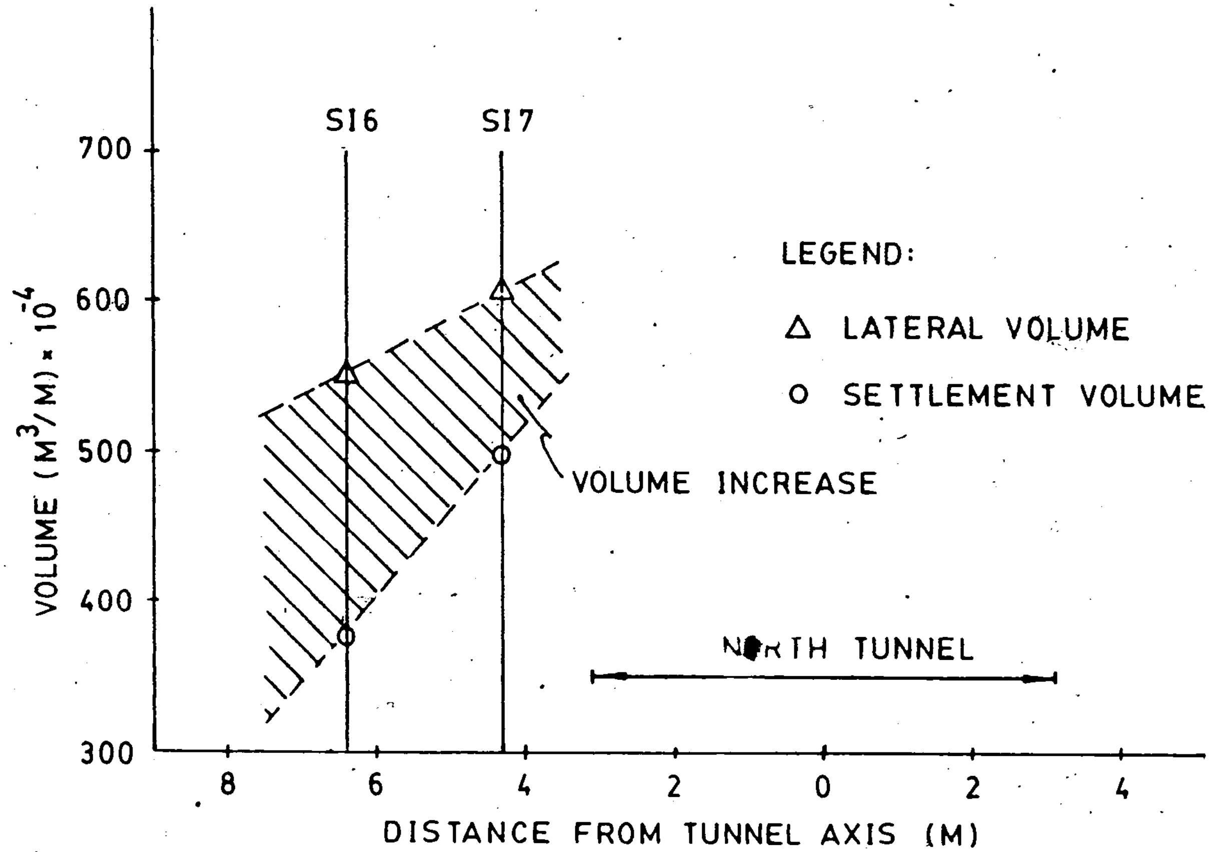

Figure 3.43 COMPARISON OF SETTLEMENT AND LATERAL DISPLACEMENT VOLUMES

from SI6, SI7 and surface settlement points. The variation of V_{lat} between February 06 and February 26 and February 01 and February 23, 1981, were chosen for SI7 and SI6, respectively, based on the inclinometer data presented in Figure 3.39.

Figure 3.43 indicates that a small portion of the ground volume increase (1.7% of ΔV), evaluated earlier in this section takes place beside the tunnel liner. This indicates that the volume changes due to LRT South Extension tunnel construction are restricted to the area above the tunnel crown.

3.5 Summary and Conclusions on Ground Displacements

This chapter reviewed the techniques most commonly used in measuring ground displacements around tunnels.

Details of the design, installation and measurement procedure of the instruments used to monitor ground displacements around the north tunnel of the LRT South Extension were presented.

From the analysis of the field data, the following was observed:

1. The surface settlement trough is not symmetric about the tunnel axis and does not fit the Gaussian distribution of surface settlements.
2. The maximum surface settlement was 10mm and occurred above the tunnel axis.

3. A small portion of the final vertical and horizontal measured displacements took place ahead of the face of the mole.
4. The magnetic extensometer ME5 indicated that no measurable vertical movements occurred 10.4 metres from the tunnel axis.
5. ME9, 1.2 metre from the springline, detected negligible vertical movements at points located below the springline level.
6. ME10, at the tunnel centreline, detected heave ahead of the mole in the magnet points close to the liner.
7. The final horizontal displacement in the direction perpendicular to the tunnel axis at the springline level was 3mm and 2mm at 1.2 metre and 3.3 metres, respectively, from the tunnel lining, directed towards the tunnel axis.
8. A ground volume increase of 1.96% of the tunnel nominal area was obtained. The inclinometers and surface settlement data indicated that over 96% of this volume increase takes place above the tunnel crown.

4. LINING LOADS AND DISPLACEMENTS

4.1 Introduction

The tunneling activities in the City of Edmonton have increased in the last decade with the growth of the city. Tunnels have been constructed for rapid transit systems and for storm and sanitary sewers.

The increase in tunneling activities has resulted in the need for improved design methods because the available methods, discussed in Chapter 5 of this thesis, do not take into account some of the details of construction and the variability of natural deposits.

Full scale field measurements have been carried out in order to verify the design methods and to provide an empirical evaluation of the behaviour of tunnels constructed in the glacial till and the Upper Cretaceous clay-shale of the Edmonton area. Soil movements and loads and deformations of the lining have been measured.

In this chapter, only the behaviour of tunnel linings is discussed.

Einsenstein et al. (1977) and Einsenstein and Thomson (1978) studied the normal loads acting on the primary lining of the north tunnel of the LRT North-East line, Edmonton, based on electrical strain gauges bonded to the steel ribs. From this study it was concluded that the determination of loads from strains measured in the strain gauges is complex and it proved difficult to separate stresses from the mole jacks from those from the soil mass.

El-Nahhas (1977) and Thomson and El-Nahhas (1980) reported lining distortion and results from pressure cells installed at the interface between the soil and the wood lagging of the temporary lining of two small diameter, deep tunnels constructed in Edmonton. They concluded that the results from the two pressure cells were of little value because the soil closing on the timber was unknown.

El-Nahhas (1980) compared the performance of two lining systems (rib and lagging and precast concrete segments) of a small diameter, deep tunnel, constructed in the glacial till of Edmonton. In this study, the precast segmented lining was extensively instrumented, with load cells and embedded strain gauges whereas the rib and lagging lining had loads evaluated from four vibrating-wire strain gauges welded to the steel ribs.

From the field instrumentation carried out in tunnels constructed in Edmonton, it can be concluded that the accurate magnitude and distribution of stresses acting on the rib and lagging lining system has not, as yet, been obtained. The lack of information concerning the behaviour of the rib and lagging lining systems led to the comprehensive instrumentation of the primary lining of the north tunnel of the LRT-South Extension.

In this chapter, the methods of determining the magnitude and distribution of stresses acting on tunnel liners are discussed in Sections 4.2 and 4.3. The instruments used in the study of the behaviour of the LRT primary lining and the discussion on the results from this instrumentation are presented in Section 4.4.

The data presented in this chapter is used in the study of soil structure interaction presented in Chapter 5.

4.2 Direct Pressure Measurement

4.2.1 Pressure Cells

There are two basic types of earth pressure measurement possible with pressure cells. One is the measurement of total pressure at a point within a soil mass (often used in earth dams) and the other is the measurement of total pressure or contact pressure against the face of a structural element (termed a boundary cell). The latter has been used to measure radial soil pressures acting at the tunnel liner interface and has yielded unsatisfactory results (Cording et al., 1975).

One reason for the poor performance of boundary cells is the difficulty in designing a pressure cell that behaves in a manner similar to the soil structure interface where the cell is installed. This similarity must include stiffness, wall roughness and simultaneous activation of cell pressure and instrumented structures.

Even in cases where these requirements are met, the scale effects may adversely affect the resulting interpretation: the contact pressures may not be uniform over the areas of contact of the pressures cell (15 to 20cm diameter). Local variation of soil contact pressures on the tunnel lining (due to ground irregularity, construction method, etc.) can cause a large variation in measured pressures. Difficulties in obtaining reliable results from boundary cells are reported by Cording et al (1975); Thomson and El-Nahhas (1980) and Delory et al (1979).

4.3 Indirect Pressure Measurement.

The pressure distribution on a lining, obtained from the measurement of thrusts, moments, shear forces and deformations can be used to evaluate the lining safety. These values can be obtained from:

- strain gauges: installed in or on the lining
- load cells: usually installed in joints of the lining
- lining deformation measurements

4.3.1 Strain Gauges

Strain Gauges are devices that measure displacements over a known length.

The commonest strain gauges in geotechnical engineering are: - electrical resistance strain gauge

- vibrating wire gauge
- mechanical gauge
- photoelastic strain gauge

Descriptions of the principles of operation, construction details, advantages and disadvantages of each gauge are extensively discussed in the literature on instrumentation (e.g. Cording et al 1975). Table 4.1 summarizes the most important features of some strain gauges (Cording et al , opt.cit.)

By installing strain gauges across the thickness of the lining one can obtain the strain distribution, and (once the elastic properties of this lining are known) the stress distribution within the instrumented section. Normal forces and bending moments can be back calculated from this stress distribution and the safety of the structure can be evaluated.

Strain gauges can be installed within the lining (concrete liners) or attached to the surface of the structural element (steel ribs in the rib and lagging system on steel segments in the liner plate system).

Strain gauges embedded in a concrete lining will not be discussed in this report. The present study, concerns the behaviour of primary lining (rib and lagging) used in the LRT South Extension tunnel.

The strains and stresses in a rib and lagging lining can be measured in either or both of the two structural members composing the system.

Type	Strain Sensitivity, Microstrains	Gage Length, Inches	Typical Range, Microstrains	Advantages	Limitations and Precautions	Reliability
Bonded electrical resistance gage	2-4	.008-6	20,000 - 50,000	Small size, low cost. Temperature compensation available.	Errors due to lead wire and circuit resistance changes unless compensated. Long term stability may be poor due to cement creep. Meticulous installation procedure. Difficult to waterproof.	Poor - Fair
Encapsulated, unbonded, electrical resistance a) Ailtech weldable gage	2-4	1 - 6	20,000	Factory waterproofing. Welded surface mount, temperature compensation available.	Errors due to lead wire and circuit resistance changes unless compensated.	Fair - Good
b) Carlson gage	4	8 - 20	700 tension, 1400 compression	Factory waterproofing, easy to install. Long experience record.	Errors due to lead wire and circuit resistance changes unless compensated. Small range. Temperature correction required.	Good
Vibrating-wire gage	1-2	4 - 14	600 - 7,000	Not as affected by lead wire resistance changes. Easy to install, factory waterproofing. Long experience record. Robust, reusable.	Small range. Temperature correction required.	Good
Mechanical gage	5-10	2 - 80	10,000 - 50,000	Simple, low cost, waterproofing not required.	Requires skill in reading. Can not be read remotely.	Excellent
Scratch gage	30	Variable, up to 30 in. or more.	40 - 1000	Self-contained, automatic recording, simple.	Limited accuracy and range.	Fair
Laser gage	0.2	6	6000	Rugged and simple.	Can not be read remotely.	

Table 4.1 STRAIN GAUGES - TYPES AND FEATURES (AFTER CORDING ET AL, 1975)

The steel ribs are the most commonly instrumented components. The variation found in the mechanical and geometric properties of the ribs is much less than that found with the timber lagging elements.

In order to obtain stress distributions across the "H" sections, usually chosen for the steel ribs, strain gauges have to be attached to both, web and flanges. Figure 4.1 illustrates the location of strain gauges used in the rib instrumentation of the north tunnel of the north-eastern section of the LRT system in Edmonton. Stresses in steel ribs were also measured by El-Nahhas (1980 and 1977) from strain gauges on the two flanges. Experience with strain gauges bonded to steel ribs is quite discouraging. Many factors lead to the poor performance of strain gauges bonded to steel ribs:

- In tunnels where ribs are subjected to longitudinal loads from the TBM, the strains induced during jacking may exceed and hence mask those from ground loads
- Flanges are subjected to secondary bending distortion effects
- Steel ribs are likely to be subjected to eccentric or torsional loadings
- The protection cap covering the strain gauge may induce a local strain field distortion.

All these factors combine to create a complex analysis of strain distribution across the rib section. It is

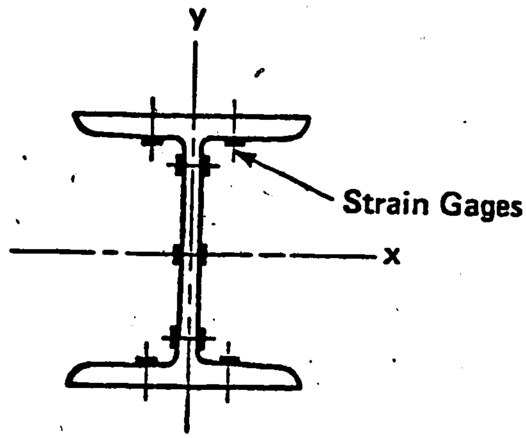

Figure 4.1 LOCATION OF STRAIN GAUGES ON RIB CROSS-SECTION - LRT NORTH-EAST LINE (AFTER EISENSTEIN ET AL, 1977)

difficult in such cases to separate the sources of deformation of the steel ribs. For geotechnical engineering research purposes, the loadings due to ground pressure are of major interest and can hardly be quantified given the preceding factors.

The wooden lagging of the primary lining is seldom instrumented due to the variation in mechanical and geometric properties of the timbers. To avoid this variability one can substitute for some pieces of wooden lagging, other pieces made of another material that present more uniform properties (e.g. steel). The piece of lagging that replaces the timber must have similar properties to the original timber lagging otherwise problems similar to those described for pressure cells will be created. The installation of strain gauges on these special pieces of lagging allows the evaluation of loads supported by these pieces.

4.3.2 Load Cells

Load cells are often used in the monitoring of loads in tunnel liners in order to minimize the difficulties in interpreting the data, as described in Section 4.3.1. Load cells also simplify the installation procedure since they are easily transported and installed.

Load cells are structural members of known mechanical properties, with strain gauges attached to measure the deformation of the element under load. The type of strain gauge attached to the load cell defines the load cell type:

- mechanical load cells
- photoelastic load cells
- electrical resistance load cells
- vibrating wire load cells

Load cells have been extensively used in segmented liners. The load cells are installed between segments, yielding no significant change in the original liner behaviour. Load cells can also be specially installed within a segment of the liner. This procedure facilitates the installation at the usually congested face of the tunnel as no deviation from the normal construction sequence occurs since this segment will have been previously prepared. However, the installation of the load cell within a segment complicates the load cell design, since its presence must not alter the mechanical behaviour of the segment. This is not easily achieved.

Usually Load cells are designed to carry only normal loads which can be achieved by providing spherical seats for the structural members (usually part of a steel sphere). The results from this type of load cell will reflect the behaviour of the lining only if the position, where the device is installed, originally carries only normal load.

Load cells designed to measure shear forces in addition to normal forces are also available. One type of these load cells is described by Kovari et al. (1977).

4.3.3 Lining Deformation

Another means of obtaining the ground stress acting on the lining is the measurement of the lining deformation.

The deformed shape of the lining can be used as a displacement boundary in any numerical analysis in which the soil-structure interaction is analysed (back analysis from known displacements)

Two of the commonest means of measuring lining deformation are described in the follow sections:

4.3.3.1 Rod or Tape Extensometer

This is an easy, accurate and relatively inexpensive way of measuring the distance between two points of the lining. Many types of extensometers have been designed and details concerning them are considered by Burke (1957), Obert and Duvall (1967), Cording et al (1975) and El-Nahhas (1977).

Tape extensometers consist of a micrometer or mechanical dial gauge connected to a rod or series of rods of known length, or to a spring loaded tape measure, kept under constant tension during readings. Measurements are taken by attaching the tape extensometer between the measurement bolts, fixed to the inside of the lining and adjusting the rods or the tension of the tapes to the required load.

The deformed shape of the tunnel can be determined by taking readings between several bolts spaced on the tunnel lining in a plane normal to the tunnel axis. The larger the number of relative displacements measured between measurement bolts, the better the definition of the deformed lining shape.

4.3.3.2 Integrated Measuring Technique

Kovari et al. (1977) proposed a technique of measuring lining displacements in order to obtain the normal loads and bending moments acting in the lining and also to obtain the external loading (radial and tangential). This procedure is termed Integrated Measuring Technique and yields reasonable results despite some simplifications inherent in the method such as deformations occur only in the plane of the monitored ring and small deformation theory. Kovari et al. (opt.cit.) reported that the deformation of the Gotthard Road Tunnel liner were monitored with the aid of three displacement measuring devices (curvometer, deformeter, distometer-ISETH), as proposed by their method. The loads predicted by the Integrated Measuring Technique were compared to those obtained from load cells installed in the same ring of the liner. This comparison showed the satisfactory performance of the method proposed by Kovari et al. (opt.cit.)

4.4 The L.R.T. South Extension Tunnel Liner Instrumentation

Loads and deformations in the primary lining were measured in the early stages of construction of the LRT tunnel in order to optimize the initial liner design and to study the soil-structure interaction.

The selection of instruments used in the monitoring of liner loads and displacements of the LRT tunnel was based mainly on previous experience in tunneling instrumentation at the University of Alberta.

The interaction between the steel ribs and wood lagging was investigated because little is known about this interaction and because it affects the construction costs and lining design to a significant extent. The study of the rib and lagging interaction was accomplished with the instrumentation of twelve steel pieces of lagging and eight load cells. Two load cells were installed on each of four steel rib rings. Convergence of other four ribs was measured with the tape extensometer and eyebolts described later in this chapter.

Pressure distribution acting on the lagging was obtained by measuring strains on the internal face of 12 pieces of hollow steel lagging that were designed to have the same bending stiffness of the wooden lagging in order to simulate its normal behaviour.

Details of each proposed instrument, including calibration tests, installation, measurement procedure, field data and data reduction is presented in the following sections of this chapter.

4.4.1 Load Cells

The choice of which method should be used to measure loads in the steel ribs was based on an analysis of the lining installation procedure. As explained in the description of the construction method (2.3.1), the four segments, composing one ring of the steel rib, are initially erected within the mole shield and kept together by two loose sets of bolts and nuts at each joint. The steel rings are exposed to the soil as the mole advances and the expansion ring (jacks) are positioned and aligned. The bolts and nuts from the upper joints are removed to allow full expansion of the joints. The expansion spacers (15.24cm long) are then placed between the end plates of the expanded joints. The bolts and nuts are then properly placed and tightened with no particular predetermined torque. By leaving the bolts and nuts relatively loose (hand tightened) the joints become free to rotate and to move radially.

The substitution of a joint spacer by a load cell designed to have the same thickness as the rib spacers and designed with spherical load caps on each end of the load cell insuring that only axial loads are transferred between ribs, would not alter the normal behaviour of the lining.

4.4.1.1 Load Cell Design Details

The structural members of the load cells were a solid cylinder of cold rolled steel (type C1018). Both ends of these cylinders had a spherical shape in order to fit the concave seatings of same radius welded to the end plates according to Figure 4.2 This allows free rotation of the structural member of the load cell in the presence of any bending moment. The mechanical properties of the structural steel are:

- Compressive yield strength = 461965 KN/m^2
- Tensile yield strength = 572285 KN/m^2
- Elastic deformation modulus = 204092000 KN/m^2

A diameter of 7.62cm was chosen for the solid steel cylinder and safety against yielding was checked as follows:

Assuming full overburden at the springline, uniformly acting around the lining, the maximum normal load in the load cell can be calculated:

$w = 20\ KN/m^3$

$h = 11.9m$ $\qquad w.h.s.R = 885.36\ KN$

$s = 1.2m$

$R = 3.1m$

where: w = soil unit weight

h = depth of springline

s = ribs spacing

R = lining radius.

Based on the load from full overburden pressure the load cells have a safety factor of 2.4 against yielding.

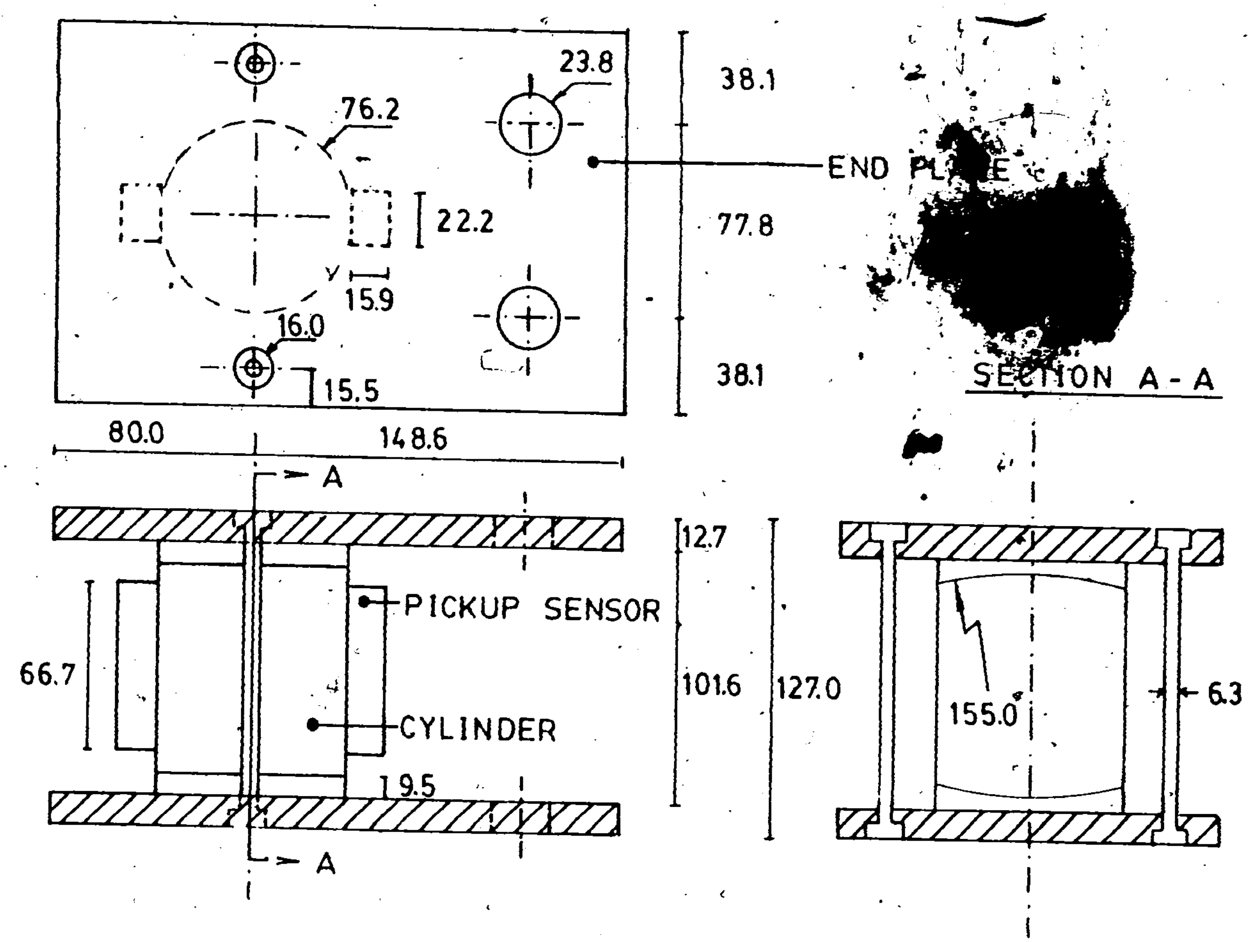

Figure 4.2 LOAD CELL - DESIGN DETAILS

UNITS: MM
SCALE 1:30

Two SINCO 52621 vibrating wire strain gauges were welded to the cylinder in diametrically opposite directions so strains could be averaged hence a more accurate normal load obtained. SINCO 52622 Pickup Sensors were placed over the vibrating wire gauges and fastened with steel belts welded to the cylinder. These sensors were connected to leads long enough to enable remote readings.

Details concerning the vibrating wire gauge, pickup sensor and strain indicator are given in the manual provided by SINCO.

Details of the load cells are depicted in Fig 4.2 and Plate 4.1.

4.4.1.2 Load Cell Calibration

Eisenstein et al. (1977) found that the maximum normal load in the ribs was approximately 630KN. Based on this information, load cells were calibrated to a load of 700KN. Each of the eight load cells was loaded and unloaded three times under a load controlled condition. Strains (from strain gauges) and loads were recorded for every increase or decrease of 100KN. Results from these calibration tests are presented in the Appendix C of this thesis. A relationship between loads and strains for each load cell was obtained by the linear regression of the data related to the loading portion of the three tests. These relationships are presented in Table C5 in Appendix C.

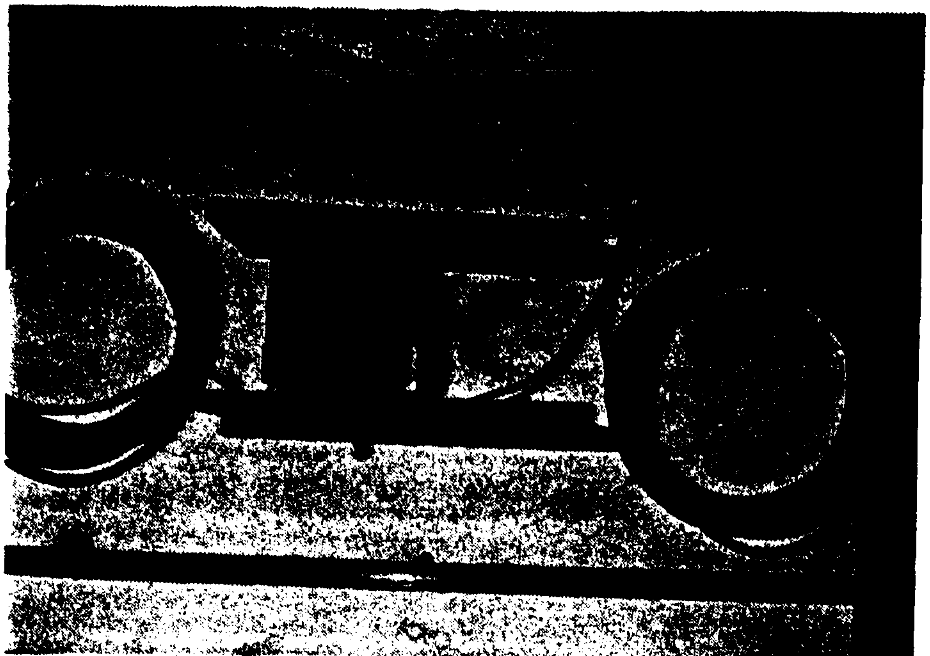

Plate 4.1 LOAD CELL DETAIL

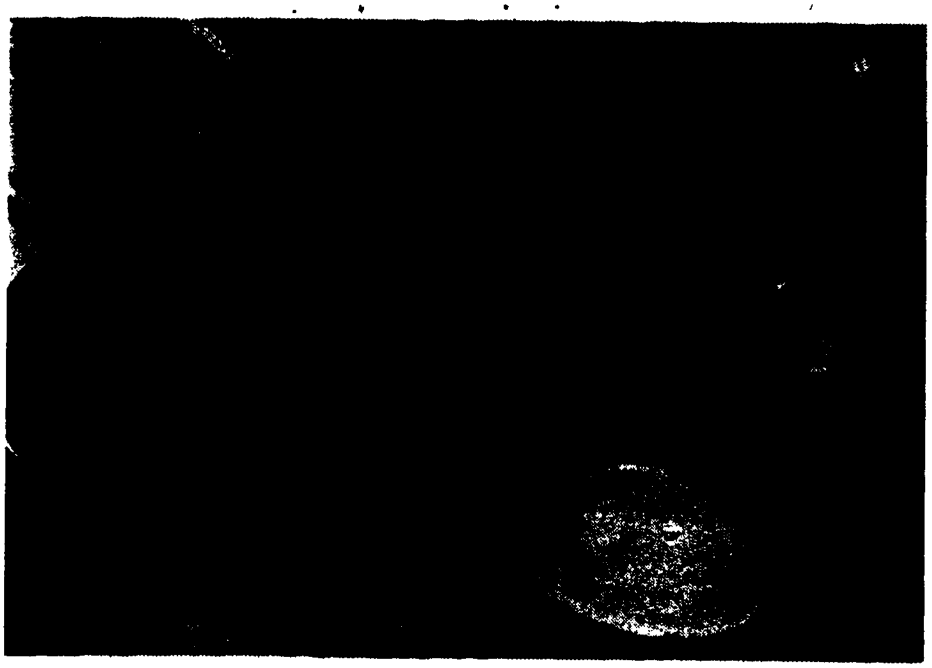

Plate 4.2 LOAD CELL INSTALLATION

4.4.1.3 Load Cell Installation

The eight load cells were installed as shown on Figure 4.3. They were installed in such a way that loads in each of the four joints of the steel sets could be measured twice.

The instrumented rings should ideally be installed exactly within the area of the tunnel where "ground instruments" had been installed (between chainage Sta.200 + 43.4 and Sta.200 + 57.1). Unfortunately, it was only possible to place the four rings in the following positions:

ring 1 - Sta. 200 + 60.6

ring 2 - Sta. 200 + 61.8

ring 3 - Sta. 200 + 63.0

ring 4 - Sta. 200 + 64.2

After the joint expansion, the load cells were placed between end plates of the steel ribs (Plate 4.2) and the bolts and nuts placed in order to be tightened later.

The load cells were positioned so that one of the strain-gauges was facing the soil and the other facing the tunnel centreline.

An additional 2.54cm long spacer (W6x25 section) had to be placed between one end of the load cell and the steel rib plate in order to complete the 15.24cm of length of the original spacer (at the time the load cells were built, it was thought that spacers were to be 12.70cm long).

A departure from the normal construction procedure was necessary in the rings where load cells had to be installed in the lower joints as the expansion joints were usually

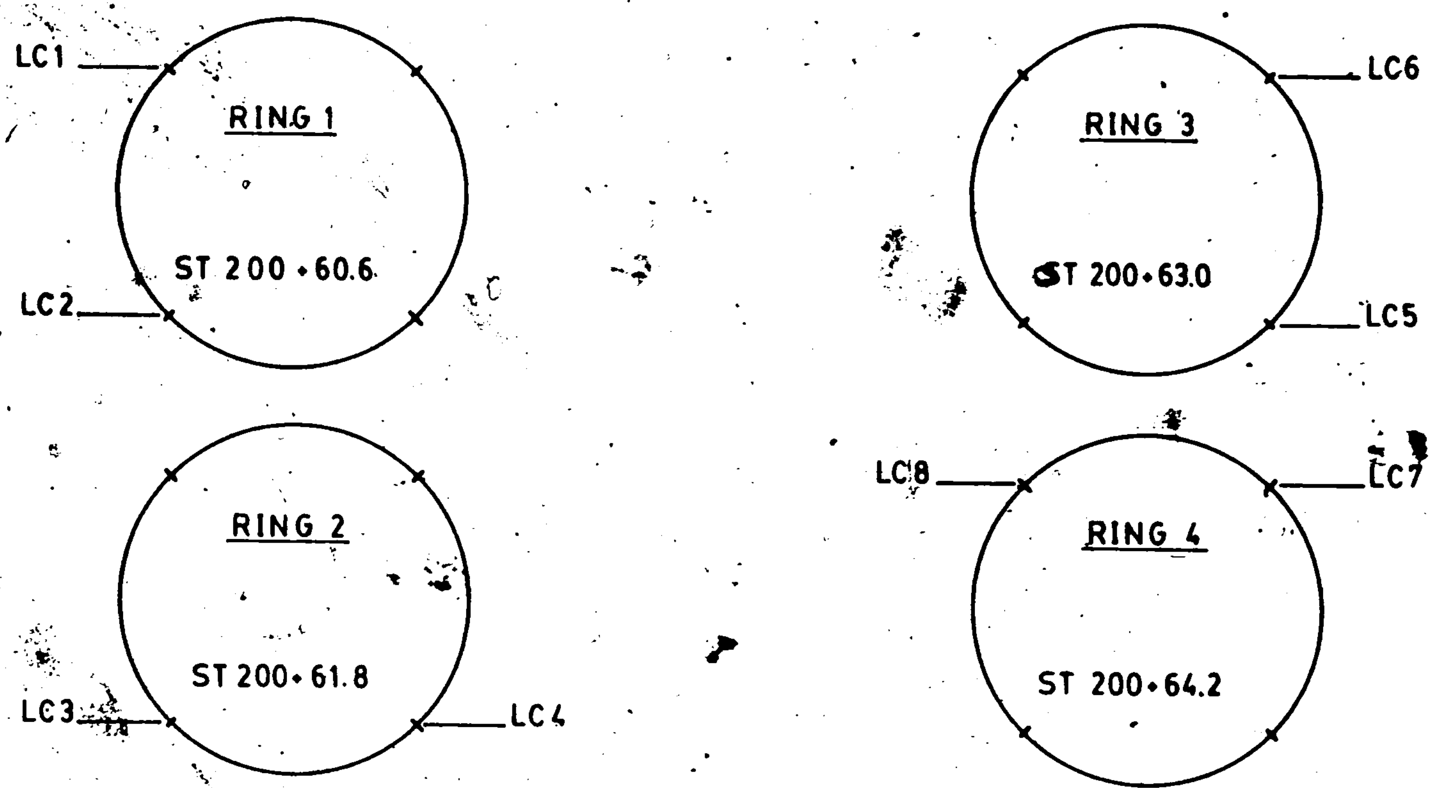

Figure 4.3 LOAD CELL LOCATION

placed in the upper joints. Expanding one or two of the lower joints instead of the upper ones, probably altered the behaviour of the lining in that region but not significantly.

After the pressure in the expansion jacks was released and the load cells activated, it was noticed that a large radial displacement of the end plates of adjoining ribs and relatively large rotation of the structural member of the load cells on the seats had taken place. The rotation of the load cells separated the sensor from the strain gauge due to a contact between sensors and end plates of load cells. The sensors were replaced and the strain gauges continued to function.

4.4.1.4 Measurement Procedure

Readings were taken with a SINCO Model 52601 strain indicator. Readings were directly displayed as microstrains, and recorded in a field sheet presented in Figure 4.4.

Zero readings for data reduction were taken for each cell immediately before installation. Subsequent readings were taken soon after the pressure in the expansion jacks was released and as often as possible in the proximity of the mole tail. The number of readings collected was restricted by other readings that had to be taken simultaneously and by the installation time required for other instruments.

LOAD CELLS FIELD SHEET

RING. NO.	CELL NO.	DATE	TIME	DISTANCE FROM THE TAIL	STRAIN GAGES READINGS A	STRAIN GAGES READINGS B	READ/ - ZERO READ/ A	READ/ - ZERO READ/ B	AVERAGE	LOAD (T)

Figure 4.4 LOAD CELL FIELD SHEET

4.4.1.5 Field Data

The data obtained from field measurements is presented in Tables C6 to C13 in Appendix C.

Measured loads were plotted versus time (Figure 4.5 and Figure 4.8), versus logarithm of time (Figure 4.6 and Figure 4.9) and versus distance from tail of mole (Figure 4.7 and Figure 4.10)

Figures 4.5 to 4.7 contain data from the load cells installed in the upper joints while Figures 4.8 to 4.10 contain data from the load cells installed in the lower joints.

4.4.1.6 Data Reduction

The loads measured at the joints of the steel ribs reflect the resultant of the stress distribution acting along the ribs and adjoining pieces of lagging.

There are many possible stress distributions acting in the perimeter of the ring that yield the same set of loads as those measured at this site.

The most often used stress distribution in the back calculation of field data is that presented in Figure 4.11. The use of this distribution is reasonable for deep tunnels where the weight of the excavated soil has a minor influence on the equilibrium of the tunnel liner (Mindlin 1940). The assumption of the stress distribution presented in Fig 4.11 in the calculation of stresses acting on the liner from the loads measured in the load cell is only reasonable when load

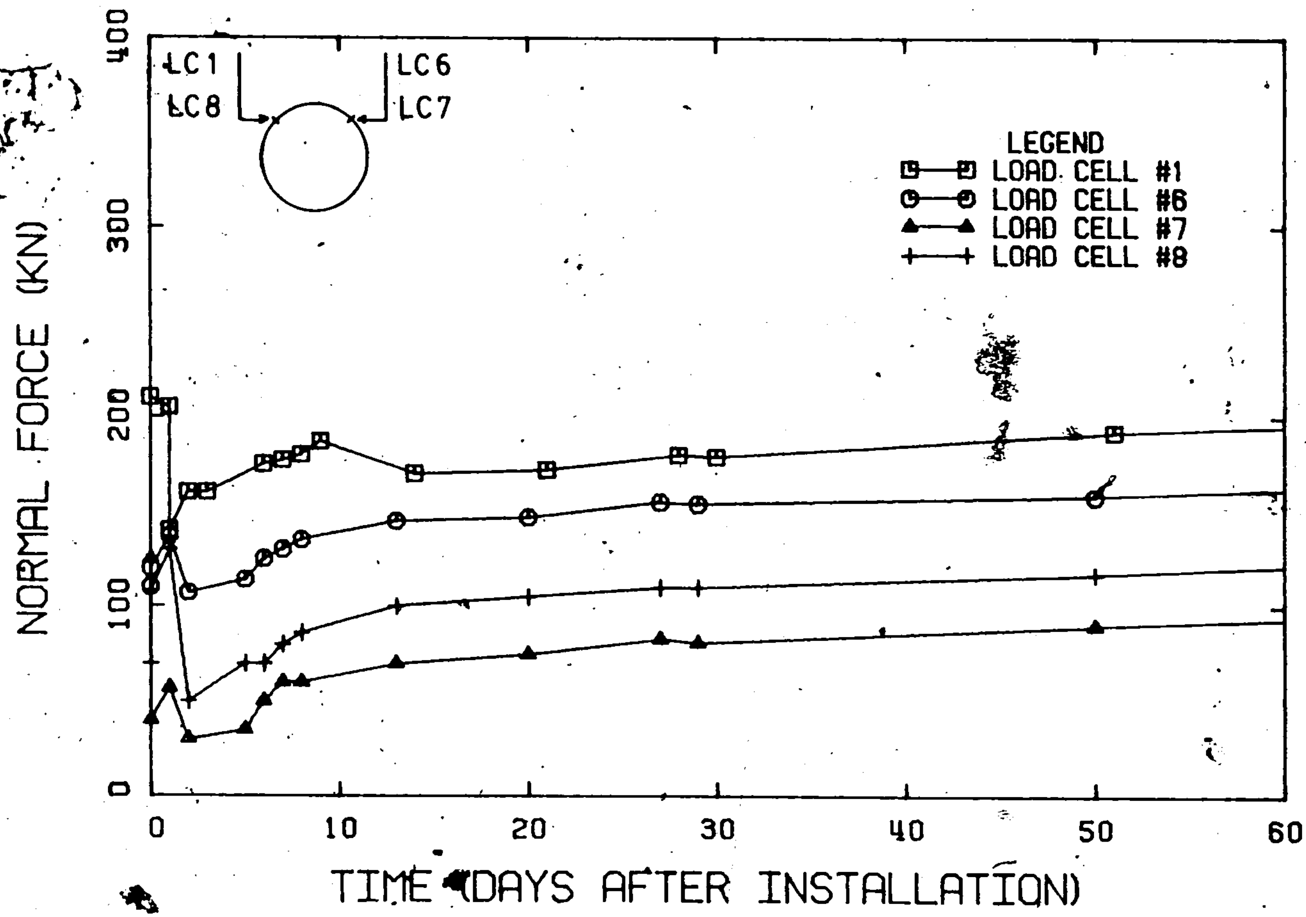

Figure 4.5 LOAD CELLS - UPPER JOINTS - LOAD VS TIME

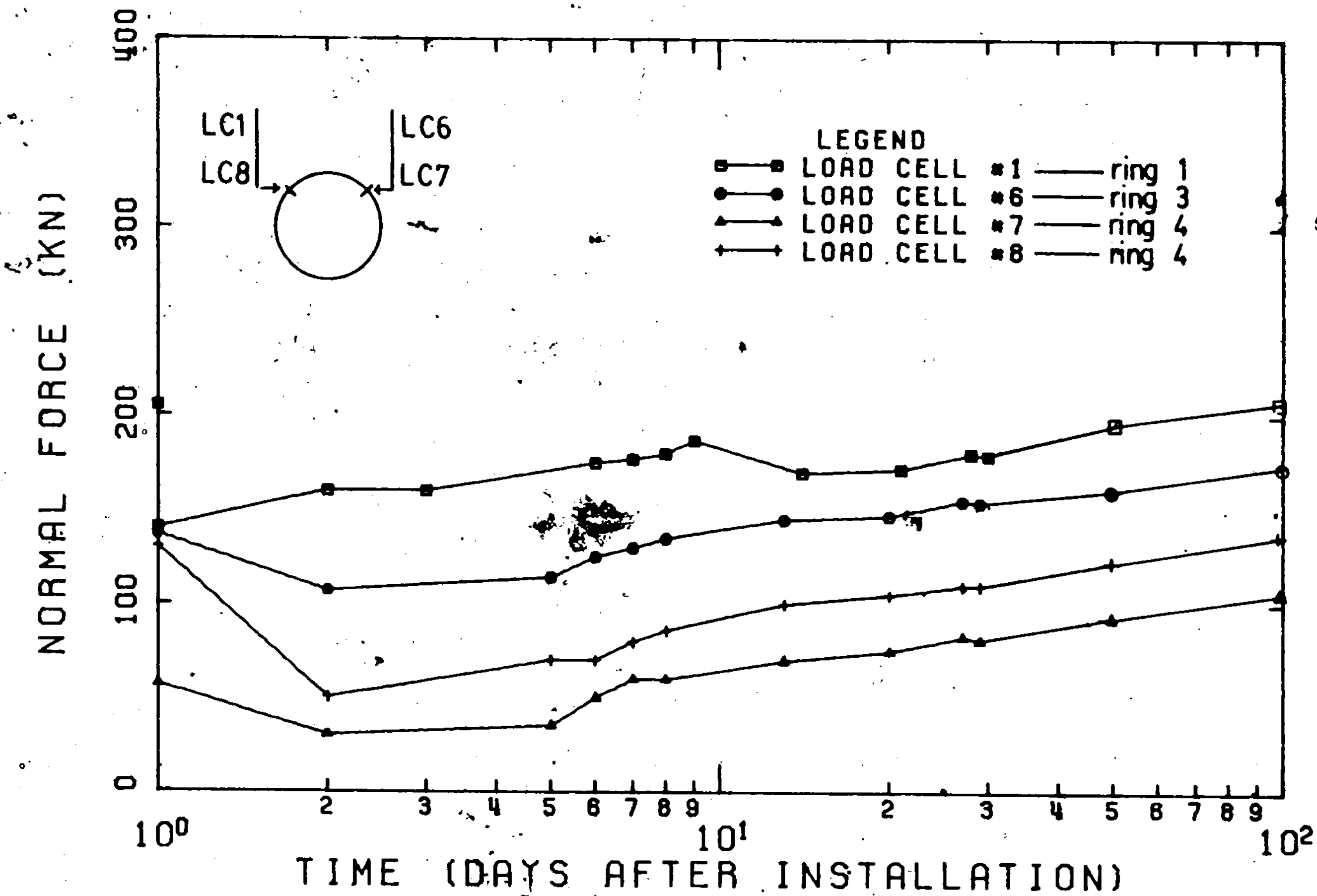

Figure 4.6 LOAD CELLS - UPPER JOINTS - LOAD VS LOG.TIME

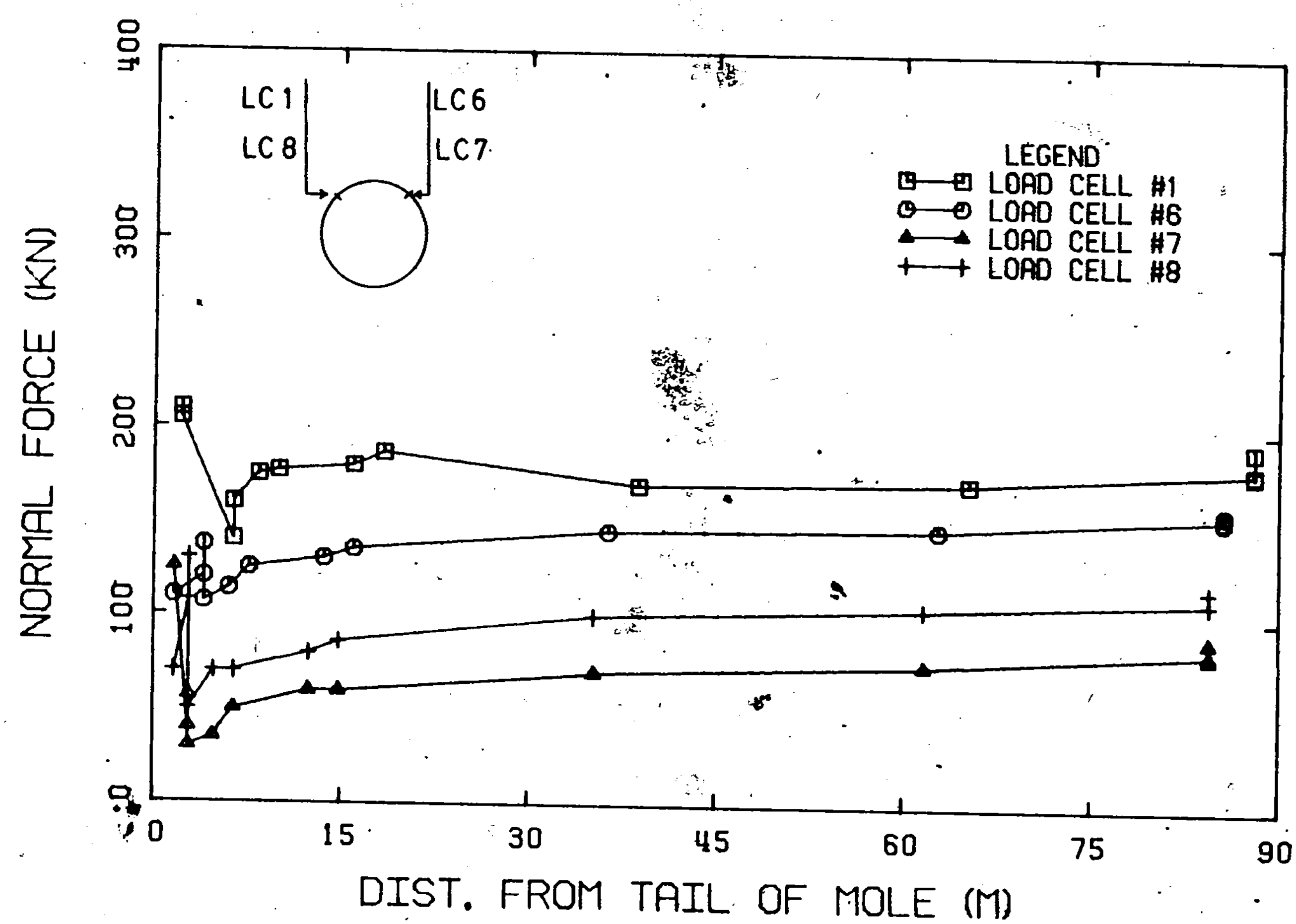

Figure 4.7 LOAD CELLS - UPPER JOINTS - LOAD VS DISTANCE FROM TAIL OF MOLE

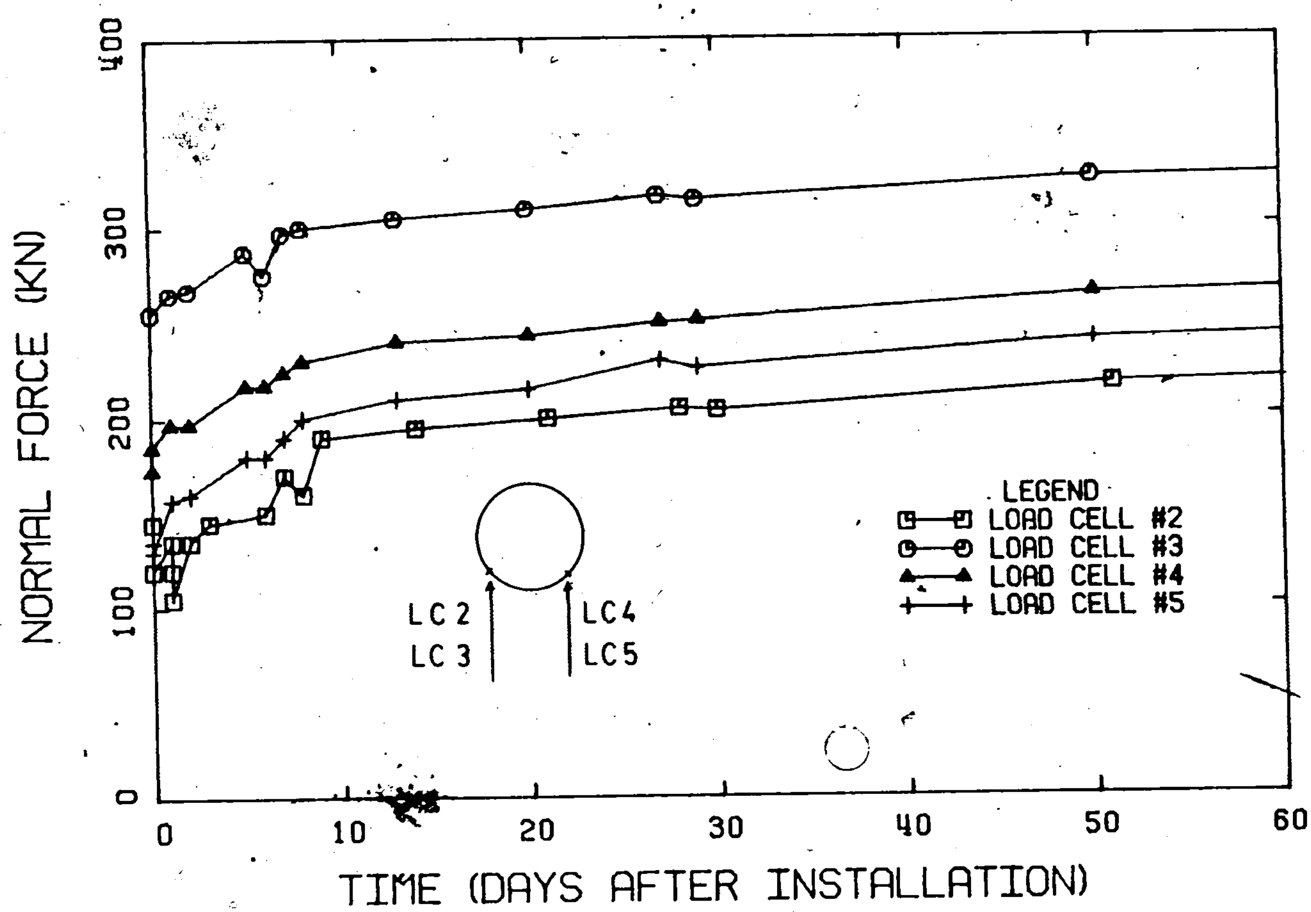

Figure 4.8 LOAD CELLS - LOWER JOINTS - LOAD VS TIME

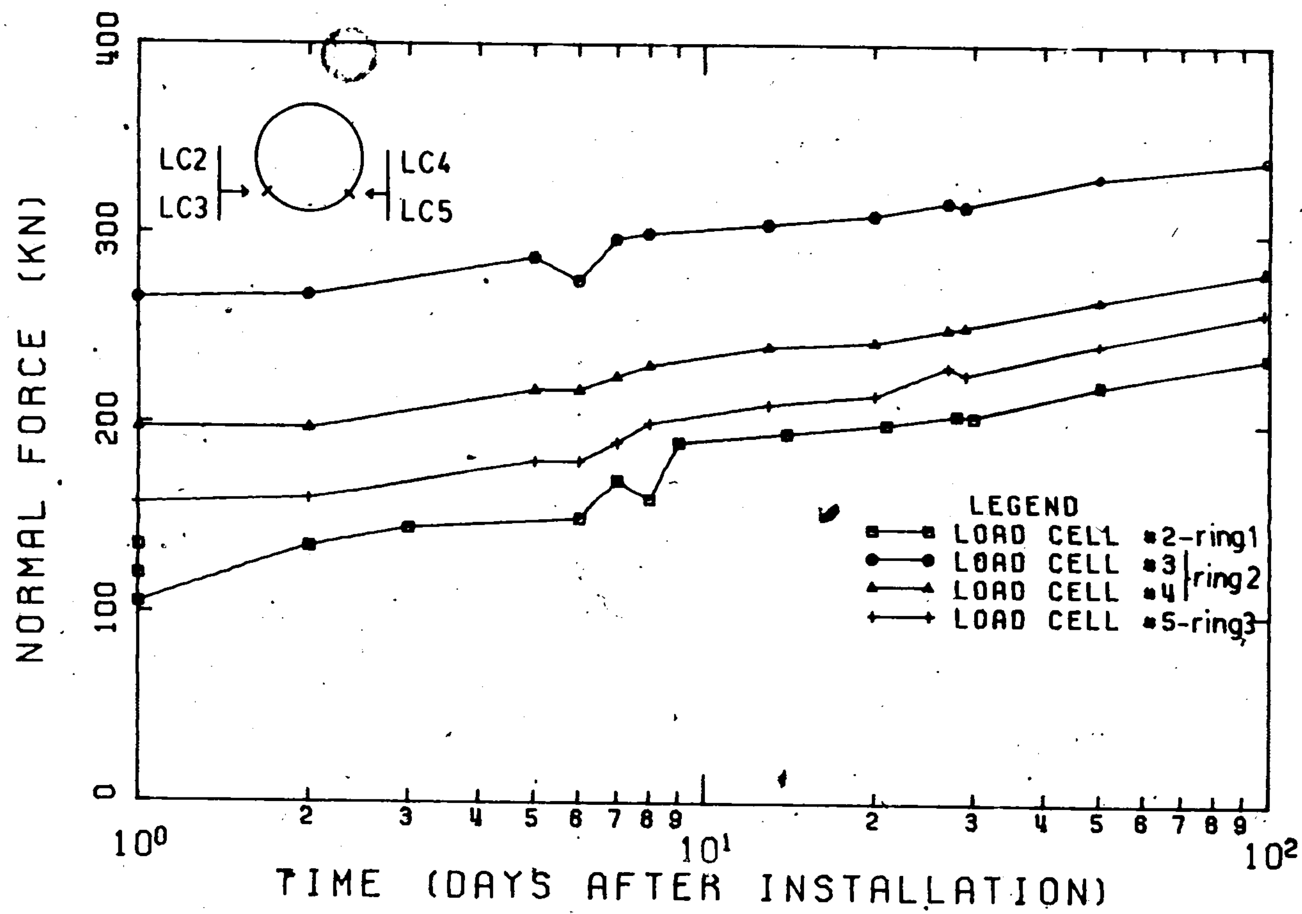

Figure 4.9 LOAD CELLS - LOWER JOINTS - LOAD VS LOG.TIME

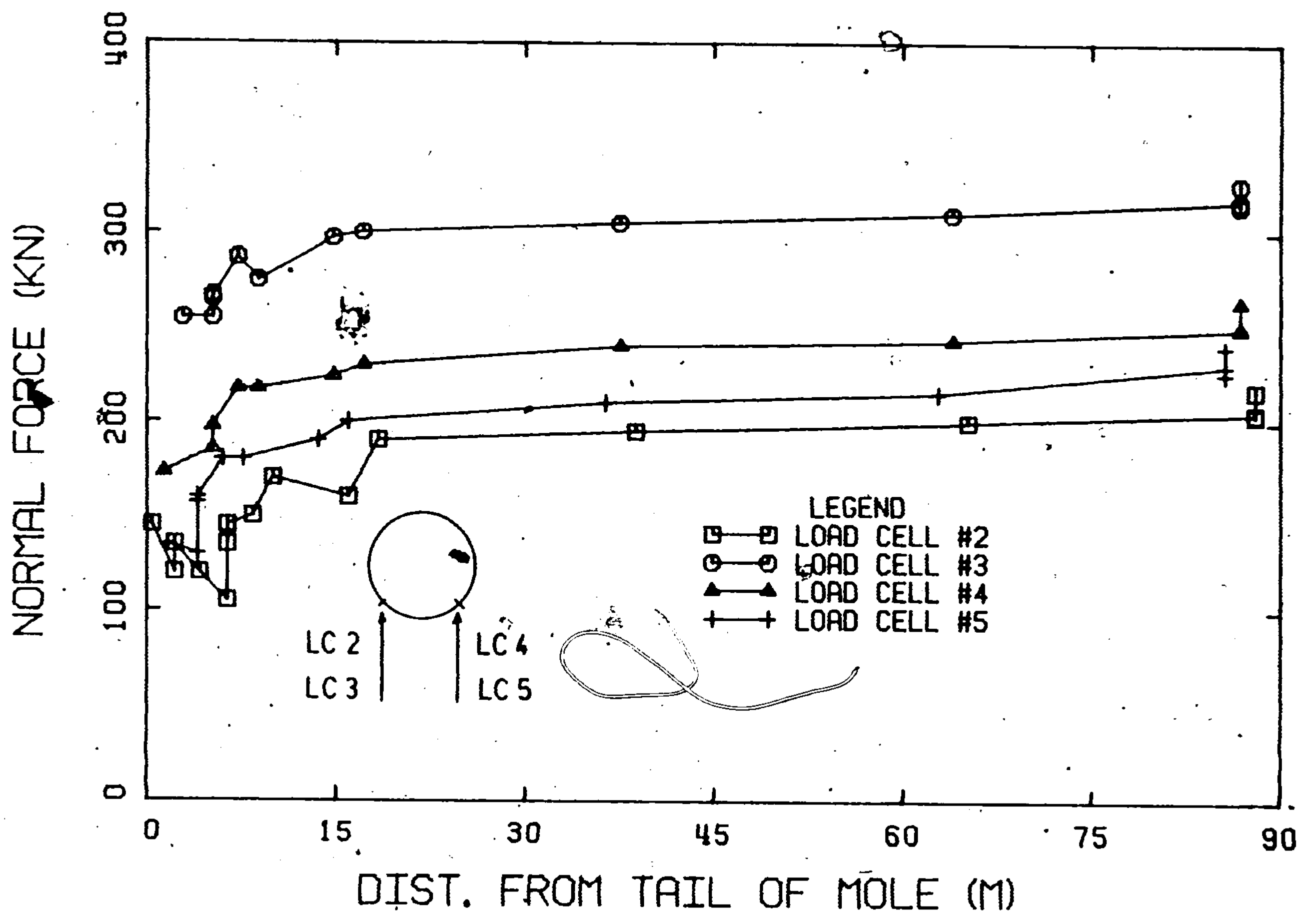

Figure 4.10 LOAD CELLS - LOWER JOINTS - LOAD VS DISTANCE FROM TAIL OF MOLE

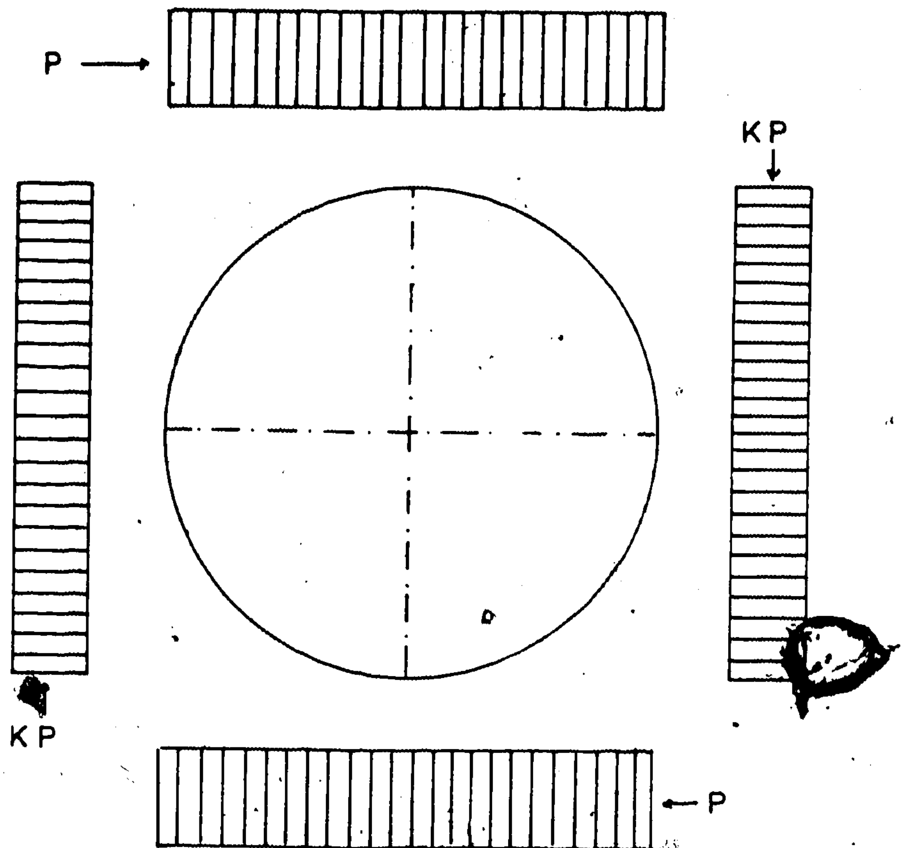

Figure 4.11 LOAD DISTRIBUTION AROUND TUNNEL LINERS: SYMMETRIC TO VERTICAL AND HORIZONTAL AXIS

cells installed in both upper and lower joints measure similar loads.

In the present study where the loads in the lower joints are significantly higher than those in the upper joints, a stress distribution taking into account the side friction along the tunnel walls seems to better explain the results, and does not complicate the analysis (many other more complex stress distributions could be used).

Figure 4.12 depicts the proposed stress distribution and it should be noted that, in this figure, the ratio between vertical and horizontal effective stresses after the tunnel construction was assumed to be unity, in order to simplify the solution.

Figure 4.13 presents the calculations carried out in order to obtain the relationship between measured loads in the upper and lower load cells and the stresses acting on the lining. These relationships are given below:

$$Rupper = 2.91p_c + 0.19p_i$$

$$Rlower = 2.91p_i + 0.19p_c \qquad 4.1$$

The meaning of each component of this equation is given in Figure 4.13.

Values of p_c and p_i (pressures at the crown and invert, respectively) can be found by substituting a pair of loads measured in the field (in the upper and lower joints) in equations 4.1.

A decision was made to study the stress distribution acting on the liner using load cell readings taken when the

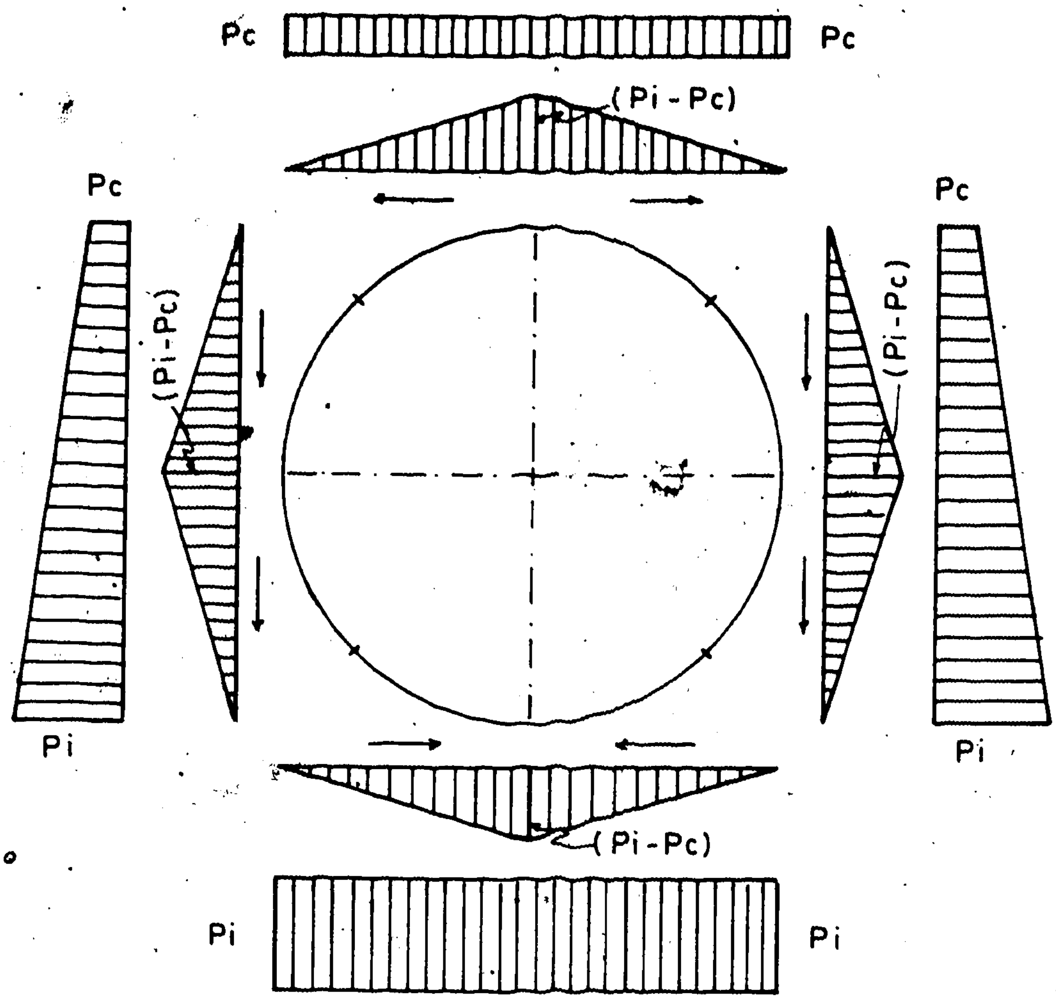

Figure 4.12 GROUND STRESS DISTRIBUTION ON STEEL RIBS TAKING INTO ACCOUNT SHEAR ALONG THE SOIL-LINER INTERFACE

UPPER JOINT

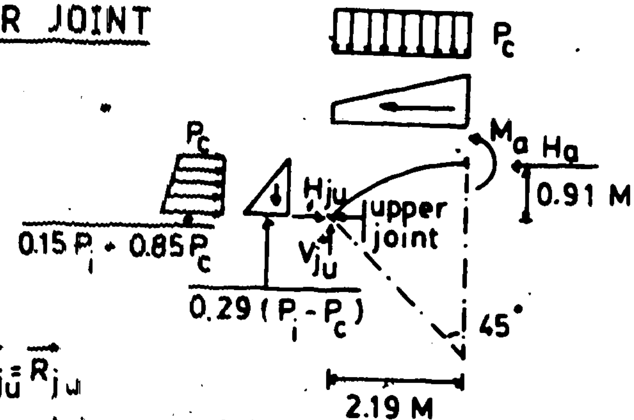

$\vec{V}_{ju} + \vec{H}_{ju} = \vec{R}_{ju}$

R_{ju} = load in upper joint

ASSUMPTIONS:

- SYMMETRY WITH RESPECT TO THE VERTICAL AXIS ($V_a = 0$)
- JOINTS DO NOT CARRY SHEAR FORCE AND BEND/ MOMENTS ($V_{ju} = H_{ju}$, $M_{ju} = 0$)

VERTICAL EQUILIBRIUM:

$$P_c\ 2.19 + \frac{0.29(P_i - P_c)\ 0.91}{2} = V_{ju}$$

$$\left.\begin{array}{l} 2.06\ P_c + 0.13\ P_i = V_{ju} \\ R_{ju} = \sqrt{2}\,.V_{ju} \end{array}\right\} \boxed{R_{ju} = 2.91\ P_c + 0.19\ P_i}$$

LOWER JOINT

$\vec{V}_{jl} + \vec{H}_{jl} = \vec{R}_{jl}$

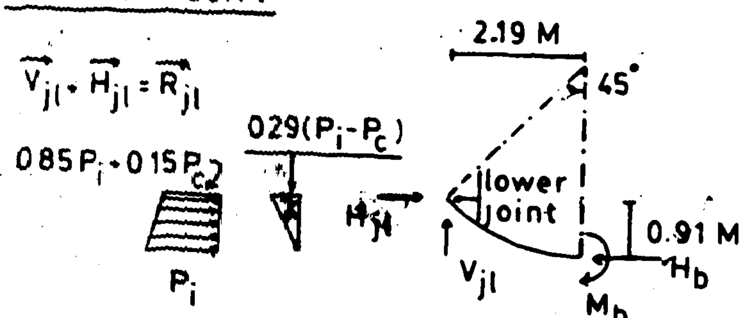

ASSUMPTIONS:

- $V_b = 0$
- $V_{jl} = H_{jl}$
- $M_{jl} = 0$

R_{jl} = load in lower joint

VERTICAL EQUILIBRIUM:

$$P_i\ 2.19 - \frac{0.29(P_i - P_c)\ 0.91}{2} = V_{jl}$$

$$\left.\begin{array}{l} 2.06\ P_i + 0.13\ P_c = V_{jl} \\ R_{jl} = \sqrt{2}\ V_{jl} \end{array}\right\} \boxed{R_{jl} = 2.91\ P_i + 0.19\ P_c}$$

Figure 4.13 EQUILIBRIUM EQUATIONS FOR THE LOAD DISTRIBUTION OF FIG 4.12

shield tail was 36.4 metres away. This distance was found to be convenient because, at this distance from the shield, the sections studied were considered to be far enough to avoid mole jacking effects and close enough to minimize the time dependent soil behavior effects on the lining pressure. Readings of load cells taken at approximately 36.4m away from the mole took place within 14 days of their installation.

Due to the fact that the use of Equations 4.1 requires load measurements in the upper and lower joints at the same ring and that not all instrumented rings had load measured in both upper and lower joints, it was proposed that the study of pressure distribution on the lining be carried out by combining the data obtained from two adjoining instrumented rings. By doing so, stress distributions can be obtained by combining loads measured in the upper and lower joints of rings 1 and 2, rings 2 and 3 and rings 3 and 4 (figure 4.3).

The values of load cell readings at 36.4m away from the mole and values of p_c and p_L obtained from the solution of Equations 4.1 are presented in Table 4.2.

4.4.2 Steel Lagging

The instrumentation and study of the lagging in the LRT tunnel primary lining was not only important from the research point of view, but also from an economic point of view since an increase in the originally specified timber

Load cell no.	Load* (kN) at 36.4 from shield
1	172.00
2	194.41
3	304.71
4	239.41
5	210.00
6	145.00
7	70.23
8	100.23

* Values linearly interpolated from readings (See Tables C6 to C13 in Appendix C)

STUDIED RINGS	COMBINED LOAD CELLS	P_{crown} (kN/m^2)	** P_{invert} (kN/m^2)
RING 1	#1 & #2	45.83	52.49
AND	#1 & #3	43.76	84.21
RING 2	#1 & #4	44.98	65.43
RING 2	#6 & #3	35.99	84.75
AND	#6 & #4	37.22	65.97
RING 3	#6 & #5	37.77	57.51
RING 3	#6 & #5	37.77	57.51
AND	#7 & #5	16.26	59.00
RING 4	#8 & #5	24.89	58.40

** 1.2m rib spacing already considered

Table 4.2 LOADS ACTING ON THE STEEL RIBS AT 36.4M FROM THE SHIELD TAIL lagging length would yield an increase in [illegible] advance rate and a decrease in the number of steel [illegible] required, thus resulting in an overall cost decrease.

The pressure acting on the timber l[illegible] be obtained by installing pressure cells at th[illegible] between the ground and lagging but this procedu[illegible] disregarded due to reasons discussed in Sec[illegible]

It was then decided to obtain ground l[illegible] by monitoring lagging strains and con[illegible] to pressures by back calcula[illegible]

Three problems had [illegible] at this [illegible]

- the difficulty of obtaini[illegible] and reproducible strain measurement[illegible]
- the variability of timber prope[illegible]
- how to separate the deformation[illegible] the mole advance from those caused [illegible] of the ground.

The first two probl[illegible] can be avo[illegible] ring strains in steel pieces of lagging, constru[illegible] the same bending stiffness as timber, and th[illegible] making these special instrumented pieces of [illegible] slightly shorter than the standard 121.92cm length.

4.4.2.1 Steel Lagging Design Details

According to the specifications for th[illegible] lining, the wooden lagging should consist of spr[illegible] equivalent material having an allowable bending fibre [illegible] not less than 6895 KN/M². Its dimensions should be

- section 100x150 (mm)
- length 121.92cm

The 150mm cross-sectional dimension should be placed against the soil.

Three pieces of timber lagging were brought to the University laboratory and loaded in bending by applying equal concentrated loads at the one-third points of the 152.4cm span (it was decided to test longer timbers than the ones that were being used in the early stages of the construction) and the central deflection versus load was recorded in order to obtain the average flexural rigidity. The flexural rigidity (EI) was found to be 105.61KN.m² and the modulus of elasticity (E) 7929.25MN/m².

It can be concluded that steel pieces of lagging with a flexural rigidity of 105.61KN.m² should be built in order to replace the original timber lagging.

Twelve pieces of lagging were made according to Figure 4.14 and the steel section HSS 5x2x0.188 was the best available, at that time, that would satisfy the requirements. The relevant mechanical properties of the beam section chosen are presented in Figure 4.14.

Weldable Ailtech electric strain gauges, Model SG129, were attached to the face of the steel lagging, facing the tunnel axis, in three locations in order to enable the evaluation of the ground stress distribution along the length of the beam. A piece of steel lagging is shown on

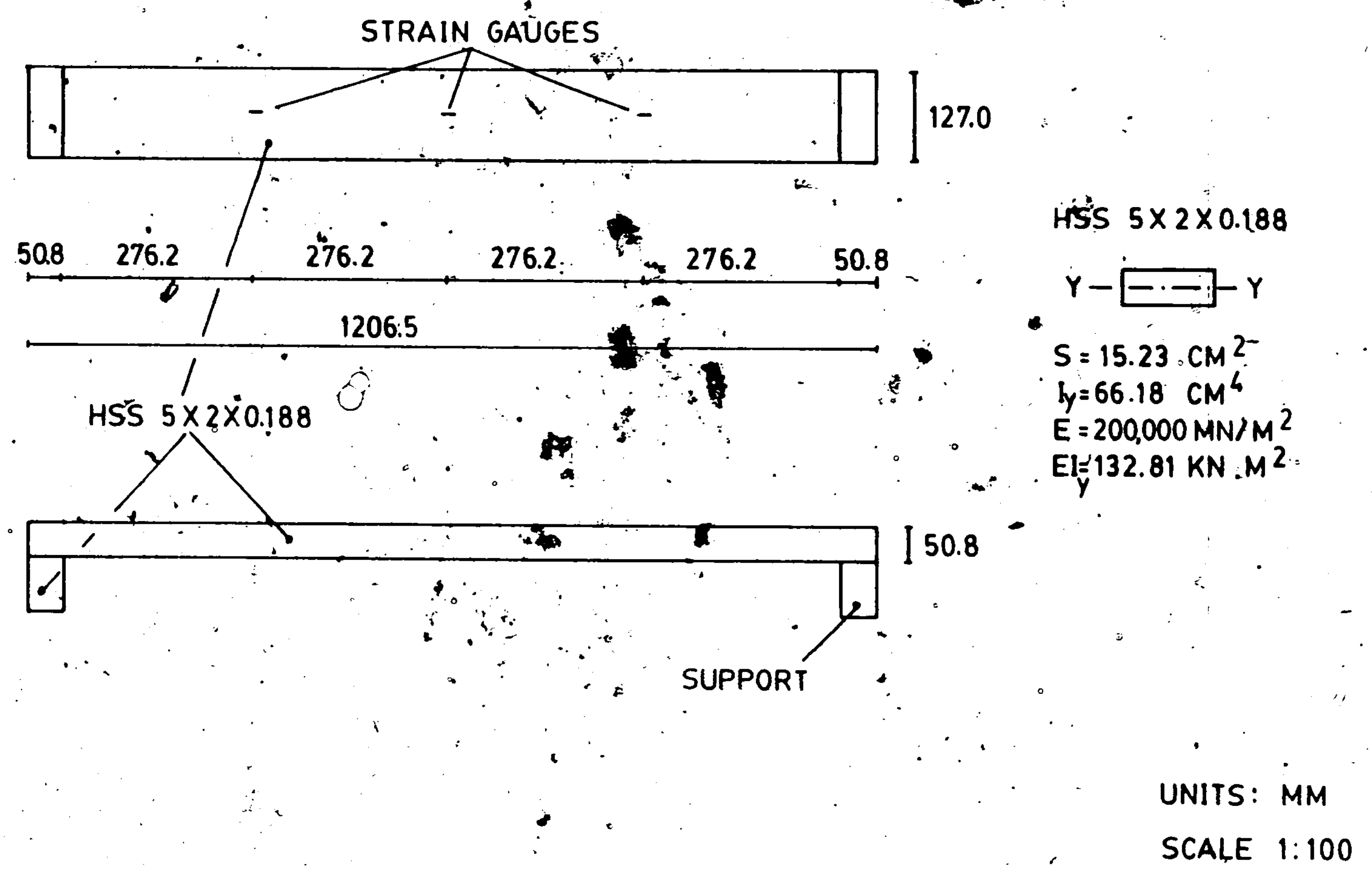

Figure 4.14 STEEL LAGGING DESIGN DETAILS

Plate 4.3.

4.4.2.2 Steel Lagging Calibration Tests

Calibration tests were carried out on each of the twelve pieces of steel lagging. Tests were carried out on a Baldwin Universal Testing Machine where the HSS 5x2x0.188 test beams were loaded in bending by applying equal concentrated loads at the one-third points of the 110.48cm free span.

Due to time constraints, strain readings during the calibration tests were taken from all three gauges only for piece SL10 while for the other beams readings were taken only at the centre strain gauge. Strains were measured with the strain indicator produced by Automation Industries Inc. The calibration test results are presented in Tables C14 to C19 in Appendix C.

As expected, the strain readings along the length of test beam SL10 were proportional to bending moment. The strains can also be expected to be proportional to bending moments for the other beams.

The inclination of the loading portion of the calibration curves were practically the same for all beams with a mean value of 6410KN.m (Fig 4.15). From this mean calibration curve, the empirical flexural rigidity of the 12 test beams can be evaluated.

For a beam under bending:

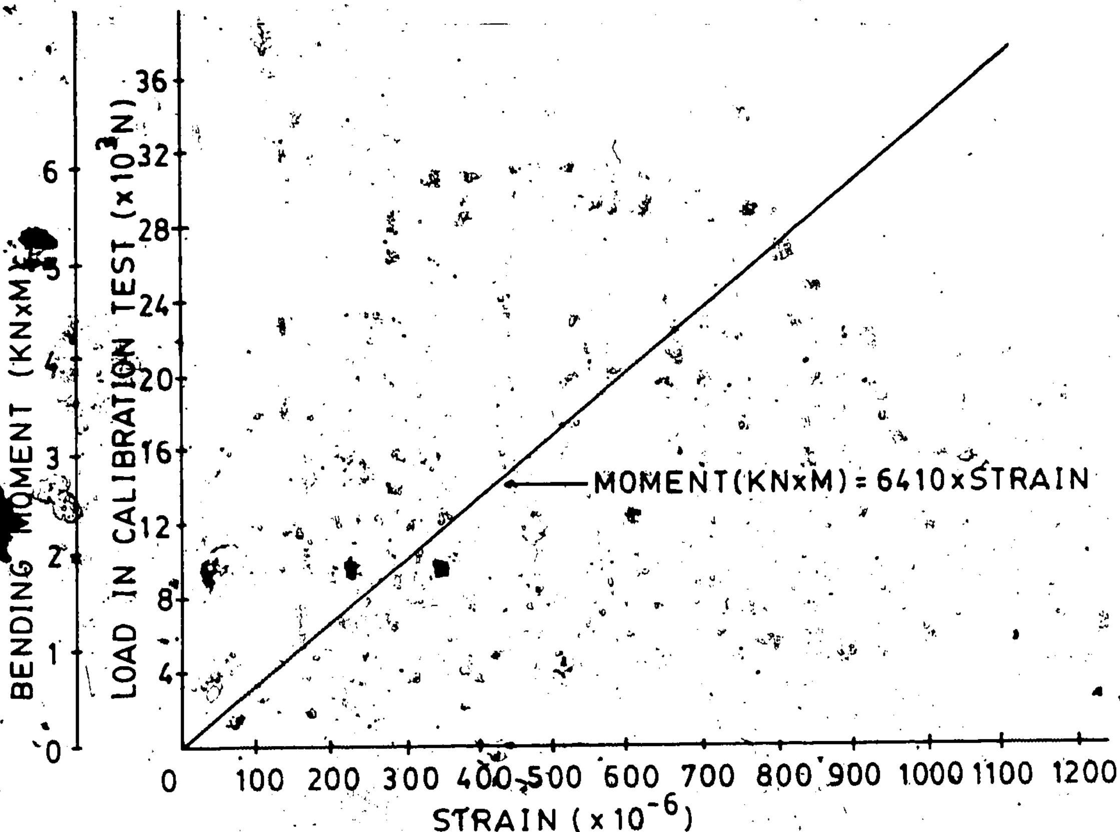

Figure 4.15 STEEL LAGGING - MEAN CALIBRATION CURVE

Plate 4.3 STEEL LAGGING DETAIL

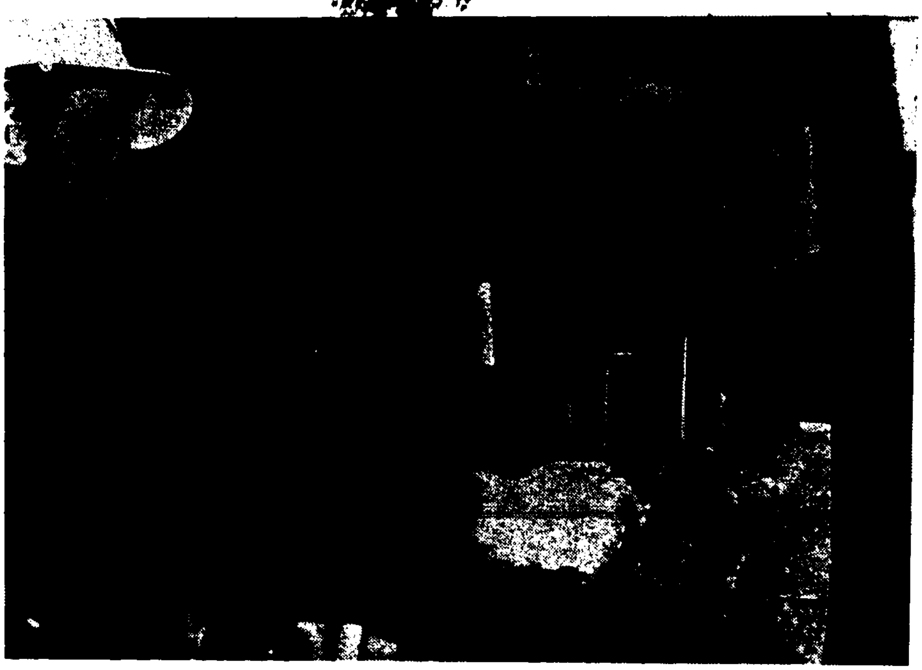

Plate 4.4 STEEL LAGGING INSTALLATION

$$\varepsilon = M.y/E.I$$

where ε = strain

M = bending moment

EI = flexural rigidity

y = 0.0254m

thus: $EI = \frac{M}{\varepsilon}\, 0.0254$

For M/ε = 6410KN.m EI = 162.81 KN.m²

which is different from the tabulated one: 132.81KN.m².

It can be concluded that the test beams have a flexural rigidity 54% higher than anticipated.

Corrections have been made to the field data in order to analyse them.

4.4.2.3 Steel lagging Installation

The pieces of steel lagging were placed in position 1, position 2 and position 3 as shown on Figure 4.16

Position 1 was located between rings 1 and 2 where load cells #1, #2, #3 and #4 were installed (see Figure 4.17), position 2, between rings 2 and 3 and position 3 between rings 3 and 4. In each of these positions, four pieces of lagging were installed. They were placed in positions that would enable the monitoring loads in most significant

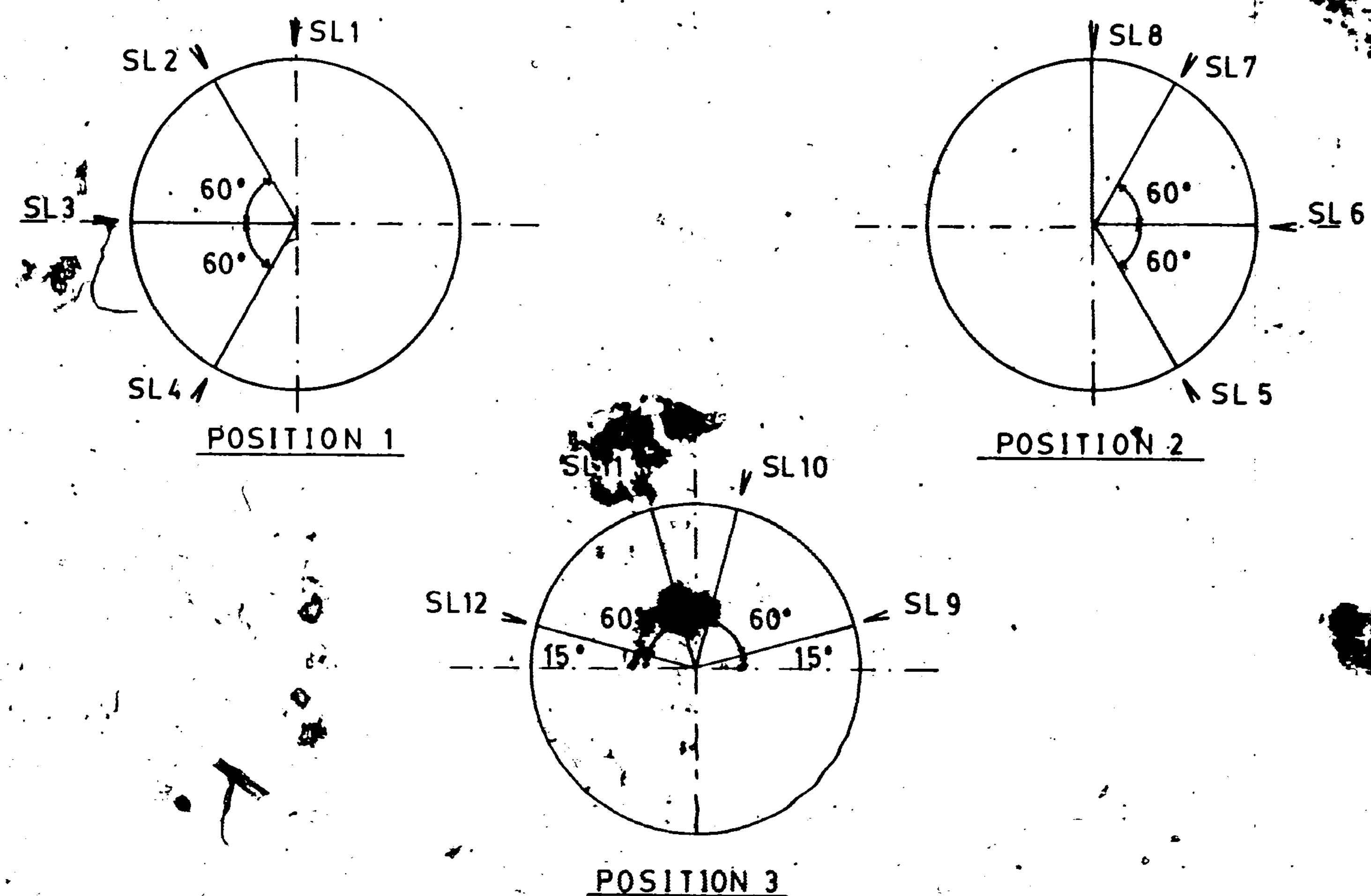

Figure 4.16 STEEL LAGGING LOCATION

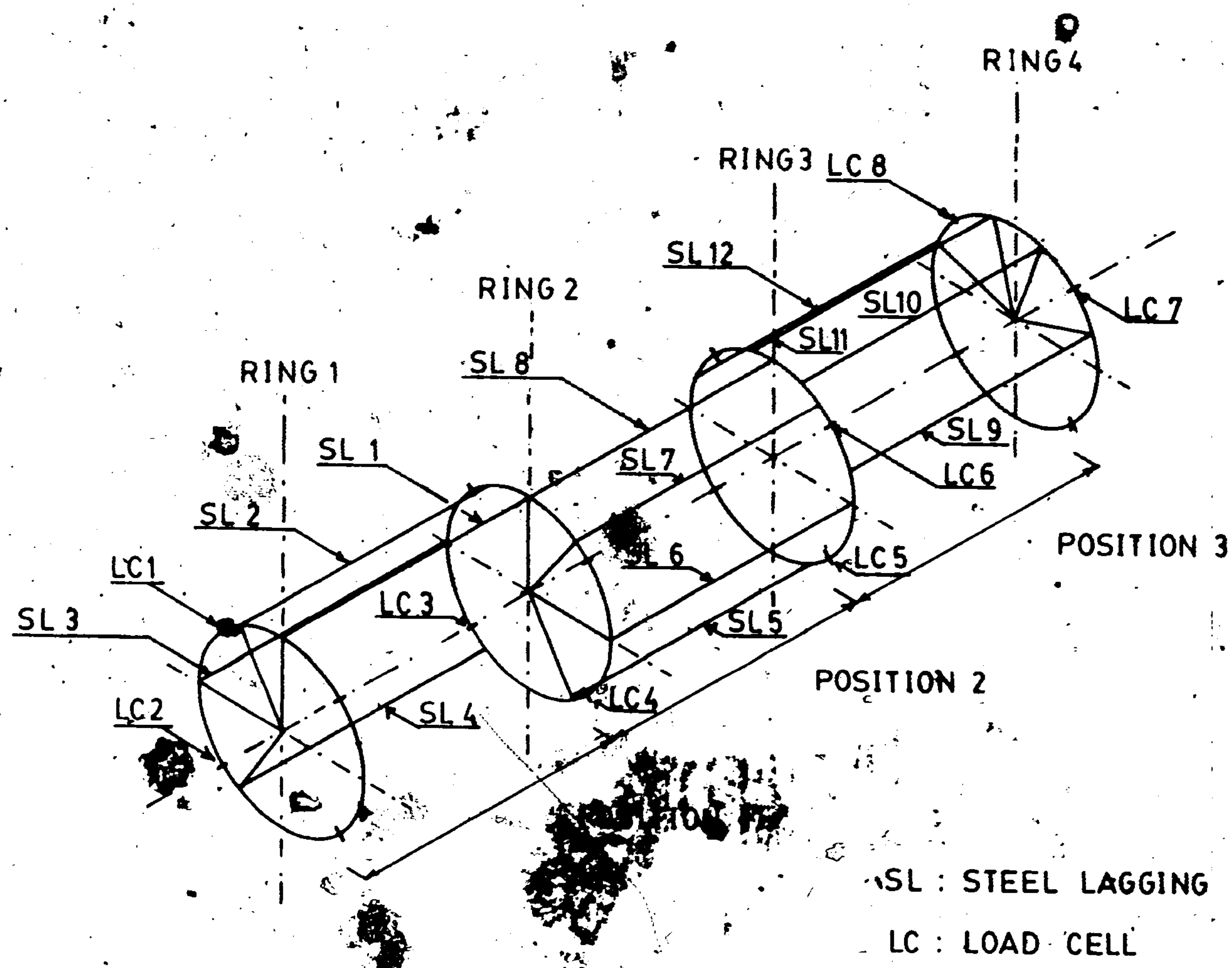

Figure 4.17 SL AND LC RELATIVE POSITION

portions of the circumference. No steel lagging was placed at the invert because this region was being used as the base for the tracks for the muck cars.

The pieces of lagging were installed soon after the erection of the steel ribs within the shield (Plate 4.4). The ribs were erected at a distance, from the previous installed ribs, slightly larger than the standard 121.92cm spacing, in order to facilitate the lagging installation.

During the steel lagging installation, a space was left between adjacent timbers by using four pieces of wood (1cm thick and 3cm wide), two at each side of the contact, to minimize side friction and to allow the measurement of overcore closure.

4.4.2.4 Measurement Procedure

Strains in the steel lagging strain gauges were measured with the read-out unit produced by Automation Industries Inc.

Zero readings from the steel lagging were taken immediately after installation, when the pieces of lagging were within the shield. The first reading following the zero reading, after installation, was taken when the steel lagging was between 1 and 3 metres from the shield tail. It was not possible to record the strains more frequently at this stage because other readings had to be taken and other instruments had to be installed simultaneously.

Strains were read for the three strain gauges of each piece of steel lagging and recorded in the field sheet presented in Figure 4.18. As the tunnel had its axis in the EAST-WEST direction, strain gauges from each piece of lagging were given the letters E (east), C (centre) and W (west).

At least four sets of readings were taken for all pieces of steel lagging, when they were within one diameter of distance from the shield tail.

4.4.2.5 Field Data

The data recorded in the field is tabulated in Tables C20 to C25 presented in Appendix C.

The strains were plotted versus time and versus distance from shield tail and are presented in figures 4.19 to 4.30.

In all figures and tables referring to the steel lagging data, the term "DISTANCE FROM TAIL OF MOLE" means the distance from the end of the steel lagging, that first leaves the shield, to the tail of the mole (shield).

In some cases, strains could not be properly recorded due to the mal-functioning of the connectors attached to the strain gauges.

Data from the steel lagging occupying the same relative position along the perimeter of the tunnel wall, were plotted in the same graph.

PIECE OF LAGGING #

DATE	DIST. TAIL	ΔE			ΔM			COMMENTS
		E	C	W	E	C	W	

PIECE OF LAGGING #

DATE	DIST. TAIL	ΔE			ΔM			COMMENTS
		E	C	W	E	C	W	

Figure 4.18 STEEL LAGGING FIELD SHEET

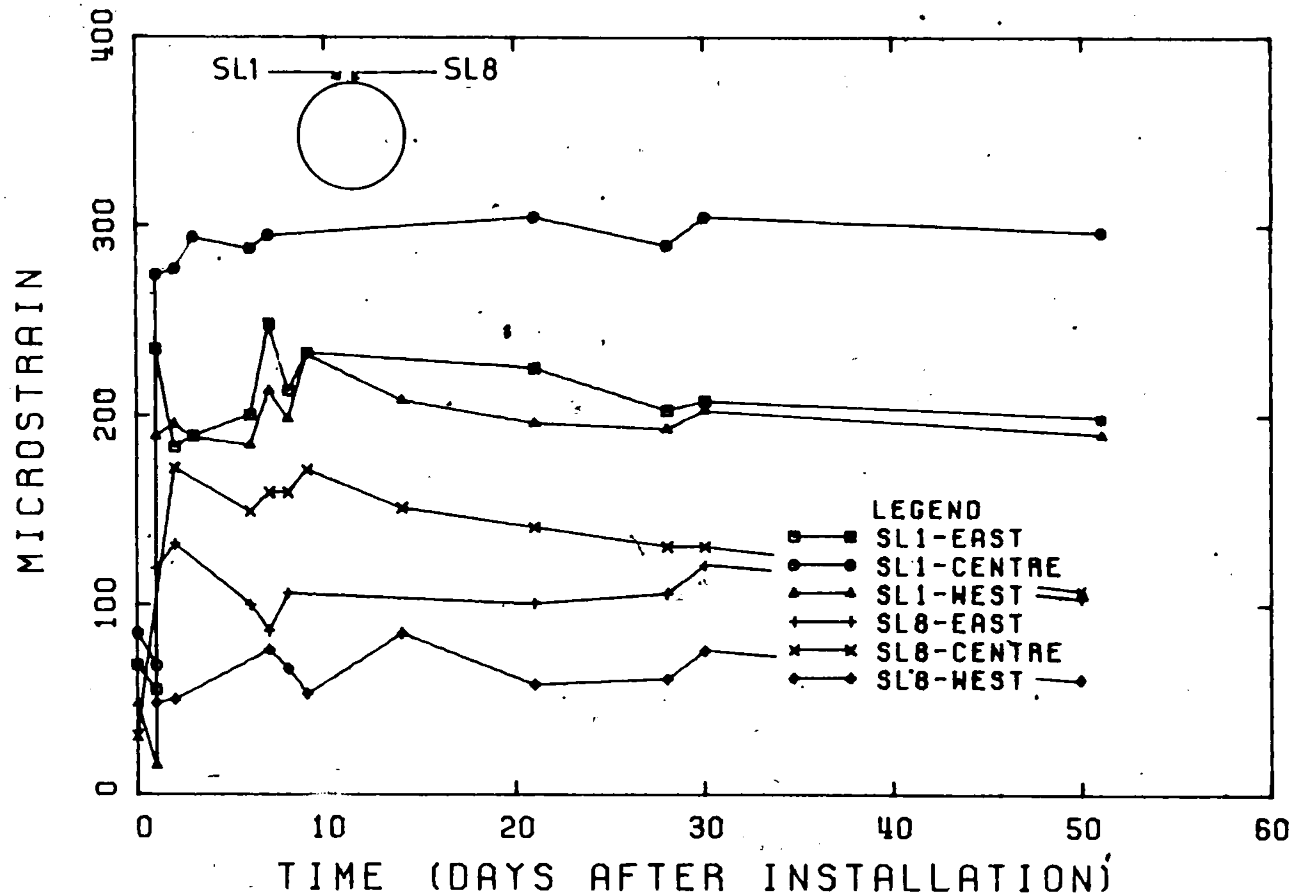

Figure 4.19 STEEL LAGGING - #1 AND #8 - STRAIN VS TIME

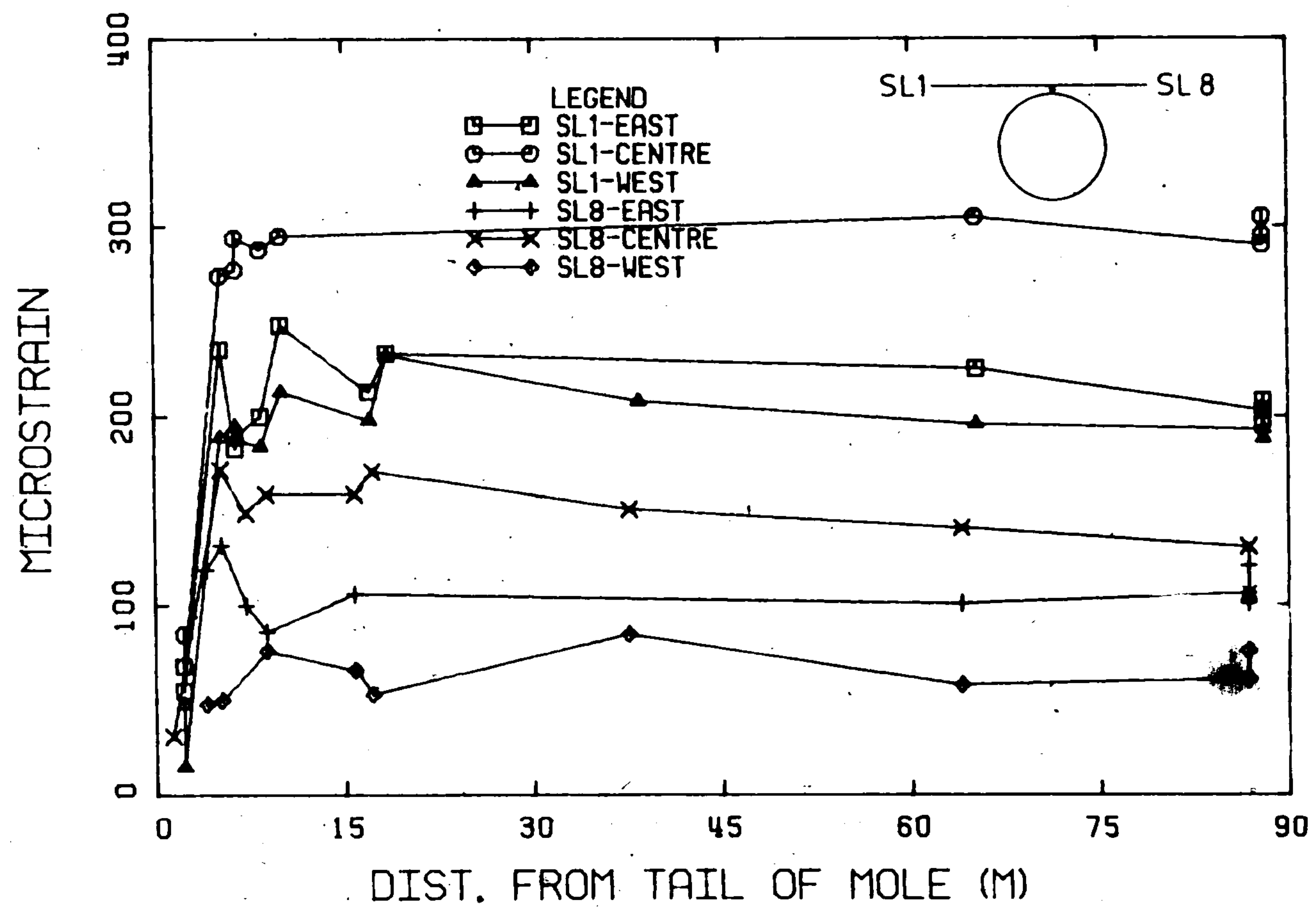

Figure 4.20 STEEL LAGGING - #1 AND #8 - STRAIN VS DIST. FROM TAIL OF MOLE

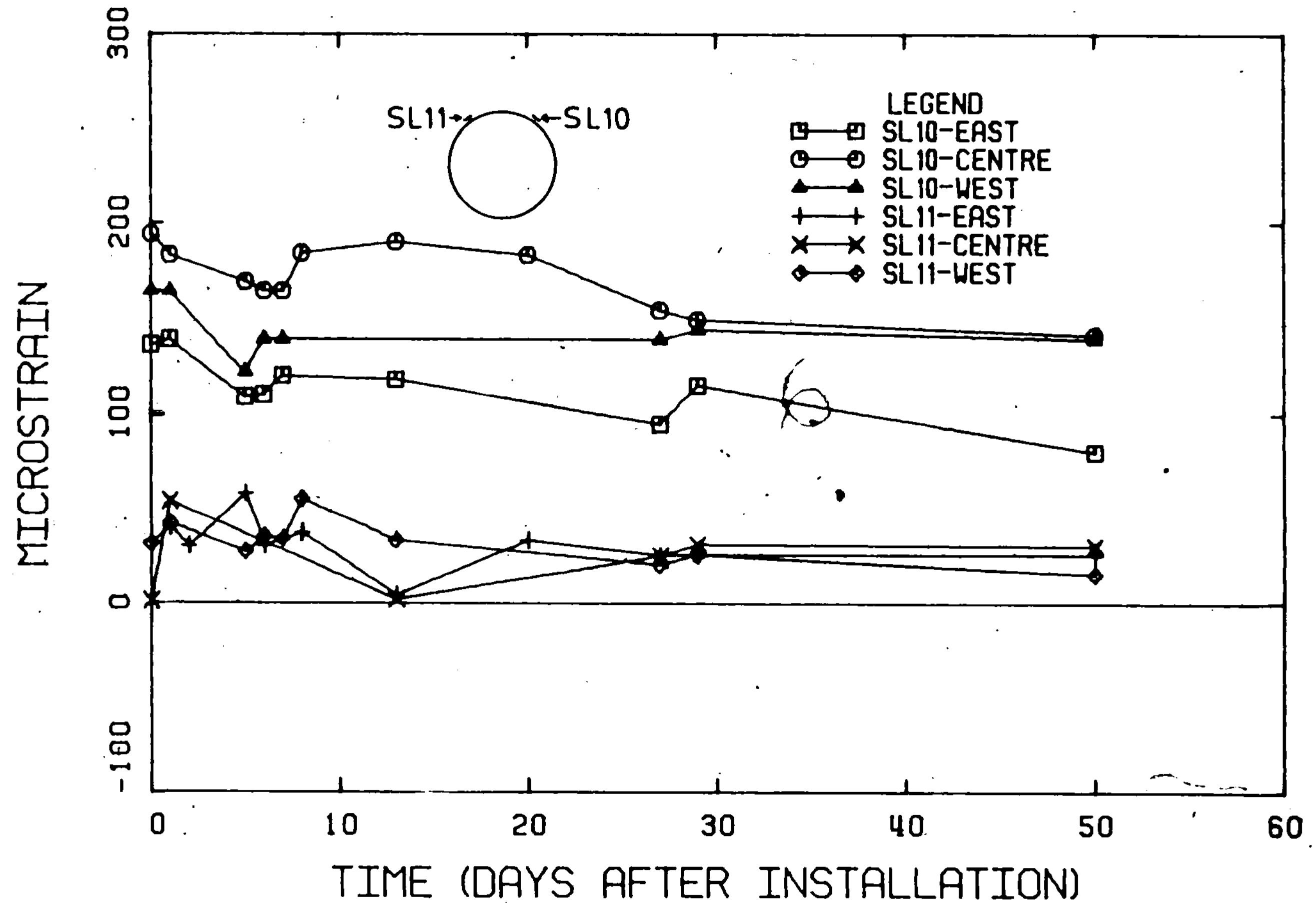

Figure 4.21 STEEL LAGGING - #10 AND #11 - STRAIN VS TIME

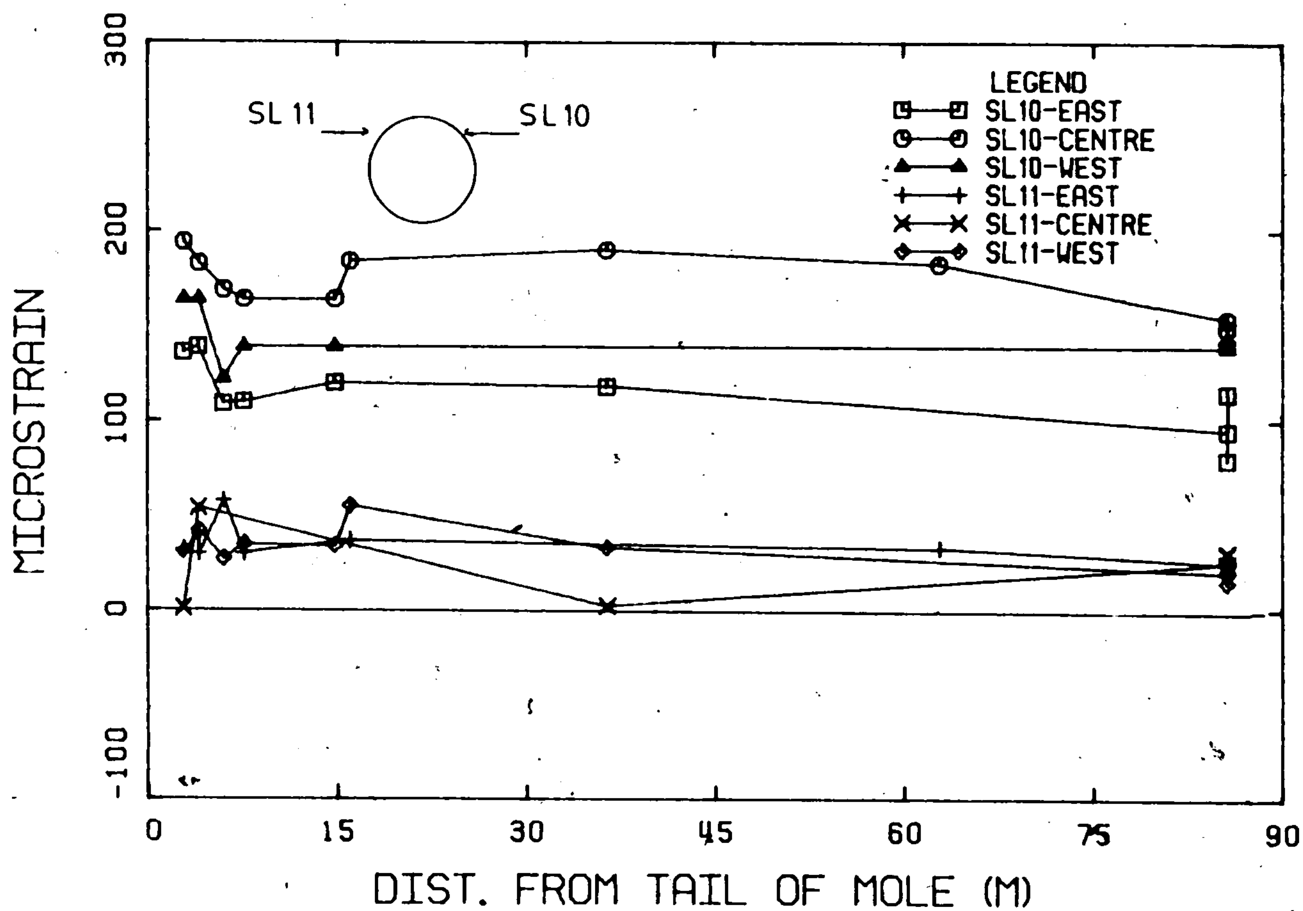

Figure 4.22 STEEL LAGGING - #10 AND #11 - STRAIN VS DIST. FROM TAIL OF MOLE

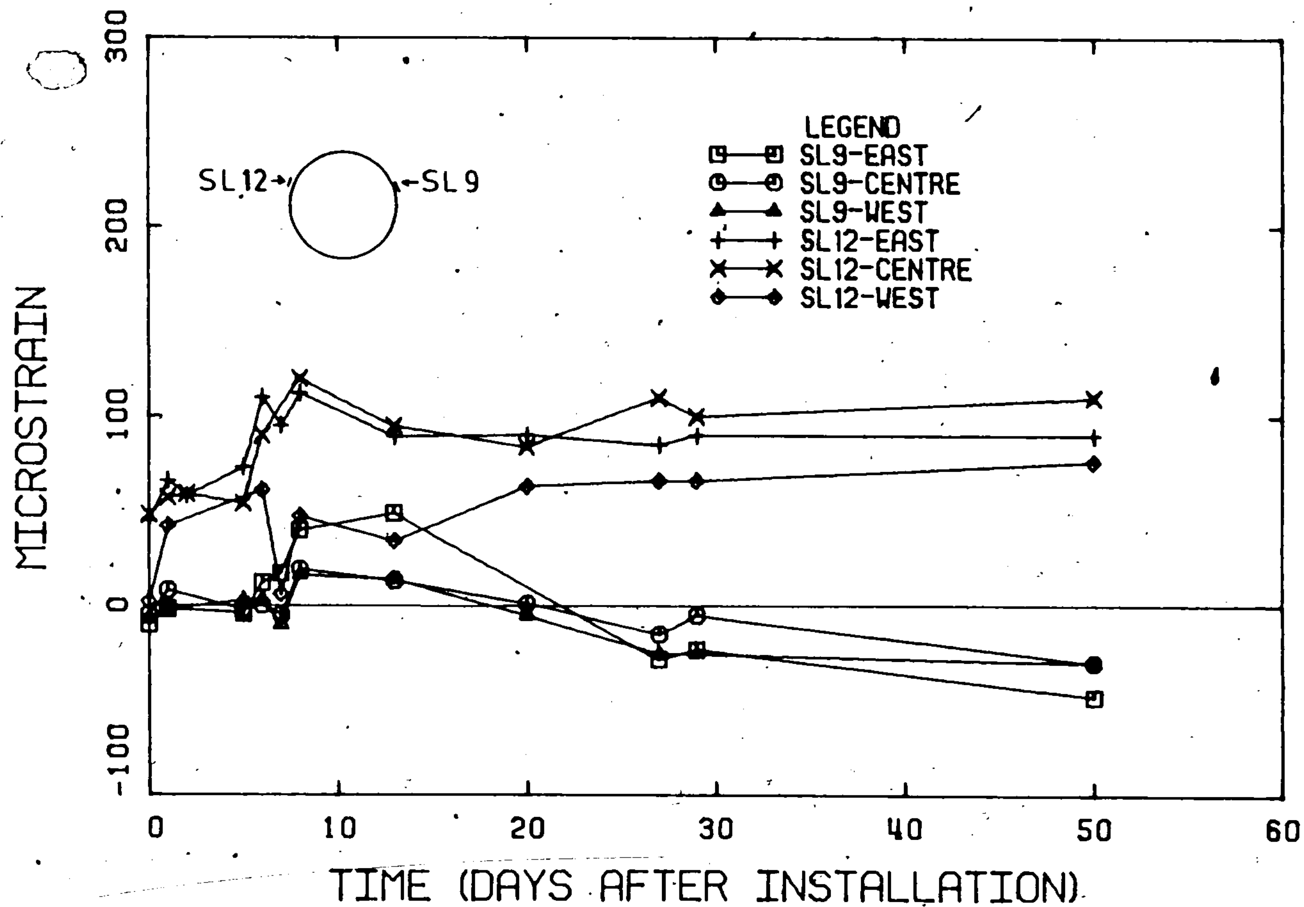

Figure 4.23 STEEL LAGGING - #9 AND #12 - STRAIN VS TIME

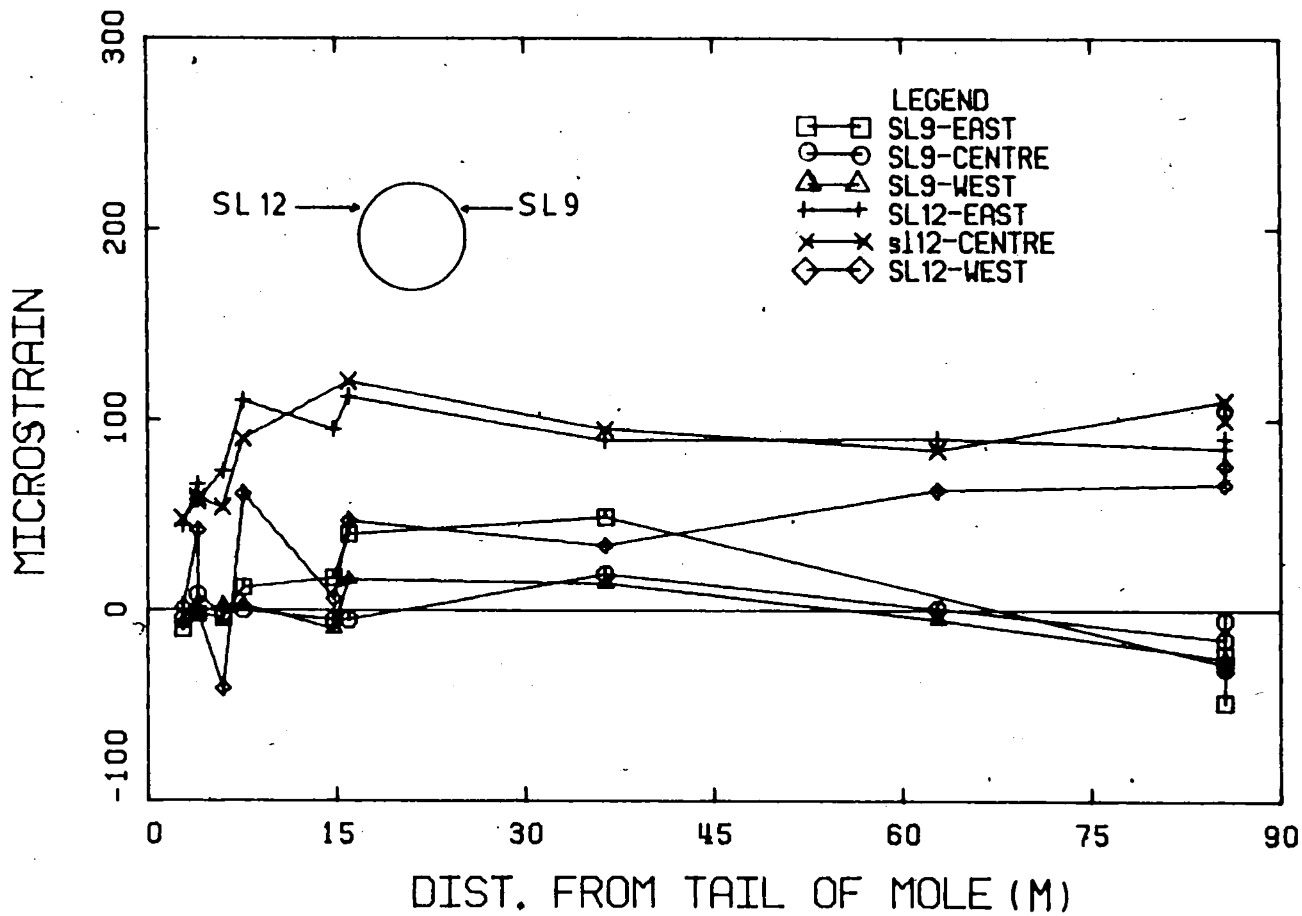

Figure 4.24 STEEL LAGGING - #9 AND #12 - STRAIN VS DIST. FROM TAIL OF MOLE

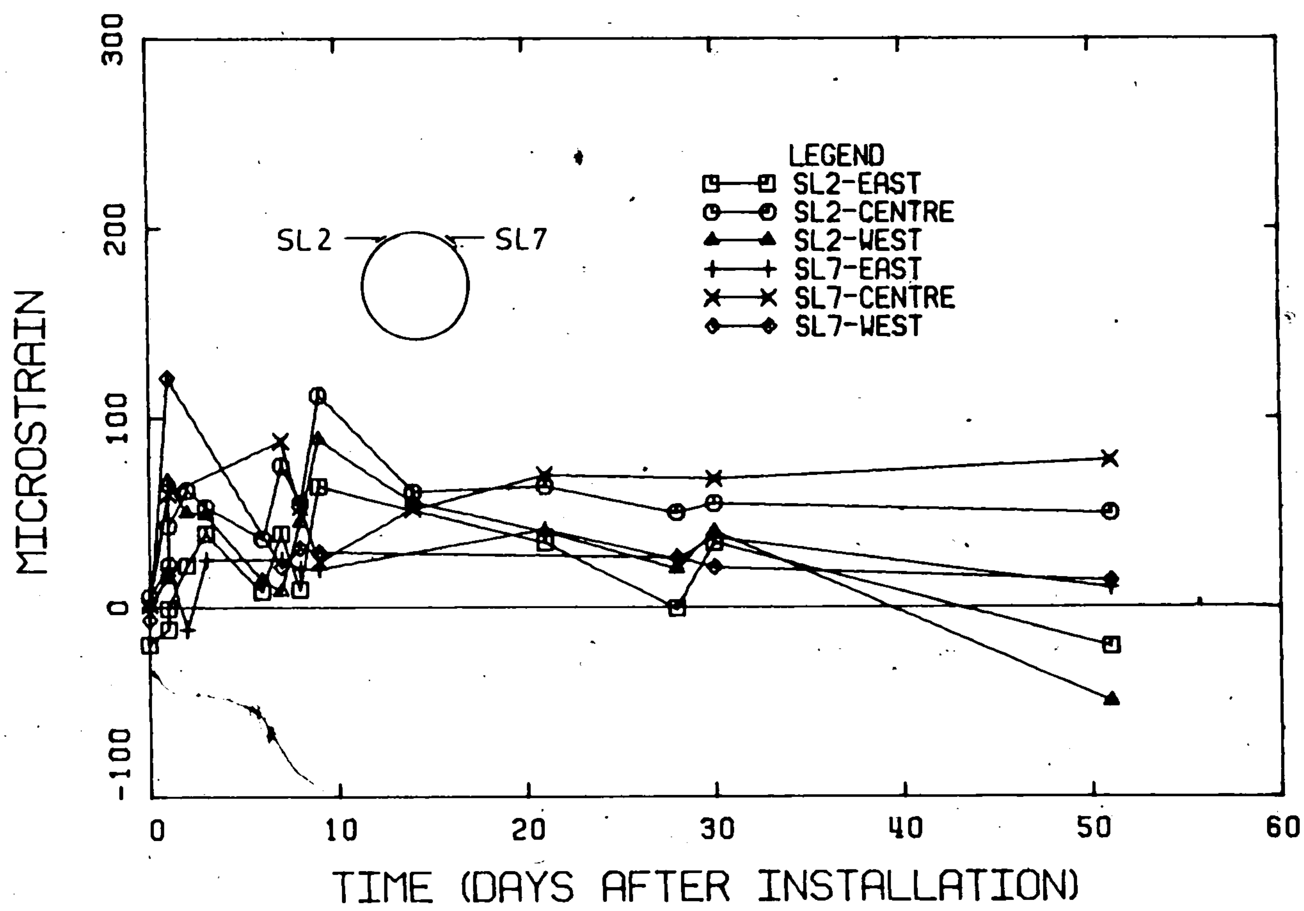

Figure 4.25 STEEL LAGGING - #2 AND #7 - STRAIN VS TIME

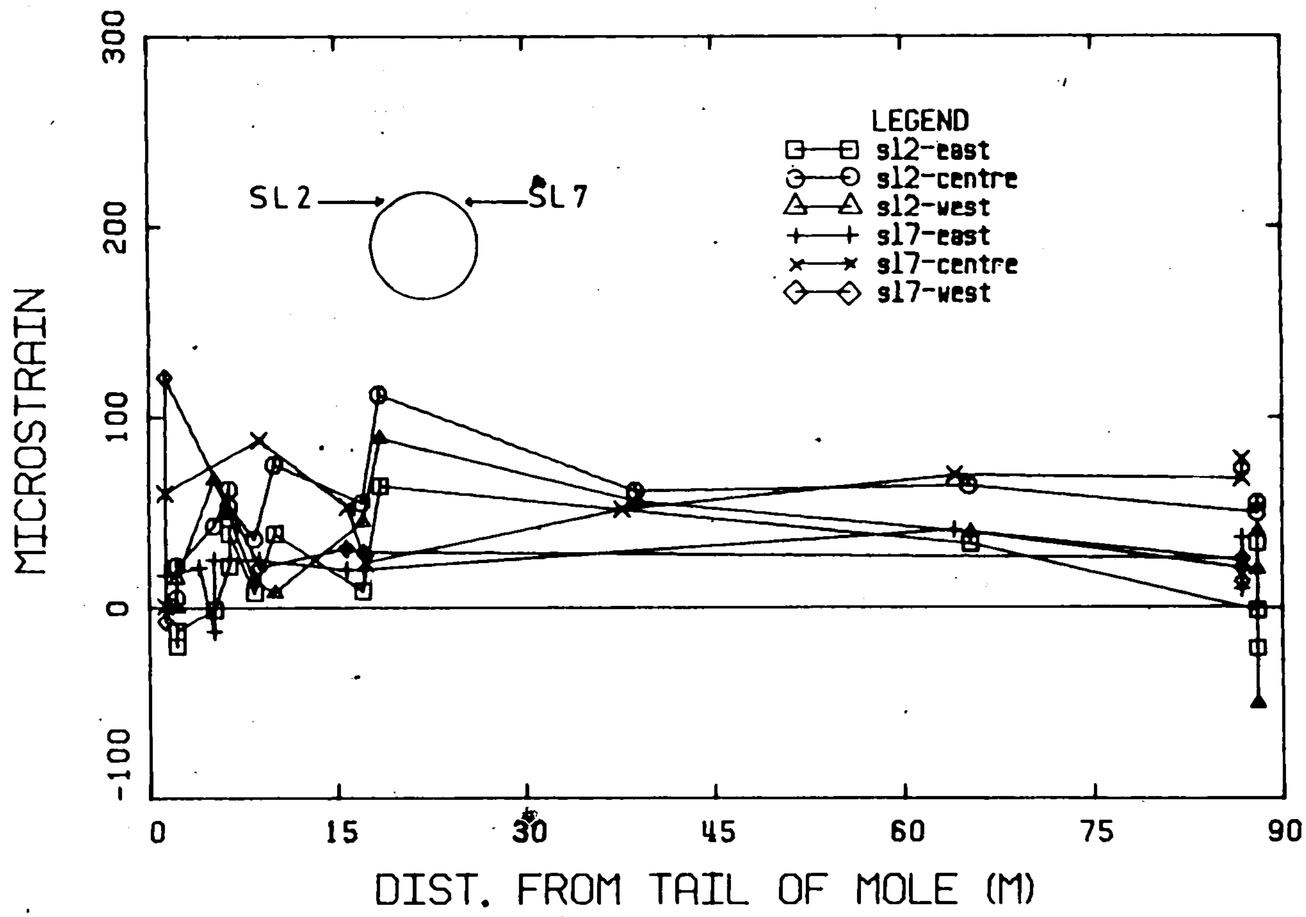

Figure 4.26 STEEL LAGGING - #2 AND #7 - STRAIN VS DIST. FROM TAIL OF MOLE

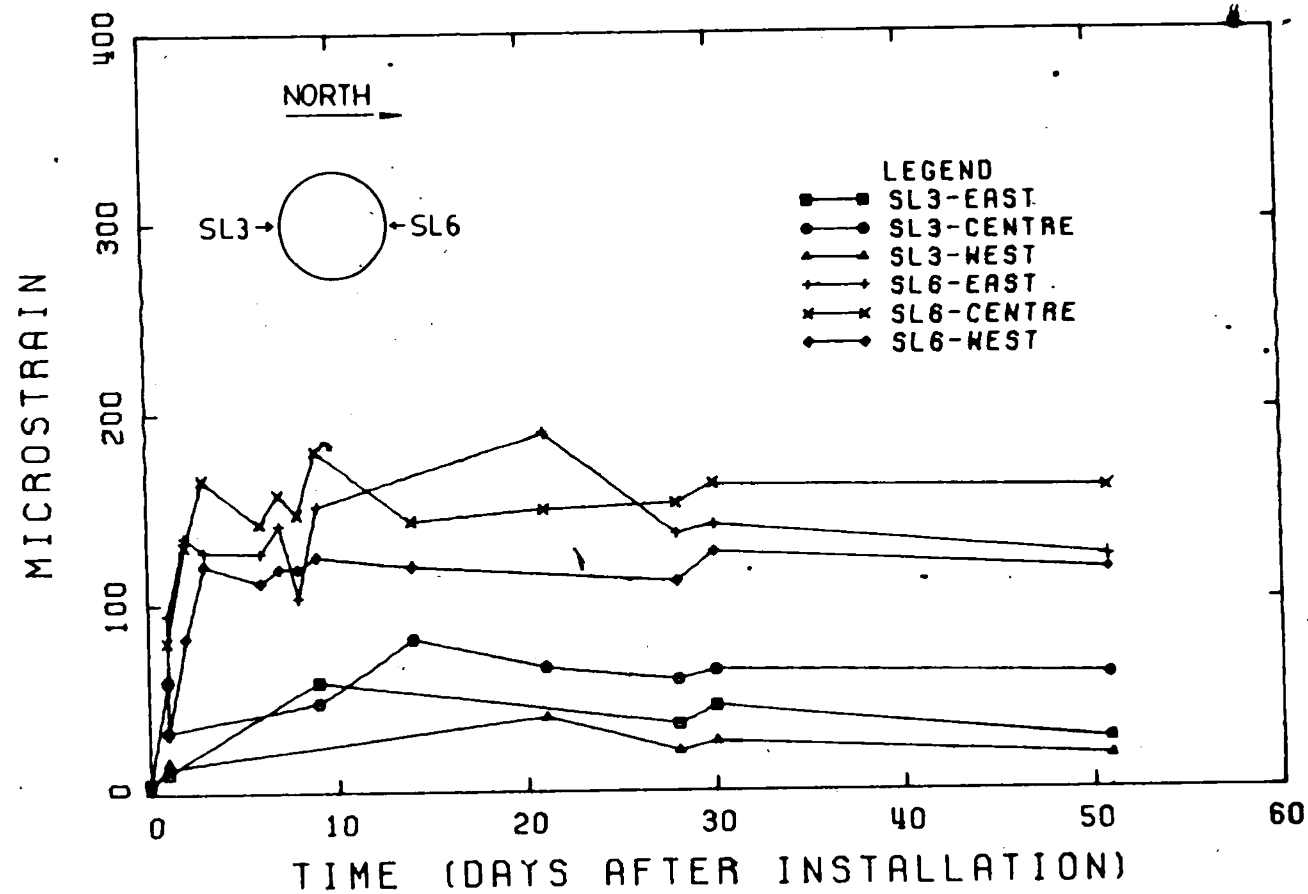

Figure 4.27 STEEL LAGGING - #3 AND #6 - STRAIN VS TIME

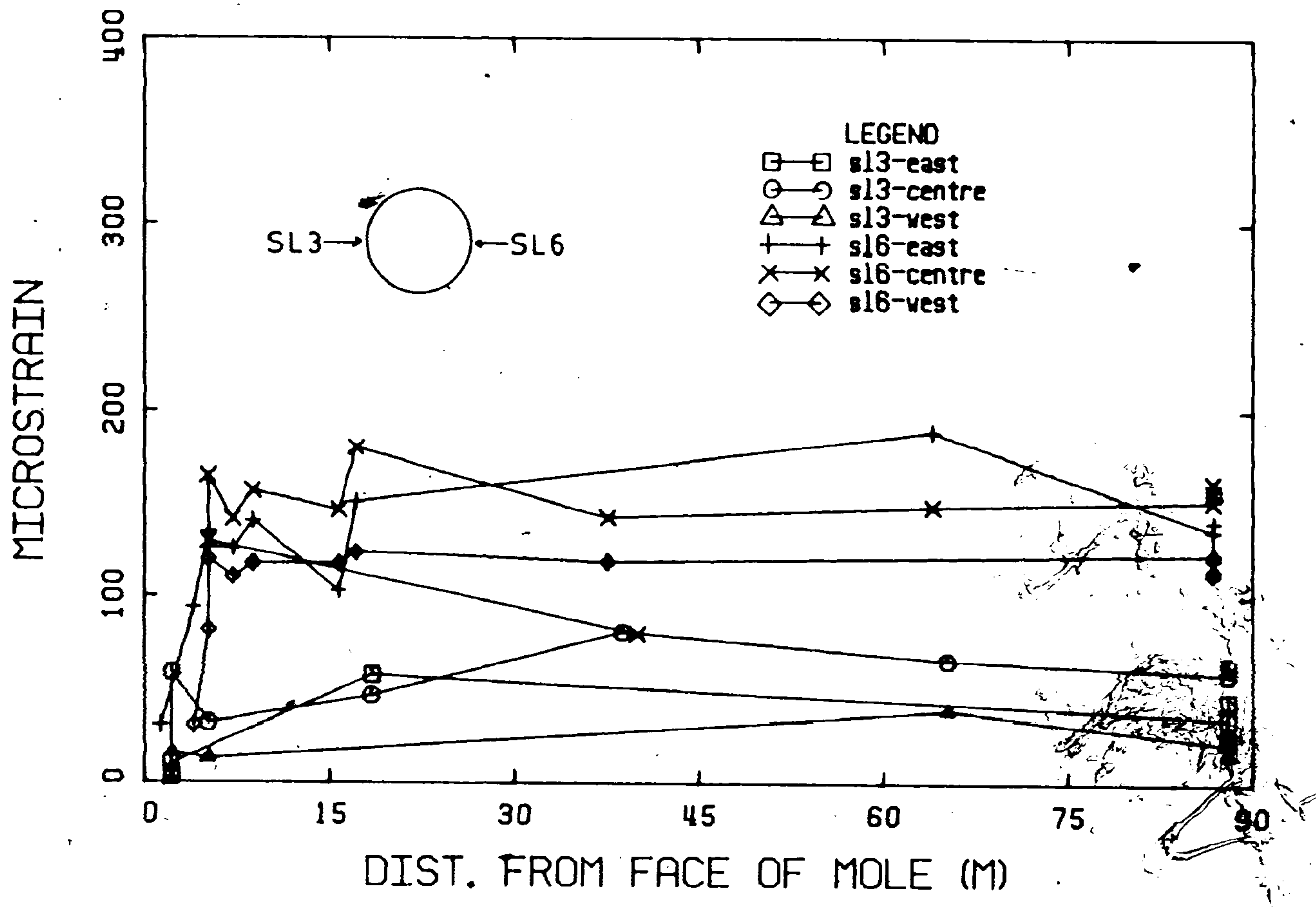

Figure 4.28 STEEL LAGGING - #3 AND #6 - STRAIN VS DIST. FROM TAIL OF MOLE

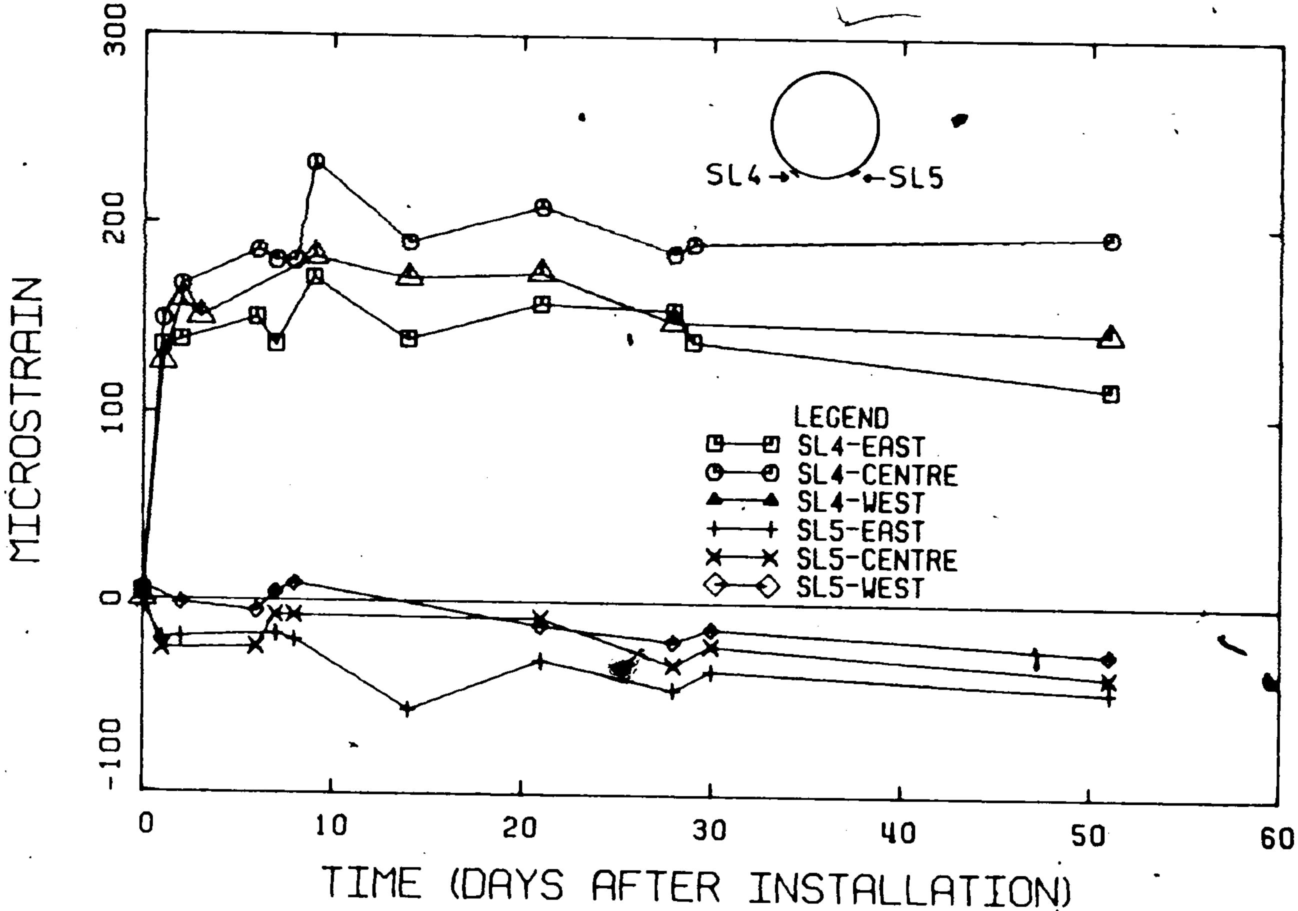

Figure 4.29 STEEL LAGGING - #4 AND #5 - STRAIN VS TIME

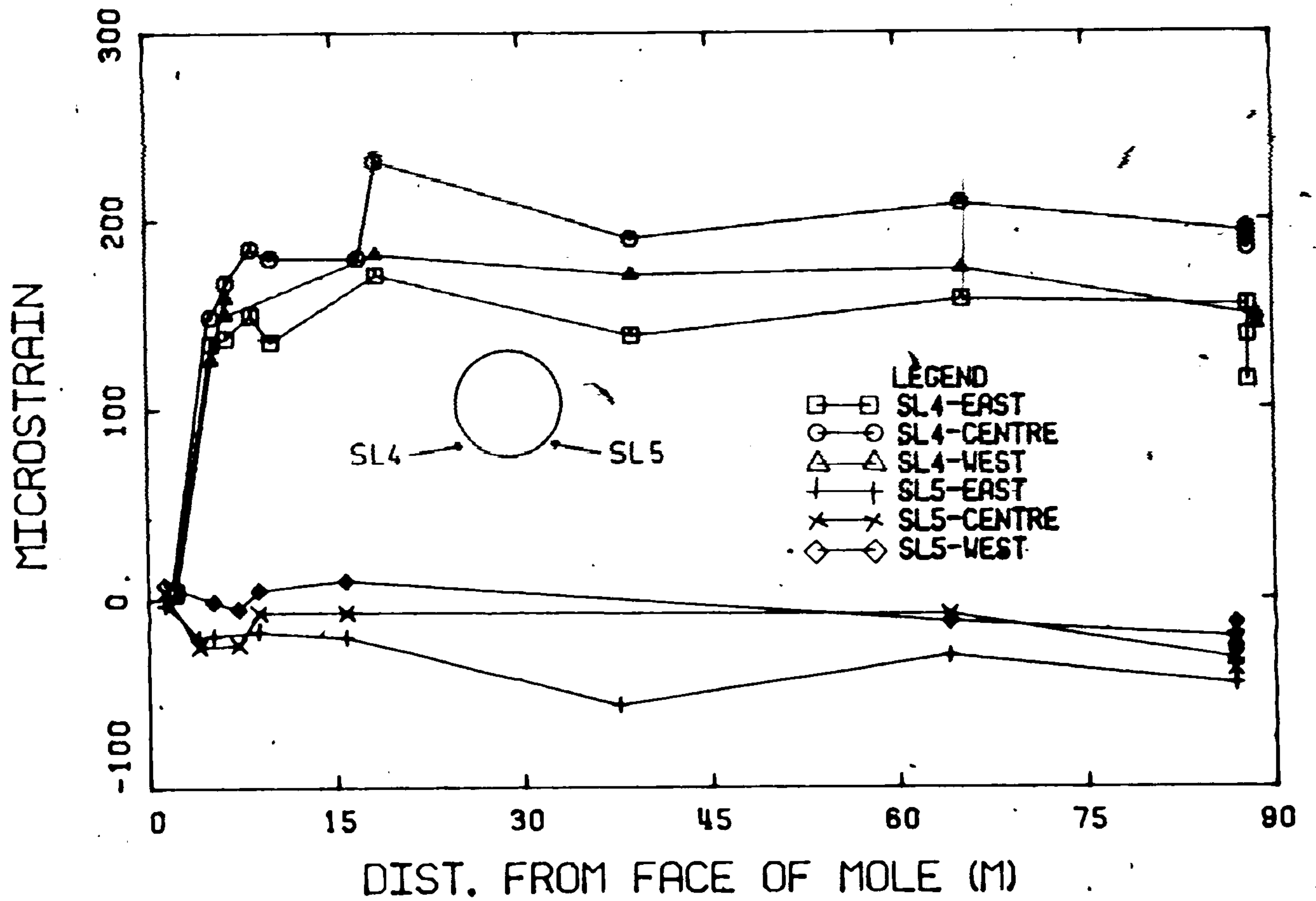

Figure 4.30 STEEL LAGGING - #4 AND #5 - STRAIN VS DIST. FROM TAIL OF MOLE

4.4.2.6 Data Reduction

The measurement of strains at three different points along the length of the pieces of steel lagging was taken to obtain the magnitude and distribution of the soil load on the lagging.

Bending moments are directly related to measured strains through the calibration curve, Figure 4.15, and are tabulated in Tables C20 to C25 in Appendix C.

Load distribution can be evaluated from bending moments through the structural concept:

$$p = \frac{\partial V}{\partial x} = \frac{\partial^2 M}{\partial x^2}$$

where p = load distribution

V = shear force

M = bending moment

As bending moments are only available at three positions along the pieces of steel lagging, the evaluation of the bending moment distribution is only approximate. The load distribution calculated from the analysis is strongly affected by the assumed initial moment distribution.

For the field data reduction, it was initially assumed that the bending moments varied linearly between strain gauges and between the outer strain gauges and the ends of the steel lagging. Shear forces could be calculated from this variation of bending moments and the same procedure is applicable to shear forces in order to calculate external load distributions.

This procedure is illustrated in Figure 4.31.

The results obtained from this analysis were clearly not reflecting the actual load distribution carried by the lining. In some cases, loads were found to be acting in the opposite of the expected direction (i.e. acting outwards).

It was then decided to submit the data to a simpler analysis that would assume:

- the ground load was uniformly distributed along the length of the steel lagging.
- no moments were carried by the ends of the steel pieces of lagging.
- no axial load was transmitted to the steel lagging.

Since, for all pieces of lagging, it was impossible to find a unique uniform load distribution that would yield values of strains identical to those obtained from the strain gauges, the uniform load distribution obtained from the data was assumed to be the average of two different uniform load distributions, calculated from the three strain gauges as follows:

$P_{u,c}$ = obtained from the strains measured by the central strain gauge.

$P_{u,o}$ = obtained from the average of the strains measured by the two outer strain gauges.

Figure 4.32 depicts these assumptions.

The load distribution along the steel lagging was calculated using the data obtained when the pieces of

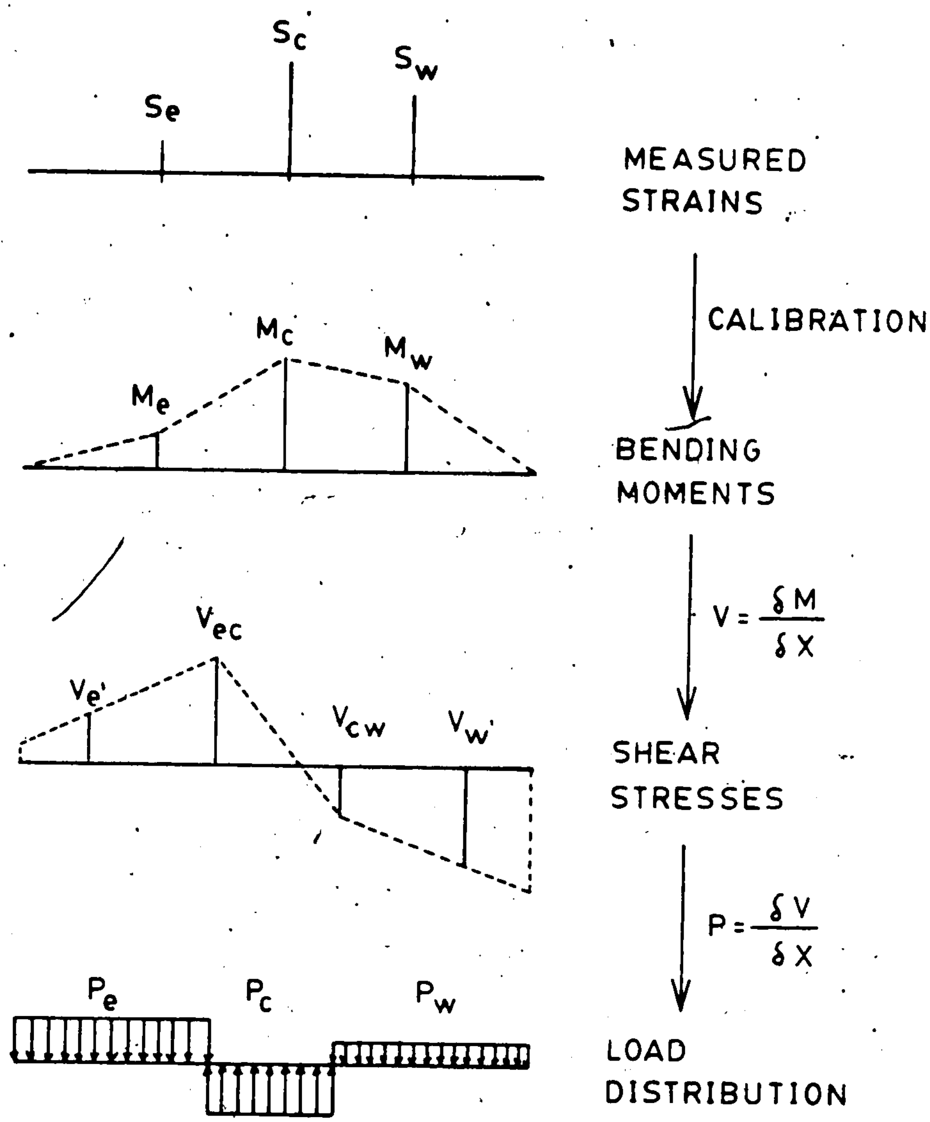

Figure 4.31 STEEL LAGGING STRESS DISTRIBUTION CALCULATED FROM STRAIN GAUGES

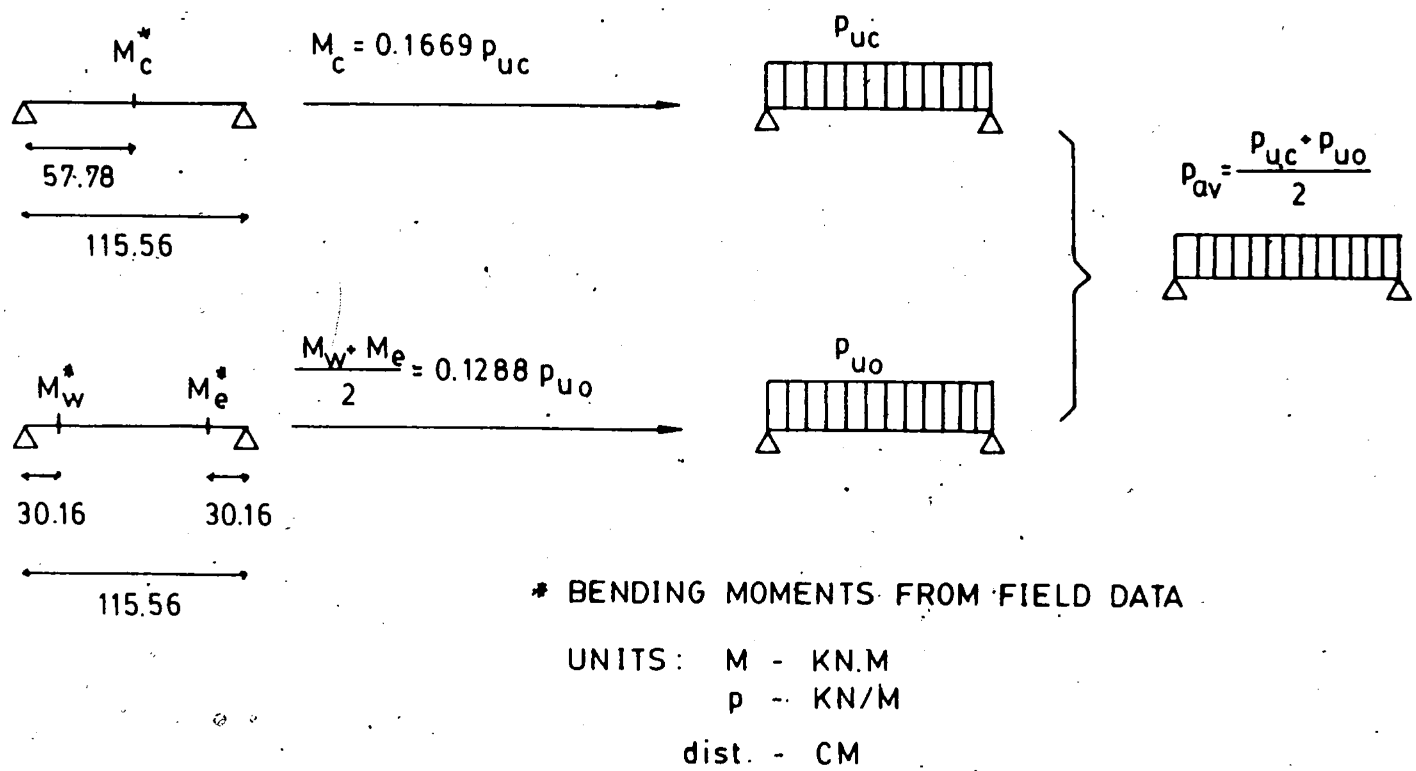

Figure 4.32 SIMPLIFIED STEEL LAGGING STRESS DISTRIBUTION ASSUMED ON THE DATA REDUCTION

lagging were at 36.4m of distance from the tail of the mole.

This distance was chosen for the same reasons discussed earlier for the load cells:

- readings taken close to the tail would be affected by the mole advance forces
- readings taken remote from the tail would be affected by the ground time dependent behavior.

The reading taken at 36.4m from the mole tail took place less than 14 days after the tail passed any instrumented ring. In most cases readings exactly at the distance of 36.4m from the tail were not taken and, in these cases, bending moments were obtained by linear interpolation of available field data. The uniform load distribution, calculated based on the assumptions described in this section, is presented in Table 4.3.

During the calibration tests, the flexural rigidity of the steel lagging was found to be 54% larger than that of the timber lagging (162.81KN.m^2 and 105.61KNm^2 respectively). This means that the load picked up by the steel lagging is probably larger than that carried by the timber. Hence, a correction is necessary since the main interest is the ground load acting on the wooden lagging. For the sake of simplicity, it was assumed that there is a linear relation between load carried and the bending stiffness. The loads originally calculated can be corrected easily and are presented in the last column of table 4.3. More complex corrections are not justified since many

MOMENTS AT 36.4m AWAY FROM TAIL (kN.m)

LAG/NO	M_e	M_c	M_w	$\frac{M_e+M_w}{2}$	Pc (kN/m)	Po (kN/m)	Pav (kN/m)	*** Pfinal (kN/m²)	**** Pfinal corr.
1	1.47	1.92	1.35	1.41	11.50	10.95	11.23	88.43	57.36
8	0.67	0.98	0.53	0.60	5.87	4.66	5.27	41.50	26.92
10	0.76	1.22	0.89	0.83	7.31	6.41	6.86	54.02	35.04
11	0.16*	0.16*	0.21	0.19	0.96	1.44	1.20	9.45	6.15
9	0.31	0.08	0.09	0.20	0.48	1.55	1.02	8.00	5.19
12	0.57	0.61	0.22	0.40	3.65	3.07	3.36	26.46	17.16
3	0.33	0.49	0.17	0.25	2.94	1.94	2.44	19.21	12.46
6	1.07	0.94	0.76	0.92	5.63	7.10	6.37	50.37	32.67
2	0.34	0.43	0.38	0.36	2.58	2.80	2.69	21.18	13.74
7	0.18	0.32	0.18	0.18	1.92	1.40	1.66	13.07	8.48
4	0.80	1.21	1.11	0.96	7.25	7.41	7.33	57.72	37.44
5	ZERO **	ZERO **	ZERO **	ZERO	ZERO	ZERO	ZERO	ZERO	ZERO

* Value not linearly interpolated -See table C25.

** These values were actually negative and, here, they were considered zero.

*** Pfinal = Pav/0.127 (m) (width correction)

**** Pcorrected = Pfinal x 105.61/162.81 (stiffness correction)

TABLE 4.3 - LOADS ACTING ON THE LAGGING AT 36.4m FROM THE SHIELD TAIL.

simplifying assumptions have been already made. The corrected values of table 4.3 are plotted in their respective locations in Figure 4.33.

4.4.3 Overcoring Measurement

The knowledge of the rate of closure of the void left between the ground and the lagging would be of great interest, with respect to loss of ground studies and helpful in interpreting the steel lagging and load cell results.

The distance between the pieces of steel lagging and the ground will be referred as overcoring. The overcoring was measured in six different locations along the length of each steel lagging installed in positions 1 and 2, soon after they left the shield.

Shortly before the second set of readings was taken (a couple of hours later) it was noticed that the ground was beeing squeezed through the space left between the steel and timber lagging. The soil that was coming towards the tunnel was a very wet soft clay mixed with medium sand which was probably coming from a inter-till water bearing sand pocket mixed with cuttings from the mole. The presence of this material around the lining determined the end of overcoring rate closure measurements which was not measured later.

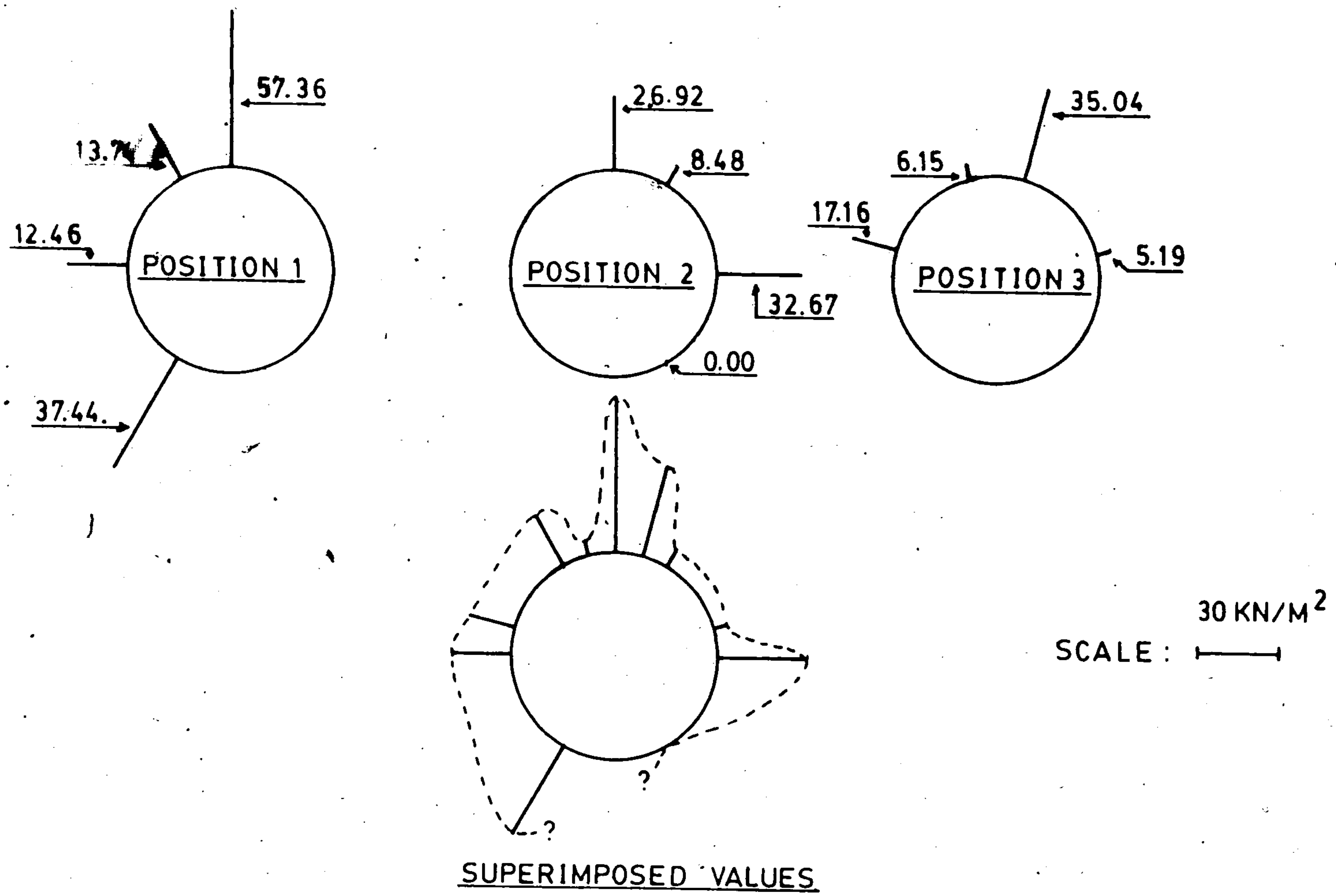

Figure 4.33 STRESS DISTRIBUTION ON THE LAGGING AT 36.4m FROM THE SHIELD TAIL

4.4.4 Lining Deformation

The monitoring of lining deformation can be very helpful in the interpretation of the steel lagging and load cell results and provides valuable input for the computer numerical analysis.

For the LRT primary lining, the distortion was recorded by measuring the change in chords of the lining with a tape extensometer and monitoring the level change of some points welded to the lining.

The quality of the distortion readings would be undoubtly improved if use had been made of the curvometer and deformeter proposed by Kovari (1977) but these instruments were not available at the moment they were needed.

4.4.4.1 Details of Instrumentation

The tape extensometer used in the distance readings was produced by Slope Indicator Co. Model P/N 518115. This tape extensometer consists of a spring loaded steel tape connected to a dial gauge. Accurate measurements of distances between two points are accomplished by hooking one end of the tape and the hook connected to the dial gauge to the eye-bolts, previously fixed to these two points.

In the primary lining, four steel ribs were chosen for deformation observation. Each of these steel rings had five eye-bolts welded according to Figure 4.34. In this figure, seven chords are indicated, which together with the level

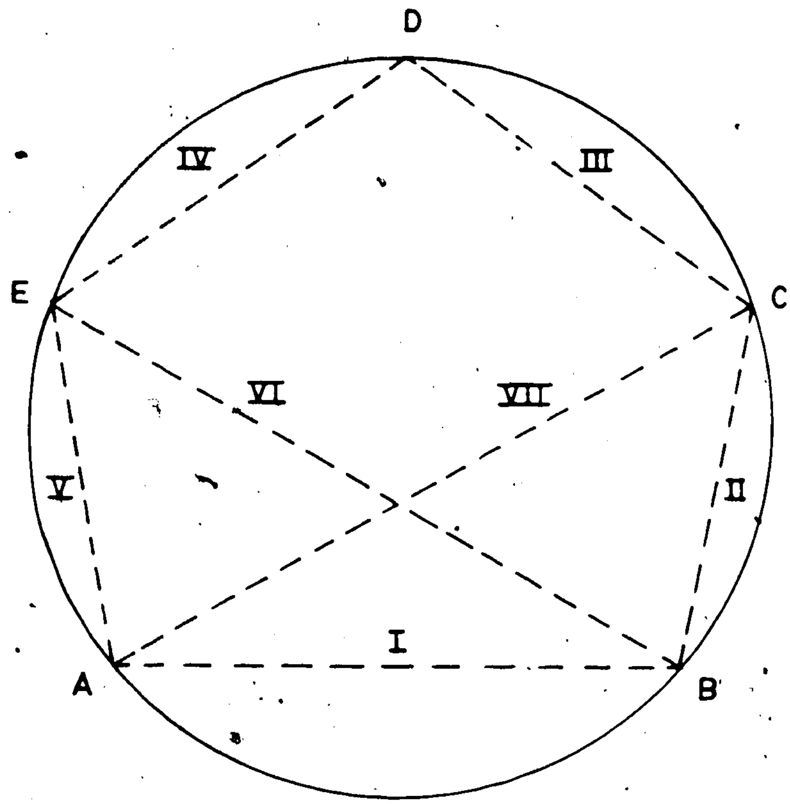

LEVEL CHANGE WAS MONITORED IN A AND B

I TO VII - MEASURED CHORDS

Figure 4.34 LINING DEFORMATION MEASUREMENT - POSITION OF THE EYE-BOLTS AND MEASURED CHORDS change of the two lower eye-bolts, made possible the location of the absolute position of the five points in the plane of that ring.

4.4.4.2 Eye-Bolts Installation

The ribs that had deformations monitored were named ring 5, ring 6, ring 7 and ring 8 located at Sta. 200 + 73.0, Sta. 200 + 74.2, Sta. 200 + 75.4 and Sta. 200 + 76.6 respectively.

The eye-bolt installations were very simple and consisted simply of welding them to the rib. The welding was only possible after the joint expansion and the spacer placement because, during expansion, the rib expansion ring was kept in contact with the ribs being expanded. The premature eye-bolt installation would inevitably have resulted in their complete destruction.

In order to improve the accuracy of the level measurements, the two lower eye-bolts of each of the four rings were welded to the lining together with a specially designed steel cylinder, with a cone-shaped depression that fits the lower end of the surveying rod.

All level measurements were referenced to a steel pin anchored to the concrete structure of the Central Station, at the tunnel entrance (approximately at 70 metres from ring 5).

A turning point was welded to the lining between the Central Station and ring 5 in order to decrease the sight distance from surveying rod to the level.

4.4.4.3 Measurement Procedure

For ring 5, the first set of readings was taken soon after the eye-bolts were installed at a distance of 0.4m from the tail. At that moment, the mole was advancing and the jacking forces on the lining, together with the vibration from the muck cars, made the readings significantly difficult to observe. This set of readings comprises the measurement of the length of seven chords and level of the two lower eye-bolts. Another difficulty that was encountered while readings were being taken was the interference of these readings with the construction procedure.

Based on these experiences it was decided to take readings only when neither the mole nor the muck cars were working. This situation happened at a distance of 1.6m away from the shield tail (1 push of the mole after the eye-bolt installation).

The second complete set of readings could not be taken within the next 15 metres of mole advance because the conveyor belt structure and the power generator (pulled by the mole) directly interfered with the chord measurements. The subsequent set of readings was taken for all rings (5 to 8) when they were at distances between three and four diameters from the shield tail. The third, and last set of readings, was taken one day after the second set.

Measurements were recorded in the field data sheet presented in Figure 4.35.

4.4.4.4 Field Data

The field data related to the lining deformation measurements is presented in Table C26, in Appendix C, and the reduced displacements are plotted in Figure 4.36.

The results shown on Figure 4.36 assume that the central point of the chord I did not move laterally.

4.5 Discussion of the LRT South Extension Tunnel Liner Instrumentation

In this section, data will be analysed independently for each set of data obtained from each instrument and, finally, a general discussion will consider all the data.

4.5.1 Discussion of Loads and Displacements of the Steel Ribs

A significant difference in normal loads obtained from load cells installed in the same relative position of the liner is noticeable (Figures 4.5 and 4.6). This variability of results happens due to the uneven application of jacking forces around the perimeter of the lining during the mole advance. This uneven force application is necessary for the steering and alignment of the mole. It can be concluded, then, that the load distribution acting on the lining is strongly affected by the construction method.

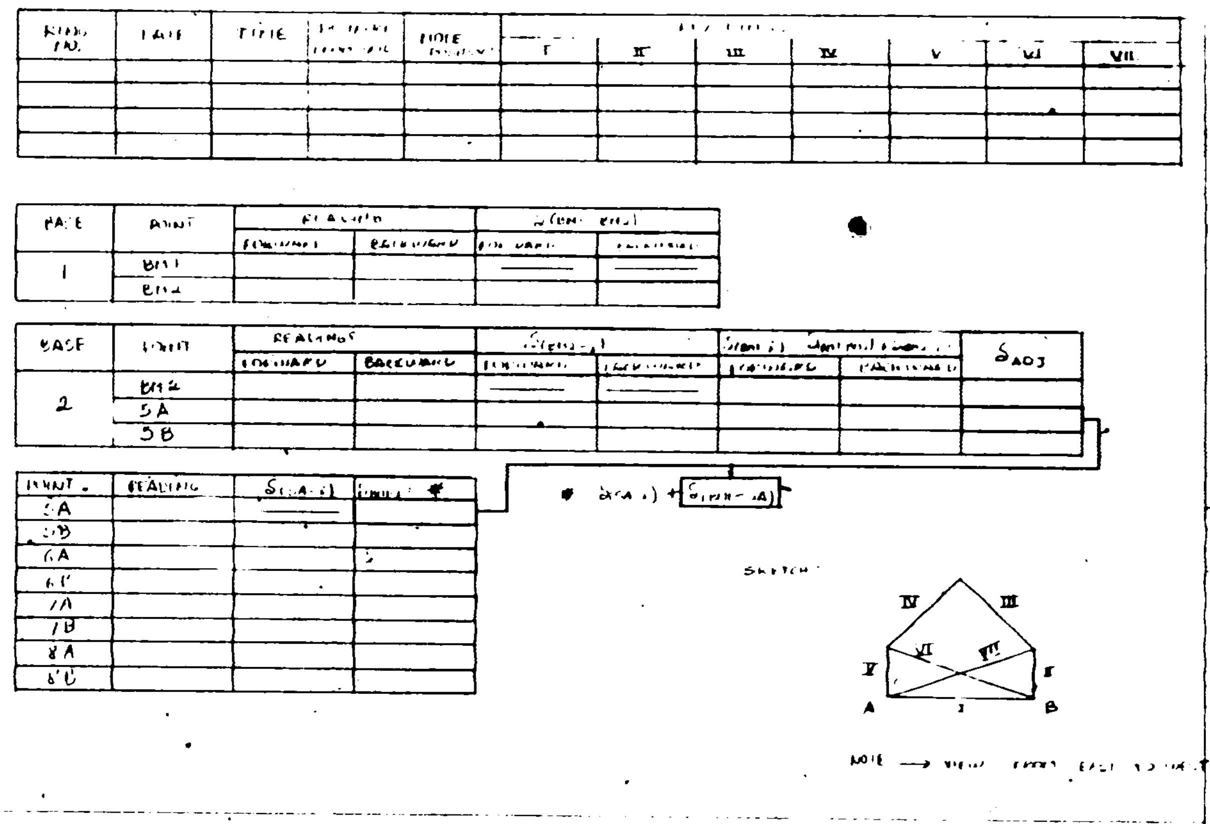

Figure 4.35 LINING DEFORMATION MEASUREMENT - FIELD DATA SHEET

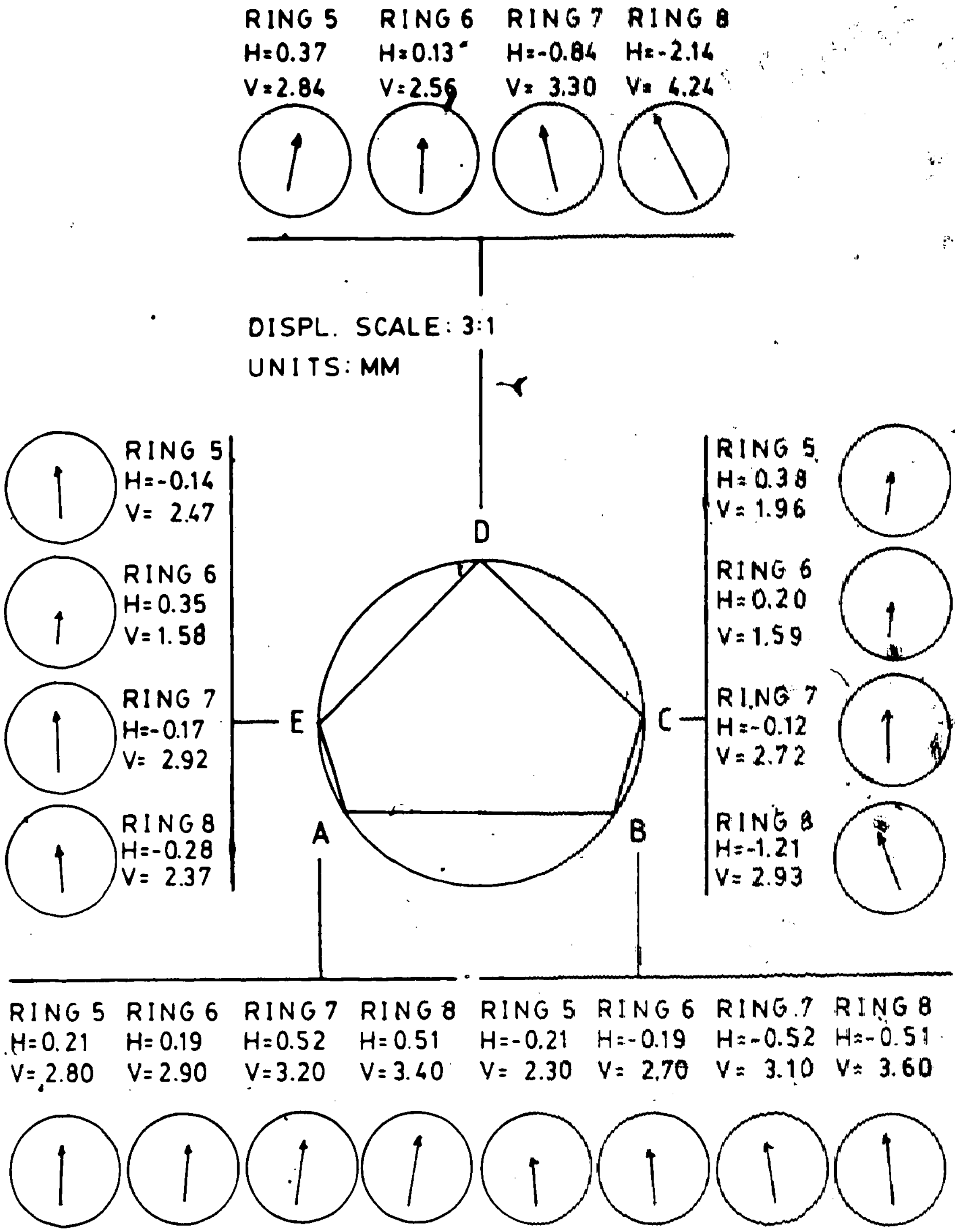

Figure 4.36 LINING DEFORMATION RESULTS

The variability of readings for each load cell was evident when these readings were taken when the mole propulsion jacks were within a distance of approximately 20 metres from the load cells (or 14 days after installation).

All figures depicting the load cell data also clearly show that the load cells installed in the upper joints picked up lower normal loads than those installed in the lower joints. This was the main justification for the analysis of Section 4.4.1.6 (Load Cell Data Reduction). Higher loads in the lower joints are probably due to the developement of shear forces between the ground and tunnel liner. The installation of load cells in the lower joints undoubtly induced this side friction because the joint expansion was done with an upward movement of the steel rib located above this joint. The tunnel construction was shut down for five days (from 18 to 23-feb-81), when ring number 4 was four metres away from the shield tail. During this period, the loads in the lower joints (numbers 2,3,4,5) increased while loads in the upper joints (numbers 6,7 and 8) decreased (see Tables in Appendix C). This enhances the interpretation that the development of shear forces along the tunnel walls is not solely due to the expansion of the lower joints.

The shear force at the soil-liner interface has a greater effect on the lining behaviour in shallow tunnels than in deep tunnels. For the latter, the shear forces are small when compared to the ring stresses induced by the stress field.

There are many methods of defining whether a tunnel is shallow or deep. These definitions can be based on the modes of failure of the opening; the similarity of ground displacements above and below the tunnel; whether the surface displacements are measurable or not; and the theory of elasticity. The knowledge of whether a tunnel will behave as a shallow or as a deep tunnel seems to be of enormous consequence in the liner design. This importance is discussed in Chapter 5 of this thesis.

The study of stress distribution around the tunnel, presented in Section 4.4.1.6 (Load Cell Data Reduction) aided in interpreting the lining behaviour. By comparing the values of load distribution acting on the crown and the invert presented in Table 4.2 with the stress at these locations before the tunnel was excavated, it can be concluded that the average stress relief at the invert ($233 KN/m^2$) is higher than that at the crown ($138 KN/m^2$). This difference in stress relief might reflect the behaviour of a shallow tunnel, since for a deep tunnel this relief should be approximately the same for crown and invert. The general upward movement of the tunnel liner presented in Figure 4.36 might also be related to the difference in stress relief in the crown and invert.

The plots of load versus time and logarithm of time show that loads continually increase after the mole passes a section. This behaviour is attributed to the time dependent transfer of loads from the soil to the tunnel liner.

The observation by Peck (1969-b) seems to be valid in this case: "For many tunnels the ring load appears to increase roughly proportionally to the logarithm of time".

It should be finally mentioned that load cells located at 36.4m away from the shield tail indicated a load distribution on the lining varying from 9 to 26 per cent of the overburden at the crown. Further comments on this variation will be offered in Section 4.5.4.

4.5.2 Discussion on Steel Lagging Results

Figures 4.19 to 4.29, which present strains measured versus time and versus distance from the tail of the mole, show some points of the lagging behaviour that are worth mentioning.

It should be noted that there is no direct relationship between the load carried and the position of the pieces of lagging as compared to the load cells that consistently measured higher loads in the lower joints of the steel ribs.

The figures also show that the strains measured in the three strain gauges attached to each of the instrumented pieces of lagging reflect the non-uniform nature of the load acting along each of these pieces. In some cases (SL2, SL5 and SL9) negative strains were measured indicating that normal load was present, probably transmitted through the four contact points of the steel lagging with the adjoining timbers and through the contact between these pieces and steel ribs. It is believed that these normal loads are very small and should not significantly alter the analysis.

In most cases, activation of the lagging occurred at a distance between 1.3 and 5.2 metres from the shield tail thus giving some indication of where the arching between the excavated soil ahead of the mole and the lining is taking place. After the lagging activation, the strains varied within a relatively narrow range except for SL9, SL2 and SL7.

It should be noted that most strain gauges reflected a decrease in the magnitude of loads supported by the steel lagging after the mole stopped with the tail at 85.6 metres from ring 5. This occurrence was probably due to the decrease in the "negative ground arching" induced by the presence of a stiffer element in the lagging and not to the increase in arching of ground between steel ribs, which probably decreases with time.

The reduced data, presented in Section 4.4.2.6 (steel lagging data reduction) involved many simplifications and assumptions but still are very useful in interpreting the lagging behaviour. Figure 4.33 depicts the reduced uniform loads and confirms the statement made at the beginning of this section: there is no direct relationship between the load carried and the position of pieces of lagging. The superimposed values presented in Figure 4.33 must be analysed with care since values of loads measured in different planes (different positions) bear no interrelationship.

The maximum measured load acting on the lagging 36.4m away from the mole is only 33% of the overburden (51% if no stiffness correction is made) which justified the increase in the rib spacing from 121.92cm to 152.40cm. This increase in rib spacing for the construction of the remainder of the tunnel was enhanced by the loads acting on the lagging measured by Thomson and El-Nahhas (1980) from 3% to 63% of overburden (tunnel in clay shale and TBM excavated). The increase in the rib spacing promoted significant economy by not only decreasing the number of steel ribs required but also increasing the rate of mole advance.

More accurate load distributions would be possible if the steel lagging comprised the entire ring rather than just a part.

4.5.3 Discussion of the Convergence / Divergence Measurements

Results from closure measurements in Figure 4.36 indicate the upward movement of the liner as a "solid body" since all these vertical displacements vary within a narrow range (from 1.58 to 3.60mm) and most of the nodes (A to E) had horizontal movements of less than 1mm.

The author is sceptical about the results of the liner movements basicly due to two reasons. First, the zero readings were taken within the region where the lining movements are basicly governed by the mole, and second, the number of readings was small. It seems, then, very difficult to be sure whether the displacements shown in Fig 4.36 are caused by ground action or by the mole action.

The valuable item of information arising from the monitoring of the liner deformation is its symmetrical behaviour with respect to the vertical line passing through the center of the tunnel and the small magnitude of displacements which is in agreement with the low normal loads measured in the load cells.

The small amount of distortion that occurred in the lining might be an indication that the ratio between vertical and horizontal ground stresses by the time the lining was installed was very close to one ($K_o = 1$).

Further discussions will be offered in the next Section, 4.5.4.

4.5.4 General Discussion of the Lining Behaviour

The data presented in Tables 4.2 and 4.3 were assembled in Table 4.4 to enable the study of the interaction between steel ribs and lagging to be made. In this table, loads obtained from the pieces of lagging located between the two lower joints were considered as acting on the invert and those located between the upper and lower joints were considered as acting on the springline.

The average values of Pcrown (stress at the crown) Pspringline and Pinvert were plotted for each of these three positions for both the steel lagging and load cell data, in

DATA FROM	Pcrown (kN/m')		Pspringline (kN/m')		Pinvert (kN/m')		AVERAGE RING STRESSES (kN/m')	
	LC	SL	LC*	SL	LC	SL	LC	SL
POSITION 1 BETWEEN RING 1 & 2	From 43.76 to 45.83 Average: 44.86	From 13.74 to 57.36 Average: 35.55	From 49.16 to 63.99 Average: 56.12	From 12.46 to 12.46 Average: 12.46	From 52.49 to 84.21 Average: 67.38	From 37.44 to 37.44 Average: 37.44	56.12	30.25
POSITION 2 BETWEEN RING 2 & 3	From 35.99 to 37.77 Average: 36.99	From 8.48 to 26.92 Average: 17.70	From 47.64 to 60.37 Average: 53.20	From 32.67 to 32.67 Average: 32.67	From 57.51 to 84.75 Average: 69.41	From 0.00 to 0.00 Average: 0.00	53.20	17.02
POSITION 3 BETWEEN RING 3 & 4	From 16.26 to 37.77 Average: 26.31	From 6.15 to 35.04 Average: 20.61	From 37.63 to 47.64 Average: 42.31	From 5.19 to 17.16 Average: 11.18	From 57.51 to 59.00 Average: 58.30	From --- to --- Average: ---	42.31	15.89

* Average of Pcrown and Pinvert.

TABLE 4.4 - LOADS ACTING ON STEEL RIBS AND LAGGING AT 36.4m FROM THE SHIELD TAIL.

Figure 4.37. In this figure, the numbers are only approximate and were plotted simply to elucidate an understanding of the lining behaviour.

The decision to plot *average* values of load distribution was made because these, when evaluated from load cell reflect the average of all loads acting along the steel ribs and the lagging, while the load distribution obtained from the steel lagging do not reflect the lining behaviour as a whole. The results plotted on this figure consistently show that loads carried by the steel ribs are higher than those carried by the neighbouring timber lagging. The opposite could be only possible if the lagging had a self supporting capacity, acting as a perfectly flexible lining. This does not happen due to the existence of the end plates welded to the steel ribs; all the radial loads carried by the lagging is transmitted to the ribs through the end plates.

Another factor affecting the load distribution along the tunnel liner is the construction method. One of the steps of the lining installation procedure is the rib expansion where the jacks, through the rib expansion ring, push the rib towards the soil, in order to minimize the ground loss around the lining. Since the expansion happens on the ribs, and these are projected 1.3cm outwards with respect to the lagging, the difference in the load carried is clearly understandable.

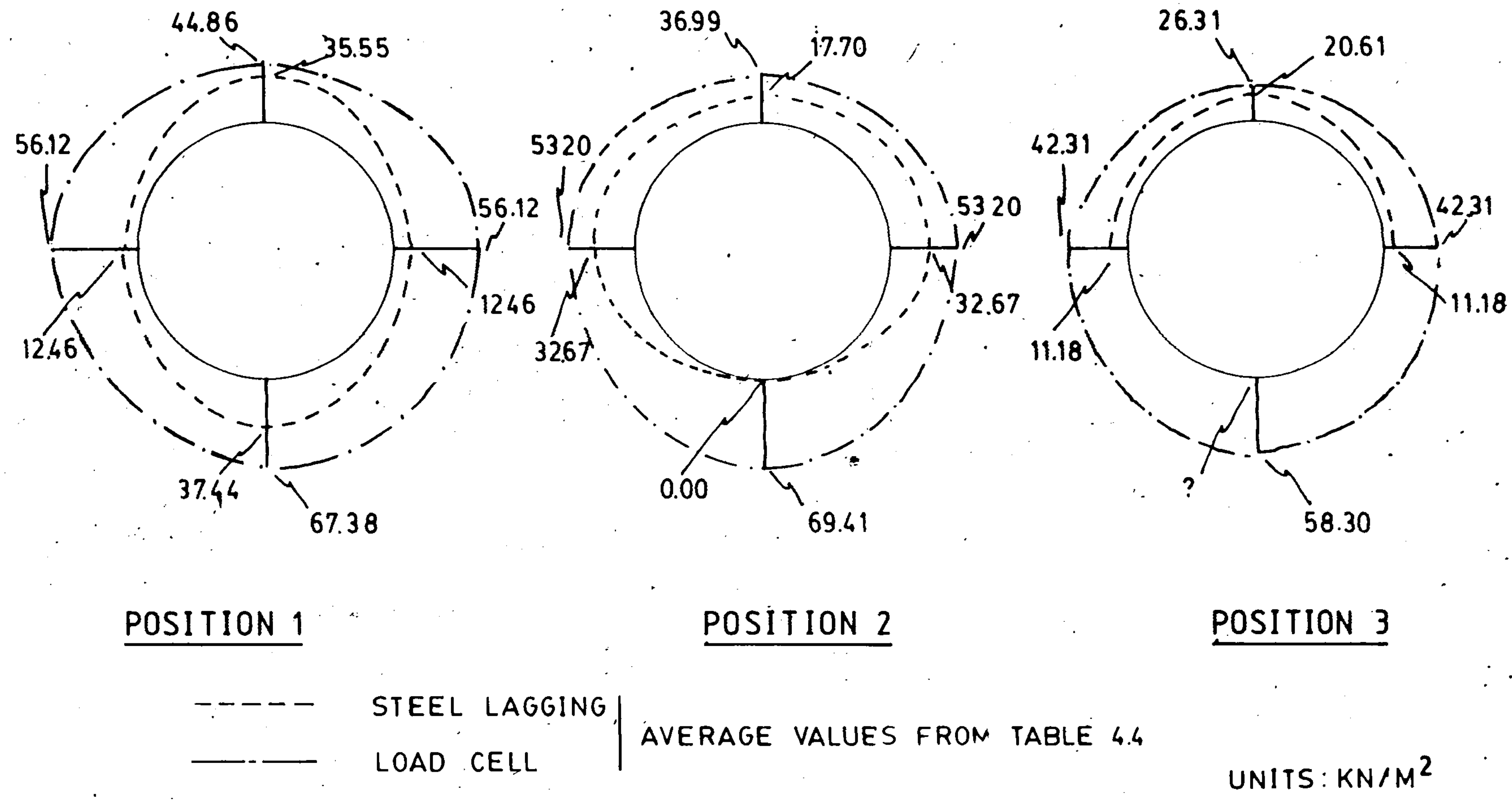

Figure 4.37 STRESS DISTRIBUTION ON RIB AND LAGGING AT 36.4M FROM THE SHIELD TAIL

The magnitude of the difference in load supported by the components of the primary lining can be roughly expressed by the average ring load values presented in the last two columns of Table 4.4. They show that ribs carry loads from 85 to 213% higher than those carried by the lagging. It is of major interest to compare the pressure on lining obtained in this study with those presented by El-Nahhas(1980) (Table 4.5). For the LRT Extension tunnel currently being studied, the height of soil carried by the steel ribs varies from 2.12m to 2.81m (obtained from average "ring loads" in Table 4.4) as compared to the 4.71m obtained from the north-eastern tunnel of the LRT. The difference in load supported by the two LRT tunnels might be due to a greater self support capacity of the ground surrounding the tunnel of the LRT South-Extension. Another reason for this difference might be due to the different methods utilized to measure normal loads in both tunnels. In the north-eastern tunnel, loads were measured with strain gauges attached to the ribs and these seem to have been affected by the advance of the mole.

The ratio (n) of height of soil carried by the lining to the tunnel diameter varies from 0.34 to 0.45 as opposed to the values presented in Table 4.5 where n varies from 0.8 to 1.09.

The great disadvantages of the comparison based on ratios such as n are that it does not take into account the construction effects that certainly have a major role in the

	Depth metre (Z)	Diam. metre (D)	Z/D	Pv (kPa)	PL (kPa)	PL/Pv x 100	h metre	n=h/D	References
LRT-NORTH EAST TUNNEL	10.2	6.1	1.7	125	100	80	4.71	0.8	Eisenstein et al. (1977) Eisenstein and Thomson (1978)
LRT-SOUTH EXTENSION	11.8	6.2	1.9	174	42.3-56.1(c) 15.9-30.3(d)	24-32 9-17	2.12-2.81 0.80-1.52	0.34-0.45 0.13-0.25	Present study
Whitemud Creek Tunnel	47.2	6.05	7.8	575	114.7	20	5.41	0.9	El-Nahhas (1977) Thomson and El-Nahhas (1980)
107th Street Tunnel	20	2.56	7.81	380	6.1-12.6(a) 112-240(b)	1.6-3.3(a) 29.5-63(b)	0.29-0.59(a) 5.28-11.31(b)	- -	El-Nahhas (1977) Thomson and El-Nahhas (1980)
Experim. Tunnel	27	2.56	10.54	550	63	12	2.79	1.09	El-Nahhas (1980)

Notes:

Pv : Overburden pressure.
PL : Pressure on lining.
h : Height of soil carried by lining = PL/soil unit weight

(a) = From pressure cells.
(b) = From lagging deflection.
(c) = From load cells - average ring stresses.
(d) = From steel lagging - average ring stresses

TABLE 4.5 - Soil pressure on the primary lining in Edmonton tunnels (After El-Nahhas 1980)

lining and ground behaviour, nor does it take into account local changes in stratigraphy.

4.6 Summary and Conclusions

In this chapter, the techniques most commonly used in the measurement of lining loads and displacements have been reviewed. Details concerning the installation, measurement procedures and design of the instruments used to monitor loads and displacements in the LRT South-Extension tunnel liner have been presented.

From the analysis of the field data, the following have been concluded:

- Load cells yielded the best results;
- Loads at the crown varied from 9 to 26% of the overburden;
- Load cell measurements indicated that the shear developed along the ribs, acting downwards, are of comparable magnitude to the ring stresses which indicates that the tunnel behaves as a shallow tunnel;
- Steel lagging picked up loads lower than those carried by the ribs, indicating arching between ribs. These loads were always less than 33% of overburden which made possible an increase of rib spacing in the continuation of the tunnel construction;

- Loads measured in the load cells increased roughly with the logarithm of time;
- Lining displacements measurements indicated a general upward movement of the liner with very small distortion of the steel ribs;
- The ratio of the height of soil carried by the lining to the tunnel diameter was found to vary from 0.34 to 0.45 which is lower than the values measured for other tunnels.
- The load distribution acting on the lining is strongly affected by the construction method.

5. SOIL-STRUCTURE INTERACTION AT TUNNELS

5.1 Introduction

The transfer of loads from the excavated ground to the tunnel lining (Soil-Structure Interaction) depends on the construction method and ground and lining deformation and strength properties. The tunnel design methods endeavour to predict the Soil-Structure Interaction. The many existing lining design methods may be divided in three classes:

- Analytical Methods:
  - Finite Element Method
  - Closed Form Solutions
  - Subgrade Reaction Theory
  - Convergence-Confinement Method
- Empirical Methods:
  - Hewett and Johannesson (1922)
  - Peck et al (1972)
  - Design Specifications
- Observational Methods

El-Nahhas (1980) provided a complete summary of some of the currently used design methods. Sophisticated methods, such as the finite element methods, require appropriate input information in order to reproduce properly the ground support interaction. In most cases appropriate information concernig construction details is not available and cannot be easily predicted.

Empirical Methods, on the other hand, do not require accurate input information, rather they are based on easily measured ground properties, qualitative geological description and local experience. Usually, the lack of more accurate input information in Empirical Methods results in substantial and indeterminable amount of overdesign. The drawbacks associated with Analytical and Empirical Methods are avoided in the Observational Method. In the Observational Method, the information obtained in the early stages of the tunnel construction is the input for the modifications of the design of sections constructed subsequently. This "learn-as-you-go" method is discussed in the Ninth Rankine Lecture presented by Peck (1969-a).

The interaction between the liner and the surrounding ground has been the subject of several recent studies because its understanding certainly leads to improved tunnel designs.

The finite element methods, closed form solutions and the convergence-confinement curves have played an important role in enlightening the complex soil-structure interaction in tunnels. Closed Form Solutions and Characteristic Lines Method (Convergence Confinement Method) are referred to in this chapter as "Simple Solutions".

The simple solutions are not only helpful in understanding the interaction problems related to tunneling but also permit the designer to rapidly investigate a range of possible support alternatives. According to Muir Wood

(1975):

"A special virtue of the simple method is that it serves quickly to indicate sensitivity of the solution across the range of the possible ground parameters."

The use of the available simple solutions in the soil-structure analysis of shallow tunnels is questionable and is the main purpose of the discussion of this chapter. Closed Form Solutions and the Convergence-Confinement Method (C.C. Method) are also discussed comprehensively in this chapter.

The applicability of Simple Solutions to shallow tunnels is discussed on the basis of the data obtained from three tunnels constructed in Edmonton. The detailed description of the three tunnels is given in Section 5.4.

5.2 Closed Form Solutions

5.2.1 Deep Tunnels

The analysis of stresses and strains around ground openings based on continuum mechanics have improved significantly in the last decade. The elastic solutions were limited to unlined openings prior to the work of Burns and Richard (1964).

Burns and Richard (opt. cit.) introduced the lining in the conventional analysis and through the extensional shell theory and derivations of the Airy's stress function, derived the stresses and displacements in both the soil and lining. The assumptions made to develop Burns and Richard (opt. cit) equations were:

1. Two dimensional problem
2. Both the lining and soil behave elastically
3. Gravity forces are ignored and soil is loaded symmetrically, with respect to both the horizontal and vertical axes, at surfaces considered as infinite (deep tunnel with external loading)
4. The lining is placed before the excavation takes place and before the medium is unstressed
5. The lining is a cylinder with constant thickness and constant elastic properties.

Burns and Richard defined two new coefficients: the compressibility and the flexibility ratios. The compressibility ratio is defined as the extensional stiffness of the médium relative to that of the liner, whereas the flexibility ratio is a measure of the flexural stiffness of the medium relative to that of the liner.

The extensional stiffness is the uniform all around pressure, applied to a circular portion of the soil with the same diameter as the tunnel liner, or the uniform pressure applied to the lining, necessary to cause a unit diametral strain.

The flexural stiffness is the pressure applied to a circular portion of the soil with the same diameter as the tunnel liner or the pressure applied to the tunnel liner, under a state of pure shear, necessary to cause a unit diametral strain.

The coefficients defined above are extremely useful in the study of deep tunnels because every in-situ stress symmetric to the horizontal and vertical axis of the tunnel can be divided into uniform all around pressure and a state of pure shear pressure distribution (Fig. 5.1).

A detailed derivation of the two ratios described above is given in Peck et al. (1972) who examined the effects of the lining flexibility and compressibility on forces and deformation in tunnel liners erected in soft ground. As the closed form solutions were limited to deep buried cylinders, the effects of the depth of cover above the tunnel crown were studied on the basis of elastic finite element solutions.

Peck et al (opt. cit.) found that the closed form solutions proposed by Burns and Richard, developed for deep tunnels, could be applied to the study of tunnels with a depth of cover (distance between the crown and the surface) greater than 1.5 times the tunnel diameter.

Mohraz et al (1975) with a series of elastic finite element solutions, investigated the effects of different lining loading conditions on the lining thrusts and deformations evaluated by the closed form solutions derived by Burns and Richard. This study was necessary since Burns and Richard's solutions assumed an external loading of the

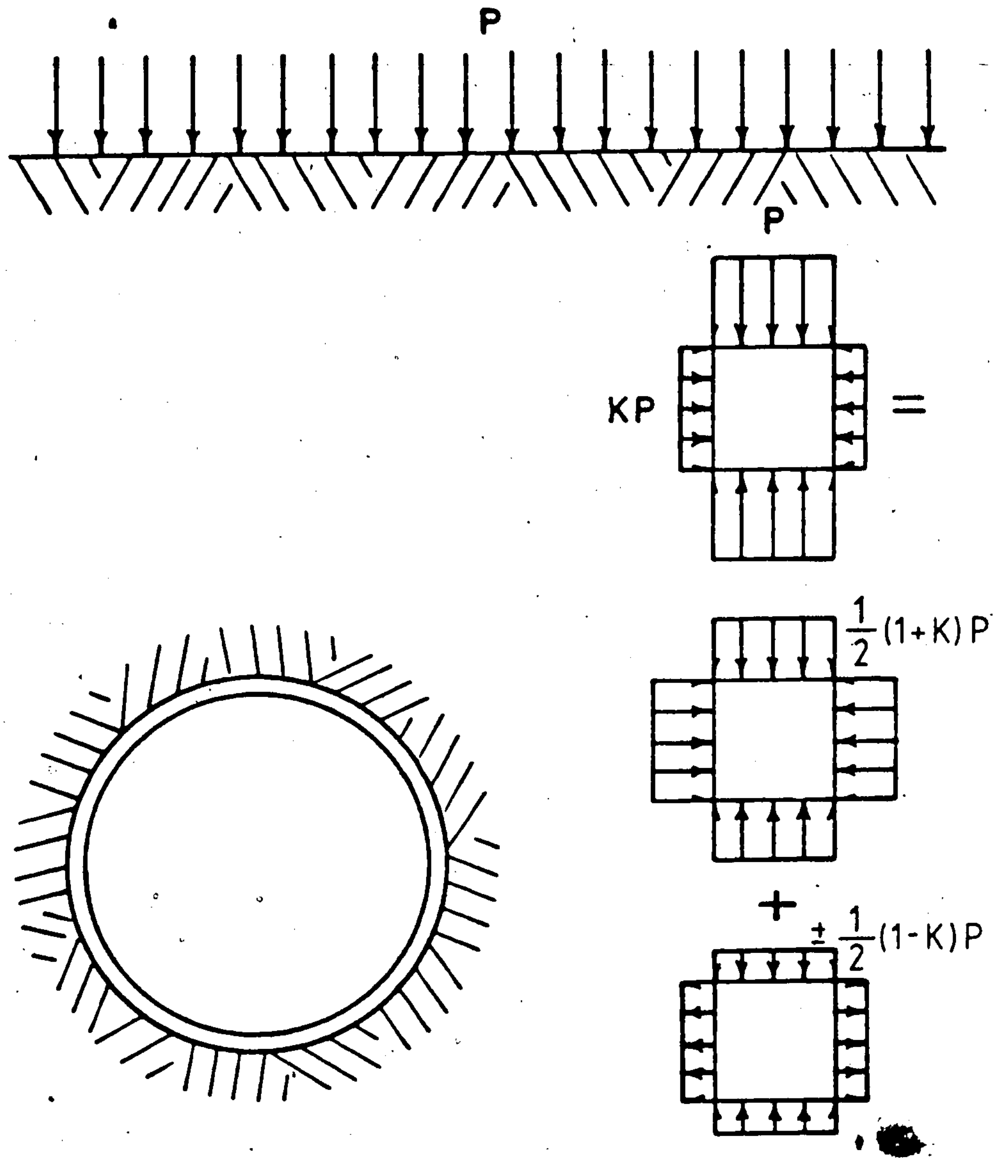

Figure 5.1 FIELD STRESSES IN BURNS AND RICHARD'S CLOSED FORM SOLUTION

lining which did not simulate the actual lining loading condition during the tunnel construction.

Mohraz et al concluded that the loading condition affects the thrust and lining deformation to a significant degree whereas transverse shear (along the soil-structure interface) and the bending moments are less affected.

Also in 1975, Muir Wood published another closed form solution for deep lined tunnels in which the unloading due to excavation was taken into account and the ground water seepage towards the tunnel was analysed.

In the report by Muir Wood, the previous closed form solution proposed by Morgan (1961) was corrected. Morgan's derivation assumed the sum of the tangential and radial stresses (σ_θ and σ_r) constant throughout the soil mass. This assumption does not reflect the plane strain condition where the strains in the direction parallel to the tunnel axis are considered equal to zero. For the plane strain case the sum of the radial and tangential stresses is given by the equation

$$\sigma_\theta + \sigma_r = \frac{\sigma_2}{\nu} \qquad 5.1$$

where σ_2 is the principal stress acting in the direction parallel to the tunnel axis and ν is the Poisson's Ratio of the medium.

Muir Wood's solution ignored the effect of the in-situ shear stresses at the ground-support interface. These shear stresses were taken into account in Curtis' derivation

(1976). Curtis extended the closed form solutions for deep lined tunnels to include the parameter of time in the context of visco-elastic behaviour of the ground.

In 1979 Einstein and Schwartz proposed another derivation for the ground-liner interaction problem. They stated that despite the fact that Curtis' solution took into account the in-situ shear stresses at the ground-support interface, neglected by Muir Wood, it still was not completely correct. Curtis' derivation assumed that the liner was inextensible for the state of pure shear loading (the loads on the lining were assumed to be the sum of two components: uniform compression and state of pure shear loading). The final equations derived by Einstein and Schwartz are presented in Figures 5.2 and 5.3 for the full-slip and no-slip cases, respectively.

Einstein and Schwartz (1980), based on parametric studies, drew the following conclusions concerning the sensitivity of the thrusts and moments relative to the variation in the lining and soil properties (the terms are defined in Figure 5.2):

1. T/PR is strongly dependent on C^* only within the range $0.05 < C^* < 50.0$ and is relatively insensitive to variations of F^*.
2. M/PR^2 is near zero for $F^* > 100$ and is insensitive to variations of C^*.
3. For excavation unloading conditions, both T/PR and M/PR^2 are insensitive to variations in Poisson's Ratio

$$C^* = \frac{ER(1-\nu_s^2)}{E_s A_s(1-\nu^2)}$$ COMPRESSIBILITY RATIO

$$F^* = \frac{ER^3(1-\nu_s^2)}{E_s I_s(1-\nu^2)}$$ FLEXIBILITY RATIO

$$\frac{T}{PR} = 0.5(1+K)(1-a_0^*) + 0.5(1-K)(1-2a_2^*)\cos 2\theta$$

$$\frac{M}{PR^2} = 0.5(1-K)(1-2a_2^*)\cos 2\theta$$

$$\frac{u_s E}{PR(1+\nu)} = 0.5(1+K)a_0^* - (1-K)[(5-6\nu)a_2^* - (1-\nu)]\cos 2\theta$$

$$\frac{v_s E}{PR(1+\nu)} = 0.5(1-K)[(5-6\nu)a_2^* - (1-\nu)]\sin 2\theta$$

WHERE : θ = ANGULAR COORDINATE MEASURED FROM THE SPRINGLINE

$$a_0^* = \frac{C^* F^*(1-\nu)}{C^* + F^* + C^* F^*(1-\nu)}$$

$$a_2^* = \frac{(F^* + 6)(1-\nu)}{2F^*(1-\nu) + 6(5-6\nu)}$$

T, M = SUPPORT THRUST AND BENDING MOMENT

P, K = IN SITU FIELD STRESS, LATERAL STRESS RATIO

E, ν = GROUND YOUNG'S MODULUS, POISSON'S RATIO

E_s, ν_s = SUPPORT YOUNG'S MODULUS, POISSON'S RATIO

A_s, I_s = SUPPORT CROSS SECTIONAL AREA AND MOMENT OF INERTIA PER UNITLENGHT OF TUNNEL

R, u_s, v_s = SUPPORT RADIUS, RADIAL AND TANGENTIAL DISPLACEMENT

Figure 5.2 FULL SLIP CASE - EINSTEIN AND SCHWARTZ, 1979-1980

$$\frac{T}{PR} = 0.5(1+K)(1-a_o^*) + 0.5(1-K)(1-2a_2^*)\cos 2\theta$$

$$\frac{M}{PR^2} = 0.25(1-K)(1-2a_2^* + 2b_2^*)\cos 2\theta$$

$$\frac{u_s E}{PR(1+\nu)} = 0.5(1+K)a_o^* + 0.5(1-K)[4(1-\nu)b_2^* - 2a_2^*]\cos 2\theta$$

$$\frac{v_s E}{PR(1+\nu)} = -(1-K)[a_2^* + (1-2\nu)b_2^*]\sin 2\theta$$

WHERE: $$b_2^* = \frac{C^*(1-\nu)}{2[C^*(1-\nu) + 4\nu - 6\underline{b} - 3\underline{b}C^*(1-\nu)]}$$

$$\underline{b} = \frac{(6+F^*)C^*(1-\nu) + 2F^*\nu}{3F^* + 3C^* + 2C^*F^*(1-\nu)}$$

$C^*, F^*, a_o^*, a_2^*, \theta, T, M, P, K, E, \nu, E_s, \nu_s, R, u_s, v_s$: DEFINED IN FIG 5.2

Figure 5.3 NO-SLIP CASE - EINSTEIN AND SCHWARTZ, 1979-1980 of the ground.

4. T/PR and M/PR^2 vary linearly with K.

5. the difference between the support forces calculated from the full-slip and no-slip solution are small.

Einstein and Schwartz (opt. cit.), with the aid of the finite element method, introduced correction factors to the lining thrusts and moments calculated by the proposed closed form solutions. Correction factors were introduced in order to take into account the spatial lag, or delay of support and the yielding in the ground mass surrounding the tunnel.

The correction factors are

λd = support delay factor

λy = ground yielding factor

The final lining thrusts and moments are:

$$Tf = T.\lambda d.\lambda y \qquad 5.2$$

$$Mf = M.\lambda d.\lambda y \qquad 5.3$$

where $$\lambda d = 0.98 - 0.57(Ld/R) \qquad 5.4$$

Ld = distance between the support and the face of the tunnel (unsupported span)

R = tunnel radius

λy is presented in the form of graphs and tables in Einstein and Schwartz (1980) as a function of the in-situ stress level, in situ stress ratio

(K), the soil strength properties and .

5.2.2 Shallow Tunnels

The existing definitions of shallow tunnels are presented in Chapter 4, Section 4.5.1.

The available closed form solutions for shallow tunnels are restricted to unlined tunnels. Mindlin (1940) presented a solution in which Gravity Loading, as opposed to External Loading, was taken into account. In the Gravity Loading case the soil mass has self weight whereas in the External Loading case the soils mass is weightless. Mindlin calculated strains and stresses around openings in an elastic medium under plane strain conditions with the help of bi-polar coordinates which simplified the solution.

In Mindlin's derivation, the effects of the proximity of the tunnel to the surface on the stress distribution in the surrounding ground mass is expressed by the difference between the weight of the excavated soil and the in-situ stresses at level of the tunnel centreline. In Mindlin's derivation, the following equation is presented:

$$[\sigma_\beta]_{\alpha=\alpha_1} = -2cw - R_2 w \frac{3-4\nu}{2-1\nu} \cos\Psi \qquad 5.5$$

where $[\sigma_\beta]_{\alpha=\alpha_1}$ = tangential stresses at the tunnel wall (unlined tunnel)

c = the depth of the centre of the tunnel

w = the unit weight of the soil (elastic)

R_2 = the tunnel radius

ν = Poisson's Ratio

ψ = the angle between the radius from the center of tunnel and the normal to the straight boundary (surface).

The second term from this equation arises from the weight of the material removed from the opening and the first term is the stress concentration effect.

Before excavation, the tangential stresses at the tunnel wall at a distance c below surface is -cw, so that the term -2cw reveals a predicted stress concentration factor of 2.

The second term of the equation is small in comparison with the first if R_2 is small in comparison to c.

The conclusion mentioned above can be verified in Figure 5.4 where values of normalized tangential stresses in the crown and invert are plotted versus the normalized depth of the tunnel. In this figure, when values of tangential stresses tend to be twice the field stress (w.c) the tunnel is said to be deep. To illustrate, the depth ratio c/R2 = 3.8 (11.3/3.1) of the LRT tunnel, in Edmonton, is indicated in Fig 5.4. It might be concluded that, according to Mindlin's derivation, the tunnel is at the boundary between a deep and shallow opening.

It is interesting to note that, according to Peck et al (1972) , the closed form solutions developed for deep lined tunnels are applicable to depth ratios (c/R2) greater than 4 which is approximately the same value found by Mindlin's

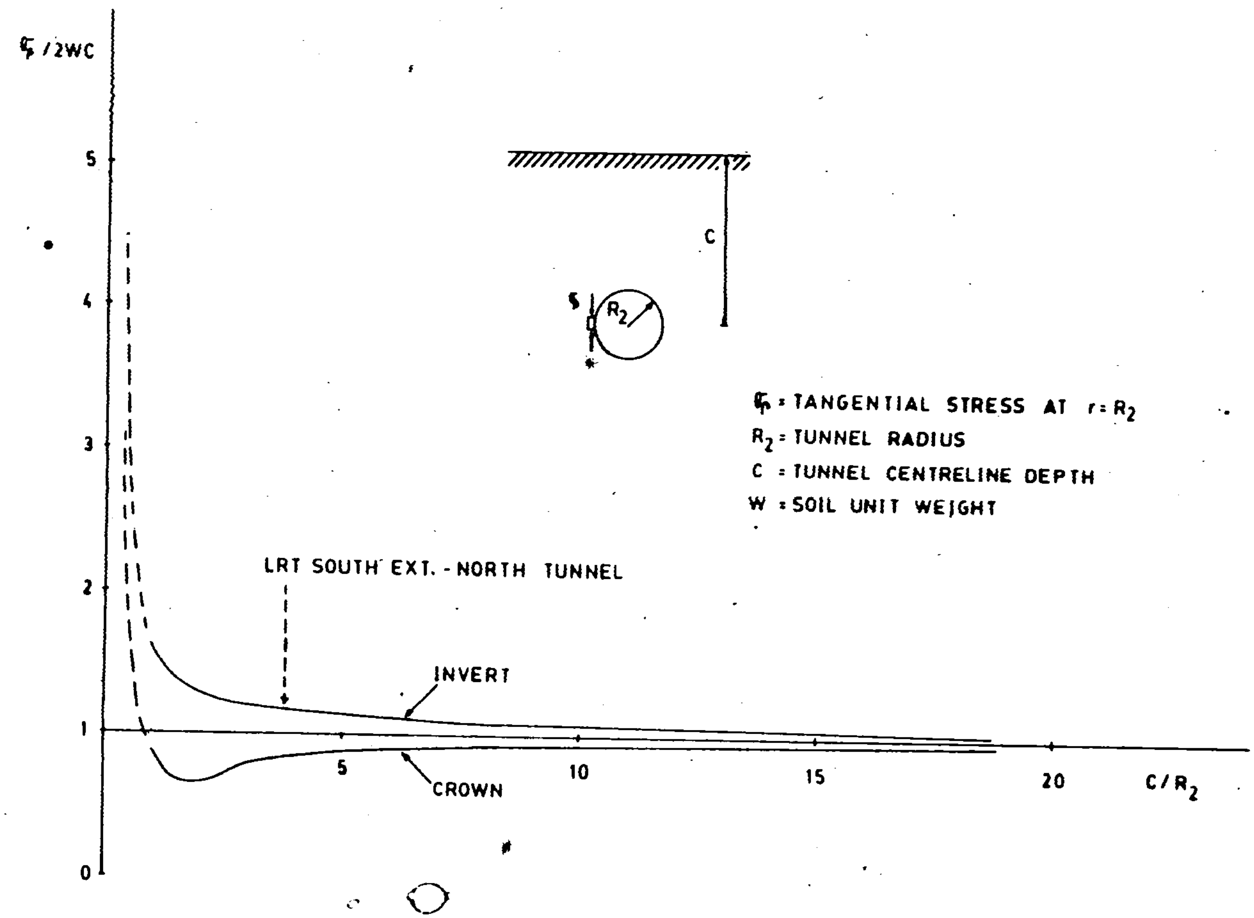

Figure 5.4. MINDLIN'S CLOSED FORM SOLUTION FOR UNLINED TUNNELS

solution for unlined tunnels (Fig 5.4).

The role of Simple Solutions in tunnel design is discussed in the introduction of this chapter. However, the lack of simple solutions for shallow lined tunnels leaves a gap in the available tools that help in the rapid investigation of alternative solutions.

5.3 The Convergence Confinement Method (Characteristic Lines Method)

The Convergence-Confinement Method is a method in which the ground structure interaction is analysed by an independent study of the behaviour of the ground and the structure.

The Convergence-Confinement Method, therefore, requires an understanding of the behaviour of the ground surrounding the opening in order to find the soil convergence in terms of the applied confining pressure and an understanding of the lining behaviour to find the confining pressure acting on the lining, in terms of deformation.

The idealization of the ground-support interaction by the two Characteristic Curves mentioned above is valid only for the symmetrical cylindrical model in which, irrespective of the lining and ground mechanical properties (E, ν), the soil and support present the same radial mode of deformation.

5.3.1 The Convergence Curve for the Ground Surrounding the Opening (Ground Reaction Curve)

The determination of the convergence curve (or Ground Reaction Curve) requires an understanding of the ground behaviour. For a homogeneous, isotropic and continuous ground mass, the parameters that reflect the ground behaviour can be separated into three categories:

a) elastic characteristics (E, ν)

b) shear strength characteristics (c, φ)

c) parameters representing the soil behaviour after maximum strength is fully mobilized (sensitivity and dilation)

A knowledge of the soil properties mentioned above allows the development of closed form solutions for unlined openings. The closed form solutions developed for the hydrostatic stress field and for the case where the loaded boundaries can be considered at infinity are of major interest in the study of Ground Reaction Curves. In the case of the hydrostatic stress field, the problem can be modelled by a thick walled hollow cylinder. Kaiser (1980) and Panet (1976) presented the derivation of a closed form solution that yields the Ground Reaction Curve of an opening excavated in a material that is assumed to be linear elastic, brittle-perfectly plastic, with yield surfaces described by the Coulomb failure criterion:

$$\sigma_1 = m\sigma_3 + s\sigma_c \qquad \text{or}$$

$$\sigma_\theta = m\sigma_r + s\sigma_c \qquad 5.6$$

where

σ_1, σ_3 = principal stresses

σ_c = unconfined compressive strength

s = strength ratio: σ_c ultimate/ σ_c peak

m = $\tan^2(45° + \varphi/2)$

φ = soil friction angle

σ_θ, σ_r = tangential and radial stresses (also principal stresses for k=1)

By imposing the continuity of radial stresses at the boundary between the elastic and plastic zone, the radius of the plastic zone can be evaluated as:

$$\frac{R}{a} = \left[\frac{(m-1)(1-\lambda c)\sigma_o + s\sigma_c}{(m-1)(1-\lambda s)\sigma_o + s\sigma_c}\right]^{\frac{1}{m-1}} \qquad 5.7$$

where: R,a = radius of the plastic zone and opening, respectively

$\sigma_o(1-\lambda_s)$ = support pressure

λs = support pressure coefficient

$$\lambda e = \frac{1}{1+m}\left[m-1+\frac{\sigma_c}{\sigma_o}\right] \qquad 5.8$$

$\lambda s = \lambda e$ if σ_θ at r = a is equal to σ_c

σ_o = in situ field stress.

The normalized radial tunnel wall displacement is given by the equation:

$$\frac{u_r^{e+p}}{u_r^e} = \frac{\lambda_e}{1+\alpha}\left[2\left(\frac{R}{r}\right)^{1+\alpha} + \alpha - 1\right] \qquad 5.9$$

where $u_r^e = \frac{\sigma_o . r}{2 . G}$ is the tunnel wall displacement under condition of elastic material behaviour

u_r^{e+p}: is the tunnel wall displacement under condition of elastic-plastic material behaviour

α : is a parameter that measures soil dilation during plastic flow $(\varepsilon_r^p + \alpha \varepsilon_\theta^p)$

α =1 when no dilation takes place

α =m for flow associated with the Coulomb failure criterion

$1 < \alpha < m$ for non-associated flow.

The combination of equations 5.6 to 5.9 enables the determination of the pressure applied to the walls of the opening as a function of the wall displacement.

The influence of friction angle, cohesion, sensitivity, time dependent behaviour and stress history on the Ground Reaction Curve have been reported by Lombardi (1970), Daemen and Fairhurst (1970 and 1972), Ladanyi (1974) and Kaiser (1980).

5.3.2 The Confinement Curve for the Support (Support Reaction Curve)

The Confinement Curve of a cylindrical support loaded by a uniform radial pressure (p_s) is defined by the relationship between and the corresponding radial displacement (u_r) given in Fig 5.5. The support parameters such as elastic properties, load capacity, behaviour after

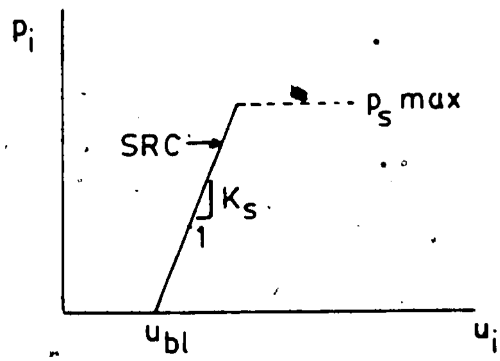

SUPPORT REACTION CURVE (SRC)

COMBINED SUPPORT STIFFNESS:

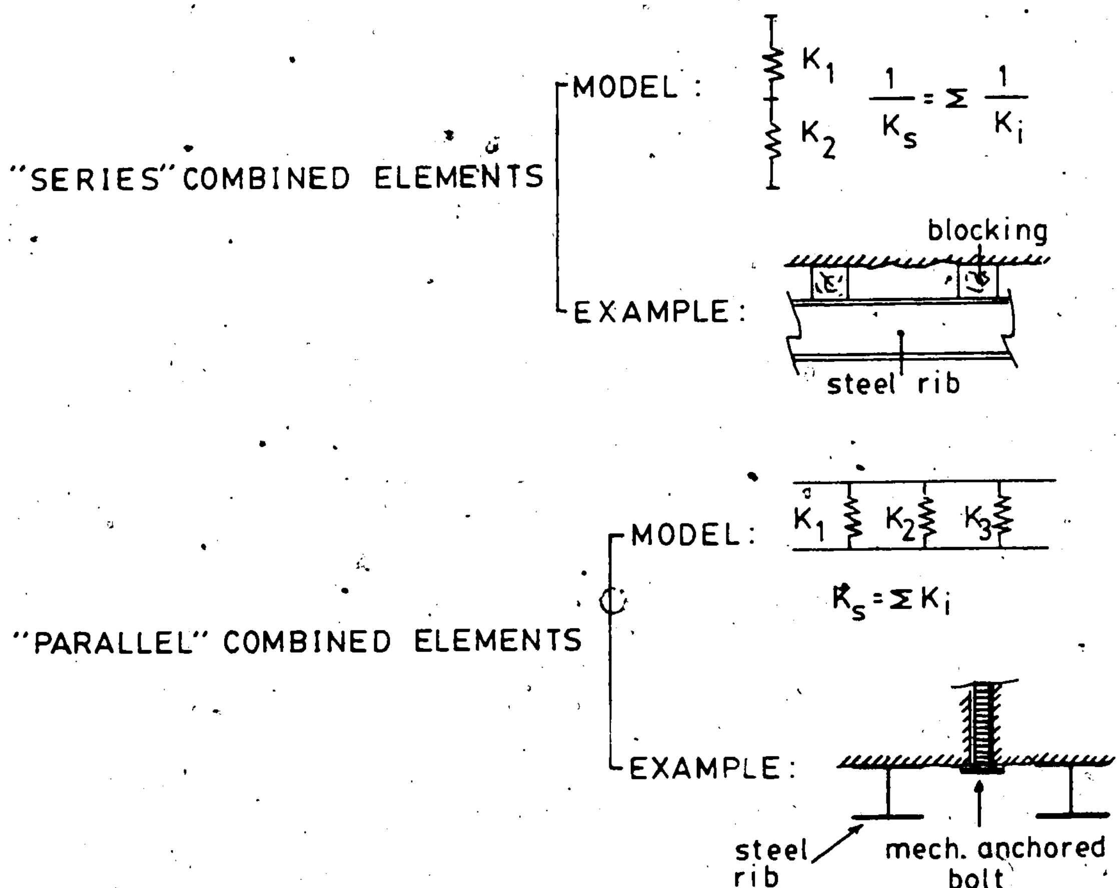

Figure 5.5 SUPPORT REACTION CURVE - COMBINED SUPPORT STIFFNESS

failure and the displacements that occured before the lining erection are necessary for the determination of the Support Reaction Curve.

The support stiffness (Ks) is defined as the uniform all around pressure required to cause unit diametral strain on the lining. Support stiffnesses for different liners such as concrete or shotcrete, block steel sets, rock bolts or cables are presented by Kaiser (1981). Lombardi (1970) also presents a variety of Support Reaction Curves. Hoek and Brown (1981) present the calculated maximum support pressures for various support systems. The study of combined support systems can be carried out with the models presented in Fig 5.5.

5.3.3 Determination of the Support Pressure and Ground Displacement at the Soil-Structure Interface

The solution for the soil-structure interaction,is given by the intersection of the two curves GRC and SRC (Fig 5.6). The simple solution of the complex ground-support interaction provided by the Characteristic Lines Method has several limitations associated with it.

The limitations of the Characteristic Lines Method were comprehensively discussed by Kerisel,J.; Duddeck,H.; Lombardi,G.; Fairhurst,C. and Daemen,J.J.K. during the Conference on "Analysis of Tunnel Stability by the Convergence-Confinement Method" held in Paris, 1978. The most significant limitations of this method are briefly

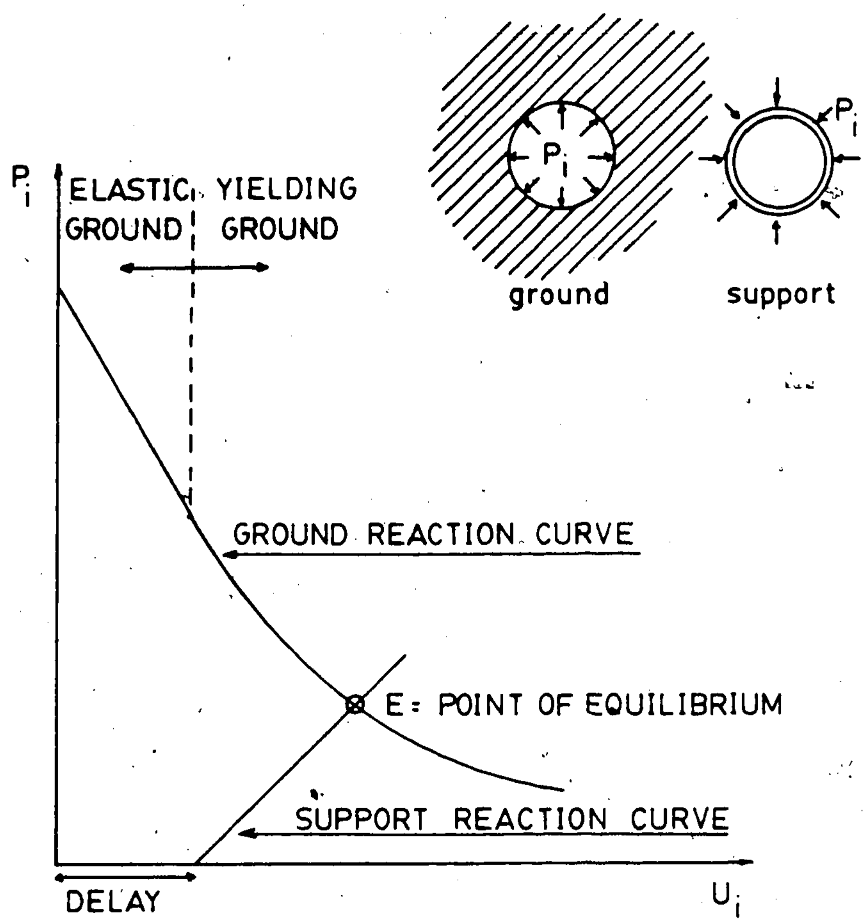

Figure 5.6 SOLUTION FOR THE SOIL-STRUCTURE INTERACTION BY THE CONVERGENCE-CONFINEMENT METHOD

discussed here. The Convergence-Confinement Method is limited to:

a) Cylindrical, or nearly cylindrical, opening and support

b) Support with constant mechanical and geometric properties (E, A, ν, I)

c) Homogeneous, isotropic and continuous ground

d) Uniform state of stresses ($\sigma_H = \sigma_V$): closed form solutions for studies of non-elastic ground masses are restricted to stress field ratio equal to one (K=1)

e) Uniform radial mode of deformation: as already noted in this chapter, the independent study of the ground and support is not possible for stress field ratios different than unity. This restriction limits the use of the Characteristic Lines Method to deep tunnels because shallow tunnels are often subjected to bending. This factor is not taken into account in the uniform radial mode of deformation

f) Time dependent soil behaviour: Fairhurst and Daemen (1972) present a qualitative discussion of the influence of the time dependent behaviour of rocks on the Ground Reaction Curve.

g) Gravity: the closed form solutions developed for the "hollow cylinder case" ignore the effects of gravity around the tunnel. The effects of gravity limit the Characteristic Lines Method to a greater degree when a "decompressed zone" develops to a significant extent around the opening and forms an unstable area in the crown.

The weight of the decompressed zone above the crown is an additional load not taken into account in the Convergence-Confinement Method. Kerisel in the Conference on Convergence-Confinement Method held in Paris proposed a method that takes the gravity loads into account. It is a method based on experiments on mini-tunnels and on the formulas for plastic equilibrium around a tunnel. The method enables a designer to calculate the gravity loads or "dead loads" as a function of the tunnel diameter, the soil unit weight and the distance between the support and face of the tunnel

h) Two dimensional behaviour of the system: Characteristic Curves are limited to plane strain/plane stress conditions. This is a significant limitation of the C.-C. Method since the face effects on the ground and lining behaviour are of utmost importance.

Egger (1978) proposed a simple method to take into account the face effects on excavation: the face is analytically modelled by a spherical face.

Lombardi (1970) proposed the simulation of the face by the sequential excavation of a core that has the tunnel diameter and length of one tunnel diameter. As the core is excavated, its load carrying capacity decreases and its wall displacements can be evaluated. The accuracy of the evaluation of the displacements that take place before the lining installation directly affects the accuracy of the prediction of loads and displacements by the Convergence-Confinement Method. Extensive finite element analyses have been carried out in order to study the three dimensional effects on tunnel design (Ranken and Ghaboussi (1975), Einstein and Schwartz (1980)).

5.3.4 Advantages of the Convergence-Confinement Method

The simplicity of the Convergence-Confinement Method is its major advantage. With the aid of only two curves, G.R.C. and S.R.C., the C.-C. Method provides a clear understanding and explanation of the process of tunnel construction.

The transfer of stresses from the ground to the lining, the effects of the delayed lining placement and concepts such as stand up time and many others are represented with ease by the C.-C. Method whereas other simple solutions, such as Closed Form Solutions, are limited to yield a "frozen picture" of strains and stresses within the ground and lining at the equilibrium condition.

The C.-C. Method is of enormous utility in complementing the tunnel design but may, however, not be suitable for direct design procedures due to the reasons discussed in this section.

5.4 Application of Simple Solutions to Tunnels Driven in Edmonton Till

In this section, the lining loads and displacements obtained from three tunnels driven in Edmonton till are compared to the loads and displacements calculated by the Simple Solutions described in the last two sections.

The three tunnels discussed in this section are:

LRT- North-East line, north tunnel (LRT-NE tunnel)

LRT- South Extension, north tunnel (LRT-SE tunnel)

Experimental tunnel (EXP tunnel)

The studies related to the LRT-NE tunnel are reported by Eisenstein et al (1977), and Eisentein and Thomson (1978). In the LRT-NE tunnel, surface settlements and stresses in the lining were measured. The LRT-SE tunnel is described in Chapters 2 to 4 in this thesis. The two tunnels mentioned above were constructed under very similar conditions. The only difference between the two LRT tunnels, despite minor local soil heterogeneities, is the size of the spacers installed in the two upper joints of the primary lining. The LRT-NE tunnel had spacers 10.2 cm long whereas in the LRT-SE the spacers were 15.2 cm long. The EXP-tunnel was comprehensively analysed by El-Nahhas (1980). It is a small diameter tunnel (D=2.56m) driven at a depth of 27 meters in the lower Edmonton till. Although the behaviour of two diffe[illegible]es of lining (rib and lagging and precast concrete[illegible] were monitored in the EXP tunnel, only measure[illegible] the rib and lagging system were related to the prese[illegible]udy.

The lining and ground parameters, related to the three tunnels , used throughout the calculations carried out in this section are presented in Table 5.1.

The three tunnels studied in this section were constructed under very similar conditions. The construction method and lining system is the same for the three tunnels.

The differences in strength and stiffness between the lower till, where the EXP tunnel was excavated, and the upper till, where the LRT tunnels were excavated are considered not to significantly alter the analysis carried out throughout this section.

The difference in the depth ratio (depth of the center of the tunnel / tunnel diameter) of the LRT tunnels and the EXP tunnel is important in the analysis of the validity of the application of "Simple Solutions" in the analysis of shallow tunnels. The EXP tunnel has a depth ratio of 10.56,

TUNNEL	SOIL ELAS. PARAMETERS		SOIL DISPLACEMENTS TOWARDS THE TUNNEL (mm) (AT THE SPRINGLINE)		
	E (MPA)	ν	BEFORE FACE	BEFORE EXPANSION	AFTER EXPANSION
LRT SE & NE	150	0.4	0*	2.5*	0.5*
EXPERIMENTAL	150	0.4	4	19	2.5+

* ONLY MEASURED AT THE LRT-SE TUNNEL

\+ Obtained from El-Nahhas (1980) Fig 4.14

STEEL RIBS

TUNNEL	ν	E(MPa)	$I_s (m^4)$ MOMENT OF INERTIA	AS(m^2) AREA CROSS SECTION	SPACING (m)	DIAM. (m)	LOADS AT THE SPRINGLINE (p_i/p_e)
LRT	0.25	207000	$22.2*10^{-8}$	$47.3*10^{-4}$	1.2*	6.1	0.18 TO 0.24 (SE) 0.62 TO 0.80 (NE)
EXPERIMENTAL	0.25	207000	$4.76*10^{-8}$	$24.7*10^{-4}$	1.5	2.56	0.02 to 0.12

TABLE 5.1 LINING AND GROUND PARAMETERS FOR THE LRT AND EXPERIMENTAL TUNNELS

and will be dealt with as a deep tunnel, whereas the LRT tunnels have a depth ratio of 1.90, and will be dealt with as shallow tunnels.

5.4.1 Analysis of the Results Obtained from Closed Form Solutions

The discussion presented in section 5.2 of this chapter showed the limitations of the available closed form solutions for deep lined tunnels. The solution proposed by Einstein and Schwartz (1979 and 1980) was chosen for this section. The assumptions involved in the derivation of this solution are summarized as:

- Plane strain condition
- Elastic behaviour of the ground and support
- Lining with constant cross section and constant mechanical properties
- Soil is isotropic and homogeneous
- The support and ground are simultaneously activated: no delayed installation of the support
- The unloading due to excavation is considered rather than external loading.

The required input for Closed Form Solutions related to ground and elastic support constants and the geometry of the support (diameter, cross sectional area, moment of inertia) is presented in Table 5.1.

The in-situ stress field is considered to be symmetric to both the vertical and horizontal tunnel axis (k=1). The magnitude of the field stress used in the calculations is calculated at the depth of the tunnel centreline.

The assumption that the in-situ stress ratio is equal to unity implies that in both cases, the full slip and no-slip between soil and structure yield identical results. The two cases yield the same results because when K=1, the shear stresses at the soil-liner interface is zero.

The equations presented in Fig 5.2 and the data presented in Table 5.1 make possible the calculation of the thrusts and deformations of the lining presented in Table 5.2. For the calculations of values presented in Table 5.2, the steel rib cross section area was divided by the rib spacing in order to obtain the effective cross section area, as recommended by Mohraz et al (1975).

The wooden lagging, installed between ribs, is assumed to have no self support capacity and does not enter into the calculations of the loads and displacements of the lining. A discussion of the self support capacity of the lagging is presented in Section 4.5.5.4.

The correction factors due to the delayed support installation and yielding ground, described in Section 5.2 are discussed in the next section.

TUNNEL	RATIOS		RIBS NORMAL LOAD (KN)		RADIAL DISPLACEMENT (mm)	
	C*	F*	CALCULATED	MEASURED	CALCULATED	MEASURED
LRT-NE LRT-SE	0.64	1302	529	461-585 100-300	2.0	- 3.0+
EXP	0.42	534	552	14-83	1.3	24.0++

+ MEASURED AT 1.2m FROM THE LINING SPRINGLINE

++ MEASURED AT .6m FROM THE LINING SPRINGLINE

TABLE 5.2- LINING THRUSTS AND DISPLACEMENTS CALCULATED BY THE CLOSED FORM SOLUTION PROPOSED BY EINSTEIN AND SCHWARTZ (1979,1980) FOR THE LRT AND THE EXPERIMENTAL TUNNELS.

5.4.2 Comments on the Evaluation of Ground Support Interaction by the Closed Form Solution by Einstein and Schwartz (1979, 1980)

For the calculation of the flexibility ratios (F*) presented in Table 5.2, the existence of the four joints of the LRT tunnel primary lining and the three joints of the EXP tunnel primary lining was neglected. Even neglecting the "hinges" in the steel ribs, the values of F* are found to be high. As discussed in section 5.2.1, for values of F* greater than 100, the bending moments on the lining are near zero and the thrust calculations are insensitive to F* which means that neglecting the lining joints does not affect the values of loads and displacements presented in Table 5.2.

The loads and lining displacements presented in Table 5.2 indicate that for the LRT-SE tunnel and the EXP tunnel, the thrusts on the lining are overestimated and the displacements underestimated when no corrections due to delay in the lining installation is applied to the linear elastic, closed form solution.

Table 5.2 also indicates that the loads measured in the LRT-NE tunnel were very close to that estimated, and that no correction factor due to delayed lining installation should be applied.

The correction due to the delayed lining installation, proposed by Einstein and Schwartz (1980), λ_d, presented in Section 5.2 is extremely difficult to estimate for the three tunnels studied in this section. The correction factor, λ_d, is a function of the distance between the face of excavation and the point where the lining first touches the ground (Ld). However, for tunnels excavated with a shielded mole, the span of unsupported ground is somewhat difficult to estimate.

In their study of some case histories on tunnel construction, Einstein and Schwartz proposed that, for tunnels excavated by a shielded mole, Ld should be the distance measured from the shield tail to the position where the lining touches the ground. This proposal assumes full contact between the shield and soil which is unreasonable for the stiff ground that surrounds the LRT and the EXP tunnels. Measurements taken from inside the LRT-SE indicate that there is a gap between the soil and the shield tail, hence, supporting the assumption that full contact between the soil and shield is unreasonable.

Values of λ_d varying from 0 to 0.8 for the LRT and EXP tunnels can be obtained from the calculations proposed by Einstein and Schwartz, which make the analysis of the results of Table 5.2 difficult. The yield factor (λ_y) based on finite element analyses carried out by Einstein and Schwartz indicate that yielding in the ground would result in an increase of up to 50% in the loads calculated from the elastic ground behaviour (Table 5.2).

If λ_y is equal to 1.5, λ_d would have to be 0.3 for the LRT-SE tunnel and 0.1 for the Experimental tunnel in order to obtain estimated loads similar to those measured at the site.

Einstein and Schwartz (1980) stated that the loads calculated by their method are overestimated up to 75%. They also verified the difficulty in the evaluation of λ_d, which is responsible for most of the inaccuracy of the method.

From the discussion presented in this chapter, it can be concluded that the prediction of lining thrusts by the Closed Form Solution is inaccurate for both deep and shallow tunnels.

It is believed that the construction details and the heterogeneity of the soil mask the inaccuracy of the application of Closed Form Solution for shallow tunnels.

The influence of the construction details and local heterogeneities on the lining thrusts can be verified by comparing the lining thrusts measured in the two LRT tunnels: the measured lining thrusts are very different despite of the fact that the two tunnels were built under identical conditions.

5.4.3 Analysis of the results obtained from the Convergence-Confinement Method

The normalized Ground Reaction Curve (GRC) for openings in the Edmonton till is plotted in Figure 5.7. The assumptions and equations involved in the plot of Ground Reaction Curves are shown in Figure 5.7 and described in Section 5.3 of this chapter. It is interesting to note that the Ground Reaction Curve, in the normalized form

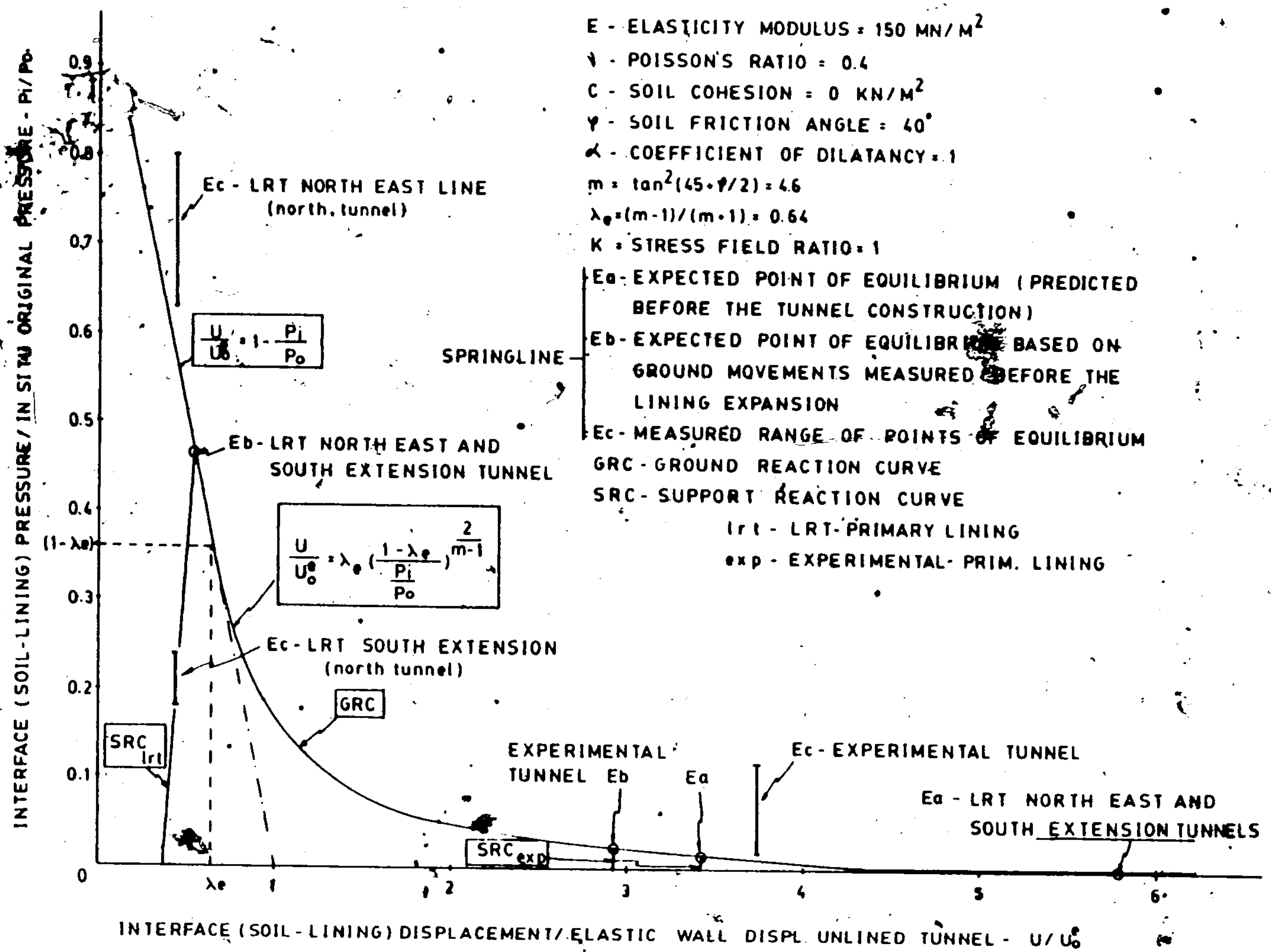

Figure 5.7 CHARACTERISTIC CURVES FOR THE LRT AND EXPERIMENTAL TUNNELS

$(Pi/Po \times Ui/U_o^e)$ is a function only of "λe" and "m" (defined in section 5.3). In the case where the soil cohesion is assumed to be zero, the normalized G.R.C. is a function only of the soil friction angle and the coefficient of dilation (α), irrespective of the soil elastic parameters in-situ stress field and size of the opening. The parameters E, ν, σ_o, D, are used when a specific displacement or pressure is to be plotted on the normalized G.R.C. plot.

The coordinates "λe", for the displacement ratio, and "$1-\lambda e$" for the pressure ratio, indicated in Fig 5.7, define the point where the onset of plasticity takes place around the opening.

Three different kinds of points of equilibrium [1] of the soil-structure interface, for the LRT and EXP tunnels, are shown in Fig 5.7 as Ea, Eb, and Ec.

1) Ea:

This is the point of equilibrium defined by the intersection of two curves, viz., the theoretical ground reaction and the support reaction curves.

The plot of the support reaction curves shown in Figure 5.7 requires a knowledge of the compressive stiffness of the support, calculated in Appendix D, and a knowledge of the ground displacement close to the ground support interface, that takes place before the lining expansion (Ubl).

---

[1] The point of equilibrium is defined by the coordinates Pi/Po, pressure ratio, and Ui/U_o^e, displacement ratio, plotted in the characteristic lines graph (Fig 5.7).

The amount of ground displacement that takes place at the soil-structure interface before the lining expansion, is defined as being the sum of two ground displacements:

a) Ground displacements that take place ahead of the face of the tunnel: assumed to be one third of the final elastic wall displacement of the unlined tunnel ($U_o^e/3$) (Ranken and Ghaboussi, 1975).

b) Ground displacements that take place along the length of the excavating machine are assumed to be one half of the difference between the excavated diameter and the diameter of the expanded primary lining.

The estimation of "Ubl" is presented in Table 5.3.

2) Eb:

This is the point of equilibrium defined by the intersection of two curves, viz., the theoretical ground reaction and the support reaction curves.

The difference between Eb and Ea is associated with the ground displacement that takes place before the lining expansion (Ubl):

In order to find Ea, "Ubl" is simply estimated based on a calculation, presented in Table 5.3, without taking into account any information from the tunnel instrumentation. On the other hand, the plot of the support reaction curve that defines the point of equilibrium, Eb, is based on the measured ground displacements that take place before the

TUNNEL	P_o (kN/m²)	$u_o^e = \frac{P_o(1+\nu)D}{2E}$	$\frac{D_{excav.} - D_{lin}}{2}$	$u_{bl} = \frac{\Delta D}{2} + \frac{u_o^e}{3}$	$\frac{u_{bl}}{u_o^e}$
LRT TUNNELS	236	6.8mm	37mm	39.3mm	5.8
EXPERIMENTAL TUNNEL	540	6.5mm	20mm	22.2mm	3.4

where:

u_{bl} = Ground displacement that takes place at the soil-structure interface, before the lining expansion.

u_o^e = Elastic wall displacements of the unlined tunnel.

P_o = In situ stress at the tunnel springline.

TABLE 5.3 - ESTIMATION OF THE GROUNG DISPLACEMENTS AT THE SOIL-STRUCTURE INTERFACE THAT OCCUR BEFORE THE LINING EXPANSION.

lining expansion (Ubl-meas) obtained from field instrumentation

The values of Ubl-meas/U_o^e are presented in Table 5.4.

3) Ec:

This is the range of points of equilibrium obtained from the lining and ground instrumentation.

Table 5.5 indicates the pressure and displacement ratios (Pi/Po and Ufinal-meas/U_o^e) calculated for three tunnels:

- LRT - South Extension - North tunnel
- LRT - North-East line - North tunnel
- Experimental tunnel

The range of points of equilibrium (Ec) related to the LRT-NE tunnel was plotted on Figure 5.7 based on certain assumptions because no ground displacements at the springline were available for this tunnel. It was assumed that the ground displacements at the springline of the LRT-Ne tunnel are equal to the ones measured in the LRT-SE tunnel. The assumption of equal lining displacement in the two LRT tunnels is based on the fact that these two tunnels were built with very similar geometry, constructions method and ground conditions, and caused similar surface settlements.

The load and displacement ratios defining "Ec" are related to the springline of the tunnels studied in this section because at the springline, more complete information was available.

TUNNEL	P_o (kN/m²)	$u_o^e = \dfrac{p_o(1+\nu)D}{2E}$	$u_{bl\text{-}meas}$	$\dfrac{u_{bl\text{-}meas}}{u_o^e}$
LRT	236	6.8mm	2.5mm	0.37
EXPERIMENTAL	540	6.5mm	19mm	2.92

where: $u_{bl\text{-}meas}$ = Measured ground displacements at the soil-structure interface that take place before the lining expansion.

u_o^e = Elastic wall displacements of the unlined tunnel.

p_o = In situ stress at the tunnel springline.

Table 5.4 CALCULATION OF THE RATIO Ubl-meas/Uo

TUNNEL	P_o (kN/m²)	P_i/P_o	$u_o^e = \frac{P_o(1+\nu)D}{2E}$	$u_{final-meas}$	$\frac{u_{final-meas.}}{u_o^e}$
LRT-SOUTH EXT	236	0.18 to 0.24	6.8mm	3mm	0.44
LRT-NORTH EAST	236	0.63 to 0.80	6.8mm	3mm	0.44
EXPERIMENTAL	540	0.02 to 0.12	6.5mm	24mm	3.75

where: $u_{final-meas}$ = Final ground displacement at the soil-structure interface;
u_o^e = Elastic wall displacements of the unlined tunnel.
P_o = In situ stress at the tunnel springline.

Table 5.5 CALCULATION OF THE RATIO Ufinal-meas/Uo

The value of the modulus of elasticity, E, chosen for the Edmonton till, 150 MN/m², is based on the pressuremeter tests reported by Morrison (1972).

5.4.4 Comments on the Evaluation of the Ground Support Interaction by the Convergence-Confinement Method

The analysis of the "points of equilibrium" plotted for the soil-structure interface of the EXP tunnel, in Fig 5.7, indicates that thrusts and lining displacements can be reasonably well predicted using the Convergence-Confinement Method.

The measured loads and displacements, in the EXP tunnel are greater than those estimated but not to a significant extent. The reason for higher measured values may be ascribed to a higher degree of soil disturbance during tunnel construction. An increase in the soil disturbance would probably result in a decrease in the soil elasticity modulus and shear strength that would yield greater loads and lining displacements.

As opposed to the EXP tunnel, the predictions of loads on the lining and ground displacements for the LRT tunnels based on the characteristic lines method yielded loads and displacements completely different than those measured.

The comparison between Ec, measured loads and displacements, and Ea, estimated loads and displacements obtained for the LRT tunnels, indicates that the convergence confinement method predicts much higher displacements and much lower thrusts in the lining than those measured.

The comparison between Ec and Eb, related to the LRT tunnels, indicate that the discrepancy between measured and expected loads and lining displacements is, basicly due to the inaccurate estimation of ground displacements ahead of the lining expansion. The estimated loads and lining displacements compare better to those measured when the point of equilibrium of the soil-structure interface is estimated on the basis of the ground movements obtained from the field instrumentation (Eb).

The inaccurate assessment of ground displacements that take place before the lining expansion is believed to be the result of the non-axisymmetric mode of deformation and development of plasticity around shallow tunnels, even in the case where K (stress field ratio) is approximately 1. The fact that the mode of deformation is responsible for the inaccuracy of the soil structure interactions predicted for the LRT is supported by the fact that after the non-axisymmetric mode of deformation ceases, i.e. when the lining is expanded against the ground, the loads and displacements predicted by the G.-C. Method become close to the measured ones.

It is believed that the soil disturbance due to tunnel construction strongly affects the boundary condition and consequently the mode of deformation of the soils around shallow tunnels.

As already mentioned in section 5.2, elastic finite element studies indicate that the LRT tunnels are at the boundary of being defined as a deep or shallow tunnel. The study of the LRT and the EXP tunnels indicated that this definition, based on finite element analyses, is not necessarily valid.

The definition of difference between deep and shallow tunnels based on stress and strain distribution around openings should take into account the construction technique used and particularly the sequence of lining installation in order to evaluate more effectively the effect of the opening excavation on the boundaries.

The study of the prediction of the soil-structure interaction for deep and shallow tunnels, constructed in a similar manner, indicated that, for the Convergence-Confinement Method (Section 5.3.3), the limitations related to the mode of deformation on the ground and of the lining are of major importance.

The discrepancy between measured and estimated ground displacements at the springline of the LRT-SE tunnel before the lining is expanded might also be due to the distance between the inclinometers and the lining. The distance between the inclinometer at the springline level and the LRT-SE lining is 1.2 metre. If soil expansion takes place within this 1.2 metre space, the measured displacements would be smaller than those at the soil-liner interface.

The comparative study of the LRT tunnels and the EXP tunnel is not invalidated by the distance between the inclinometer and LRT lining because in the EXP tunnel, the inclinometer that yielded the results reported in this section was installed at 0.6 metre from the liner which is considered large compared to the tunnel diameter.

5.5 Summary and Conclusions of the Evaluation of Soil-Structure Interaction by "Simple Solutions"

In this chapter, the applicability of Closed Form Solutions and the Convergence-Confinement Method for the evaluation of the soil-structure interaction in shallow tunnels was analysed. This analysis was based on the data collected from two types of tunnels constructed under very similar conditions, viz., the shallow LRT tunnels and the deep EXP tunnel.

It was concluded that the thrusts and lining displacements predicted by the closed form solution proposed by Einstein and Schwartz (1979,1980) were only comparable to those measured in the LRT-NE tunnel.

For the LRT-SE and EXP tunnels, the measured thrusts were much smaller than those predicted.

The correction to the lining thrusts and moments calculated by the Closed Form Solution due to delayed lining installation and yelding ground was discussed in this chapter. It was concluded that the delayed lining installation correction factor (λd) is difficult to predict for tunnels excavated in stiff ground by shielded tunnel boring machines.

The difficulty in predicting λd masks the effects of the proximity of the surface on the thrusts and lining displacements calculated by the Closed Form Solutions.

The evaluation of the soil-structure interaction by the Characteristic Lines Method was found to be good for the deep tunnel, i.e. the EXP tunnel. The boundary conditions and mode of deformation in the Experimental tunnel are probably closer to those assumed by the Characteristic Lines Method.

The lining loads and ground deformations predicted by the Characteristic Lines Method for the LRT tunnels, were different than those observed. The predicted displacements at the tunnel springline were much greater than those measured. The reasons for the discrepancy between predicted and measured displacements were ascribed to the fact that the mode of deformation of the soil surrounding the LRT tunnels was not equal to that assumed in the derivation of the characteristic lines in the Convergence-Confinement Method.

A departure from the uniform radial mode of behaviour (axisymmetric) assumed by the C.-C. Method might be due to:

- A lower value of the in-situ stress ratio (K<1)
- The heterogeneous nature of the upper till, with the presence of the inter-till sand in the

proximity of the tunnel.

- the proximity of the tunnel to the surface

The fact that an in-situ stress ratio close to unity has been verified in the upper Edmonton till and that only small sand pockets were detected close to the tunnel instrumentation might be an indication of the importance of proximity of the tunnel to the surface on the departure from the axisymmetric behaviour in the LRT-SE tunnel.

The use of the Convergence-Confinement Method in the study of the soil-structure interaction of the tunnels presented in this section was extremely useful. The plot of estimated and measured loads and displacements on the ground and lining on Figure 5.7 gave an indication of the importance of the proper assumptions concerning the mode of behaviour around shallow openings.

There is a great need for the development of simple solutions for shallow tunnels. The existence of Simple Solutions would help the tunnel design but its limitations can be foreseen because the discrepancy between the loads measured in the two LRT tunnels can only be explained by the complete knowledge of minor construction details and local heterogeneity. These can hardly be incorporated in a Simple Solution.

6. CONCLUSIONS

6.1 Introduction

The research [illegible] examined the behaviour of a large diameter, shallow tunnel, built in stiff ground for the extension of the Light Rail Transit System of the City of Edmonton, Alberta.

The analysis of the factors affecting the behaviour of the tunnel lining and surrounding ground was based on the data collected from a comprehensive monitoring program. The comparison of the results from a deeper, small diameter tunnel, with a different depth ratio (depth of the centre of the tunnel/tunnel diameter) allowed the analysis of the influence of the depth ratio on the mode of deformation and plastic behaviour of the soil and how these affect the lining behaviour.

The following sections summarize the major findings of this research.

6.2 Soil Response to Tunneling

6.2.1 Surface Vertical Displacements

The surface settlement points indicated that the surface settlement trough was not symmetric to the tunnel axis. This asymmetry might be due to the presence of inter-till sand pockets, non-symmetric to the tunnel axis or/and due to the presence of buildings at only one side of the tunnel axis. The shallow foundations of these buildings might locally increase the soil stiffness, resulting in smaller settlements.

The asymmetry observed in the transverse sections of the surface settlements troughs indicates that they do not fit the Gaussian distribution of surface settlements proposed by Litviniszyn (1956) and Peck (1969).

The steeper portions of the transverse section of the settlement troughs occur in a narrow region above the tunnel and do not affect the buildings located 10 metres from the tunnel axis, where the differential settlements are approximately 1:17000.

Negligible surface vertical displacements were [illegible] ahead of the face of the mole. These displacements stabilized 15 metres behind the face of the mole.

6.2.2 Deep Vertical Displacements

Before the mole reached a section, points close to the soil to be excavated along a vertical line passing through the tunnel axis experienced heave of up to 3mm. Negligible downward movements were detected ahead of the face of the mole.

During the tunnel excavation, the extensometers located beside the tunnel liner did not measure significant soil straining in the vertical direction ($\varepsilon_{vert} < 0.1\%$)

The stabilization of vertical displacements of the soil occurred approximately 15 metres from the face of the mole..

The monitoring of vertical movements above a roof failure indicated that large vertical displacements (larger than 50mm) propagated up to 3.4 metres to 4.5 metres above the tunnel crown. The settlements at the surface, above this roof failure, were small and should not affect the nearby building foundations.

6.2.3 Deep Horizontal Displacements

The inclinometers located at 1.2 metre and 3.3 metres from the tunnel liner, at the springline, measured horizontal displacements of 3.0mm and 2.0mm, respectively, towards the tunnel axis. The development of horizontal movements towards the tunnel axis started 3.0 metres ahead of the face of the mole and stabilized approximately 6.0 metres from the tail of the mole, where the primary lining was expanded against the ground. It can be concluded that the horizontal displacements in the soil stabilized faster than the vertical ones.

The development of soil movements in the direction parallel to the tunnel axis indicated that analytical studies of tunnel behaviour based on plane strain analyses do not reflect reality. The fact that the points in the ground move in a direction parallel to the tunnel axis during tunneling and return to their initial position, after the mole passes, enhances the fact that studies of the final displacements about tunnels that do not take into account the soil "strain history" are not acceptable.

6.2.4 Loss of Ground

The coupled analysis of vertical and horizontal displacements around the LRT tunnel yielded the conclusion that the ground experienced an average volume increase of 0.59 m³/lineal metre (1.96% of the tunnel nominal volume) due to tunnel construction. Similar ground volume increases were measured by Hansmire (1975) in a tunnel dug in dense sand.

More than 96% of the ground volume increase due to the LRT tunnel construction occurred in the region above the tunnel crown.

6.3 Lining Loads and Displacements

The loads carried by the steel lagging and load cells were affected by the action of the longitudinal propulsion jacks of the mole on the primary lining.

The load cells installed in the lower rib joints consistently picked up higher loads than those installed in the upper joints. This reflects the development of shear at the soil-liner interface, probably due to the upward movement of the liner detected in the lining displacement measurements. The load cells also indicated higher soil stress relief at the invert than at the crown. This difference in soil stress relief might also be due to the upward movement of the liner.

The coupled study of the steel lagging and load cell data indicated that the steel ribs carried average loads 85% to 213% higher than those carried by the lagging. This might be an indication that soil arching occurred between ribs.

The steel ribs at the crown carried loads from 9% to 26% of the overburden. These loads are smaller than those measured in the LRT North East tunnel (71% of overburden).

The lining displacements measurements indicated that after rib expansion, there is very little liner distortion.

6.4 Soil-Structure Interaction

The [illegible] of the soil displacements associated with the loads on the primary lining in tunnels constructed in Edmonton with different depth ratios (depth of center of the tunnel/tunnel diameter) enabled the analysis of the applicability of Closed Form Solutions and the Convergence-Confinement Method, termed Simple Solutions, to shallow tunnels. This analysis showed that the prediction of lining loads and displacements with Closed Form Solutions is inaccurate for both deep and shallow tunnels, basically due to the difficulty of taking into account the delayed installation of the lining. It was concluded that the prediction of tunnel behaviour based on the Confinement-Convergence Method yielded good results for deep tunnels but not for shallow tunnels.

The discrepancy between predicted and measured displacements is ascribed to the fact that the mode of deformation and development of plasticity of the soil surrounding the LRT tunnels was not axisymmetric, as assumed by the Convergence-Confinement Method. The departure from the uniform radial mode of behaviour (axisymmetric) was ascribed to the proximity of the LRT tunnels to the surface.

6.5 Recommendations for Further Studies

The conclusions presented in this Chapter indicate that there is no simple method that permits the engineer to rapidly investigate alternatives to problems related to shallow tunnels. It is suggested that further studies to develop Closed Form Solutions for shallow lined tunnels should be carried out. These Closed Form Solutions would probably lead to simple design methods applicable to shallow tunnels.

REFERENCES

Attewell, P.B., and Farmer, I.W. 1974a. Ground deformation resulting from shield tunnelling in London clay, Canadian Geotechnical Journal, Vol. 11, pp. 380-395.

Attewell, P.B., and Farmer, I.W. 1974b. Ground disturbance caused by shield tunnelling in stiff overconsolidated clay. Engineering Geology, Vol. 8, pp.361-381.

Attewell, P.B., and Farmer, I.W. 1975. Ground settlement above shield driven tunnels in clay. Tunnels and Tunnelling, Vol. 7, No. 1, pp.58-62.

Burke, H. 1957. Garrison Dam tunnel test section investigation. Journal of Soil Mechanics and Foundations Division, ASCE, Vol. 83, paper no. 1438.

Burland, J.B., and Moore, J.F.A. 1973. The measurement of ground displacements around deep excavations. Field Instrumentation in Geotechnical Engineering, Butterworth and Co., London, pp.70-84.

Burns, J.Q. and Richard, R.M. 1964. Attenuation of stresses for buried cylinders. Proceedings on Symposium on Soil-Structure Interaction, Tucson, pp. 378-392

Chatterji, P.K., Smith, L.B., Insley, A.E., and Sharma, L. 1979. Construction of Saline Creek Tunnel in Athabasca Oil Sand. Canadian Geotechnical Journal, Vol. 16, pp. 90-103.

Cording, E.J., Hendron, A.J., Pa[illegible]erson, H.H. Hansmire, W.H., Jones, R.A., Mahar, J.W. and O'Rourke, T.D. 1975. Methods for geotechnical observations and instrumentation in tunneling. Report prepared for U.S.

Curtis, D.J. 1976. The circular tunnel in elastic ground: Discussion. Geotechnique, Vol. 26, pp.231-237.

Daemen, J.J.K. and Fairhurst, C. 1970. Influence of failed rock properties in tunnel stability. 12th Symposium on Rock Mechanics, Rolla, Missouri, pp. 855-875.

Daemen, J.J.K. and Fairhurst, C. 1972. Rock failure and tunnel support loading. Proceedings of the International Symposium on Underground Openings. Luzern, Switzerland

Delory, F.A., Crawford, A.M., and Gibson, M.E.M. 1979. Measurements on a tunnel lining in very dense till. Canadian Geotechnical Journal, Vol. 16, pp. 190-199.

Eisenstein, Z., Kulak, G.I., MacGregor, J.G., and Thomson, S. , 1977. Report on Geotechnical and Construction Performance of the Twin Tunnels. Unpublished report prepared for the City of Edmonton Engineering Dpt., Edmonton, Alberta, 77 pp.

Eisenstein, Z., and Thomson, S. 1978. Geotechnical performance of a tunnel in till. Canadian Geotechnical Journal, Vol. 15, pp. 332-345.

Einstein, H.H. and Schwartz, C.W. 1979. Simplified analysis for tunnel supports. [illegible] Journal of Geotechnical Engineering Division, [illegible], pp. 499-518.

Einstein, H.H. and Schwartz, C.W. 1980. Improved design of tunnel supports volumes 1 and 2. Report prepared for the U.S. Dept of Transportations. Report numbers: UMTA-MA-06-0100-80-4 and 5.

El-Nahhas, F. 1977. Field measurements in two tunnels in the City of Edmonton. M.Sc. Thesis, Departement of Civil Engineering, University of Alberta, Edmonton, Alberta, 85p.

El-Nahhas, F. 1980. The behaviour of tunnels in stiff soils. Ph.D. Thesis, Dpt. of Civil Engineering, University of Alberta. Edmonton, Alberta, 305 pp.

Figueiredo, A.F. and Negro, A. 1981. A new sensing system for boreholes extensometers. Unpublished technical note.

Gould, J.D. and Dunnicliff, C.J. 1971. Accuracy of field deformation measurements. Proceedings of the 4th Pan American Conference on Soil Mechanics and Foundation Engineering, Puerto Rico, Vol. 1, pp.313-366.

Hanna, T.H. 1973. Foundation instrumentation. Trans. Tech. Publications, Cleveland.

Hansmire, W. 1975. Field measurements of ground displacements about a tunnel in soil. Ph.D. Thesis, University of Illinois at Urbana-Champaign.

Hedley, D.G.F. 1969. Design criteria for multi-wire borehole extensometer systems. First Canadian Symposium on Mining Surveying and Rock Deformation Measurements.

Hoek, E. and Brown, E.T. 1981. Underground excavations in rock. Inst. Min. and Met., London

Kaiser, P.K. 1980. Effect of stress history on the deformation behaviour of underground openings. 13th Canadian Rock Mechnics Symposium, pp. 133-140.

Kaiser, P.K. 1981. University of Alberta CIVE 699 Unpublished class notes.

Kanji, M.A. 1979. Surface displacement as a consequence of excavation activities (General Report, Theme IV). Proc. 4th Rock Mech. Congress, Int. Soc. Rock Mech., Montreux, Vol 3, pp 345-368.

Kathol, C.P. and McPherson, R.A. 1975. Urban geology of Edmonton. Alberta Research Counsil, Bulletin 32, 61p.

Kerisel, J.; Duddeck, H.; Lombardi, G.; Fairhurst, C. and Daemen, J.J.K; Egger, P. 1978. Proceedings of the Conference on Analysis of Tunnel Stability by the Convergence-Confinement Method, Underground Space, 1980, Vol. 4, No. 4, 5 and 6, pp.221-258, 297-318 and 361-402.

Kovari, K., Amstad, C.H., Fritz, P. 1977. Integrated measuring technique for rock pressure. Int. Symposium on Field measurements in Rock Mechanics, Zurich, pp.

289-316.

Ladanyi, B. 1974. Use of long-term strength concept in the determination of ground pressure on tunnel linings. Proc. of the 3rd Inter. Cong. on Rock Mechnics, Vol. 2B, pp. 1150-1156.

Litviniszyn, J. 1956. Application of the equation of stochastic processes to mechanics of loose bodies. Arch. Mech. Stosow, Vol.8, pp.393-411.

Lombardi, G. 1970. The influence of rock characteristics on the stability of rock cavities. Tunnels and Tunnelling, Vol. 2, pp. 104-109.

Lombardi, G. 1973. Dimensioning of tunnel linings with regards to constructional procedure. Tunnels and Tunnelling, Vol. 5, pp. 340-351.

May, R.W. and Thomson, S. 1978. The geology and geotechnical properties of till and related deposits in the Edmonton, Alberta, area. Canadian Geotechnical Journal, Vol. 15, pp. 362-370.

Medeiros, L. 1979. Deep excavations in stiff soils. Ph.D. Thesis, Departement of Civil Engineering, University of Alberta.

Mello, V.F.B. 1981. Proposed bases for collating experiences for urban tunneling design. Proceedings of the Symposium on Tunneling and Deep Excavations in Soils, Sao Paulo, Brazil, pp. 197-235.

Mendes, R.H., Brown, E.L., Moreau, R. and Boyer, B. 1970. Supervision of the behaviour of Daniel Johnson Dam (Manicouagan 5). Trans. 10th Intl. Cong. on Large Dams, Montreal, Vol III, pp. 1183-1205.

Mindlin, R.D. 1940. Stress distribution around a tunnel. Trans. American Society of Civil Engineering, Vol 105, pp. 1117-1140.

Mohraz, B., Hendron, A.J., Ranken, R.E. and Salem, M.H. 1975. Liner medium interaction in tunnels ASCE

Journal of the Construction Division, March 1975, pp. 127-141.

Morgan, H.D. 1961. A contribution to the analysis of stress in a circular tunnel, Geotechnique, Vol. 11, pp. 37-46.

Muir Wood, A.M. 1975. The circular tunnel in elastic ground. Geotechnique, Vol. 25, pp. 115-127.

Obert, L. and Duvall, W.I. 1967. Rock mechanics and the design of structures in rock. New-York, John Wiley and Sons.

Panet, M. 1976. Stabilite et Soutenement des tunnels. La mechanique des roches appliquee aux ouvrages du Genie Civil, Chapitre IX, pp 143-168. L'Ecole Nationale des Ponts et Chausses.

Peck, R.B. 1969-a. Advantages and limitations of the Observational method in applied soil mechanics. 9th Rankine Lecture, Geotechnique, Vol. 19, pp 171-187.

Peck, R.B. 1969-b. Deep excavations and tunnelling in soft ground. State of the Art Report. Proc. 7th Int. Conf. on Soil Mech. and Found. Eng., Vol. 3, Mexico City, Mexico, pp. 225-290.

Peck, R.B., Hendron, A.J. and Mohraz, B. 1972. State of the srt of soft-ground tunneling. Proceedings of the 1st North American Rapid Excavation and Tunneling Conference, Vol. 1, pp. 259-286.

Ranken, R.E. and Ghaboussi, J. 1975. Tunnel design considerations: Analysis of stresses and deformations around advancing tunnels. Report prepared for U.S. Department of transportation, UILU-ENG75-2016.

Ryzuk, C.N. 1977. Details of multipoint extensometers used to monitor deformation in a tunnel in oil sands. Memorandum to Dr. N.R. Morgenstern, unpublished.

Savigny, K.W. 1980. In situ analysis of naturally occurring creep in ice-rich permafrost soil. Ph.D. Thesis, Dpt.

of Civil Engineering, University of Alberta, Edmonton, Alberta. pp 439.

Schmidt, B. 1969. Settlement and ground movement associated with tunnelling in soil. Ph.D. Thesis, Department of Civil Engineering, University of Illinois, Urbana.

Thomson, S. and El-Nahhas, F. 1980. Field measurements in two tunnels in Edmonton, Alberta. Canadian Geotechnical Journal, Vol. 17, pp. 20-33.

Terzaghi, K. 1938. Settlement of structures in Europe and methods of measurement. Transactions, ASCE, Vol. 103, 1432.

Thurber Consultants Ltd. 1980. Subsurface conditions, Central Station to Government Centre Station. Unpublished report prepared for the City of Edmonton, LRT, Edmonton, Alberta.

U.S.B.R. 1963. Earth manual, U.S. Bureau of Reclamation, Denver Colorado.

Ward, W.H., Burland, J.B. and Gallois, R.W. 1968. Geotechnical assessment of site at Mundford, Norfolk for a large proton accelerator. Geotechnique, Vol. 18, No.4, pp. 399-431.

Westgate, J.A. 1969. The Quaternary geology of the Edmonton area, Alberta. In Pedology and Quaternary research. Edited by S. Pawluk. University of Alberta Printing Department, Edmonton, Alberta, pp.129-151.

Wilson, S.D. 1962. The use of slope measuring devices to determine movements in earth masses. ASTM STP 322, Field Testing of Soils, pp.187-197.

A. APPENDIX - LABORATORY TEST RESULTS

TEST HOLE	DEPTH (m)	Wi (%)	Wp (%)	Wl (%)	Ip (%)	% SAND	% SILT	% CLAY	BULK DENSITY (Mg/m3)	UNDRAINED SHEAR STRENGTH (kPa)
A. CLAYS										
79-1	3.8-4.3	26.4	29.4	65.0	35.6	9.0	47.0	44.0	2.01	63
79-2	3.8-4.3	33.2	19.1	61.9	42.8	6.0	54.0	40.0	1.98	101
79-3	3.8-4.3	32.3	23.8	70.9	47.8	7.0	38.0	55.0	1.95	141
79-6	5.3-5.6	38.2	20.9	46.5	25.6	-	70.0	30.0	1.95	60
79-10	3.8-4.3	33.7	22.9	59.1	36.2	-	64.5	35.5	1.94	81
79-15	3.8-4.3	31.5	18.2	32.9	14.7	5.0	85.0	10.0		
79-18	2.4-2.9	32.3	27.2	64.6	37.4	5.0	51.0	44.0		
79-20	5.8-6.2	39.4	27.7	49.9	22.2	1.5	69.5	29.0	1.81	44
79-21	4.1-4.6	34.6	27.7	57.5	29.8	12.5	50.0	37.5	1.91	96
79-23	3.7-4.1	28.0	32.6	78.7	46.1	2.0	36.0	62.0	1.84	86
79-23	5.2-5.6	34.3							1.86	137
B. SILTS										
79-13	6.9-7.3	33.3	27.8	35.3	7.5	5.0	82.0	13.0	-	-
79-14	6.9-7.3	35.7	26.2	34.2	8.0	10.0	81.0	9.0	-	-
79-16	5.3-5.8	21.1	27.7	30.4	2.7	1.0	89.0	10.0	-	-

Table A.1 SUMMARY OF LABORATORY TEST RESULTS - LAKE EDMONTON SEDIMENTS

TEST HOLE	DEPTH (m)	Wi (%)	Wp (%)	Wl (%)	Ip (%)	% SAND	% SILT	% CLAY	BULK DENSITY (Mg/m^3)	UNDRAINED SHEAR STRENGTH (kPa)
79-1	8.4- 8.7	14.4	18.1	34.9	16.8	40.0	40.0	20.0	2.15	344
79-2	9.9-10.2	14.1	16.4	26.8	10.4	45.0	47.5	7.5	2.16	54*
79-3	8.4- 8.7	12.7	16.8	27.8	11.0	41.0	43.0	16.0	2.24	339
79-3	13.1-13.5	12.1	14.9	31.9	17.0	42.0	37.0	21.0	2.23	342
79-4	5.3- 5.8	28.7	18.2	43.2	25.0	24.0	49.0	27.0	2.01	54*
79-5	8.4- 8.7	16.3	16.9	38.4	21.05	37.5	39.0	23.5	2.25	175
79-8	8.4- 8.7	13.6	15.9	30.5	14.6	45.0	40.0	15.0	2.30	198
79-11	8.4- 8.7	14.5	15.8	34.3	18.5	37.0	45.0	17.5	2.27	365
79-19	11.6-11.9		16.7	34.2	17.5	40.0	41.0	19.0		
79-22	7.3- 7.8	24.2	16.2	29.9	13.7	47.5	36.5	16.0	2.12	325

*Sheared along vertical crack.

LEGEND: Wi in situ water content
Wp plastic limit
Wl liquid limit
Ip plasticity index

Table A.2 SUMMARY OF LABORATORY TEST RESULTS - BROWN TILL

TEST HOLE	DEPTH (m)	Wi (%)	Wp (%)	Wl (%)	Ip (%)	% SAND	% SILT	% CLAY	BULK DENSITY (Mg/m^3)	UNDRAINED SHEAR STRENGTH (kPa)
79-1	13.0-13.4	11.3	19.3	34.8	15.4	40.0	40.0	20.0	2.33	363
79-1	16.0-16.5	12.0	15.6	38.0	22.4	36.0	40.0	24.0	2.24	540
79-2	14.8-15.2	13.2	16.4	29.1	12.7	45.0	40.0	15.0	2.24	315
79-2	17.8-18.3	14.9	15.5	39.6	24.1	36.0	40.0	24.0	2.19	259
79-2	20.6-21.0	24.6	20.8	66.8	46.0	9.0	36.0	55.0	2.03	176
79-2	22.1-22.6	24.5	21.5	49.5	28.0	20.0	53.0	27.0	2.00	192
79-2	23.6-24.1	18.0	20.6	51.8	31.2	16.0	42.5	41.5	2.17	240
79-3	17.5-17.8	15.5	14.2	38.0	23.8	36.0	39.0	25.0	2.17	218
79-3	19.0-19.5	15.7	18.3	40.6	22.3	32.0	40.5	27.5	2.12	254
79-3	20.6-21.0	15.9	14.8	38.1	23.3	36.0	39.0	25.0	2.19	187
79-3	22.1-22.6	14.2	18.8	40.2	21.4	32.0	41.0	27.0	2.17	383
79-5	16.0-16.3	15.0	14.9	36.6	21.7	35.0	42.0	23.0	2.31	225
79-5	19.1-19.4	16.3	15.6	35.4	19.8	39.0	39.5	21.5	-	-
79-5	22.1-22.6	12.7	16.6	34.9	18.3	42.5	35.5	22.0	2.21	380
79-6	22.1-22.6	12.6	18.7	42.5	23.8	35.0	36.5	28.5	2.21	680

Table A.3 SUMMARY OF LABORATORY TEST RESULTS - GREY TILL

TEST HOLE	DEPTH (m)	Wi (%)	Wp (%)	Wl (%)	Ip (%)	% SAND	% SILT	% CLAY	BULK DENSITY (Mg/m^3)	UNDRAINED SHEAR STRENGTH (kPa)
79-10	16.0-16.5	14.6	14.2	36.2	22.0	35.5	43.5	21.0	2.25	250*
79-18	14.8-15.2	18.7	18.7	29.4	10.7	13.0	77.0	10.0	2.06	180
79-18	20.7-21.2	16.6	16.8	35.0	18.2	42.0	35.5	22.5	1.97	163
79-20	13.0-13.4	19.8	17.2	30.9	13.7	41.0	42.0	17.0	2.32	220
79-21	22.1-22.6	15.9	16.8	37.4	20.6	41.0	36.0	23.0	2.13	245
79-22	7.3- 7.8	17.4	16.2	29.9	13.7	47.5	36.5	16.0	2.12	225
79-22	10.4-10.8	15.5	16.3	32.7	16.4	41.5	41.0	17.5	2.21	183
79-22	16.2-16.6	16.3	17.4	33.6	16.2	38.0	41.0	21.0	2.20	243
79-24	14.8-15.3	10.1	15.7	32.9	17.2	44.5	35.0	20.5	2.24	662
79-25	16.3-16.8	11.1	17.2	31.5	14.3	41.0	42.0	17.0	2.22	486
79-26	14.8-15.3	14.5	16.3	36.9	20.6	40.5	37.0	22.5	2.10	155
79-26	17.5-18.0	14.2	16.1	34.7	18.6	42.0	38.0	20.0	2.03	139
79-26	22.1-22.6	18.6	22.7	50.6	27.9	27.5	42.5	30.0	2.06	94

* Modulus of Elasticity as measured in Cyclic Compressive Test was 110 MPa.

Table A.4 SUMMARY OF LABORATORY TEST RESULTS - GREY TILL (cont)

Table A.5 SUMMARY OF LABORATORY TEST RESULTS - INTER-TILL SANDS

Test Hole	Depth (m)	Wi	% Sand	% Silt	%Clay
79-6	8.4 - 8.7	15.5	66.0	24.0	5.0
79-6	11.7 - 12.0	19.9	65.0	31.0	4.0
79-6	14.5 - 14.7	22.9	38.0	62.0	0.0
79-19	14.7 - 15.0	22.0	60.0	35.5	4.5
79-19	17.7 - 18.0	18.3	78.5	17.0	4.5

Table A.6 SUMMARY OF LABORATORY TEST RESULTS - SASKATCHEWAN SANDS AND GRAVELS

Test Hole	Depth (m)	Wi	% Sand	% Silt	%Clay
79-28			97.5	2.5	0.0

B. APPENDIX - GROUND INSTRUMENTS - FIELD DATA

POINTS POSITION 1981

INSTR.		SP2	SP3	SP4	ME5	SI6	SI7	SP8	ME9	ME10	SP11	SI12	SP13	SP14	SP15	SP16
ST.		55.2	46.5	46.6	44.6	43.4	48.7	46.6	43.4	48 7	46.6	43.6	46.5	55.5	56.9	57.1
DATE	TIME					DIST	FROM	THE	FACE	OF	THE	MOLE				
JAN18	15:00	-50.2	-41.5	-46.6	-39.6	-38.4	-43.7	-41.6	-38.4	-43.7	-41.6	-38.6	-41.5	-50.5	-51.9	-52.1
JAN30	15:00	-30.9	-22.2	-22.3	-20.3	-19.1	-24.4	-22.3	-19.1	-24.4	-22.3	-19.3	-22.2	-31.2	-32.6	-32.8
FEB 2	15:45	-27.5	-18.8	-18.9	-16.9	-15.7	-21.0	-18.9	-15.7	-21.0	-18.9	-15.9	-18.8	-27.8	-29.2	-29.4
FEB 3	7--15	-27.5	-18.8	-18.9	-16.9	-15.7	-21.0	-18.9	-15.7	-21.0	-18.9	-15.9	-18.8	-27.8	-29.2	-29.4
FEb 4	15:00	-26.3	-17.6	-17.7	-15.7	-14.5	-19.8	-17.7	-14.5	-19.8	-17.7	-14.7	-17.6	-26.6	-28.0	-28.2
FEB 5	11:10	-23.9	-15.2	-15.3	-13.3	-12.1	-17.4	-15.3	-12.1	-17.4	-15.3	-12.3	-15.2	-24.2	-25.6	-25.8
FEB 5	15:00	-21.5	-12.8	-12.9	-10.9	- 9.7	-15.0	-12.9	- 9.7	-15.0	-12.9	- 9.9	-12.8	-21.8	-23.2	-23.4
FEB 6	13:00	-17.8	- 9.1	- 9.2	- 7.2	- 6.0	-11.3	- 9.2	- 6.0	-11.3	- 9.2	- 6.2	- 9.1	-18.1	-19.5	-19.7
FEB7/8	all	-17.8	- 9.1	- 9.2	- 7.2	- 6.0	-11.3	- 9.2	- 6.0	-11.3	- 9.2	- 6.2	- 9.1	-18.1	-19.5	-19.7
FEB 9	12:45	-14.8	- 6.1	- 6.2	- 4.2	- 3.4	- 8.3	- 6.2	- 3.4	- 8.3	- 6.2	- 3.6	- 6.1	-15.1	-16.5	-16.7
FEB10	7:35	-13.4	- 4.7	- 4.8	- 2.8	- 1.6	- 6.9	- 4.8	- 1.6	- 6.9	- 4.8	- 1.8	- 4.7	-13.7	-15.1	-15.3
FEB10	8:30	-13.1	- 4.4	- 4.5	- 2.5	- 1.3	- 6.6	- 4.5	- 1.3	- 6.6	- 4.5	- 1.5	- 4.4	-13.4	-14.8	-15.0
FEB10	9:20	-12.8	- 4.1	- 4.2	- 2.2	- 1.0	- 6.3	- 4.2	- 1.0	- 6.3	- 4.2	- 1.2	- 4.1	-13.1	-14.5	-14.7
FEB10	10:10	-12.5	- 3.8	- 3.9	- 1.9	- 0.7	- 6.0	- 3.9	- 0 7	- 6.0	- 3.9	- 0.9	- 3.9	-12.8	-14.2	-14.4
FEB10	11:30	-12.3	- 3.6	- 3.7	- 1.7	- 0.5	- 5.8	- 3.7	- 0.5	- 5.8	- 3.7	- 0.7	- 3.7	-12.6	-14.0	-14.2
FEB10	13:45	-10.0	- 1.3	- 1.4	- 0.4	+ 1.8	- 3.5	- 1.4	+ 1.8	- 3.5	- 1.4	+ 1.6	- 1.3	-10.3	-11.7	-11.9
FEB10	15:00	- 8.7	+ 0.0	- 0.1	+ 1.9	+ 3.1	- 2.2	- 0.1	+ 3.1	- 2.2	- 0.1	+ 2.9	+ 0.0	- 9.0	-10.4	-10.6
FEB11	9:05	- 7.7	+ 1.0	+ 0.9	+ 2.9	+ 4.1	- 1.2	+ 0.9	+ 4.1	- 1.2	+ 0.9	+ 3.9	+ 1.0	- 8.0	- 9.4	- 9.6
FEB11	11:05	- 6.4	+ 2.3	+ 2.2	+ 4.2	+ 5.4	+ 0.1	+ 2.2	+ 5.4	+ 0.1	+ 2.2	+ 5.2	+ 2.2	- 6.7	- 8.1	- 8.3
FEB 0	13:10	- 5.2	+ 3.5	+ 3.4	+ 5.4	+ 6.6	+ 1.3	+ 3.4	+ 6.6	+ 1.3	+ 3.4	+ 6.4	+ 3.5	- 5.5	- 6.9	- 7.1
FEB 0	15:00	- 3.9	+ 4.8	+ 4.7	+ 6.7	+ 7.9	+ 2.6	+ 4.7	+ 7.9	+ 2.6	+ 4.7	+ 7.7	+ 4.8	- 4.2	- 5.6	- 5.8
FEB12	9:45	- 1.6	+ 7.1	+ 7.0	+ 9.0	+10.2	+ 4.9	+ 7.0	+10.2	+ 4.9	+ 7.0	+10.0	+ 7.1	- 1.9	- 3.3	- 3.5
FEB12	12:20	- 0.3	+ 8.4	+ 8.3	+10.3	+11.5	+ 6.2	+ 8.3	+11.5	+ 6.2	+ 8.3	+11.[illegible]	+ 8.4	- 0.6	- 2.0	- 2.2
FEB12	13-15	+ 1.0	+ 9.7	+ 9.6	+11.6	+12.8	+ 7.5	+ 9.6	+12.8	+ 7.5	+ 9.6	+12.[illegible]	+ 9.7	+ 0.7	- 0.7	- 0.8
FEB13	7:30	+ 2.3	+11.0	+10.9	+12.9	+14.1	+ 8.8	+10.9	+14.1	+ 8.8	+10.9	[illegible]	+11.0	+ 2.0	+ 0.6	+ 0.4
FEB13	8-15	+ 3.6	+12.3	+12.2	+14.2	+15.4	+10.1	+12.2	+15.4	+10.1	+12.2	+15.2	+12.3	+ 3.3	+ 1.9	+ 1.7
FEB16	7:50	+ 4.8	+13.5	+13.4	+15.4	+16.6	+11.3	+13.4	+16.6	+11.3	+13.4	+16.4	+13.[illegible]	+ 4.5	+ 3.1	+ 2.9
FEB16	9:45	+ 6.0	+14.7	+14.6	+16.6	+17.8	+12.5	+14.6	+17.8	+12.5	+14.6	+17.6	+14.[illegible]	+ 5.7	+ 4.3	+ 4.1
FEB16	12:20	+ 7.1	+15.8	+15.7	+17.7	+18.9	+13.6	+15.7	+18.9	+13.6	+15.7	+18.7	+15.8	+ 6.8	+ 5.4	+ 5.2

TABLE B1 - DISTANCE FROM GROUND INSTRUMENTS TO THE NOSE OF MOLE

POINTS POSITION 1981

INST.		SP2	SP3	SP4	ME5	SI6	SI7	SP8	ME9	ME10	SP11	SI12	SP13	SP14	SP15	SP16
ST.		55.2	46.5	46.6	44.6	43.4	48.7	46.6	43.4	48.7	46.6	43.6	46.5	55.5	56.9	57.1
DATE	TIME					DIST	FROM	THE	FACE	OF	THE	MOLE				
FEB16	13:40	8.3	17.0	16.9	18.9	20.1	14.8	16.8	20.1	14.8	16.9	19.9	17.0	8.0	6.6	6.4
FEB17	07:45	9.5	18.2	18.1	20.1	21.3	16.0	18.1	21.3	16.0	18.1	21.1	18.2	9.2	7.8	7.6
FEB17	08:50	10.7	19.4	19.3	21.3	22.5	17.2	19.3	22.5	17.2	19.3	22.3	19.4	10.4	9.0	8.8
FEB17	12:50	12.0	20.7	20.6	22.6	23.8	18.5	20.6	23.8	18.5	20.6	23.6	20.7	11.7	10.3	10.1
FEB17	13:55	13.3	22.0	21.9	23.9	25.1	19.8	21.9	25.1	19.8	21.9	24.9	22.0	13.0	11.6	11.4
FEB18	08:20	14.5	23.2	23.1	25.1	26.3	21.0	23.1	26.3	21.0	23.1	26.1	23.2	14.2	12.8	12.6
FEB18	09:45	15.6	24.3	24.2	26.2	27.4	22.1	24.2	27.4	22.1	24.2	27.2	24.3	15.3	13.9	13.7
FEB18	12:00	16.8	25.5	25.4	27.4	28.6	23.3	25.4	28.6	23.3	25.4	28.4	15.5	16.5	15.1	14.9
FEB18	13:30	18.0	26.7	26.6	28.6	29.8	24.5	26.6	29.8	24.5	26.6	29.6	26.7	17.7	16.3	16.1
FEB19	13:30	18.0	26.7	26.6	28.6	29.8	24.5	26.6	29.8	24.5	26.6	29.6	26.7	17.7	16.3	16.1
FEB20	13:30	18.0	26.7	26.6	28.6	29.8	24.5	26.6	29.8	24.5	26.6	29.6	26.7	17.7	16.3	16.1
FEB21	13:30	18.0	26.7	26.6	28.6	29.8	24.5	26.6	29.8	24.5	26.6	29.6	26.7	17.7	16.3	16.1
FEB22	13:30	18.0	26.7	26.6	28.6	29.8	24.5	26.6	29.8	24.5	26.6	29.6	26.7	17.7	16.3	16.1
FEB23	07:35	19.5	28.2	28.1	30.1	31.3	26.0	28.1	31.3	26.0	28.1	25.8	28.2	19.2	17.8	17.6
FEB23	12:10	20.6	29.3	29.2	31.2	32.4	27.1	29.2	32.4	27.1	29.2	32.2	29.3	20.3	18.9	18.7
FEB24	09:15	21.8	30.5	30.4	32.4	33.6	28.3	30.4	33.6	28.3	30.4	33.4	30.5	21.5	20.1	19.9
FEB24	10:35	23.1	31.8	31.7	33.7	34.9	29.6	31.7	34.9	29.6	31.7	34.7	31.8	22.8	21.4	21.2
FEB24	13:45	24.4	33.1	33.0	35.0	36.2	30.9	33.0	36.2	30.9	33.0	36.0	33.1	24.1	22.7	22.5
FEB25	10:20	25.6	34.3	34.2	36.2	37.4	32.1	34.2	37.4	32.1	34.2	37.2	34.3	25.3	23.9	23.7
FEB25	12:10	26.9	35.6	35.5	37.5	38.5	33.4	35.5	38.7	33.4	35.5	38.5	35.6	26.6	25.2	25.0
FEB25	13:30	28.1	36.8	36.7	38.7	39.9	34.6	36.7	39.9	34.6	36.7	39.7	36.8	27.8	26.4	26.2
FEB25	14:50	29.3	38.0	37.9	39.9	41.1	35.8	37.9	41.1	35.8	37.9	40.9	38.0	28.0	27.6	27.4
FEB26	07:00	29.3	38.0	37.9	39.9	41.1	35.8	37.9	41.1	35.8	37.9	40.9	38.0	28.0	27.6	27.4
FEB26	08-30	30.5	39.2	39.1	41.1	42.3	37.0	39.1	42.3	37.0	39.1	42.1	39.2	30.2	28.2	28.6
FEB26	12:50	31.7	40.4	40.3	42.3	43.5	38.2	40.3	43.5	38.2	40.3	43.3	40.4	31.4	30.0	29.8
FEB26	13:55	32.9	41.6	41.5	43.5	44.7	39.4	41.5	44.7	39.4	41.5	44.5	41.6	32.6	31.2	31.0
FEB26	15:00	34.1	42.8	42.7	44.7	45.9	40.6	42.7	45.9	40.6	42.7	45.7	42.9	33.8	32.4	32.2
FEB27	07:00	34.1	42.8	42.7	44.7	45.9	40.6	42.7	45.9	40.6	42.7	45.7	42.9	33.8	32.4	32.2
FEB27	07:45	35.3	44.0	43.9	45.9	47.1	41.8	43.9	47.1	41.8	43.9	46.9	44.0	35.0	33.6	33.4
FEB27	09:05	36.9	45.2	45.1	47.1	48.3	43.0	45.1	48.3	43.0	45.1	48.1	45.2	36.2	34.8	34.6

TABLE B2 - DISTANCE FROM GROUND INSTRUMENTS TO THE NOSE OF MOLE (cont)

POINTS POSITION 1981

INSTR.		SP2	SP3	SP4	ME5	SI6	SI7	SP8	ME9	ME10	SP11	SI12	SP13	SP14	SP15	SP16
ST.		55.2	46.5	46.6	44.6	43.4	48.7	46.6	43.4	48.7	46.6	43.6	46.5	55.5	56.9	57.1
DATE	TIME					DIST	FROM	THE	FACE	OF	THE	MOLE				
FEB27	10:40	37.7	46.4	46.3	48.3	49.5	44.2	46.3	49.5	44.2	46.3	49.3	46.4	37.4	36.0	35.8
FEB27	13:00	38.9	47.6	47.5	49.5	50.7	45.4	47.5	50.7	45.4	47.5	50.5	47.6	38.6	37.2	37.0
FEB27	14:00	40.1	48.8	48.7	50.7	51.9	46.6	48.7	51.9	46.6	48.7	50.7	48.8	39.8	38.4	38.2
FEB27	14:45	41.3	50.0	49.9	51.9	53.1	47.8	49.9	53.1	47.8	49.9	52.9	50.0	41.0	39.6	39.4
MAR02	07:00	41.3	50.0	49.9	51.9	53.1	47.8	49.9	53.1	47.8	49.9	52.9	50.0	41.0	39.6	39.4
MAR02	09:30	42.5	51.2	51.1	53.1	54.3	49.0	51.1	54.3	49.0	51.1	54.1	51.2	42.2	40.8	40.6
MAR02	11:00	43.7	52.4	52.3	54.3	55.5	50.2	52.3	55.5	50.2	52.3	55.3	52.4	43.4	42.0	41.8
MAR02	13:50	44.9	53.6	53.5	55.5	56.7	51.5	53.5	56.7	51.5	53.7	56.7	53.8	44.6	43.2	43.0
MAR02	15:00	46.1	54.8	54.7	56.7	57.9	52.6	54.7	57.9	52.6	54.7	57.7	54.8	45.8	44.4	44.2
MAR03	07:00	46.1	54.8	54.7	56.7	57.9	52.6	54.7	57.9	52.6	54.7	57.7	54.8	45.8	44.4	44.2
MAR03	08:15	47.3	56.0	55.9	57.9	59.1	53.8	55.9	59.1	53.8	55.9	58.9	56.0	47.0	45.6	45.4
MAR03	09:30	48.5	57.2	57.1	59.1	60.3	55.0	57.1	60.3	55.0	57.1	60.1	57.2	48.2	46.8	46.8
MAR03	12:55	49.7	58.4	58.3	60.3	61.5	56.2	58.3	61.5	56.2	58.3	61.3	58.4	49.4	48.0	47.8
MAR03	14:10	50.9	59.6	59.5	61.5	62.7	57.4	59.5	62.7	57.4	59.5	62.5	59.6	50.6	49.2	49.0
MAR04	07:00	50.9	59.6	59.5	61.5	62.7	57.4	59.5	62.7	57.4	59.5	62.5	59.6	50.6	49.2	49.0
MAR04	07:30	52.1	60.8	60.7	62.7	63.9	58.6	60.7	63.9	58.6	60.7	63.7	60.8	51.8	50.4	50.2
MAR04	09:15	53.5	62.0	61.9	63.9	65.1	59.8	61.9	65.1	59.8	61.9	64.9	62.0	53.0	51.6	51.4
MAR04	10:30	54.5	63.2	63.1	65.1	66.2	61.0	63.1	66.2	61.0	63.1	66.0	63.2	54.2	52.8	52.6
MAR04	12:15	55.7	64.4	64.3	66.3	67.5	62.2	64.3	67.5	62.2	64.3	67.3	64.4	55.4	54.0	53.8
MAR04	14:00	56.9	65.5	65.6	67.5	68.7	63.4	65.5	68.7	63.4	65.5	68.5	65.6	56.6	55.2	55.0
MAR05	07:00	56.9	65.5	65.6	67.5	68.7	63.4	65.5	68.7	63.4	65.5	68.5	65.6	56.6	55.2	55.0
MAR05	07:25	58.5	67.2	67.1	69.1	70.3	65.0	67.1	70.3	65.0	67.1	70.1	67.2	58.2	56.8	56.6
MAR05	09:30	59.7	68.4	68.3	70.3	72.5	66.2	68.3	71.5	66.2	68.3	71.3	68.4	59.4	58.0	57.8
MAR05	10:35	60.9	69.6	69.5	71.5	72.7	67.4	69.5	72.7	67.4	69.5	72.5	69.6	60.6	59.2	59.0
MAR05	12:30	62.1	70.8	70.7	72.7	73.9	68.6	70.7	73.9	62.6	70.7	73.7	70.8	61.8	60.4	60.2
MAR05	14:00	63.4	72.1	72.0	74.0	75.2	69.9	72.0	75.2	69.9	72.0	75.0	72.1	63.1	61.8	61.6
MAR06	07:00	63.4	72.1	72.0	74.0	75.2	69.9	72.0	75.2	69.9	72.0	75.0	72.1	63.1	61.8	61.6
MAR06	07:45	64.9	73.6	73.5	75.5	76.7	71.4	73.5	76.7	71.4	73.5	76.5	73.6	64.6	63.2	63.0
MAR06	08:50	66.1	74.8	74.7	76.7	77.9	72.6	74.7	77.9	72.6	74.7	77.7	74.8	65.8	64.4	64.2
MAR06	10:00	67.3	76.0	75.9	77.9	79.1	73.8	75.9	79.1	73.8	75.9	78.9	76.0	67.0	66.6	66.4
MAR06	11:15	68.8	77.5	77.4	79.4	80.6	75.3	77.4	80.6	75.3	77.4	80.4	77.5	[illegible]	67.1	66.9
MAR06	13:15	70.0	78.7	78.6	80.6	81.8	76.5	78.6	81.8	76.5	78.6	81.6	78.7	69.7	68.3	68.1
MAR06	14:40	71.2	79.9	79.8	81.8	83.0	77.7	79.8	83.0	77.7	79.8	82.9	79.9	69.9	68.5	68.3

TABLE B3 - DISTANCE FROM GROUND INSTRUMENTS TO THE NOSE OF MOLE (cont)

POINTS POSITION 1981

INSTR.		SP2	SP3	SP4	ME5	SI6	SI7	SP8	ME9	ME10	SP11	SI12	SP13	SP14	SP15	SP16
ST.		55.2	46.5	46.6	44.6	43.4	48.7	46.6	43.4	48.7	46.6	43.6	46.5	55.5	56.9	57.1
DATE	TIME					DIST	FROM	THE	FACE	OF	THE	MOLE				
MAR09	07:00	71.2	79.9	79.8	81.8	83.0	77.7	79.8	83.0	77.7	79.8	82.8	79.9	70.9	69.5	69.3
MAR09	08:30	72.4	81.1	81.0	83.0	84.2	78.9	81.0	84.2	78.9	81.0	84.0	81.1	72.1	70.7	70.5
MAR09	09:30	73.6	82.3	82.2	84.2	85.4	80.1	82.2	85.4	80.1	82.2	85.2	82.3	73.3	71.9	71.7
MAR09	10:40	74.9	83.6	83.5	85.5	86.7	81.7	83.5	86.7	81.7	83.5	86.5	83.6	74.6	73.2	73.0
MAR09	15:00	74.9	83.6	83.5	85.5	86.7	81.7	83.5	86.7	81.7	83.5	86.5	83.6	74.6	73.2	73.0
MAR10	07:00	74.9	83.6	83.5	85.5	86.7	81.7	83.5	86.7	81.7	83.5	86.5	83.6	74.6	73.2	73.0
MAR10	08:15	76.1	84.8	84.7	86.7	87.9	82.6	84.7	87.9	82.6	84.7	87.7	84.8	75.8	74.8	74.6
MAR10	09:30	78.3	87.0	86.9	88.9	90.1	84.8	86.9	90.1	84.8	86.9	89.9	87.0	78.0	76.6	76.4
MAR10	10:30	79.5	88.2	88.1	90.1	91.3	86.0	88.1	91.3	86.0	88.1	91.1	88.2	79.2	77.8	77.6
MAR10	12:00	80.0	89.5	89.4	91.4	92.6	87.3	89.4	92.6	87.3	89.4	92.4	89.5	80.5	79.1	78.9
MAR10	13:15	82.1	90.8	90.7	92.7	93.9	88.6	90.7	93.9	88.6	90.7	93.7	90.8	81.8	80.4	80.2
MAR10	14:20	83.4	92.1	92.0	94.0	95.2	89.9	92.0	95.2	89.9	92.0	95.0	92.1	83.3	81.9	81.7
MAR11	07:00	83.4	92.1	92.0	94.0	95.2	89.9	92.0	95.2	89.9	92.0	95.0	92.1	83.3	81.9	81.7
MAR11	09:30	84.6	93.3	93.2	95.2	96.4	91.1	93.2	96.4	91.1	93.2	96.2	93.3	84.3	82.9	82.7
MAR11	10:35	86.0	94.7	94.6	96.6	97.8	92.5	94.6	97.8	92.5	94.6	97.6	94.7	85.7	84.3	84.1
MAR11	12:29	87.3	96.0	95.9	97.9	99.1	93.8	95.9	99.1	93.8	95.9	98.9	96.0	87.0	85.6	85.4
MAR11	13:35	88.5	97.2	97.1	99.1	100.3	95.0	97.1	100.3	95.0	97.1	100.1	97.2	88.2	86.8	86.6
MAR11	14:30	89.7	98.4	98.3	100.3	101.5	96.2	98.3	101.5	96.2	98.3	101.3	98.4	89.4	88.0	87.8
MAR12	07:00	89.7	98.4	98.3	100.3	101.5	96.2	98.3	101.5	96.2	98.3	101.3	98.4	89.4	88.0	87.8
MAR12	09:10	91.2	99.9	99.8	101.8	103.0	97.7	99.8	103.0	97.7	99.8	102.8	99.9	89.9	87.5	87.2
MAR12	12:30	92.7	100.4	100.3	102.3	104.5	98.2	100.3	104.5	98.2	100.3	104.3	100.4	92.4	91.0	90.8
MAR12	14:00	94.2	101.9	101.8	103.8	106.0	99.7	100.8	106.0	99.7	100.8	105.8	100.9	93.9	92.5	92.3
MAR12	15:00	95.5	102.2	102.1	104.1	107.3	101.0	102.1	107.3	101.0	102.1	107.1	102.2	95.2	93.8	93.6
MAR13	07:00	95.5	102.2	102.1	104.1	107.3	101.0	102.1	107.3	101.0	102.1	107.1	102.2	95.2	93.8	93.6
MAR13	09:10	96.7	103.4	103.3	105.3	108.5	102.3	103.3	108.5	102.3	103.3	108.3	103.4	96.4	95.0	95.8
MAR13	10:45	97.9	104.6	104.5	106.5	109.7	103.5	104.5	109.7	103.5	104.5	109.5	104.6	97.6	96.2	96.0
MAR13	13:50	99.1	105.8	105.7	107.7	110.9	104.7	105.7	110.9	104.7	105.7	110.7	105.8	98.8	97.4	97.2
MAR13	14:45	100.3	107.0	106.9	108.9	112.1	105.9	106.9	112.1	105.9	106.9	111.9	107.0	100.0	98.6	98.4
MAR16	07:00	100.3	107.0	106.9	108.9	112.1	105.9	106.9	112.1	105.9	106.9	111.9	107.0	100.0	98.6	98.4
MAR16	07:30	100.8	107.5	107.4	109.4	112.6	106.4	107.3	112.6	106.4	107.3	112.4	107.4	100.5	99.1	98.9
MAR16	09:00	102.0	108.7	108.6	110.6	113.8	107.6	108.5	113.8	107.6	108.5	113.6	108.6	101.7	100.3	100.1
MAR16	10:45	103.2	109.9	109.8	111.8	115.0	108.8	109.7	115.0	108.8	109.7	114.8	108.9	102.9	101.5	101.3

TABLE B4 - DISTANCE FROM GROUND INSTRUMENTS TO THE NOSE OF MOLE (cont)

MARKER POINT NO. 1

	TIME DAYS	INIT. READ.	READINGS	DISPL CMS	LOCATION	
DECEMBER 29 1980	76.0	2.3027	2.3027	0.0	-30.00	0.0
FEBRUARY 1 1981	77.0	2.3027	2.2926	0.0040	-20.20	0.0100
FEBRUARY 2 1981	78.0	2.3027	2.3026	0.0000	-15.00	0.0250
FEBRUARY 5 1981	81.0	2.3027	2.2630	0.0000	-10.00	0.0050
FEBRUARY 6 1981	82.0	2.3027	2.2933	0.1100	-7.20	0.0000
FEBRUARY 8 1981	84.0	2.3027	2.2912	0.0400	-7.00	-0.1000
FEBRUARY 9 1981	85.0	2.3027	2.2408	0.1200	-4.20	-0.1000
FEBRUARY 10 1981	86.0	2.3027	2.2408	0.0400	-1.70	-0.2500
FEBRUARY 10 1981	86.0	2.3027	——	——	1.00	-0.2000
FEBRUARY 11 1981	87.0	2.3027	2.2400	0.1200	6.40	-0.2400
FEBRUARY 11 1981	87.0	2.3027	2.2428	-0.0000	6.70	-0.3400
FEBRUARY 12 1981	88.0	2.3027	2.2402	-0.0061	8.00	-0.4100
FEBRUARY 13 1981	89.0	2.3027	2.2408	-0.0000	14.00	-0.3100
FEBRUARY 16 1981	92.0	2.3027	2.2810	0.0200	17.70	-0.1000
FEBRUARY 17 1981	93.0	2.3027	2.2818	-0.0010	22.00	-0.1000
FEBRUARY 18 1981	94.0	2.3027	2.2810	0.0000	26.20	-0.1200
FEBRUARY 19 1981	95.0	2.3027	2.2820	-0.0000	28.00	-0.1200
FEBRUARY 23 1981	99.0	2.3027	2.2820	-0.0450	31.20	-0.1100
FEBRUARY 26 1981	102.0	2.3027	2.2820	-0.1000	42.20	-0.1000
MARCH 7 1981	111.0	2.3027	2.2820	-0.1101	51.80	-0.1050

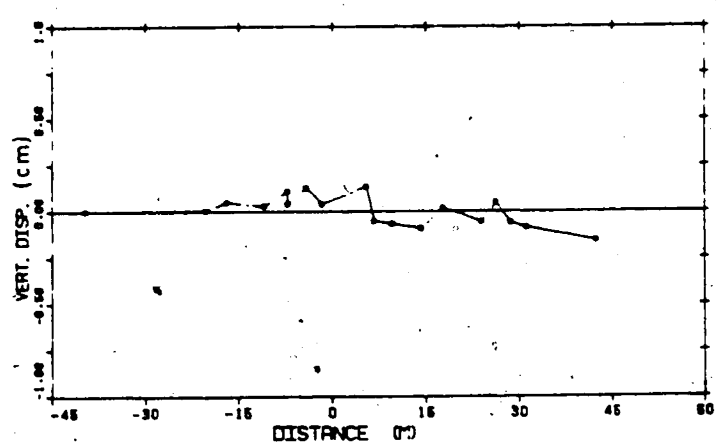

Figure B.1 ME5 MP#1 D=2.35m

MAGNET POINT NO. 2

	TIME DAYS	INIT. READ.	READINGS	DISPL. CMS	LOCATION	
DECEMBER 22 1980	36.0	4.8785	4.8785	0.0	-38.60	0.0
FEBRUARY 1 1981	77.0	4.8785	4.8765	-0.0200	-20.30	0.0100
FEBRUARY 3 1981	79.0	4.8785	4.8768	0.0250	-18.80	0.0350
FEBRUARY 5 1981	81.0	4.8785	4.8782	0.0750	-10.80	0.0650
FEBRUARY 6 1981	82.0	4.8785	4.8782	0.0650	-7.30	0.0850
FEBRUARY 8 1981	84.0	4.8785	4.8776	-0.0060	-7.30	-0.1060
FEBRUARY 9 1981	85.0	4.8785	4.8788	0.1300	-4.30	-0.1850
FEBRUARY 10 1981	86.0	4.8785	4.8785	0.0150	-1.70	-0.2050
FEBRUARY 10 1981	86.0	4.8785	4.8785	0.0100	1.00	-0.3000
FEBRUARY 11 1981	87.0	4.8785	4.8740	0.0000	5.40	-0.3400
FEBRUARY 11 1981	87.0	4.8788	4.8788	-0.0480	6.70	-0.3450
FEBRUARY 12 1981	88.0	4.8785	4.8745	-0.0100	8.80	-0.4100
FEBRUARY 13 1981	89.0	4.8785	4.8728	-0.0450	14.30	-0.5150
FEBRUARY 16 1981	92.0	4.8785	4.8773	-0.0350	17.70	-0.1850
FEBRUARY 17 1981	93.0	4.8785	4.8775	-0.0600	23.00	-0.1800
FEBRUARY 18 1981	94.0	4.8785	4.8772	-0.0050	26.30	-0.1200
FEBRUARY 19 1981	95.0	4.8785	4.8773	-0.0150	28.00	-0.1300
FEBRUARY 23 1981	99.0	4.8785	4.8785	-0.1100	31.30	-0.1100
FEBRUARY 26 1981	102.0	4.8785	4.8780	-0.1300	42.30	-0.1800
MARCH 7 1981	111.0	4.8785	4.8788	-0.1300	51.00	-0.1050

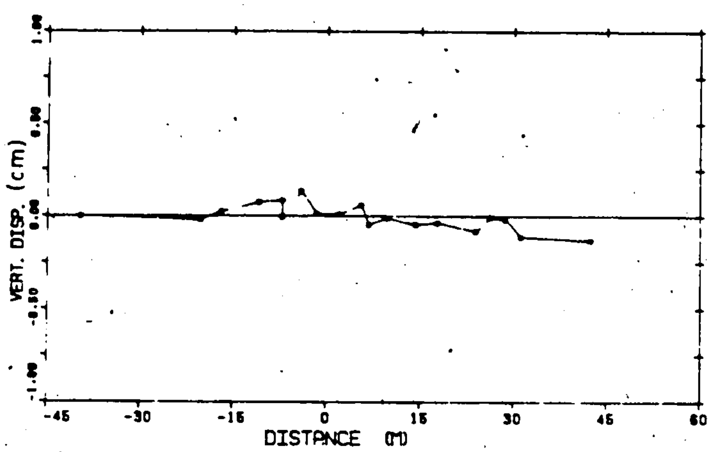

Figure B.2 ME5 MP#2 D=4.88m

MAGNET POINT NO. 3

	TIME DAYS	INIT. READ.	READINGS	DISPL CMS	LOCATION	
DECEMBER 22 1980	36.0	0.8803	0.8803	0.0	-30.00	0.0
FEBRUARY 1 1981	77.0	0.8803	0.8806	-0.0440	-20.20	0.0100
FEBRUARY 3 1981	79.0	0.8803	0.8813	-0.0800	-15.00	0.0250
FEBRUARY 5 1981	81.0	0.8803	0.8803	0.0600	-10.00	0.0650
FEBRUARY 6 1981	82.0	0.8803	0.8806	0.1100	-7.20	0.0800
FEBRUARY 8 1981	84.0	0.8803	0.8803	-0.0001	-7.20	-0.1000
FEBRUARY 9 1981	85.0	0.8803	0.8873	0.1301	-4.20	-0.1050
FEBRUARY 10 1981	86.0	0.8803	0.8875	-0.0100	-1.70	-0.2050
FEBRUARY 10 1981	86.0	0.8803	0.8806	0.0650	1.00	-0.2000
FEBRUARY 11 1981	87.0	0.8803	0.8808	0.0085	5.40	-0.2400
FEBRUARY 11 1981	87.0	0.8803	0.8805	0.0301	6.70	-0.3450
FEBRUARY 12 1981	88.0	0.8803	0.8883	-0.0150	8.00	-0.4100
FEBRUARY 13 1981	89.0	0.8803	0.8853	-0.0100	14.20	-0.5150
FEBRUARY 16 1981	92.0	0.8803	0.8843	0.0400	17.70	-0.1550
FEBRUARY 17 1981	93.0	0.8803	0.8883	0.0150	22.00	-0.1600
FEBRUARY 18 1981	94.0	0.8803	0.8800	0.0000	25.20	-0.1250
FEBRUARY 19 1981	95.0	0.8803	0.8868	0.0101	26.80	-0.1350
FEBRUARY 23 1981	99.0	0.8803	0.8803	-0.1100	31.20	-0.1100
FEBRUARY 26 1981	102.0	0.8803	0.8806	-0.1200	42.20	-0.1000
MARCH 7 1981	111.0	0.8803	0.8803	-0.1100	51.00	-0.1050

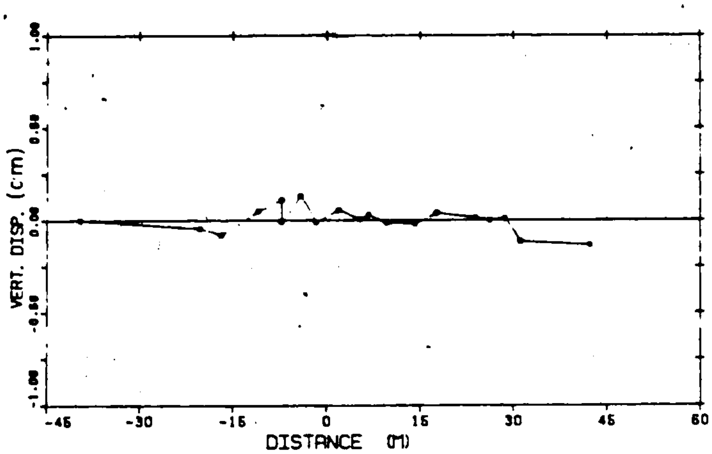

Figure B.3 ME5 MP#3 D=6.85m

MAGNET POINT NO. 4

	TIME DAYS	INIT. READ	READINGS	DISPL CMS	LOCATION	
DECEMBER 31 1980	45.0	0.1226	0.1226	0.0	-38.00	0.0
FEBRUARY 1 1981	77.0	0.1226	0.1236	-0.0050	-20.30	0.0100
FEBRUARY 2 1981	78.0	0.1226	0.1236	-0.0800	-18.00	0.0350
FEBRUARY 5 1981	81.0	0.1226	0.1230	0.0300	-10.90	0.0650
FEBRUARY 6 1981	82.0	0.1226	0.1230	0.0400	-7.20	0.0850
FEBRUARY 8 1981	84.0	0.1226	0.1215	0.0200	-7.20	-0.1000
FEBRUARY 9 1981	85.0	0.1226	0.1203	0.0600	-4.20	-0.1050
FEBRUARY 10 1981	86.0	0.1226	0.1215	-0.1000	-1.70	-0.2850
FEBRUARY 10 1981	86.0	0.1226	0.1198	0.0350	1.90	-0.2000
FEBRUARY 11 1981	87.0	0.1226	0.1188	0.0850	5.40	-0.2400
FEBRUARY 11 1981	87.0	0.1226	0.1200	-0.0750	5.70	-0.3400
FEBRUARY 12 1981	88.0	0.1226	0.1188	0.0151	8.80	-0.4100
FEBRUARY 13 1981	89.0	0.1226	0.1178	-0.0188	14.20	-0.3150
FEBRUARY 16 1981	92.0	0.1226	0.1203	0.0000	17.70	-0.1850
FEBRUARY 17 1981	93.0	0.1226	0.1208	0.0481	22.00	-0.1800
FEBRUARY 18 1981	94.0	0.1226	0.1210	0.0600	26.20	-0.1250
FEBRUARY 19 1981	95.0	0.1226	0.1215	-0.0100	28.60	-0.1350
FEBRUARY 23 1981	99.0	0.1226	0.1228	-0.0600	31.20	-0.1100
FEBRUARY 26 1981	102.0	0.1226	0.1230	-0.1040	42.30	-0.1200
MARCH 7 1981	111.0	0.1226	0.1233	-0.1100	51.00	-0.1000

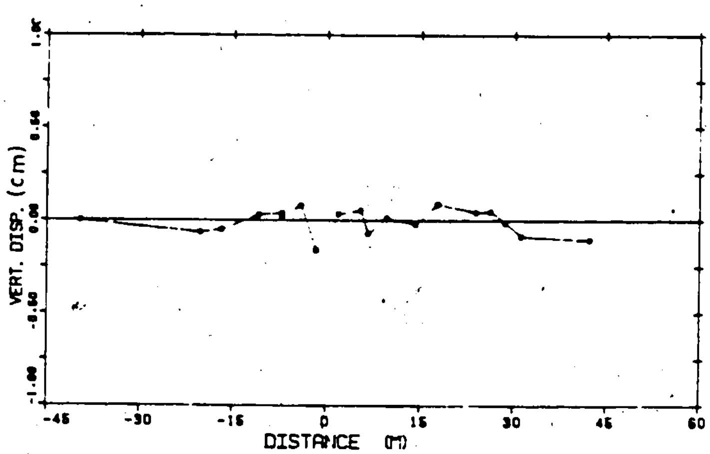

Figure B.4 ME5 MP#4 D=8.13m

MAGNET POINT NO. 5

	TIME DAYS	INIT READ	READINGS	DISPL CMS	LOCATION	
DECEMBER 23, 1980	30.0	10.8860	10.8860	0.0	-30.60	0.0
FEBRUARY 1 1981	77.0	10.8865	10.8805	-0.0600	-30.30	0.0100
FEBRUARY 3 1981	79.0	10.8680	10.8803	-0.0650	-18.60	0.0300
FEBRUARY 5 1981	81.0	10.8860	10.8900	0.0040	-10.90	0.0650
FEBRUARY 6 1981	82.0	10.8860	10.8683	0.0048	-7.30	0.0600
FEBRUARY 8 1981	84.0	10.8865	10.8870	0.0440	-7.30	-0.1000
FEBRUARY 9 1981	85.0	10.8860	10.8800	0.0850	-4.30	-0.1800
FEBRUARY 10 1981	86.0	10.8865	10.8808	0.0140	-1.70	-0.2800
FEBRUARY 10 1981	86.0	10.8865	10.8855	0.0001	1.80	-0.2000
FEBRUARY 11 1981	87.0	10.8668	10.8848	0.0600	5.40	-0.3400
FEBRUARY 11 1981	87.0	10.8868	10.8880	-0.0481	5.70	-0.3450
FEBRUARY 12 1981	88.0	10.8848	10.8843	0.0100	8.80	-0.4100
FEBRUARY 13 1981	89.0	10.8865	10.8838	-0.0450	14.30	-0.5100
FEBRUARY 16 1981	92.0	10.8866	10.8605	0.0450	17.70	-0.1800
FEBRUARY 17 1981	93.0	10.8868	10.8603	0.0300	23.90	-0.1600
FEBRUARY 18 1981	94.0	10.8565	10.8888	0.0440	26.30	-0.1250
FEBRUARY 19 1981	96.0	10.8850	10.8808	0.0340	28.80	-0.1300
FEBRUARY 23 1981	99.0	10.8885	10.8842	-0.0001	31.30	-0.1100
FEBRUARY 26 1981	102.0	10.8865	10.8878	-0.0001	42.30	-0.1800
MARCH 7, 1981	111.0	10.8800	10.8878	-0.0081	61.30	-0.1050

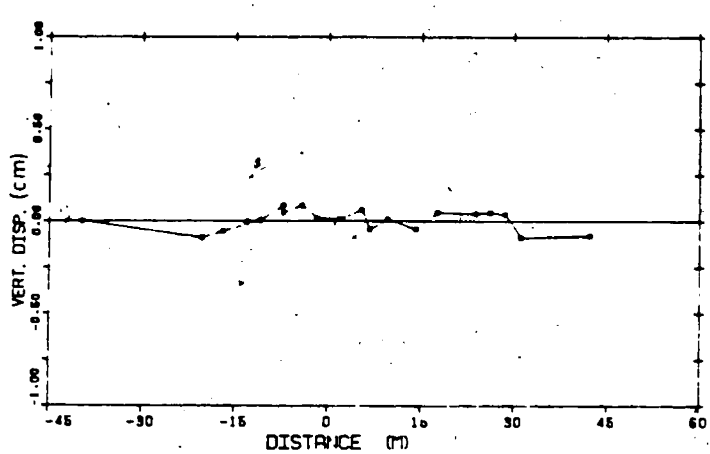

Figure B.5 ME5 MP#5 D=10.86m

MAGNET POINT NO 6

		TIME DAYS	INIT READ	READINGS	DISPL [illegible]	LOCATION	
DECEMBER 22	1980	30.0	12.9065	12.9065	0.0	-30.00	0.0
FEBRUARY 1	1981	77.0	12.9065	12.8105	-0.1701	-30.30	0.0100
FEBRUARY 3	1981	79.0	12.9065	12.8100	-0.1250	-18.80	0.0250
FEBRUARY 5	1981	81.0	12.9065	12.9005	-0.0450	-10.80	0.0650
FEBRUARY 6	1981	82.0	12.9065	12.9000	0.0140	-9.20	0.0850
FEBRUARY 8	1981	84.0	12.9065	12.8973	0.0150	-7.30	-0.1000
FEBRUARY 9	1981	85.0	12.9065	12.9065	0.0250	-6.20	-0.1650
FEBRUARY 10	1981	86.0	12.9065	12.9000	-0.0250	-1.70	-0.2650
FEBRUARY 10	1981	86.0	12.9065	12.9065	0.0065	1.80	-0.2000
FEBRUARY 11	1981	87.0	12.9065	12.9065	0.0000	5.40	-0.2400
FEBRUARY 11	1981	87.0	12.9065	12.9063	-0.0250	8.70	-0.2450
FEBRUARY 12	1981	88.0	12.9065	12.8045	-0.0100	9.00	-0.4100
FEBRUARY 13	1981	88.0	12.9065	12.9035	0.0650	14.30	-0.5100
FEBRUARY 16	1981	92.0	12.9065	12.9063	0.0650	17.70	-0.1550
FEBRUARY 17	1981	93.0	12.8000	12.8063	0.0600	23.00	-0.1800
FEBRUARY 18	1981	94.0	12.9065	12.9070	0.0250	25.30	-0.1250
FEBRUARY 19	1981	95.0	12.9065	12.9065	0.0240	28.60	-0.1200
FEBRUARY 23	1981	99.0	12.9065	12.9065	-0.7100	31.30	-0.1100
FEBRUARY 26	1981	102.0	12.9065	12.9075	-0.0801	42.30	-0.1000
MARCH 7	1981	111.0	12.9065	12.9073	0.0150	61.80	-0.1000

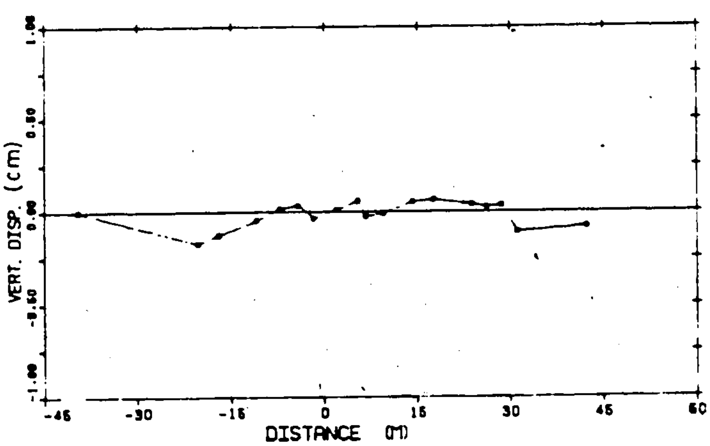

Figure B.6 ME5 MP#6 D=12.91m

MAGNET POINT NO 7

	TIME DAYS	INIT. READ.	READINGS	DISPL CMS	LOCATION	
DECEMBER 22 1980	36.0	14.8825	14.8825	0.0	-28.60	0.0
FEBRUARY 1 1981	77.0	14.8825	14.8806	-13.7500	-20.20	0.0100
FEBRUARY 3 1981	79.0	14.8825	14.8826	-13.0700	-18.00	0.0200
FEBRUARY 5 1981	81.0	14.8825	14.8825	-14.0450	-10.50	0.0050
FEBRUARY 6 1981	82.0	14.8825	14.8845	-14.1350	-7.20	0.0000
FEBRUARY 8 1981	84.0	14.8825	14.8860	-14.2850	-7.20	-0.1000
FEBRUARY 9 1981	85.0	14.8825	14.8865	-14.4050	-4.20	-0.1050
FEBRUARY 10 1981	86.0	14.8825	14.8860	-14.5000	-1.70	-0.2050
FEBRUARY 10 1981	86.0	14.8825	14.8850	-14.6400	1.00	-0.2000
FEBRUARY 11 1981	87.0	14.8825	14.8865	-14.8400	5.40	-0.2400
FEBRUARY 11 1981	87.0	14.8825	14.8865	-14.8400	8.70	-0.2400
FEBRUARY 12 1981	88.0	14.8825	14.8845	-14.8100	9.80	-0.4100
FEBRUARY 13 1981	89.0	14.8825	14.8842	-14.8850	14.20	-0.5100
FEBRUARY 16 1981	92.0	14.8825	14.8873	-14.8255	17.70	-0.1550
FEBRUARY 17 1981	93.0	14.8825	14.0070	84.2700	23.00	-0.1800
FEBRUARY 18 1981	94.0	14.8825	14.8873	-14.8060	26.20	-0.1250
FEBRUARY 19 1981	95.0	14.8825	14.8880	-14.8850	28.80	-0.1200
FEBRUARY 23 1981	99.0	14.8825	15.0006	-14.8100	31.20	-0.1100
FEBRUARY 26 1981	102.0	14.8825	14.8855	-14.8100	42.20	-0.1000
MARCH 7 1981	111.0	14.8825	15.0000	-14.9000	81.80	-0.1050

DISREGARD

Figure B.7 ME5 MP#7 @=14.81m

MAGNET POINT NO. 8

		TIME DAYS	INIT. READ.	READINGS	DISPL CMS	LOCATION	
DECEMBER 22	1980	36.0	16.7742	16.7742	0.0	-38.00	0.0
FEBRUARY 1	1981	77.0	16.7742	16.7765	-0.2267	-20.20	0.0100
FEBRUARY 3	1981	79.0	16.7742	16.7763	-0.1740	-16.00	0.0200
FEBRUARY 5	1981	81.0	16.7742	16.7758	-0.0045	-10.00	0.0650
FEBRUARY 6	1981	82.0	16.7742	16.7750	-0.0037	-7.20	0.0650
FEBRUARY 8	1981	84.0	16.7742	16.7733	-0.0042	-7.30	-0.1000
FEBRUARY 9	1981	85.0	16.7742	16.7723	0.0364	-4.20	-0.1050
FEBRUARY 10	1981	86.0	16.7742	16.7716	-0.0042	-1.70	-0.2250
FEBRUARY 10	1981	86.0	16.7742	16.7713	0.0106	1.00	-0.2000
FEBRUARY 11	1981	87.0	16.7742	16.7664	0.1101	5.40	-0.2400
FEBRUARY 11	1981	87.0	16.7742	16.7716	-0.0045	5.70	-0.2450
FEBRUARY 12	1981	88.0	16.7742	16.7666	0.0461	8.00	-0.4100
FEBRUARY 13	1981	89.0	16.7742	16.7660	0.0160	14.20	-0.5150
FEBRUARY 16	1981	92.0	16.7742	16.7720	0.0764	17.70	-0.1550
FEBRUARY 17	1981	93.0	16.7742	16.7716	0.1008	23.00	-0.1650
FEBRUARY 18	1981	94.0	16.7742	16.7735	-0.0441	20.20	-0.1250
FEBRUARY 19	1981	95.0	16.7742	16.7720	0.0064	26.00	-0.1250
FEBRUARY 23	1981	99.0	16.7742	16.7730	-0.0251	31.20	-0.1100
FEBRUARY 26	1981	102.0	16.7742	16.7736	-0.0248	42.20	-0.1000
MARCH 7	1981	111.0	16.7742	16.7733	-0.0042	51.00	-0.1050

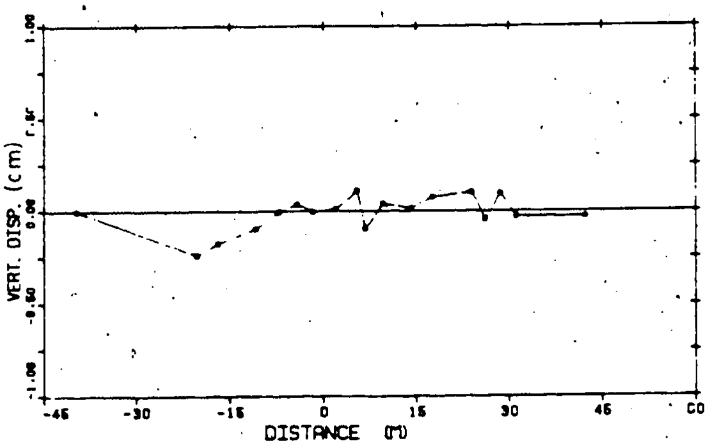

Figure B.8 ME5 MP#8 D=16.78m

MAGNET POINT NO. 9

	TIME DAYS	INIT. READ	READINGS	DISPL (CM)	LOCATION	
DECEMBER 22 1980	30.0	18.0773	18.0773	0.0	-38.50	0.0
FEBRUARY 1 1981	77.0	18.0773	18.0788	-0.1500	-20.50	0.0100
FEBRUARY 2 1981	78.0	18.0773	18.0790	-0.1666	-18.00	0.0250
FEBRUARY 5 1981	81.0	18.0773	18.0778	0.0048	-10.50	0.0084
FEBRUARY 6 1981	82.0	18.0773	18.0760	0.1184	-7.20	0.0080
FEBRUARY 8 1981	84.0	18.0773	18.0783	-0.0043	-7.30	-0.1000
FEBRUARY 9 1981	85.0	18.0773	18.0768	0.0452	-4.20	-0.1050
FEBRUARY 10 1981	86.0	18.0773	18.0743	0.0188	-1.70	-0.2050
FEBRUARY 10 1981	86.0	18.0773	18.0730	0.0400	1.80	-0.2800
FEBRUARY 11 1981	87.0	18.0773	18.0730	0.0300	4.40	-0.3400
FEBRUARY 11 1981	87.0	18.0773	18.0733	0.0648	5.70	-0.3450
FEBRUARY 12 1981	88.0	18.0773	18.0723	0.0808	8.80	-0.4100
FEBRUARY 13 1981	89.0	18.0773	18.0768	0.1280	14.30	-0.5150
FEBRUARY 16 1981	92.0	18.0773	18.0748	0.1284	17.70	-0.1550
FEBRUARY 17 1981	93.0	18.0773	18.0733	0.2182	23.90	-0.1800
FEBRUARY 18 1981	94.0	18.0773	18.0760	0.2048	25.20	-0.1250
FEBRUARY 19 1981	95.0	18.0773	18.0742	0.1588	28.80	-0.1300
FEBRUARY 23 1981	99.0	18.0773	18.0782	-0.0083	31.20	-0.1100
FEBRUARY 26 1981	102.0	18.0773	18.0765	0.0702	42.30	-0.1000
MARCH 7 1981	111.0	18.0773	18.0783	-0.0043	51.80	-0.1000

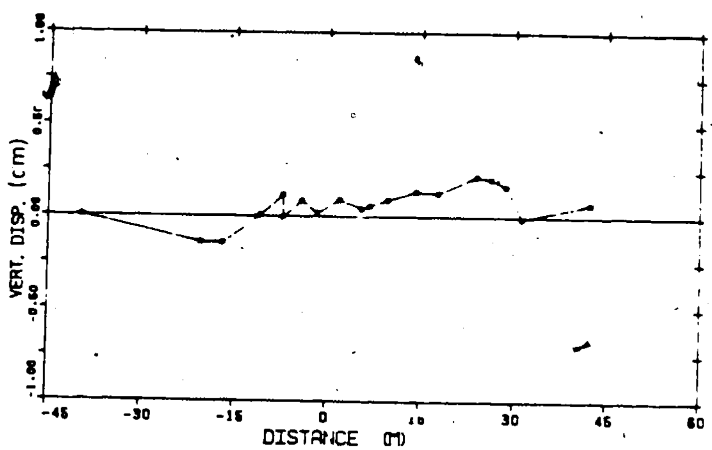

Figure B.9 ME5 MP#9 D=18.08m

MARKER POINT NO 1

	TIME DAYS	INIT. READ.	READINGS	DISPL CMS	LOCATION	
DECEMBER 22 1980	38.0	1.4348	1.4348	0.0	-40.00	0.0
FEBRUARY 3 1981	79.0	1.4348	1.4352	0.0500	-15.00	0.1000
FEBRUARY 5 1981	81.0	1.4348	1.4352	0.1100	-8.70	0.1000
FEBRUARY 8 1981	82.0	1.4348	1.4355	0.0900	-6.00	-0.1000
FEBRUARY 8 1981	84.0	1.4348	1.4355	-0.0200	-6.00	0.0450
FEBRUARY 9 1981	85.0	1.4348	1.4348	0.0500	-3.60	0.0300
FEBRUARY 10 1981	86.0	1.4348	1.4363	-0.1500	-0.50	-0.0550
FEBRUARY 10 1981	86.0	1.4348	1.4360	-0.1150	3.10	-0.1050
FEBRUARY 11 1981	87.0	1.4348	1.4363	-0.1850	5.60	-0.2350
FEBRUARY 11 1981	87.0	1.4348	1.4366	-0.2000	7.90	-0.2600
FEBRUARY 12 1981	88.0	1.4348	1.4538	-0.3100	11.00	-0.4400
FEBRUARY 13 1981	89.0	1.4348	1.4383	-0.4100	15.40	-0.4600
FEBRUARY 13 1981	90.0	1.4348	1.4366	-0.5250	15.40	-0.5200
FEBRUARY 16 1981	92.0	1.4348	1.4393	-0.4500	18.30	-0.0400
FEBRUARY 17 1981	93.0	1.4348	1.4399	-0.5100	25.10	-0.0100
FEBRUARY 18 1981	94.0	1.4348	1.4403	-0.4700	27.40	0.0000
FEBRUARY 19 1981	95.0	1.4348	1.4402	-0.4650	29.60	0.0050
FEBRUARY 23 1981	99.0	1.4348	1.4402	-0.4600	32.40	0.0000
FEBRUARY 26 1981	102.0	1.4348	1.4413	-0.5650	43.50	0.0450
MARCH 18 1981	122.0	1.4348	1.4416	-0.5900	115.00	0.0700

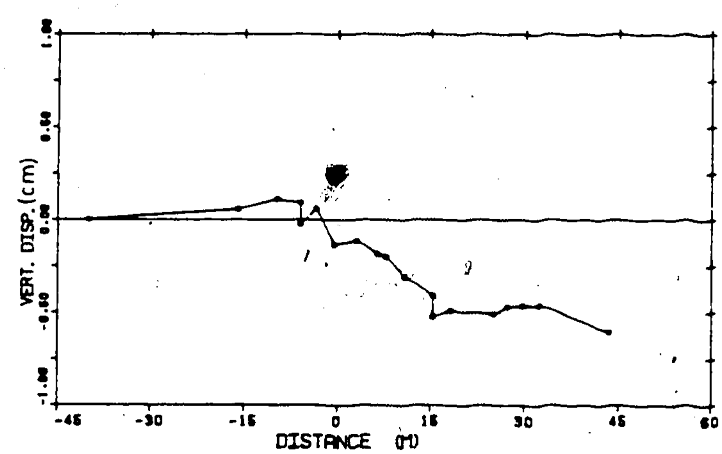

Figure B.10 ME9 MP#1 D=1.43m

MAGNET POINT NO. 2

	TIME DAYS	INIT. READ	READINGS	DISPL CM	LOCATION	
DECEMBER 22 1980	50.0	2.0316	2.0316	0.0	-48.00	0.0
FEBRUARY 5 1981	79.0	2.0316	2.0333	0.0851	-15.00	0.1000
FEBRUARY 5 1981	81.0	2.0316	2.0316	0.1301	-9.70	0.1000
FEBRUARY 6 1981	82.0	2.0316	2.0333	0.0001	-6.00	0.1000
FEBRUARY 8 1981	84.0	2.0316	2.0316	0.0450	-5.00	0.0450
FEBRUARY 9 1981	85.0	2.0316	2.0316	0.0001	-3.40	0.0300
FEBRUARY 10 1981	86.0	2.0316	2.0333	-0.1640	-0.80	-0.0850
FEBRUARY 10 1981	86.0	2.0316	2.0302	-0.0740	2.10	-0.1050
FEBRUARY 11 1981	87.0	2.0316	2.0300	-0.0850	5.00	-0.2250
FEBRUARY 11 1981	87.0	2.0316	2.0302	-0.1500	7.90	-0.2000
FEBRUARY 12 1981	88.0	2.0316	2.0306	-0.3400	11.00	-0.4400
FEBRUARY 13 1981	89.0	2.0316	2.0306	-0.2500	15.40	-0.4800
FEBRUARY 13 1981	89.0	2.0316	2.0306	-0.4850	15.40	-0.5250
FEBRUARY 16 1981	92.0	2.0316	2.0300	-0.4883	18.30	-0.5400
FEBRUARY 17 1981	93.0	2.0316	2.0303	-0.4000	25.10	-0.6100
FEBRUARY 18 1981	94.0	2.0316	2.0275	-0.5500	27.40	0.0800
FEBRUARY 19 1981	95.0	2.0316	2.0305	-0.4100	29.80	0.0250
FEBRUARY 23 1981	99.0	2.0316	2.0276	-0.5100	33.00	0.0000
FEBRUARY 26 1981	102.0	2.0316	2.0276	-0.5550	43.50	0.0450
MARCH 18 1981	122.0	2.0316	2.0288	-0.6200	118.00	0.0700

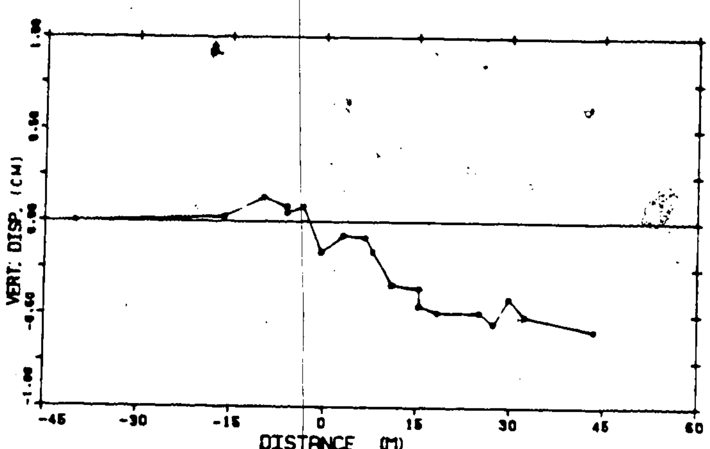

Figure B.11 ME9 MP#2 D=2.93m

MAGNET POINT NO 3

	TIME DAYS	INIT. READ	READINGS	DISPL CMS	LOCATION	
DECEMBER [illegible] 1980	[illegible]	[illegible]	[illegible]	[illegible]	[illegible]	[illegible]
FEBRUARY [illegible] 1981	[illegible]	[illegible]	[illegible]	[illegible]	[illegible]	[illegible]
FEBRUARY [illegible] 1981	[illegible]	[illegible]	[illegible]	[illegible]	[illegible]	[illegible]
FEBRUARY [illegible] 1981	[illegible]	[illegible]	[illegible]	[illegible]	[illegible]	[illegible]
FEBRUARY [illegible] 1981	[illegible]	[illegible]	[illegible]	[illegible]	[illegible]	[illegible]
FEBRUARY [illegible] 1981	[illegible]	[illegible]	[illegible]	[illegible]	[illegible]	[illegible]
FEBRUARY [illegible] 1981	[illegible]	[illegible]	[illegible]	[illegible]	[illegible]	[illegible]
FEBRUARY [illegible] 1981	[illegible]	[illegible]	[illegible]	[illegible]	[illegible]	[illegible]
FEBRUARY [illegible] 1981	[illegible]	[illegible]	[illegible]	[illegible]	[illegible]	[illegible]
FEBRUARY [illegible] 1981	[illegible]	[illegible]	[illegible]	[illegible]	[illegible]	[illegible]
FEBRUARY [illegible] 1981	[illegible]	[illegible]	[illegible]	[illegible]	[illegible]	[illegible]
FEBRUARY [illegible] 1981	[illegible]	[illegible]	[illegible]	[illegible]	[illegible]	[illegible]
FEBRUARY [illegible] 1981	[illegible]	[illegible]	[illegible]	[illegible]	[illegible]	[illegible]
FEBRUARY [illegible] 1981	[illegible]	[illegible]	[illegible]	[illegible]	[illegible]	[illegible]
FEBRUARY [illegible] 1981	[illegible]	[illegible]	[illegible]	[illegible]	[illegible]	[illegible]
FEBRUARY [illegible] 1981	[illegible]	[illegible]	[illegible]	[illegible]	[illegible]	[illegible]
FEBRUARY [illegible] 1981	[illegible]	[illegible]	[illegible]	[illegible]	[illegible]	[illegible]
FEBRUARY [illegible] 1981	[illegible]	[illegible]	[illegible]	[illegible]	[illegible]	[illegible]
FEBRUARY [illegible] 1981	[illegible]	[illegible]	[illegible]	[illegible]	[illegible]	[illegible]
MARCH [illegible] 1981	[illegible]	[illegible]	[illegible]	[illegible]	[illegible]	[illegible]

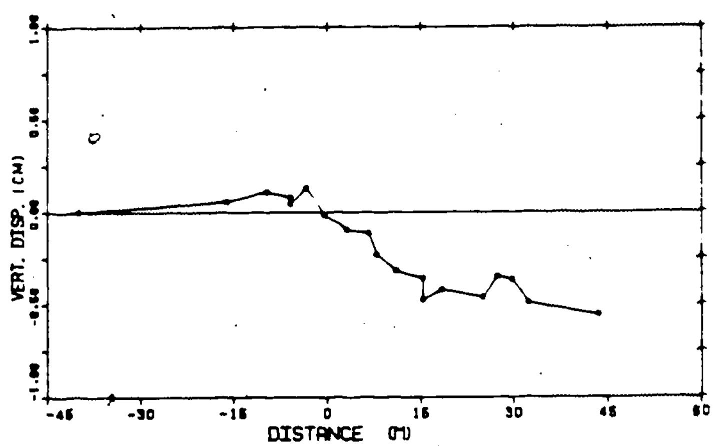

Figure B.12 ME9 MP#3 D=4.89m

MARKET POINT NO 4

	TIME DAYS	INIT. READ	READINGS	DISPL. CMS	LOCATION	
DECEMBER 22 1980	36.0	7.0043	7.0043	0.0	-40.00	0.0
FEBRUARY 3 1981	78.0	7.0043	7.0026	-0.0700	-15.00	0.1000
FEBRUARY 6 1981	81.0	7.0043	7.0040	0.0000	-8.70	0.1000
FEBRUARY 6 1981	82.0	7.0043	7.0043	0.0001	-5.00	0.1000
FEBRUARY 8 1981	84.0	7.0043	7.0044	-0.0000	-3.00	0.0250
FEBRUARY 9 1981	85.0	7.0043	7.0035	0.1100	-3.40	0.0300
FEBRUARY 10 1981	86.0	7.0043	7.0053	-0.0000	-0.00	-0.0000
FEBRUARY 10 1981	86.0	7.0043	7.0055	-0.1100	3.10	-0.1000
FEBRUARY 11 1981	87.0	7.0043	7.0071	-0.1300	5.00	-0.2000
FEBRUARY 11 1981	87.0	7.0043	7.0055	-0.1300	7.00	-0.2000
FEBRUARY 12 1981	88.0	7.0043	7.0033	-0.3000	11.00	-0.4400
FEBRUARY 12 1981	88.0	7.0043	7.0050	-0.3000	15.40	-0.4000
FEBRUARY 13 1981	89.0	7.0043	7.0033	-0.4300	15.40	-0.3200
FEBRUARY 16 1981	91.0	7.0043	7.0070	-0.3000	16.30	-0.4400
FEBRUARY 17 1981	93.0	7.0043	7.0040	-0.5000	25.10	-0.2100
FEBRUARY 18 1981	94.0	7.0043	7.0043	-0.3300	27.40	0.0000
FEBRUARY 19 1981	95.0	7.0043	7.0044	-0.3640	30.50	0.0450
FEBRUARY 23 1981	99.0	7.0043	7.0055	-0.4300	33.40	0.0000
FEBRUARY 26 1981	102.0	7.0043	7.0100	-0.5300	43.50	0.0450
MARCH 10 1981	123.0	7.0043	7.0104	-0.5600	115.00	0.0700

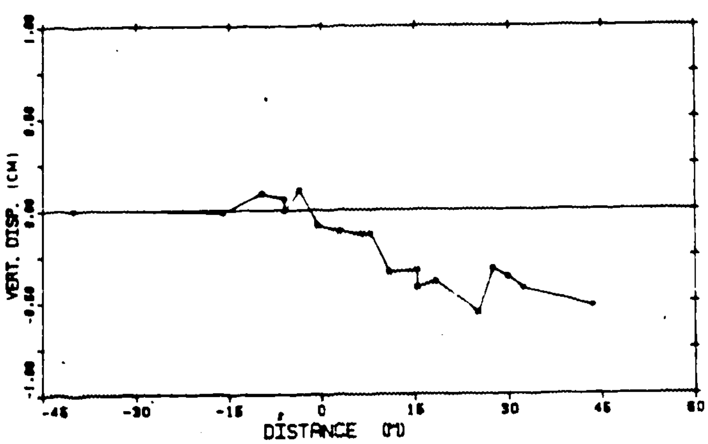

Figure B.13 ME9 MP#4 D=7.01m

[illegible]

	[illegible]	[illegible]	[illegible]	[illegible]	[illegible]	
DECEMBER [illegible] 1980	[illegible]	[illegible]	[illegible]	[illegible]	[illegible]	[illegible]
FEBRUARY [illegible] 1981	[illegible]	[illegible]	[illegible]	[illegible]	[illegible]	[illegible]
FEBRUARY [illegible] 1981	[illegible]	[illegible]	[illegible]	[illegible]	[illegible]	[illegible]
FEBRUARY [illegible] 1981	[illegible]	[illegible]	[illegible]	[illegible]	[illegible]	[illegible]
FEBRUARY [illegible] 1981	[illegible]	[illegible]	[illegible]	[illegible]	[illegible]	[illegible]
FEBRUARY [illegible] 1981	[illegible]	[illegible]	[illegible]	[illegible]	[illegible]	[illegible]
FEBRUARY [illegible] 1981	[illegible]	[illegible]	[illegible]	[illegible]	[illegible]	[illegible]
FEBRUARY [illegible] 1981	[illegible]	[illegible]	[illegible]	[illegible]	[illegible]	[illegible]
FEBRUARY [illegible] 1981	[illegible]	[illegible]	[illegible]	[illegible]	[illegible]	[illegible]
FEBRUARY [illegible] 1981	[illegible]	[illegible]	[illegible]	[illegible]	[illegible]	[illegible]
FEBRUARY [illegible] 1981	[illegible]	[illegible]	[illegible]	[illegible]	[illegible]	[illegible]
FEBRUARY [illegible] 1981	[illegible]	[illegible]	[illegible]	[illegible]	[illegible]	[illegible]
FEBRUARY [illegible] 1981	[illegible]	[illegible]	[illegible]	[illegible]	[illegible]	[illegible]
FEBRUARY [illegible] 1981	[illegible]	[illegible]	[illegible]	[illegible]	[illegible]	[illegible]
FEBRUARY [illegible] 1981	[illegible]	[illegible]	[illegible]	[illegible]	[illegible]	[illegible]
FEBRUARY [illegible] 1981	[illegible]	[illegible]	[illegible]	[illegible]	[illegible]	[illegible]
FEBRUARY [illegible] 1981	[illegible]	[illegible]	[illegible]	[illegible]	[illegible]	[illegible]
FEBRUARY [illegible] 1981	[illegible]	[illegible]	[illegible]	[illegible]	[illegible]	[illegible]
FEBRUARY [illegible] 1981	[illegible]	[illegible]	[illegible]	[illegible]	[illegible]	[illegible]
MARCH [illegible] 1981	[illegible]	[illegible]	[illegible]	[illegible]	[illegible]	[illegible]

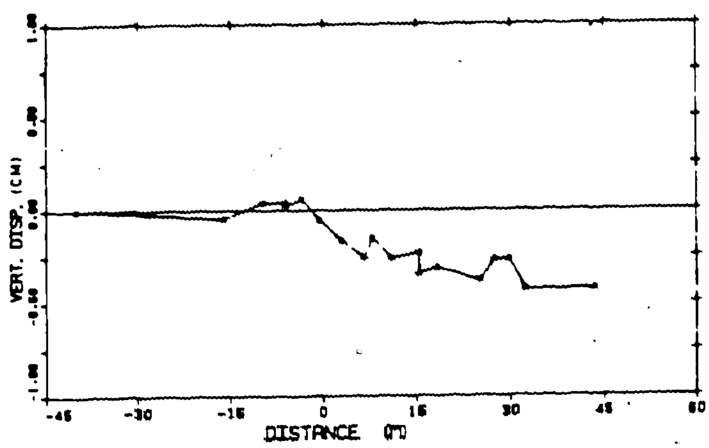

Figure B.14 ME9 MP#5 D=8.93m

MAGNET POINT NO. 6

	TIME DAYS	INIT. READ.	READINGS	DISPL CMS	LOCATION	
DECEMBER 22 1980	[illegible]	11.1000	11.1000	0.0	-[illegible]	0.0
FEBRUARY 3 1981	70.0	11.1000	11.1010	[illegible]	-10.00	0.1000
FEBRUARY [illegible] 1981	[illegible]	11.1000	11.100[illegible]	[illegible]	-9.70	0.1000
FEBRUARY [illegible] 1981	[illegible]	11.1000	11.1010	[illegible]	-6.00	0.1000
FEBRUARY [illegible] 1981	[illegible]	11.1000	11.100[illegible]	-0.0[illegible]	-[illegible]	0.0[illegible]
FEBRUARY [illegible] 1981	[illegible]	11.1000	11.100[illegible]	0.1000	-2.[illegible]	0.0[illegible]
FEBRUARY 10 1981	[illegible]	11.1000	11.1000	-0.0[illegible]	-0.[illegible]	-0.0[illegible]
FEBRUARY 10 1981	[illegible]	11.1000	11.10[illegible]	-0.0[illegible]	3.10	-0.1[illegible]
FEBRUARY 11 1981	[illegible]	11.1000	11.107[illegible]	-0.0100	[illegible]	-0.[illegible]
FEBRUARY 11 1981	[illegible]	11.1000	11.10[illegible]	0.0700	7.[illegible]	-0.[illegible]
FEBRUARY 1[illegible] 1981	[illegible]	11.1000	11.1070	-0.1400	11.00	-0.4400
FEBRUARY 1[illegible] 1981	[illegible]	11.1000	11.10[illegible]	-0.0400	1[illegible]	-0.[illegible]
FEBRUARY 1[illegible] 1981	[illegible]	11.1000	11.10[illegible]	-0.1700	1[illegible]	-0.[illegible]
FEBRUARY 1[illegible] 1981	[illegible]	11.1000	11.101[illegible]	-0.1000	1[illegible]	-0.0400
FEBRUARY 17 1981	[illegible]	11.1000	11.101[illegible]	-0.1000	[illegible]	-0.0100
FEBRUARY 1[illegible] 1981	[illegible]	11.1000	11.1010	-0.0200	27.[illegible]	0.0[illegible]
FEBRUARY 1[illegible] 1981	[illegible]	11.1000	11.1010	-0.0[illegible]	[illegible]	0.0[illegible]
FEBRUARY [illegible] 1981	[illegible]	11.1000	11.10[illegible]	-0.[illegible]	[illegible]	0.0[illegible]
FEBRUARY [illegible] 1981	10[illegible]	11.1000	11.10[illegible]	-0.1[illegible]	[illegible]	0.0[illegible]
MARCH 1[illegible] 1981	1[illegible]	11.1000	11.10[illegible]	-0.[illegible]	1[illegible]	0.0700

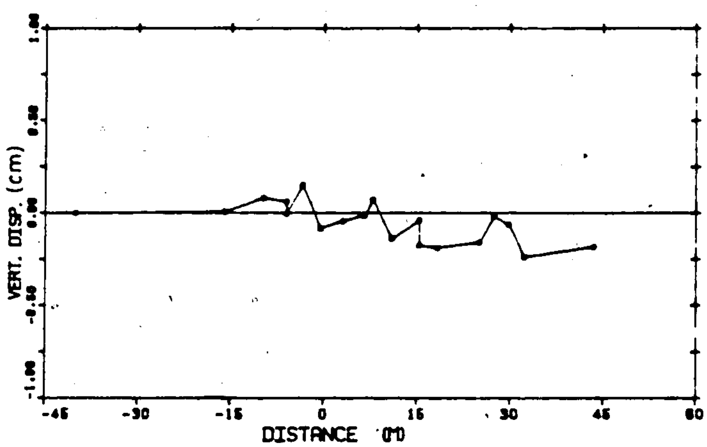

Figure B.15 ME9 MP#6 D=11.16m

MAGNET POINT NO 7

	TIME DAYS	INIT. READ.	READINGS	DISPL CM	LOCATION	
DECEMBER 22 1980	36.0	12.8840	12.8840	0.0	-40.00	0.0
FEBRUARY 2 1981	78.0	12.8840	12.8855	-0.0751	-15.00	0.1000
FEBRUARY 5 1981	81.0	12.8840	12.8852	0.0500	-8.70	0.1600
FEBRUARY 6 1981	82.0	12.8840	12.8850	0.0000	-6.00	0.1600
FEBRUARY 8 1981	84.0	12.8840	12.8845	-0.0050	-5.00	0.0450
FEBRUARY 9 1981	85.0	12.8840	12.8820	0.1200	-3.40	0.0200
FEBRUARY 10 1981	86.0	12.8840	12.8825	-0.0250	-0.50	-0.0850
FEBRUARY 10 1981	86.0	12.8840	12.8816	0.0250	3.10	-0.1000
FEBRUARY 11 1981	87.0	12.8840	12.8800	0.0850	6.00	-0.2250
FEBRUARY 11 1981	87.0	12.8840	12.8788	0.1800	7.00	-0.2000
FEBRUARY 12 1981	88.0	12.8840	12.8780	0.0400	11.00	-0.4400
FEBRUARY 13 1981	89.0	12.8840	12.8788	0.0500	15.40	-0.4000
FEBRUARY 13 1981	89.0	12.8840	12.8780	-0.0250	15.60	-0.5250
FEBRUARY 16 1981	92.0	12.8840	12.8826	0.0100	18.30	-0.0400
FEBRUARY 17 1981	93.0	12.8840	12.8845	-0.0500	25.10	-0.0100
FEBRUARY 18 1981	94.0	12.8840	12.8860	0.0000	27.40	0.0000
FEBRUARY 19 1981	95.0	12.8840	12.8825	0.1000	30.60	0.0550
FEBRUARY 23 1981	99.0	12.8840	12.8852	-0.0400	32.40	0.0000
FEBRUARY 26 1981	102.0	12.8840	12.8865	-0.0050	43.50	0.0450
MARCH 19 1981	123.0	12.8840	12.8870	-0.2200	115.00	0.0700

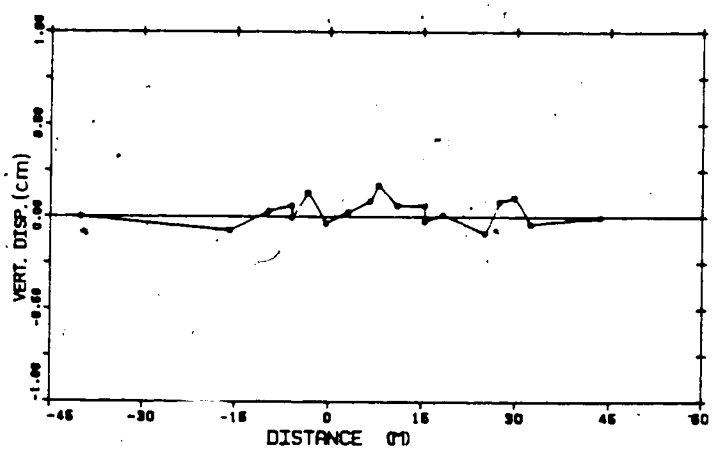

Figure B.16 ME9 MP#7 D=13.89m

MAGNET POINT NO. 8

	TIME DAYS	INIT READ.	READINGS	DISPL CMS	LOCATION	
DECEMBER 22 1980	58.0	15.0030	15.0035	0.0	-40.00	0.0
FEBRUARY 3 1981	75.0	15.0030	15.0000	-0.1400	-15.00	0.1050
FEBRUARY 5 1981	81.0	15.0035	15.0000	0.0101	-9.70	0.1000
FEBRUARY 6 1981	82.0	15.0035	15.0045	0.0001	-6.00	0.1000
FEBRUARY 8 1981	84.0	15.0035	15.0045	-0.0040	-5.00	0.0450
FEBRUARY 9 1981	85.0	15.0035	15.0024	0.1000	-3.40	0.0200
FEBRUARY 10 1981	86.0	15.0035	15.0035	-0.0500	-0.50	-0.0450
FEBRUARY 10 1981	86.0	15.0035	[illegible]	0.1050	3.10	-0.1050
FEBRUARY 11 1981	87.0	15.0035	[illegible]	0.0650	5.50	-0.2250
FEBRUARY 11 1981	87.0	15.0030	15.0000	0.1700	7.50	-0.2000
FEBRUARY 12 1981	88.0	15.0035	15.0000	0.1101	11.00	-0.4400
FEBRUARY 13 1981	89.0	15.0035	15.0075	0.1401	13.40	-0.4000
FEBRUARY 13 1981	89.0	15.0035	15.0075	0.0751	15.40	-0.5300
FEBRUARY 16 1981	92.0	15.0035	15.0035	0.0000	16.30	-0.0400
FEBRUARY 17 1981	93.0	15.0035	15.0035	0.0000	25.10	-0.0100
FEBRUARY 18 1981	94.0	15.0035	15.0023	0.2001	27.40	0.0000
FEBRUARY 19 1981	95.0	15.0035	15.0034	0.1550	30.50	0.0450
FEBRUARY 23 1981	99.0	15.0035	15.0045	-0.0001	33.40	0.0000
FEBRUARY 26 1981	102.0	15.0035	15.0035	0.0450	43.50	0.0450
MARCH 18 1981	122.0	15.0035	15.1000	45.5200	115.00	0.0700

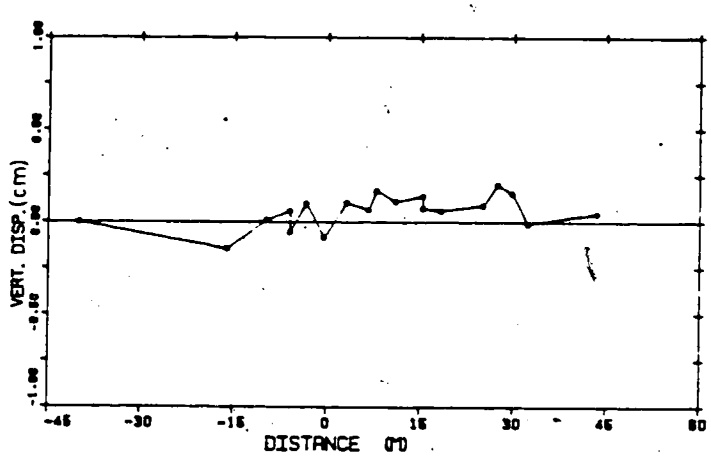

Figure B.17 ME9 MP#8 D=15.61m

MAGNET POINT NO. 9

	TIME DAYS	INIT. READ	READINGS	DISPL CMS	LOCATION	
DECEMBER 22 1980	38.0	10.0182	10.0182	0.0	-40.00	0.0
FEBRUARY 3 1981	79.0	10.0182	10.0210	-0.1001	-18.00	0.1080
FEBRUARY 5 1981	81.0	10.0182	10.0105	0.0410	-8.70	0.1800
FEBRUARY 6 1981	83.0	10.0182	10.0105	0.0410	-6.00	0.1800
FEBRUARY 8 1981	84.0	10.0182	10.0180	0.0282	-6.00	0.0480
FEBRUARY 9 1981	85.0	10.0182	10.0176	0.1007	-3.40	0.0300
FEBRUARY 10 1981	86.0	10.0182	10.0100	0.0081	-0.80	-0.0080
FEBRUARY 10 1981	86.0	10.0182	10.0158	0.0654	3.10	-0.1080
FEBRUARY 11 1981	87.0	10.0182	10.0146	0.1100	5.00	-0.2200
FEBRUARY 11 1981	87.0	10.0182	10.0133	0.2208	7.80	-0.2600
FEBRUARY 12 1981	88.0	10.0182	10.0123	0.1012	11.00	-0.4400
FEBRUARY 12 1981	88.0	10.0182	10.0118	0.1000	13.40	-0.4800
FEBRUARY 13 1981	89.0	10.0182	10.0116	0.1280	15.00	-0.5250
FEBRUARY 16 1981	92.0	10.0182	10.0105	0.1401	15.30	-0.0400
FEBRUARY 17 1981	93.0	10.0182	10.0105	0.1701	20.10	-0.0100
FEBRUARY 18 1981	94.0	10.0182	10.0152	0.2700	27.40	0.0100
FEBRUARY 19 1981	95.0	10.0182	10.0106	0.2601	28.80	0.0880
FEBRUARY 22 1981	98.0	10.0182	10.0140	0.1200	32.40	0.0000
FEBRUARY 26 1981	102.0	10.0182	10.0170	0.1280	43.50	0.0480
MARCH 19 1981	123.0	10.0182	10.0200	-0.0084	115.00	0.0700

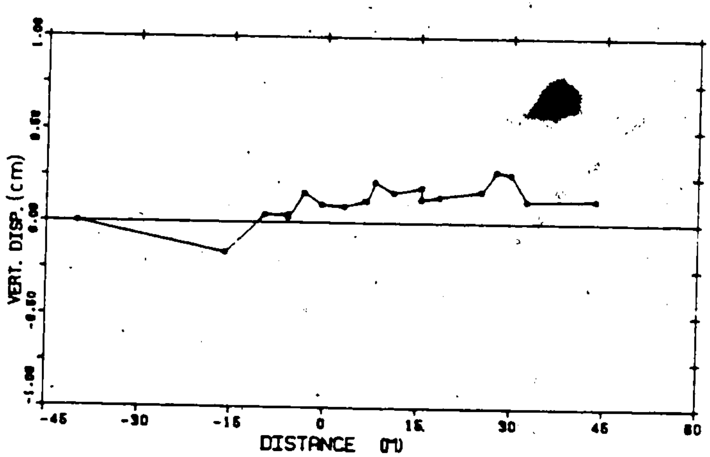

Figure B.18 ME9 MP#9 D=16.92m

MAGNET POINT NO 10

	TIME DAYS	INIT. READ	READINGS	DISPL CM	LOCATION	
DECEMBER 22 1980	36.0	16.3023	16.3023	0.0	-40.00	0.0
FEBRUARY 2 1981	79.0	16.3023	16.3040	-0.1482	-18.00	0.1000
FEBRUARY 5 1981	81.0	16.3023	16.3040	-0.0004	-8.70	0.1000
FEBRUARY 6 1981	82.0	16.3023	16.3026	0.0106	-8.00	0.1000
FEBRUARY 8 1981	84.0	16.3023	16.3033	-0.0642	-6.00	0.0400
FEBRUARY 9 1981	85.0	16.3023	16.3013	0.1207	-3.40	0.0200
FEBRUARY 10 1981	86.0	16.3023	16.2716	-1.0001	-0.50	-0.0450
FEBRUARY 10 1981	86.0	16.3023	16.3006	0.0481	3.10	-0.1050
FEBRUARY 11 1981	87.0	16.3023	16.2963	0.1066	6.00	-0.2350
FEBRUARY 11 1981	87.0	16.3023	16.2970	0.3010	7.00	-0.2800
FEBRUARY 12 1981	88.0	16.3023	16.3005	0.1258	11.00	-0.4400
FEBRUARY 13 1981	88.0	16.3023	16.3056	0.1000	16.40	-0.4800
FEBRUARY 13 1981	89.0	16.3023	16.3001	0.1250	18.40	-0.5250
FEBRUARY 16 1981	92.0	16.3023	16.3004	0.1111	15.30	-0.0400
FEBRUARY 17 1981	93.0	16.3023	16.3006	0.1701	20.10	-0.0100
FEBRUARY 18 1981	94.0	16.3023	16.3004	0.3311	27.40	0.0000
FEBRUARY 19 1981	95.0	16.3023	16.3005	0.3051	30.00	0.0050
FEBRUARY 23 1981	99.0	16.3023	16.3030	0.0702	33.40	0.0000
FEBRUARY 26 1981	102.0	16.3023	16.3080	-0.5242	43.50	0.0450
MARCH 18 1981	122.0	16.3023	16.3045	-0.1427	115.00	0.0700

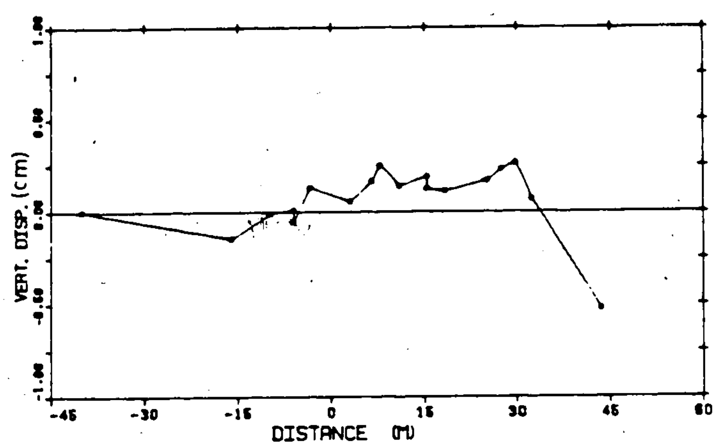

Figure B.19 ME9 MP#10 D=18.36m

MAGNET POINT NO. 1

	TIME DAYS	INIT. READ.	READINGS	DISPL CMS	LOCATION	
DECEMBER 22 1980	50.0	2.5200	2.5200	0.0	-45.00	0.0
FEBRUARY 1 1981	77.0	2.5200	2.5205	-0.0520	-24.00	0.0100
FEBRUARY 3 1981	79.0	2.5200	2.5202	-0.0100	-21.00	0.0190
FEBRUARY 5 1981	81.0	2.5200	2.5202	-0.0100	-15.00	0.0100
FEBRUARY 6 1981	82.0	2.5200	2.5262	0.0020	-11.00	0.0270
FEBRUARY 8 1981	84.0	2.5200	2.5202	-0.0120	-11.00	0.0170
FEBRUARY 9 1981	85.0	2.5200	2.5276	0.1371	-8.00	0.0170
FEBRUARY 10 1981	86.0	2.5200	2.5266	0.0500	-6.00	0.0190
FEBRUARY 10 1981	86.0	2.5200	2.5250	0.0200	-2.00	0.0040
FEBRUARY 11 1981	87.0	2.5200	2.5240	0.0250	-1.00	0.0000

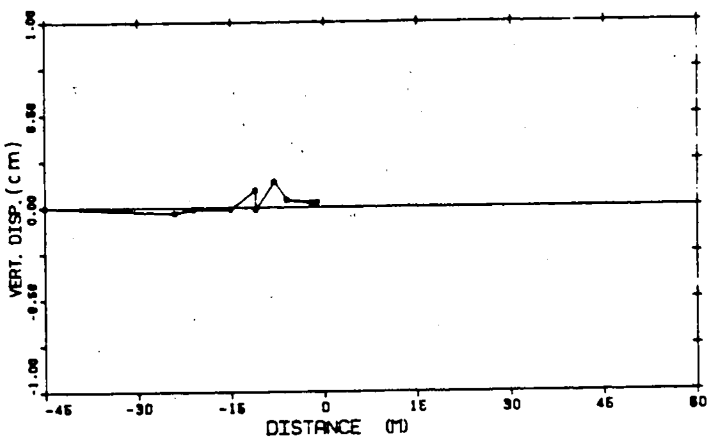

Figure B.20 ME10 MP#1 D=253 m

MAGNET POINT NO. 2

	TIME DAYS	INIT READ.	READINGS	DISPL CMS	LOCATION	
DECEMBER 22 1980	30.0	4.5770	4.5770	0.0	-45.00	0.0
FEBRUARY 1 1981	77.0	4.5770	4.5758	-0.0620	-24.00	0.0180
FEBRUARY 3 1981	79.0	4.5770	4.5760	-0.0610	-21.00	0.0180
FEBRUARY 5 1981	81.0	4.5770	4.5753	-0.0311	-15.00	0.0180
FEBRUARY 6 1981	83.0	4.5770	4.5773	0.0720	-11.00	0.0230
FEBRUARY 6 1981	84.0	4.5770	4.5773	0.0870	-11.00	0.0170
FEBRUARY 9 1981	86.0	4.5770	4.5786	0.1105	-8.00	0.0170
FEBRUARY 10 1981	86.0	4.5770	4.5770	0.0180	-5.00	0.0180
FEBRUARY 10 1981	86.0	4.5770	4.5778	0.0640	-3.00	0.0040
FEBRUARY 11 1981	87.0	4.5770	4.5775	0.0570	-1.00	0.0060

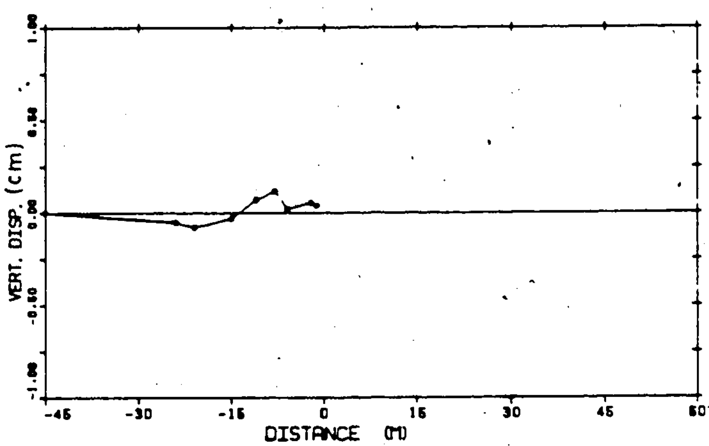

Figure B.21 ME10 MP# 2 D = 4.58 m

MAGNET POINT NO. 3

	TIME DAYS	INIT. READ.	READINGS	DISPL CMS	LOCATION	
DECEMBER 22 1980	36.0	0.3603	0.3603	0.0	-48.00	0.0
FEBRUARY 1 1981	77.0	0.3603	0.3613	-0.0820	-24.00	0.0100
FEBRUARY 3 1981	79.0	0.3603	0.3612	-0.0810	-21.00	0.0100
FEBRUARY 5 1981	81.0	0.3603	0.3602	0.0100	-15.00	0.0100
FEBRUARY 6 1981	82.0	0.3603	0.2798	0.0720	-11.00	0.0220
FEBRUARY 8 1981	84.0	0.3603	0.3602	0.0170	-11.00	0.0170
FEBRUARY 9 1981	85.0	0.3603	0.2790	0.1470	-8.00	0.0170
FEBRUARY 10 1981	86.0	0.3603	0.2786	0.0880	-6.00	0.0100
FEBRUARY 10 1981	86.0	0.3603	0.2783	0.1020	-3.00	0.0040
FEBRUARY 11 1981	87.0	0.3603	0.2782	0.1070	-1.00	0.0030

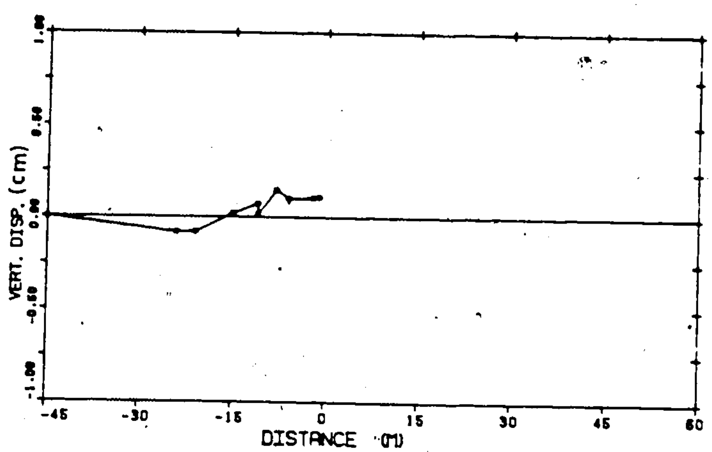

FIG B.22 ME10 MP# 3 D= 638m

MAGNET POINT NO. 4

	TIME DAYS	INIT. READ.	READINGS	DISPL CMS	LOCATION	
DECEMBER 22 1980	36.0	8.4016	8.4018	0.0	-45.00	0.0
FEBRUARY 1 1981	77.0	8.4016	8.4030	-0.1090	-24.00	0.0180
FEBRUARY 3 1981	79.0	8.4016	8.4028	-0.0600	-21.00	0.0100
FEBRUARY 5 1981	81.0	8.4016	8.4030	-0.1010	-15.00	0.0100
FEBRUARY 6 1981	82.0	8.4016	8.4018	0.0220	-11.00	0.0220
FEBRUARY 8 1981	84.0	8.4016	8.4018	0.0470	-11.00	0.0170
FEBRUARY 9 1981	86.0	8.4016	8.4006	0.1070	-8.00	0.0170
FEBRUARY 10 1981	86.0	8.4016	8.4006	0.1100	-6.00	0.0190
FEBRUARY 10 1981	86.0	8.4016	8.4010	0.0640	-3.00	0.0040
FEBRUARY 11 1981	87.0	8.4016	8.4002	0.1000	-1.00	0.0060

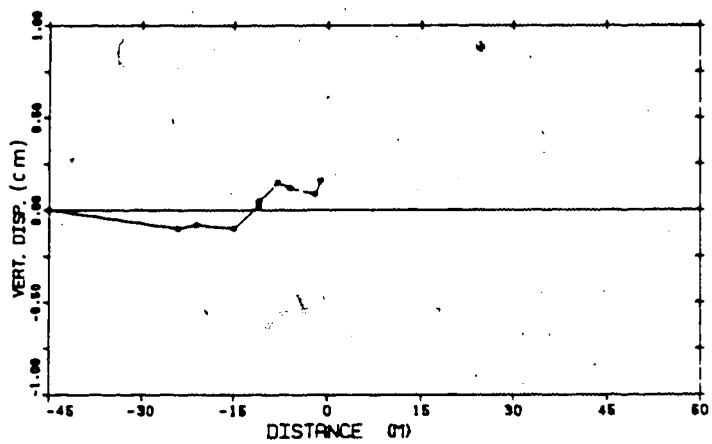

FIG B.23 ME10 MP#4 D= 8.40 m

MAGNET POINT NO 5

	TIME DAYS	INIT. READ	READINGS	DISPL CMS	LOCATION	
DECEMBER 22 1980	30.0	10.2185	10.2185	0.0	-45.00	0.0
FEBRUARY 1 1981	77.0	10.2185	10.2300	-0.1320	-24.00	0.0160
FEBRUARY 2 1981	78.0	10.2185	10.2302	-0.1610	-21.00	0.0100
FEBRUARY 5 1981	81.0	10.2185	10.2195	-0.0600	-15.00	0.0100
FEBRUARY 6 1981	82.0	10.2185	10.2165	0.0220	-11.00	0.0170
FEBRUARY 8 1981	84.0	10.2185	10.2165	0.0170	-11.00	0.0170
FEBRUARY 9 1981	85.0	10.2185	10.2175	0.1170	-8.00	0.0170
FEBRUARY 10 1981	86.0	10.2185	10.2285	-1.0810	-6.00	0.0150
FEBRUARY 10 1981	86.0	10.2185	10.2176	0.0740	-2.00	0.0060
FEBRUARY 11 1981	87.0	10.2185	10.2172	0.1260	-1.00	0.0060

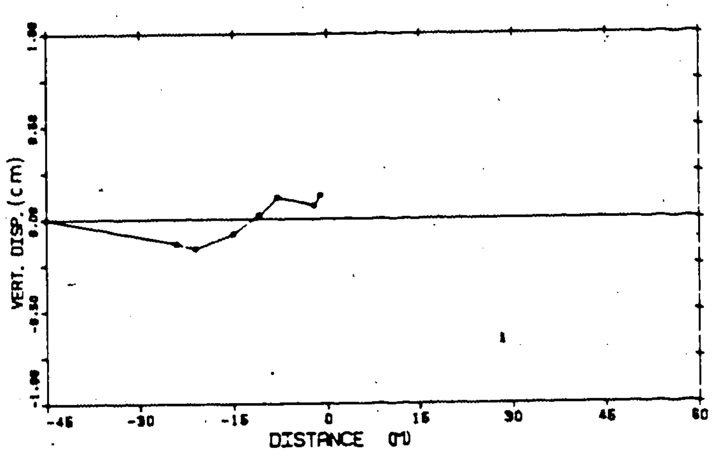

Figure B.24 ME10 MP#5 D=10.22m

MAGNET POINT NO. 6

	TIME DAYS	INIT. READ.	READINGS	DISPL DMM	LOCATION	
DECEMBER 22 1980	36.0	12.2770	12.2770	0.0	-45.00	0.0
FEBRUARY 1 1981	77.0	12.2770	12.2756	-0.1520	-24.00	0.0100
FEBRUARY 2 1981	78.0	12.2770	12.2756	-0.1510	-21.00	0.0100
FEBRUARY 5 1981	81.0	12.2770	12.2762	-0.1110	-15.00	0.0100
FEBRUARY 6 1981	82.0	12.2770	12.2772	-0.0070	-11.00	0.0620
FEBRUARY 8 1981	84.0	12.2770	12.2772	-0.0120	-11.00	0.0170
FEBRUARY 9 1981	85.0	12.2770	12.2790	0.1170	-8.00	0.0170
FEBRUARY 10 1981	86.0	12.2770	12.2770	0.0100	-6.00	0.0100
FEBRUARY 10 1981	86.0	12.2770	12.2790	0.1040	-2.00	0.0040
FEBRUARY 11 1981	87.0	12.2770	12.2788	0.1580	-1.00	0.0050

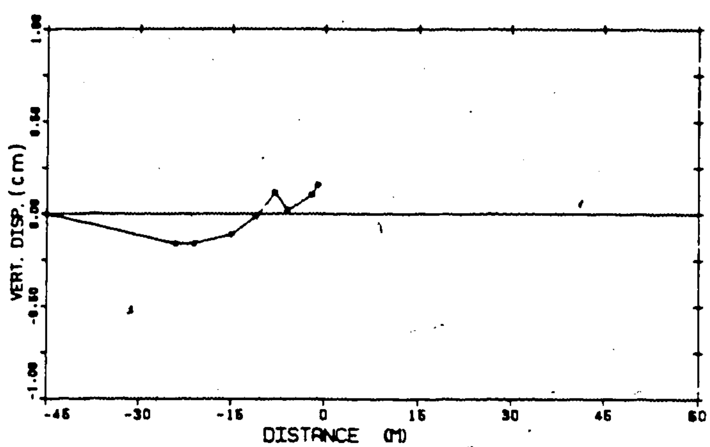

Figure B.25 ME10 MP#6 D=12.28m

MAGNET POINT NO. 7

	TIME DAYS	INIT READ	READINGS	DISPL (MM)	LOCATION	
DECEMBER 22 1980	38.0	14.2[illegible]	14.2[illegible]	0.0	-45.00	0.0
FEBRUARY 1 1981	77.0	14.2[illegible]	14.2[illegible]	-0.1820	-24.00	0.0100
FEBRUARY 3 1981	79.0	14.2[illegible]	14.2[illegible]	-0.1610	-21.00	0.0100
FEBRUARY 5 1981	81.0	14.2[illegible]	14.2[illegible]	-0.1610	-15.00	0.0100
FEBRUARY 6 1981	82.0	14.2[illegible]	14.2[illegible]	0.00[illegible]0	-11.00	0.0220
FEBRUARY 8 1981	84.0	14.2[illegible]	14.2[illegible]	-0.0231	-11.00	0.0170
FEBRUARY 9 1981	85.0	14.2[illegible]	14.2[illegible]	0.0470	-8.00	0.0170
FEBRUARY 10 1981	86.0	14.2[illegible]	14.2[illegible]	-0.0010	-6.00	0.0100
FEBRUARY 10 1981	86.0	14.2[illegible]	14.2810	0.1020	-2.00	0.0040
FEBRUARY 11 1981	87.0	14.2[illegible]	14.2800	0.2270	-1.00	0.0040

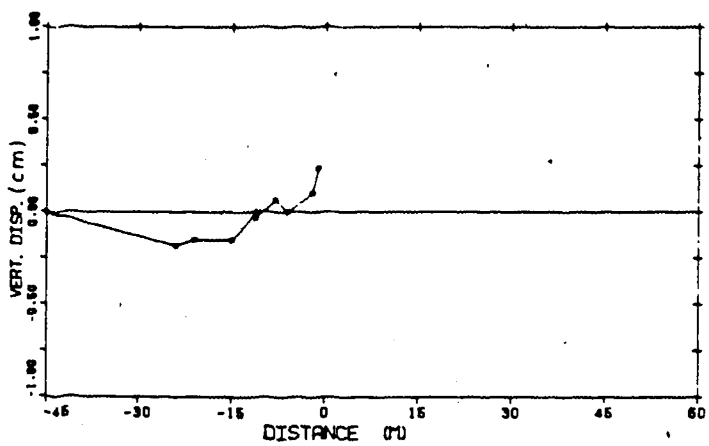

Figure B.26 ME10 MP#7 D=14.29m

MAGNET POINT NO. 8

	TIME DAYS	INIT. READ.	READINGS	DISPL. CMS	LOCATION	
DECEMBER 31 1980	56.0	10.3426	10.3430	0.0	-45.00	0.0
FEBRUARY 1 1981	77.0	10.3426	10.3445	-0.1820	-34.00	0.0100
FEBRUARY 3 1981	79.0	10.3426	10.3442	-0.1306	-31.00	0.0100
FEBRUARY 5 1981	81.0	10.3426	10.3430	-0.0613	-16.00	0.0100
FEBRUARY 6 1981	82.0	10.3426	10.3426	0.0325	-11.00	0.0230
FEBRUARY 8 1981	84.0	10.3426	10.3430	0.0475	-11.00	0.0170
FEBRUARY 9 1981	85.0	10.3426	10.3413	0.1085	-8.00	0.0170
FEBRUARY 10 1981	86.0	10.3426	10.3416	0.1182	-6.00	0.0150
FEBRUARY 10 1981	86.0	10.3426	10.3410	0.1641	-2.00	0.0040
FEBRUARY 11 1981	87.0	10.3426	10.3304	0.2971	-1.00	0.0060

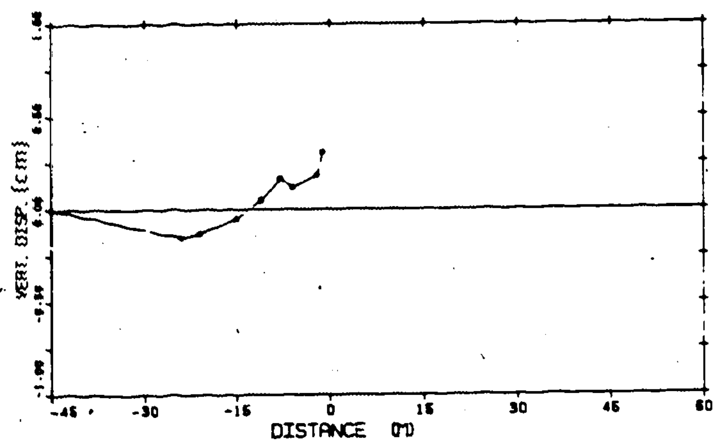

Figure B.27 ME1,0 MP#8 D=16.25m

MAGNET POINT NO 1

	TIME DAYS	INIT READ	READINGS	DISPL CMS	LOCATION	
MARCH 3 1981	107.0	3.0087	3.0087	0.0	-27.40	0.0
MARCH 4 1981	108.0	3.0087	3.0087	0.1100	-21.40	0.1100
MARCH 5 1981	109.0	3.0087	3.0082	0.1700	-15.50	0.1800
MARCH 7 1981	111.0	3.0087	3.0082	0.2700	-7.10	0.2800
MARCH 8 1981	112.0	3.0087	3.0082	-0.1200	-3.40	-0.1700
MARCH 10 1981	114.0	3.0087	3.0082	0.0800	0.0	0.0800
MARCH 10 1981	114.0	3.0087	3.0000	-0.2100	3.60	-0.2000
MARCH 11 1981	115.0	3.0087	2.9982	-0.2700	10.20	-0.1200
MARCH 13 1981	117.0	3.0087	2.9500	-0.7551	19.80	-0.8200
MARCH 19 1981	123.0	3.0087	2.9982	-1.1350	24.90	-0.8800

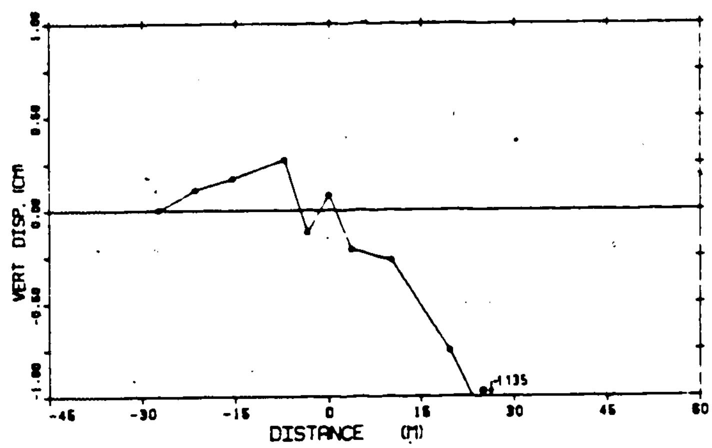

Figure 8.28 ME17 MP#1 D=3.01m

MAGNET POINT NO 2

	TIME DAYS	INIT READ	READINGS	DISPL CMS	LOCATION	
MARCH 3 1981	107.0	4.2005	4.2005	0.0	-27.40	0.0
MARCH 4 1981	108.0	4.2005	4.2003	0.1300	-21.40	0.1100
MARCH 5 1981	109.0	4.2005	4.2000	0.1700	-16.50	0.1200
MARCH 7 1981	111.0	4.2005	4.1987	0.2990	-7.10	0.2200
MARCH 8 1981	112.0	4.2005	4.1987	-0.0801	-3.40	-0.1700
MARCH 10 1981	114.0	4.2005	4.1987	0.1000	0.0	0.0300
MARCH 10 1981	114.0	4.2005	4.1002	-0.2500	3.60	-2.2000
MARCH 11 1981	115.0	4.2005	4.1243	-0.4800	10.20	-0.1200
MARCH 13 1981	117.0	4.2005	4.1247	-0.8850	16.80	-0.8200
MARCH 19 1981	123.0	4.2005	4.1252	-1.4551	24.00	-0.8850

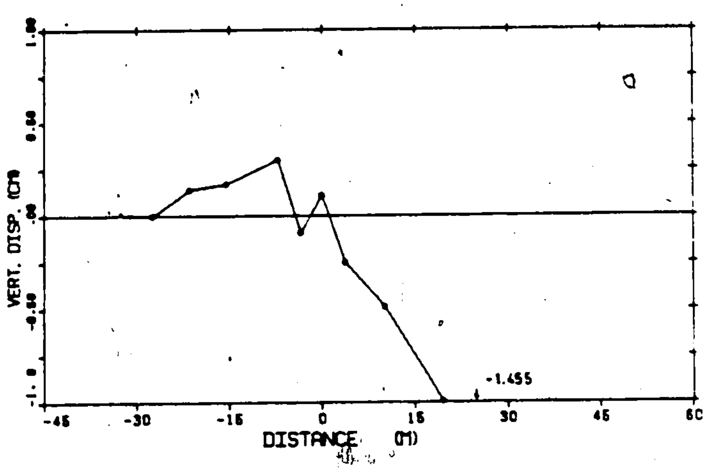

Figure B.29 ME17 MP#2 D=4.20m

MAGNET POINT NO 3

	TIME DAYS	INIT READ	READINGS	DISPL CMS	LOCATION	
MARCH 3 1981	107.0	5.2437	5.2437	0.0	-27.40	0.0
MARCH 4 1981	108.0	5.2437	5.2430	0.0800	-21.40	0.1100
MARCH 5 1981	109.0	5.2437	5.2422	0.1700	-15.50	0.1200
MARCH 7 1981	111.0	5.2437	5.2420	0.2500	-7.10	0.2200
MARCH 8 1981	112.0	5.2437	5.2432	-0.1200	-3.40	-0.1700
MARCH 10 1981	114.0	5.2437	5.2422	0.0800	0.0	0.0200
MARCH 10 1981	114.0	5.2437	5.2222	-0.2201	3.50	-2.2600
MARCH 11 1981	115.0	5.2437	5.2037	-4.1200	10.30	-5.1200
MARCH 12 1981	117.0	5.2437	5.2062	-4.9750	10.50	-5.6250
MARCH 18 1981	123.0	5.2437	5.2057	-5.2850	24.90	-5.9850

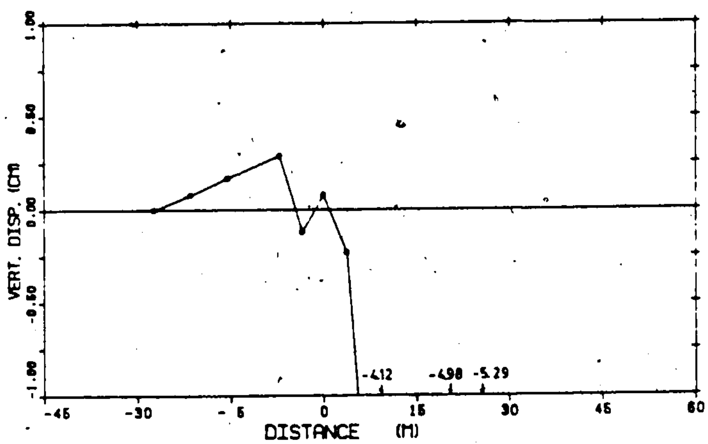

Figure B.30 ME17 MP#3 D=5.24m

MAGNET POINT NO 4

	TIME DAYS	INIT READ	READINGS	DISPL CMS	LOCATION	
MARCH 3 1981	107.0	0.6652	0.6652	0.0	-27.40	0.0
MARCH 4 1981	108.0	0.6652	0.6650	0.1200	-21.40	0.1100
MARCH 6 1981	110.0	0.6652	0.6650	0.1200	-15.50	0.1200
MARCH 7 1981	111.0	0.6652	0.6647	0.2700	-7.10	0.2200
MARCH 8 1981	112.0	0.6652	0.6645	-0.1000	-3.40	-0.1700
MARCH 10 1981	114.0	0.6652	0.6650	0.0400	0.0	0.0200
MARCH 10 1981	114.0	0.6652	0.6607	-0.4201	3.60	-3.2800
MARCH 11 1981	115.0	0.6652	0.5775	-7.3500	10.20	-8.1200
MARCH 12 1981	117.0	0.6652	0.5826	-8.3600	19.80	-8.8200
MARCH 19 1981	123.0	0.6652	0.5825	-8.7200	24.90	-8.8850

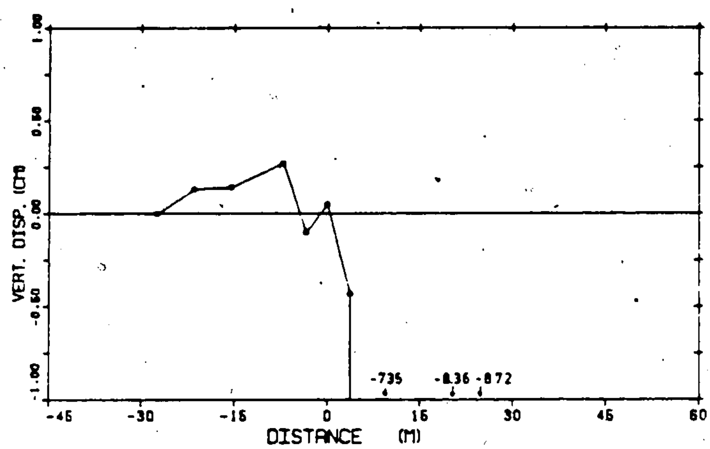

Figure B.31 ME17 MP#4 D=6.69m

MAGNET POINT NO 5

	TIME DAYS	INIT READ	READINGS	DISPL CMS	LOCATION	
MARCH 3 1981	107.0	7.8820	7.8820	0.0	-27.00	0.0
MARCH 4 1981	108.0	7.8820	7.8875	0.1801	-21.40	0.1100
MARCH 5 1981	109.0	7.8820	7.8825	0.1701	-15.50	0.1200
MARCH 7 1981	111.0	7.8820	7.8822	0.3000	-7.10	0.2200
MARCH 9 1981	113.0	7.8820	7.8830	-0.0700	-3.40	-0.1700
MARCH 10 1981	114.0	7.8820	8.4115	-61.8155	0.0	0.0300
MARCH 10 1981	114.0	7.8820	8.4115	-64.1255	3.50	-2.2500
MARCH 11 1981	115.0	7.8820	8.4115	-60.8855	10.20	-5.1200
MARCH 12 1981	117.0	7.8820	8.4115	-60.4740	15.00	-5.8250
MARCH 16 1981	123.0	7.8820	8.4115	-60.8340	24.00	-5.8850

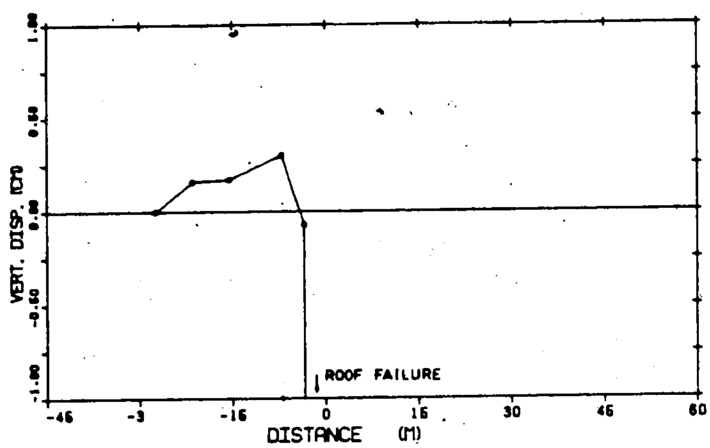

Figure B.32 ME17 MP#5 D=7.59m

BASIC DATA FOR COMPUTATION

```
            THE HOLE HAS BEEN READ ON     7 OCCASIONS
CALIBRATION READINGS WERE TAKEN ON      DECEMBER 22  1980
            THE DEEPEST READING IS     88.00 FEET
         THE SHALLOWEST READING IS    2.00 FEET
                  THE CLAMP RISES    3.00 FEET ABOVE GROUND

THE ANGLE BETWEEN THE "A" AXIS
AND THE AXIS OF PRINCIPAL
DEFORMATION IS     21.00 DEGREES
```

ALGEBRAIC DIFFERENCE IN CALIBRATION READINGS

	A DIRECTION			B DIRECTION		
DEPTH	A1	A2	DIFFERENCE IN A	B1	B2	DIFFERENCE IN B
-26.82	60	30	30	-110	62	-172
-26.21	-224	305	-529	-182	140	-322
-25.60	-462	526	-988	-238	180	-418
-24.99	-492	550	-1042	-592	448	-1040
-24.38	405	-296	701	-589	591	-1180
-23.77	570	-503	1073	-530	474	-1004
-23.16	510	-648	1158	-454	404	-858
-22.56	788	-700	1488	-375	326	-701
-21.95	790	-723	1513	-300	258	-558
-21.34	1004	-850	1854	-149	101	-250
-20.73	879	-809	1688	-148	109	-257
-20.12	767	-670	1437	-120	82	-202
-19.51	584	-519	1103	-100	78	-178
-18.90	532	-464	996	-30	-5	-25
-18.29	420	-348	768	-57	9	-66
-17.68	408	-341	749	-100	45	-145
-17.07	576	-516	1092	15	-79	94
-16.46	628	-559	1187	67	-134	201
-15.85	758	-710	1468	124	-107	231
-15.24	970	-908	1878	166	-210	376
-14.63	1045	-979	2024	246	-301	547
-14.02	990	-928	1918	340	-384	724
-13.41	888	-930	1818	394	-442	836
-12.80	1027	-860	1887	257	-298	555
-12.19	973	-899	1872	-32	-25	-7
-11.58	940	-876	1816	-70	23	-93
-10.97	980	-664	1644	1	-55	56
-10.36	909	-847	1756	97	-149	246
-9.75	904	-842	1746	66	-185	251
-9.14	795	-731	1526	7	-63	70
-8.53	590	-620	1210	-10	-36	26
-7.92	636	-574	1210	-88	35	-123
-7.32	558	-446	1004	3	-57	60
-6.71	508	-441	949	20	-62	82
-6.10	290	-193	483	-73	24	-97
-5.49	185	-124	309	-258	210	-468
-4.88	387	-216	603	-265	220	-485
-4.27	484	-402	886	-140	82	-222
-3.66	555	-488	1043	-81	40	-121
-3.05	375	-314	689	-340	274	-614
-2.44	164	-106	270	-588	523	-1111
-1.83	159	-98	257	-670	609	-1279
-1.22	177	-120	297	-733	680	-1413
-0.61	182	-105	287	-830	774	-1604

Figure B.33 SI6-FIELD DATA

ALGEBRAIC DIFFERENCE FOR SET 2 OBTAINED ON FEBRUARY 01 1981

DEFLECTION COMPONENTS RESOLVED INTO PREFERRED DEFORMATION DIRECTIONS

DEPTH	A1	A2	DIFFERENCE IN A (A DIRECTION)	B1	B2	DIFFERENCE IN B (B DIRECTION)	DEPTH IN MS	TRUE DEFLECTION OF A IN CMS	TRUE DEFLECTION OF B IN CMS
[illegible]	[illegible]	[illegible]	[illegible]	[illegible]	[illegible]	[illegible]	[illegible]	[illegible]	[illegible]

ALGEBRAIC DIFFERENCE FOR SET 3 OBTAINED ON FEBRUARY 08 1981

DEFLECTION COMPONENTS RESOLVED INTO PREFERRED DEFORMATION DIRECTIONS

DEPTH	A1	A2	DIFFERENCE IN A (A DIRECTION)	B1	B2	DIFFERENCE IN B (B DIRECTION)	DEPTH IN MS	TRUE DEFLECTION OF A IN CMS	TRUE DEFLECTION OF B IN CMS
[illegible]	[illegible]	[illegible]	[illegible]	[illegible]	[illegible]	[illegible]	[illegible]	[illegible]	[illegible]

Figure B.34 SI6-FIELD DATA

ALGEBRAIC DIFFERENCE FOR SET 4 OBTAINED ON FEBRUARY [illegible] 1981

DEPTH	A1	A2	DIFFERENCE IN A	B1	B2	DIFFERENCE IN B
	A DIRECTION			B DIRECTION		
[illegible]	[illegible]	[illegible]	[illegible]	[illegible]	[illegible]	[illegible]

DEFLECTION COMPONENTS RESOLVED INTO PREFERRED DEFORMATION DIRECTIONS

DEPTH IN MS.	TRUE DEFLECTION OF A IN CMS	TRUE DEFLECTION OF B IN CMS
[illegible]	[illegible]	[illegible]

ALGEBRAIC DIFFERENCE FOR SET 5 OBTAINED ON FEBRUARY [illegible] 1981

DEPTH	A1	A2	DIFFERENCE IN A	B1	B2	DIFFERENCE IN B
	A DIRECTION			B DIRECTION		
[illegible]	[illegible]	[illegible]	[illegible]	[illegible]	[illegible]	[illegible]

DEFLECTION COMPONENTS RESOLVED INTO PREFERRED DEFORMATION DIRECTIONS

DEPTH IN MS	TRUE DEFLECTION OF A IN CMS	TRUE DEFLECTION OF B IN CMS
[illegible]	[illegible]	[illegible]

Figure B.35 SI6-FIELD DATA

ALGEBRAIC DIFFERENCE FOR SET 6 OBTAINED ON FEBRUARY 11 1981

DEFLECTION COMPONENTS RESOLVED INTO PREFERRED DEFORMATION DIRECTIONS

		A DIRECTION			B DIRECTION				
DEPTH	A1	A2	DIFFERENCE IN A	B1	B2	DIFFERENCE IN B	DEPTH IN MS	TRUE DEFLECTION OF A IN CMS	TRUE DEFLECTION OF B IN CMS
-26.82	47	5	42	-140	62	-202	-26.82	1.8463E-02	-2.4670E-03
-26.21	-229	204	-433	-205	128	-333	-26.21	2.0605E-02	-2.2673E-02
-25.60	-460	517	-977	-253	180	-433	-25.60	5.2085E-02	-3.7631E-02
-24.99	-518	566	-1084	-406	437	-843	-24.99	-3.3435E-03	-6.6370E-02
-24.38	381	-339	720	-507	657	-1164	-24.38	-6.2205E-02	-8.8850E-02
-23.77	500	-507	1007	-533	466	-999	-23.77	-7.4290E-02	-5.0763E-02
-23.16	597	-546	1143	-458	397	-855	-23.16	-9.4374E-02	-6.3930E-02
-22.55	746	-701	1447	-383	327	-710	-22.55	-1.0623E-01	-1.0346E-01
-21.95	778	-730	1508	-311	241	-552	-21.95	-1.1952E-01	-1.0327E-01
-21.34	887	-952	1839	-188	66	-254	-21.34	-1.2073E-01	-1.1858E-01
-20.73	874	-979	1853	-164	110	-274	-20.73	-1.2202E-01	-1.3775E-01
-20.12	748	-700	1448	-134	89	-223	-20.12	-9.7366E-02	-1.6233E-01
-19.51	586	-530	1116	-120	60	-180	-19.51	-7.1015E-02	-1.7473E-01
-18.90	523	-475	998	-50	0	-50	-18.90	-5.3077E-02	-2.0605E-01
-18.29	415	-360	775	-70	12	-82	-18.29	-3.4882E-02	-2.3785E-01
-17.68	398	-350	748	-104	25	-129	-17.68	-4.4850E-02	-2.1386E-01
-17.07	556	-510	1066	8	-53	61	-17.07	-5.0520E-02	-2.2003E-01
-16.46	612	-563	1175	58	-129	187	-16.46	-5.5667E-02	-2.3874E-01
-15.85	752	-718	1470	97	-103	200	-15.85	-4.8510E-02	-2.6356E-01
-15.24	855	-801	1656	147	-221	368	-15.24	-5.6404E-02	-2.8006E-01
-14.63	1040	-982	2022	238	-299	537	-14.63	-6.6847E-02	-3.0434E-01
-14.02	983	-939	1922	333	-395	728	-14.02	-6.7481E-02	-3.1055E-01
-13.41	982	-840	1822	374	-437	811	-13.41	-3.4760E-02	-3.4240E-01
-12.80	1019	-867	1886	330	-304	634	-12.80	-2.4282E-02	-3.7775E-01
-12.19	861	-810	1671	-46	-25	-21	-12.19	-1.7710E-02	-3.5212E-01
-11.58	933	-884	1817	-26	11	-37	-11.58	-1.6856E-02	-3.9341E-01
-10.97	946	-881	1827	-8	-92	84	-10.97	-2.5820E-02	-4.0518E-01
-10.36	907	-857	1764	86	-151	237	-10.36	-5.1821E-02	-4.1023E-01
-9.75	898	-850	1748	91	-156	247	-9.75	-6.0032E-02	-4.1885E-01
-9.14	800	-757	1557	-3	-71	68	-9.14	6.0651E-02	-4.0408E-01
-8.53	685	-633	1318	-20	-43	23	-8.53	6.1067E-02	-3.8664E-01
-7.92	637	-687	1324	-94	29	-123	-7.92	7.0613E-02	-3.8672E-01
-7.32	552	-508	1060	0	-56	56	-7.32	8.1511E-02	-3.9067E-01
-6.71	504	-451	955	18	-63	81	-6.71	9.0653E-02	-3.8097E-01
-6.10	281	-218	499	-60	22	-82	-6.10	1.4050E-01	-3.4104E-01
-5.49	170	-130	300	-269	204	-473	-5.49	1.4720E-01	-3.4653E-01
-4.88	268	-216	484	-267	210	-477	-4.88	1.1570E-01	-3.6031E-01
-4.27	461	-409	870	-248	81	-329	-4.27	1.0562E-01	-3.6489E-01
-3.66	547	-491	1038	-80	37	-117	-3.66	8.2777E-02	-3.8707E-01
-3.05	385	-342	727	-347	278	-625	-3.05	1.5455E-01	-3.5560E-01
-2.44	155	-118	273	-296	821	-1117	-2.44	1.3290E-01	-3.6230E-01
-1.83	153	-105	258	-600	604	-1204	-1.83	1.0976E-01	-3.6555E-01
-1.22	172	-127	299	-740	868	-1608	-1.22	1.0576E-01	-3.5107E-01
-0.61	150	-100	250	-810	750	-1560	-0.61	1.2261E-01	-3.2164E-01

ALGEBRAIC DIFFERENCE FOR SET 7 OBTAINED ON FEBRUARY 26 1981

DEFLECTION COMPONENTS RESOLVED INTO PREFERRED DEFORMATION DIRECTIONS

		A DIRECTION			B DIRECTION				
DEPTH	A1	A2	DIFFERENCE IN A	B1	B2	DIFFERENCE IN B	DEPTH IN MS	TRUE DEFLECTION OF A IN CMS	TRUE DEFLECTION OF B IN CMS
-26.82	46	10	36	-150	61	-211	-26.82	1.8488E-02	-4.1007E-02
-26.21	-229	303	-532	-202	128	-330	-26.21	2.5745E-02	-3.4260E-02
-25.60	-460	516	-976	-261	147	-408	-25.60	3.7944E-02	-1.3070E-02
-24.99	-513	571	-1084	-493	426	-919	-24.99	-3.1095E-02	-8.3810E-03
-24.38	384	-326	710	-542	652	-1194	-24.38	-5.7263E-02	-5.2339E-02
-23.77	563	-505	1068	-540	473	-1013	-23.77	-8.0215E-02	-6.7808E-02
-23.16	602	-545	1147	-462	394	-856	-23.16	-1.1194E-01	-7.3024E-02
-22.55	748	-700	1448	-390	327	-717	-22.55	-1.1840E-01	-1.0180E-01
-21.95	781	-727	1508	-316	250	-566	-21.95	-1.0790E-01	-1.1578E-01
-21.34	880	-947	1827	-166	106	-272	-21.34	-1.3132E-01	-1.5055E-01
-20.73	677	-918	1595	-172	108	-280	-20.73	-1.0635E-01	-1.6610E-01
-20.12	747	-700	1447	-138	86	-224	-20.12	-8.1703E-02	-2.1352E-01
-19.51	587	-529	1116	-126	67	-193	-19.51	-5.3085E-02	-2.3159E-01
-18.90	525	-471	996	-58	2	-60	-18.90	-2.3103E-02	-2.5106E-01
-18.29	420	-356	776	-69	6	-75	-18.29	-1.3369E-02	-2.6852E-01
-17.68	404	-346	750	-113	39	-152	-17.68	-7.6758E-03	-2.8688E-01
-17.07	571	-519	1090	4	-85	89	-17.07	-7.0616E-03	-3.0707E-01
-16.46	620	-561	1181	54	-129	183	-16.46	-1.1330E-02	-3.2231E-01
-15.85	755	-715	1470	88	-156	244	-15.85	1.1118E-02	-3.7405E-01
-15.24	864	-802	1666	139	-203	342	-15.24	1.7146E-02	-4.3673E-01
-14.63	1047	-984	2031	226	-295	521	-14.63	4.1824E-02	-4.5052E-01
-14.02	992	-935	1927	374	-337	711	-14.02	5.7824E-02	-4.6593E-01
-13.41	988	-839	1827	375	-434	809	-13.41	6.8528E-02	-5.1006E-01
-12.80	1024	-867	1891	235	-398	633	-12.80	1.1728E-01	-5.4910E-01
-12.19	871	-810	1681	-66	-27	-39	-12.19	1.4761E-01	-5.6752E-01
-11.58	938	-884	1822	-83	32	-115	-11.58	1.5577E-01	-6.1005E-01
-10.97	946	-890	1836	-19	-52	33	-10.97	1.7038E-01	-6.5705E-01
-10.36	910	-853	1763	78	-145	223	-10.36	1.9233E-01	-6.6113E-01
-9.75	902	-849	1751	83	-151	234	-9.75	2.1006E-01	-7.0233E-01
-9.14	805	-753	1558	-8	-65	57	-9.14	2.6270E-01	-7.0252E-01
-8.53	684	-628	1312	-20	-23	3	-8.53	2.7581E-01	-7.2465E-01
-7.92	638	-581	1219	-102	25	-127	-7.92	2.8729E-01	-7.3653E-01
-7.32	566	-503	1069	-13	-40	27	-7.32	3.1743E-01	-7.6721E-01
-6.71	508	-448	956	10	-58	68	-6.71	3.3672E-01	-7.8362E-01
-6.10	277	-210	487	-76	20	-96	-6.10	3.4674E-01	-7.6514E-01
-5.49	170	-134	304	-254	206	-460	-5.49	3.7428E-01	-7.6036E-01
-4.88	272	-216	488	-276	217	-493	-4.88	3.5182E-01	-7.6033E-01
-4.27	453	-400	853	-147	81	-228	-4.27	3.8378E-01	-7.6085E-01
-3.66	560	-481	1041	-100	42	-142	-3.66	3.8648E-01	-8.3082E-01
-3.05	381	-330	711	-340	266	-606	-3.05	3.8476E-01	-8.1040E-01
-2.44	156	-107	263	-606	520	-1126	-2.44	3.8238E-01	-8.3558E-01
-1.83	164	-87	251	-483	819	-1302	-1.83	3.0287E-01	-8.5660E-01
-1.22	173	-130	303	-747	670	-1417	-1.22	3.0048E-01	-8.6072E-01
-0.61	160	-87	247	-802	722	-1524	-0.61	3.1573E-01	-7.6407E-01

Figure B.36 SI6-FIELD DATA

BASIC DATA FOR COMPUTATION

THE HOLE HAS BEEN READ ON 7 OCCASIONS
CALIBRATION READINGS WERE TAKEN ON DECEMBER 22 1988
THE DEEPEST READING IS 88.00 FEET
THE SHALLOWEST READING IS 2.00 FEET
THE CLAMP RISES 2.00 FEET ABOVE GROUND

THE ANGLE BETWEEN THE "A" AXIS
AND THE AXIS OF PRINCIPAL
DEFORMATION IS 3.15 DEGREES

ALGEBRAIC DIFFERENCE IN CALIBRATION READINGS

	A DIRECTION			B DIRECTION		
DEPTH	A1	A2	DIFFERENCE IN A	B1	B2	DIFFERENCE IN B
-26.82	882	-927	1809	-446	374	-820
-26.21	754	-705	1459	61	-123	184
-25.60	1106	-1053	2159	96	-167	263
-24.99	1308	-1282	2590	-85	44	-129
-24.38	677	-641	1318	-806	740	-1546
-23.77	494	-421	915	-1014	839	-1853
-23.16	527	-472	999	-1082	1034	-2116
-22.56	504	-446	950	-1149	1102	-2251
-21.95	446	-377	823	-1187	1135	-2322
-21.34	306	-346	652	-1218	1136	-2354
-20.73	233	-180	413	-1116	1048	-2164
-20.12	288	-223	511	-1060	978	-2038
-19.51	166	-109	275	-892	822	-1714
-18.90	265	-162	427	-850	781	-1631
-18.29	350	-300	650	-537	467	-1004
-17.68	413	-354	767	-427	370	-797
-17.07	437	-362	799	-344	282	-626
-16.46	404	-427	831	-223	138	-361
-15.85	270	-308	578	-67	5	-72
-15.24	329	-271	600	-59	15	-74
-14.63	348	-280	628	-60	10	-70
-14.02	366	-304	670	-4	-92	88
-13.41	410	-348	758	66	-125	191
-12.80	304	-232	536	-39	-22	-17
-12.19	148	-84	232	-258	180	-438
-11.58	215	-141	356	-300	236	-536
-10.97	287	-243	530	-321	288	-609
-10.36	334	-287	621	-493	366	-859
-9.75	425	-357	782	-533	469	-1002
-9.14	471	-414	885	-603	537	-1140
-8.53	565	-507	1072	-650	590	-1240
-7.92	590	-535	1125	-681	616	-1297
-7.32	478	-424	902	-807	730	-1537
-6.71	485	-422	907	-738	670	-1408
-6.10	316	-256	572	-680	606	-1286
-5.49	221	-155	376	-614	554	-1168
-4.88	159	-82	241	-543	480	-1023
-4.27	125	-67	192	-458	397	-855
-3.66	79	-5	84	-400	340	-740
-3.05	-62	118	-180	-393	328	-721
-2.44	-128	190	-318	-240	188	-428
-1.83	-115	170	-285	-312	277	-589
-1.22	-44	122	-166	-380	328	-708
-0.61	-89	148	-237	-426	373	-799

Figure B.37 SI7-FIELD DATA

ALGEBRAIC DIFFERENCE FOR SET 2 OBTAINED ON FEBRUARY 1 1981 — DEFLECTION COMPONENTS RESOLVED INTO PREFERRED DEFORMATION DIRECTIONS

	A DIRECTION			B DIRECTION					
DEPTH	A1	A2	DIFFERENCE IN A	B1	B2	DIFFERENCE IN B	DEPTH IN MS	TRUE DEFLECTION OF A IN CMS	TRUE DEFLECTION OF B IN CMS
-26.82	988	-934	1922	-451	373	-824	-26.82	2.01200E-02	-4.98708E-03
-26.21	762	-709	1472	90	-130	106	-26.21	2.38708E-03	1.35308E-02
-25.60	1130	-1046	2176	98	-174	272	-25.60	4.08838E-02	2.01808E-02
-24.99	1333	-1304	2637	-122	38	-160	-24.99	1.09838E-02	-3.11008E-02
-24.38	781	-567	1348	-709	325	-1034	-24.38	8.18278E-02	-9.03138E-02
-23.77	682	-639	1321	-1015	839	-1848	-23.77	7.01888E-02	6.48878E-04
-23.16	834	-470	1003	-1088	1015	-2103	-23.16	7.81838E-02	2.09888E-02
-22.56	582	-458	958	-1153	1089	-2242	-22.56	8.88858E-02	3.83208E-02
-21.95	460	-364	824	-1102	1130	-2323	-21.95	8.80878E-02	3.84218E-02
-21.34	318	-243	858	-1317	1138	-2383	-21.34	8.70478E-02	3.68728E-02
-20.73	327	-107	414	-1121	1046	-2167	-20.73	1.00348E-01	3.48788E-02
-20.12	382	-231	613	-1053	988	-2038	-20.12	1.03308E-01	3.67488E-02
-19.51	185	-118	303	-890	818	-1708	-19.51	1.18088E-01	4.48818E-02
-18.90	242	-188	428	-867	777	-1624	-18.90	1.18888E-01	5.52378E-02
-18.29	349	-304	853	-837	667	-1004	-18.29	1.30858E-01	5.56418E-02
-17.68	408	-357	765	-427	371	-798	-17.68	1.17588E-01	6.38808E-02
-17.07	422	-373	795	-348	270	-618	-17.07	1.24378E-01	7.10118E-02
-16.46	408	-448	833	-217	141	-356	-16.46	1.27088E-01	7.87488E-02
-15.85	370	-308	678	-87	6	-71	-15.85	1.21488E-01	7.90438E-02
-15.24	324	-276	600	-67	5	-72	-15.24	1.31288E-01	8.30888E-02
-14.63	340	-285	625	-88	0	-88	-14.63	1.30888E-01	8.80448E-02
-14.02	360	-313	673	-12	-71	59	-14.02	1.33048E-01	8.83138E-02
-13.41	408	-350	764	84	-122	108	-13.41	1.41348E-01	9.33288E-02
-12.80	282	-241	523	-40	-31	-17	-12.80	1.38748E-01	9.30758E-02
-12.19	162	-67	229	-284	161	-448	-12.19	1.31848E-01	7.78208E-02
-11.58	205	-151	356	-303	233	-528	-11.58	1.31868E-01	7.78208E-02
-10.97	208	-248	544	-341	288	-607	-10.97	1.38838E-01	8.77708E-02
-10.36	328	-287	823	-486	351	-887	-10.36	1.43708E-01	8.80238E-02
-9.75	418	-378	785	-623	402	-985	-9.75	1.37808E-01	7.83808E-02
-9.14	470	-422	892	-885	531	-1128	-9.14	1.47818E-01	1.01278E-01
-8.53	562	-511	1073	-888	580	-1335	-8.53	1.48118E-01	1.08878E-01
-7.92	588	-542	1138	-888	810	-1284	-7.92	1.58818E-01	1.14128E-01
-7.32	474	-428	903	-810	728	-1538	-7.32	1.58878E-01	1.11088E-01
-6.71	481	-429	810	-740	885	-1608	-6.71	1.53348E-01	1.11338E-01
-6.10	307	-288	585	-883	803	-1268	-6.10	1.58878E-01	1.22888E-01
-5.49	218	-153	378	-518	847	-1162	-5.49	1.58588E-01	1.21888E-01
-4.88	146	-98	245	-882	480	-1032	-4.88	1.53418E-01	1.08288E-01
-4.27	170	-75	185	-460	588	-858	-4.27	1.67888E-01	1.10078E-01
-3.66	68	-17	85	-403	384	-747	-3.66	1.68248E-01	1.13188E-01
-3.05	-88	98	-158	-388	237	-623	-3.05	1.58178E-01	8.88418E-02
-2.44	-130	183	-313	-380	175	-418	-2.44	2.01288E-01	1.13488E-01
-1.83	-121	166	-287	-218	243	-861	-1.83	1.87888E-01	1.20458E-01
-1.22	-68	113	-182	-381	212	-683	-1.22	2.07888E-01	1.48878E-01
-0.61	-88	108	-243	-430	288	-708	-0.61	1.93048E-01	1.51188E-01

ALGEBRAIC DIFFERENCE FOR SET 3 OBTAINED ON FEBRUARY 8 1981 — DEFLECTION COMPONENTS RESOLVED INTO PREFERRED DEFORMATION DIRECTIONS

	A DIRECTION			B DIRECTION					
DEPTH	A1	A2	DIFFERENCE IN A	B1	B2	DIFFERENCE IN B	DEPTH IN MS	TRUE DEFLECTION OF A IN CMS	TRUE DEFLECTION OF B IN CMS
-26.82	984	-940	1924	-442	385	-827	-26.82	2.36178E-02	-8.38348E-03
-26.21	766	-711	1477	85	-127	183	-26.21	2.48288E-02	4.08778E-03
-25.60	1092	-1030	2120	104	-171	275	-25.60	-2.40088E-02	2.00358E-02
-24.99	1388	-1313	2681	-87	18	-116	-24.99	6.84738E-03	4.18938E-02
-24.38	712	-667	1378	-88	723	-1634	-24.38	8.88548E-02	5.50058E-02
-23.77	882	-641	833	-1011	828	-1840	-23.77	1.28718E-01	7.28178E-02
-23.16	927	-476	1002	-1088	1033	-2127	-23.16	1.32308E-01	6.38258E-02
-22.56	808	-457	958	-1188	1108	-2289	-22.56	1.58408E-01	8.88078E-02
-21.95	448	-383	831	-1198	1128	-2324	-21.95	1.88148E-01	5.08538E-02
-21.34	328	-288	678	-1214	1161	-2388	-21.34	2.07708E-01	5.12308E-02
-20.73	338	-181	428	-1118	1081	-2188	-20.73	2.38928E-01	4.48058E-02
-20.12	293	-233	528	1088	988	-2048	-20.12	2.53188E-01	3.08858E-02
-19.51	170	-118	288	-885	821	-1718	-19.51	2.73148E-01	2.80128E-02
-18.90	248	-187	438	-884	770	-1633	-18.90	2.88488E-01	2.60458E-02
-18.29	342	-287	638	-842	472	-1014	-18.29	2.88888E-01	1.02058E-02
-17.68	411	-357	768	-428	378	-802	-17.68	2.71138E-01	2.87608E-03
-17.07	422	-288	787	-329	278	-617	-17.07	[illegible]	1.82188E-03
-16.46	487	-448	943	-218	137	-347	-16.46	[illegible]	2.88248E-02
-15.85	386	-287	678	-68	3	-71	-15.85	2.81808E-01	4.18938E-02
-15.24	321	-278	601	-63	14	-77	-15.24	2.83378E-01	3.71128E-02
-14.63	342	-288	637	-63	4	-68	-14.63	2.84588E-01	4.32838E-02
-14.02	380	-302	682	3	-84	88	-14.02	2.73848E-01	3.88848E-02
-13.41	410	-284	784	68	-133	198	-13.41	2.81088E-01	8.07338E-02
-12.80	304	-342	647	-35	-29	-6	-12.80	2.88088E-01	8.43018E-02
-12.19	180	-48	235	-268	188	-443	-12.19	3.08818E-01	8.32488E-02
-11.58	203	-141	344	-301	223	-524	-11.58	2.88378E-01	8.78448E-02
-10.97	287	-242	530	-238	267	-505	-10.97	2.85788E-01	6.08248E-02
-10.36	327	-283	670	-483	300	-883	-10.36	2.85788E-01	8.68088E-02
-9.75	420	-368	788	-834	402	-887	-9.75	2.77108E-01	8.57708E-02
-9.14	474	-421	885	-802	533	-1138	-9.14	2.81008E-01	7.42348E-02
-8.53	563	-601	1063	-664	582	-1248	-8.53	2.78000E-01	8.43338E-02
-7.92	583	-543	1138	-887	818	-1288	-7.92	2.83838E-01	8.67008E-02
-7.32	488	-438	920	-804	728	-1530	-7.32	3.10218E-01	7.87088E-02
-6.71	487	-428	915	-738	687	-1408	-6.71	3.21138E-01	8.60308E-02
-6.10	325	-282	607	-678	808	-1284	-6.10	3.84338E-01	8.00338E-02
-5.49	228	-188	407	-618	550	-1164	-5.49	4.08238E-01	8.74718E-02
-4.88	180	-88	248	-564	488	-1032	-4.88	4.21188E-01	8.44838E-02
-4.27	128	-76	204	-480	402	-882	-4.27	4.38838E-01	7.83388E-02
-3.66	72	-14	88	-397	347	-744	-3.66	4.42888E-01	8.41188E-02
-3.05	-43	104	-147	-303	321	-624	-3.05	4.74288E-01	8.14108E-02
-2.44	-128	187	-315	-238	186	-423	-2.44	4.78828E-01	8.88758E-02
-1.83	-119	171	-290	-313	288	-604	-1.83	4.88338E-01	8.70748E-02
-1.22	-66	115	-181	-386	324	-710	-1.22	4.78288E-01	8.14108E-02
-0.61	-88	180	-268	-428	383	-811	-0.61	4.82808E-01	8.23898E-02

Figure B.38 SI7-FIELD DATA

ALGEBRAIC DIFFERENCE FOR SET 4 OBTAINED ON FEBRUARY 10 1981

DEFLECTION COMPONENTS RESOLVED INTO PREFERRED DEFORMATION DIRECTIONS

	A DIRECTION			B DIRECTION					
DEPTH	A1	A2	DIFFERENCE IN A	B1	B2	DIFFERENCE IN B	DEPTH IN MS	TRUE DEFLECTION OF A IN CMS	TRUE DEFLECTION OF B IN CMS
-26.82	877	-926	1801	-412	300	-708	-26.82	[illegible]	[illegible]
-26.21	700	-704	1404	85	-127	212	-26.21	[illegible]	[illegible]
-25.60	1115	-1071	2186	109	-168	276	-25.60	[illegible]	[illegible]
-24.99	1250	-1207	2658	-50	46	-104	-24.99	[illegible]	[illegible]
-24.38	695	-646	1380	-600	742	-1342	-24.38	[illegible]	[illegible]
-23.77	467	-421	818	-1005	841	-1846	-23.77	[illegible]	[illegible]
-23.16	530	-477	1007	-1077	1036	-2111	-23.16	[illegible]	[illegible]
-22.55	504	-455	861	-1140	1104	-2249	-22.55	[illegible]	[illegible]
-21.95	449	-364	833	-1181	1161	-2332	-21.95	[illegible]	[illegible]
-21.34	313	-356	669	-1213	1163	-2356	-21.34	[illegible]	[illegible]
-20.73	231	-164	415	-1110	1064	-2109	-20.73	[illegible]	[illegible]
-20.12	200	-231	421	-1081	802	-2033	-20.12	[illegible]	[illegible]
-19.51	105	-117	222	-860	851	-1713	-19.51	[illegible]	[illegible]
-18.90	245	-100	434	-865	779	-1624	-18.90	[illegible]	[illegible]
-18.29	350	-209	642	-834	677	-1011	-18.29	[illegible]	[illegible]
-17.68	400	-253	762	-419	377	-796	-17.68	[illegible]	[illegible]
-17.07	430	-307	767	-332	304	-616	-17.07	[illegible]	[illegible]
-16.46	493	-644	837	-307	144	-381	-16.46	[illegible]	[illegible]
-15.85	300	-306	678	-88	13	-78	-15.85	[illegible]	[illegible]
-15.24	337	-371	598	-63	21	-74	-15.24	[illegible]	[illegible]
-14.63	343	-364	577	-60	14	-60	-14.63	[illegible]	[illegible]
-14.02	356	-300	606	3	-84	81	-14.02	[illegible]	[illegible]
-13.41	410	-353	763	76	-126	200	-13.41	[illegible]	[illegible]
-12.80	307	-236	533	-37	-22	-15	-12.80	[illegible]	[illegible]
-12.19	150	-46	236	-247	100	-437	-12.19	[illegible]	[illegible]
-11.58	200	-143	357	-301	230	-530	-11.58	[illegible]	[illegible]
-10.97	300	-243	543	-320	277	-602	-10.97	[illegible]	[illegible]
-10.36	330	-261	590	-483	302	-605	-10.36	[illegible]	[illegible]
-9.75	433	-356	787	-523	466	-991	-9.75	[illegible]	[illegible]
-9.14	473	-410	888	-601	645	-1136	-9.14	[illegible]	[illegible]
-8.53	566	-507	1073	-842	805	-1242	-8.53	[illegible]	[illegible]
-7.92	503	-536	1133	-875	824	-1299	-7.92	[illegible]	[illegible]
-7.32	466	-430	916	-801	730	-1531	-7.32	[illegible]	[illegible]
-6.71	465	-430	911	-730	676	-1412	-6.71	[illegible]	[illegible]
-6.10	317	-370	687	-673	610	-1203	-6.10	[illegible]	[illegible]
-5.49	230	-105	351	-612	556	-1166	-5.49	[illegible]	[illegible]
-4.88	153	-100	253	-641	601	-1022	-4.88	[illegible]	[illegible]
-4.27	127	-74	201	-485	404	-601	-4.27	[illegible]	[illegible]
-3.66	73	-14	87	-301	304	-747	-3.66	[illegible]	[illegible]
-3.05	-48	103	-137	-303	326	-626	-3.05	[illegible]	[illegible]
-2.44	-125	188	-316	-330	100	-436	-2.44	[illegible]	[illegible]
-1.83	-116	173	-282	-305	256	-562	-1.83	[illegible]	[illegible]
-1.22	-68	120	-188	-300	325	-507	-1.22	[illegible]	[illegible]
-0.61	-108	157	-265	-628	298	-626	-0.61	[illegible]	[illegible]

ALGEBRAIC DIFFERENCE FOR SET 5 OBTAINED ON FEBRUARY 11 1981

DEFLECTION COMPONENTS RESOLVED INTO PREFERRED DEFORMATION DIRECTIONS

	A DIRECTION			B DIRECTION					
DEPTH	A1	A2	DIFFERENCE IN A	B1	B2	DIFFERENCE IN B	DEPTH IN MS	TRUE DEFLECTION OF A IN CMS	TRUE DEFLECTION OF B IN CMS
-26.82	874	-936	1806	-418	308	-721	-26.82	[illegible]	[illegible]
-26.21	783	-700	1472	75	-131	208	-26.21	[illegible]	[illegible]
-25.60	1127	-1068	2171	103	-167	270	-25.60	[illegible]	[illegible]
-24.99	1359	-1206	2557	-103	62	-165	-24.99	[illegible]	[illegible]
-24.38	893	-683	1540	-814	752	-1566	-24.38	[illegible]	[illegible]
-23.77	485	-440	926	-1010	843	-1853	-23.77	[illegible]	[illegible]
-23.16	537	-474	1001	-1001	1023	-2114	-23.16	[illegible]	[illegible]
-22.55	603	-452	955	-1148	1101	-2249	-22.55	[illegible]	[illegible]
-21.95	444	-383	827	-1184	1128	-2316	-21.95	[illegible]	[illegible]
-21.34	312	-258	571	-1212	1148	-2358	-21.34	[illegible]	[illegible]
-20.73	234	-190	424	-1113	1040	-2152	-20.73	[illegible]	[illegible]
-20.12	200	-231	521	-1052	866	-2036	-20.12	[illegible]	[illegible]
-19.51	148	-118	304	-890	820	-1710	-19.51	[illegible]	[illegible]
-18.90	248	-190	438	-867	770	-1626	-18.90	[illegible]	[illegible]
-18.29	348	-301	647	-632	670	-1002	-18.29	[illegible]	[illegible]
-17.68	408	-356	765	-418	272	-701	-17.68	[illegible]	[illegible]
-17.07	422	-359	781	-232	278	-510	-17.07	[illegible]	[illegible]
-16.46	466	-444	920	-208	143	-349	-16.46	[illegible]	[illegible]
-15.85	306	-310	678	-87	-11	-66	-15.85	[illegible]	[illegible]
-15.24	325	-277	602	-62	16	-89	-15.24	[illegible]	[illegible]
-14.63	341	-286	627	-61	11	-73	-14.63	[illegible]	[illegible]
-14.02	300	-309	608	6	-80	81	-14.02	[illegible]	[illegible]
-13.41	405	-356	761	71	-125	196	-13.41	[illegible]	[illegible]
-12.80	359	-365	644	-66	-22	-33	-12.80	[illegible]	[illegible]
-12.19	145	-80	225	-288	106	-400	-12.19	[illegible]	[illegible]
-11.58	202	-143	346	-301	230	-530	-11.58	[illegible]	[illegible]
-10.97	293	-244	537	-321	274	-595	-10.97	[illegible]	[illegible]
-10.36	325	-285	620	-450	301	-650	-10.36	[illegible]	[illegible]
-9.75	423	-258	702	-525	404	-930	-9.75	[illegible]	[illegible]
-9.14	470	-418	888	-603	548	-1146	-9.14	[illegible]	[illegible]
-8.53	581	-506	1057	-648	552	-1241	-8.53	[illegible]	[illegible]
-7.92	502	-546	1137	-688	516	-1200	-7.92	[illegible]	[illegible]
-7.32	485	-436	921	-806	724	-1530	-7.32	[illegible]	[illegible]
-6.71	402	-430	812	-720	872	-1611	-6.71	[illegible]	[illegible]
-6.10	318	-277	595	-675	612	-1287	-6.10	[illegible]	[illegible]
-5.49	230	-169	391	-610	580	-1164	-5.49	[illegible]	[illegible]
-4.88	150	-103	253	-530	480	-1026	-4.88	[illegible]	[illegible]
-4.27	125	-61	206	-461	305	-846	-4.27	[illegible]	[illegible]
-3.66	73	-17	85	-302	380	-742	-3.66	[illegible]	[illegible]
-3.05	-61	106	-168	-300	227	-612	-3.05	[illegible]	[illegible]
-2.44	-128	108	-316	-226	102	-410	-2.44	[illegible]	[illegible]
-1.83	-122	171	-293	-304	352	-657	-1.83	[illegible]	[illegible]
-1.22	-68	118	-187	-353	320	-663	-1.22	[illegible]	[illegible]
-0.61	-111	161	-272	-415	378	-700	-0.61	[illegible]	[illegible]

Figure B.39 SI7-FIELD DATA

ALGEBRAIC DIFFERENCE FOR SET 6 OBTAINED ON FEBRUARY 17 1981

DEFLECTION COMPONENTS RESOLVED INTO PREFERRED DEFORMATION DIRECTIONS

	A DIRECTION			B DIRECTION					
DEPTH	A1	A2	DIFFERENCE IN A	B1	B2	DIFFERENCE IN B	DEPTH IN MS	TRUE DEFLECTION OF A IN CMS	TRUE DEFLECTION OF B IN CMS
[illegible]	[illegible]	[illegible]	[illegible]	[illegible]	[illegible]	[illegible]	[illegible]	[illegible]	[illegible]

ALGEBRAIC DIFFERENCE FOR SET 7 OBTAINED ON FEBRUARY 17

DEFLECTION COMPONENTS RESOLVED INTO PREFERRED DEFORMATION DIRECTIONS

	A DIRECTION			B DIRECTION					
DEPTH	A1	A2	DIFFERENCE IN A	B1	B2	DIFFERENCE IN B	DEPTH IN MS	TRUE DEFLECTION OF A IN CMS	TRUE DEFLECTION OF B IN CMS
[illegible]	[illegible]	[illegible]	[illegible]	[illegible]	[illegible]	[illegible]	[illegible]	[illegible]	[illegible]

Figure B.40 SI7-FIELD DATA

```
****************************************************************************

    BASIC DATA FOR COMPUTATION

          THE HOLE HAS BEEN READ ON     5 OCCASIONS
CALIBRATION READINGS WERE TAKEN ON      DECEMBER 22  1988
             THE DEEPEST READING IS     88.00 FEET
          THE SHALLOWEST READING IS    2.00 FEET
                    THE CLAMP RISES   3.00 FEET ABOVE GROUND

          THE ANGLE BETWEEN THE "A" AXIS
          AND THE AXIS OF PRINCIPAL
          DEFORMATION IS       2.32 DEGREES

****************************************************************************
```

ALGEBRAIC DIFFERENCE IN CALIBRATION READINGS

DEPTH	A1	A2	DIFFERENCE IN A	B1	B2	DIFFERENCE IN B
	A DIRECTION			B DIRECTION		
-26.82	325	-548	873	-127	53	-180
-26.21	220	-170	390	-551	465	-1016
-25.60	263	-299	562	-620	605	-1225
-24.99	366	-334	700	-478	413	-891
-24.38	582	-430	1012	-145	58	-203
-23.77	688	-822	1510	-218	136	-354
-23.16	672	-830	1502	-180	130	-310
-22.55	676	-920	1596	-161	81	-242
-21.95	959	-901	1860	-224	180	-404
-21.34	1184	-1077	2261	-348	268	-616
-20.73	1275	-1231	2506	-297	227	-524
-20.12	1073	-1021	2094	-313	249	-562
-19.51	1013	-950	1963	-272	198	-470
-18.90	885	-822	1707	-174	92	-266
-18.29	900	-843	1743	322	-404	726
-17.68	1370	-1330	2700	663	-760	1423
-17.07	1280	-1021	2301	324	-410	734
-16.46	1329	-1285	2614	-13	-72	59
-15.85	1301	-1227	2528	36	-80	116
-15.24	1064	-1024	2088	-117	36	-153
-14.63	880	-823	1703	-256	187	-443
-14.02	827	-768	1595	-295	230	-525
-13.41	807	-747	1554	-356	290	-646
-12.80	803	-747	1550	-475	406	-881
-12.19	654	-589	1243	-509	451	-960
-11.58	565	-502	1067	-349	269	-618
-10.97	540	-480	1020	-223	100	-323
-10.36	627	-556	1183	-398	318	-716
-9.75	636	-573	1209	-483	360	-843
-9.14	540	-474	1014	-416	332	-748
-8.53	594	-537	1131	-407	334	-741
-7.92	532	-574	1106	-474	396	-870
-7.32	580	-523	1103	-431	287	-718
-6.71	526	-575	1101	-318	306	-624
-6.10	562	-482	1044	-127	53	-180
-5.49	533	-478	1011	-33	-43	10
-4.88	446	-380	826	18	-87	105
-4.27	335	-270	605	65	-135	200
-3.66	287	-236	523	103	-167	270
-3.05	300	-239	539	114	-190	304
-2.44	273	-215	488	93	-188	281
-1.83	330	-171	501	145	-218	363
-1.22	202	-144	346	169	-244	413
-0.61	84	-34	118	206	-280	486

Figure B.41 SI12-FIELD DATA

ALGEBRAIC DIFFERENCE FOR SET [illegible] OBTAINED ON FEBRUARY [illegible] [illegible]

DEPTH	A1	A2	DIFFERENCE IN A	B1	B2	DIFFERENCE IN B	DEPTH IN MS	TRUE DEFLECTION OF A IN CMS	TRUE DEFLECTION OF B IN CMS
	A DIRECTION			B DIRECTION			DEFLECTION COMPONENTS RESOLVED INTO PREFERRED DEFORMATION DIRECTIONS		
[illegible]	[illegible]	[illegible]	[illegible]	[illegible]	[illegible]	[illegible]	[illegible]	[illegible]	[illegible]

ALGEBRAIC DIFFERENCE FOR SET [illegible] OBTAINED ON FEBRUARY [illegible] [illegible]

DEPTH	A1	A2	DIFFERENCE IN A	B1	B2	DIFFERENCE IN B	DEPTH IN MS	TRUE DEFLECTION OF A IN CMS	TRUE DEFLECTION OF B IN CMS
	A DIRECTION			B DIRECTION			DEFLECTION COMPONENTS RESOLVED INTO PREFERRED DEFORMATION DIRECTIONS		
[illegible]	[illegible]	[illegible]	[illegible]	[illegible]	[illegible]	[illegible]	[illegible]	[illegible]	[illegible]

Figure B.42 SI.12-FIELD DATA

ALGEBRAIC DIFFERENCES FOR SET A OBTAINED ON FEBRUARY 06 1981

DEPTH	A DIRECTION A1	A2	DIFFERENCE IN A	B DIRECTION B1	B2	DIFFERENCE IN B
[illegible]	[illegible]	[illegible]	[illegible]	[illegible]	[illegible]	[illegible]

DEFLECTION COMPONENTS RESOLVED INTO PREFERRED DEFORMATION DIRECTIONS

DEPTH IN MS	TRUE DEFLECTION OF A IN CMS	TRUE DEFLECTION OF B IN CMS
[illegible]	[illegible]	[illegible]

ALGEBRAIC DIFFERENCES FOR SET B OBTAINED ON FEBRUARY 06 1981

DEPTH	A DIRECTION A1	A2	DIFFERENCE IN A	B DIRECTION B1	B2	DIFFERENCE IN B
[illegible]	[illegible]	[illegible]	[illegible]	[illegible]	[illegible]	[illegible]

DEFLECTION COMPONENTS RESOLVED INTO PREFERRED DEFORMATION DIRECTIONS

DEPTH IN MS	TRUE DEFLECTION OF A IN CMS	TRUE DEFLECTION OF B IN CMS
[illegible]	[illegible]	[illegible]

Figure B.43 SI12-FIELD DATA

ALGEBRAIC DIFFERENCE FOR SET 6 OBTAINED ON FEBRUARY 10 1981

DEFLECTION COMPONENTS RESOLVED INTO PREFERRED DEFORMATION DIRECTIONS

	A DIRECTION			B DIRECTION					
DEPTH	A1	A2	DIFFERENCE IN A	B1	B2	DIFFERENCE IN B	DEPTH IN MS.	TRUE DEFLECTION OF A IN CMS	TRUE DEFLECTION OF B IN CMS
[illegible]	[illegible]	[illegible]	[illegible]	[illegible]	[illegible]	[illegible]	[illegible]	[illegible]	[illegible]

Figure B.44 SI12-FIELD DATA

C. APPENDIX - LINING INSTRUMENTS - FIELD DATA

LOAD CELL #5

LOAD(N)	Δε (1)	Δε (2)	Δε (3)
0	0	0	0
100,000	145	257	202
200,000	273	404	379
300,000	423	546	537
400,000	583	709	710
500,000	750	870	881
600,000	928	1043	202
700,000	1113	1214	1219
600,000	932	1031	1039
500,000	754	850	858
400,000	580	667	680
300,000	409	492	500
200,000	249	325	325
100,000	120	187	171
0	0	0	0

LOAD CELL #3

LOAD(N)	Δε (1)	Δε (2)	Δε (3)
0	0	0	0
100,000	200	256	237
200,000	364	414	413
300,000	518	563	578
400,000	673	722	748
500,000	822	885	912
600,000	974	1052	1073
700,000	1118	1212	1198
600,000	956	1045	1066
500,000	798	877	902
400,000	638	708	734
300,000	483	535	566
200,000	431	386	401
100,000	179	226	231
0	4	-6	12

$\Delta\varepsilon$ is the sum of channels A and B.

TABLE C1 - LOAD CELLS #3 AND #5 - CALIBRATION

LOAD CELL #1

LOAD(N)	(1)	(2)	(3)
	ΔƐ		
0	0	0	0
100,000	185	209	232
200,000	335	364	406
300,000	447	522	571
400,000	620	686	733
500,000	768	849	887
600,000	918	997	1029
700,000	1074	1156	1147
600,000	919	1990	1020
500,000	762	829	858
400,000	607	660	706
300,000	453	505	540
200,000	305	336	369
100,000	163	176	200
0	8	0	11

LOAD CELL #4

		ΔƐ	
0	0	0	0
100,000	115	161	158
200,000	250	299	330
300,000	401	458	504
400,000	563	622	681
500,000	735	797	846
600,000	907	970	1016
700,000	1083	1140	1152
600,000	906	963	1008
500,000	737	782	833
400,000	564	607	652
300,000	400	424	476
200,000	250	265	300
100,000	113	130	140
0	5	0	7

$\Delta\varepsilon$ is the sum of channels A and B..

TABLE C2 - LOAD CELLS #1 AND #4 - CALIBRATION

LOAD CELL #2

LOAD(N)	$\Delta\varepsilon$ (1)	(2)	(3)
0	0	0	0
100,000	202	246	240
200,000	356	369	407
300,000	506	500	576
400,000	668	646	748
500,000	824	812	924
600,000	981	979	1097
700,000	1142	1149	1227
600,000	978	971	1087
500,000	811	794	904
400,000	645	619	725
300,000	477	451	541
200,000	314	295	364
100,000	153	164	188
0	-1	0	-1

LOAD CELL #7

	$\Delta\varepsilon$		
0	0	0	0
100,000	156	170	191
200,000	301	283	367
300,000	460	423	537
400,000	613	574	705
500,000	781	738	872
600,000	891	908	1036
700,000	1107	1082	1169
600,000	942	909	1016
500,000	770	734	848
400,000	599	565	671
300,000	439	398	500
200,000	274	244	326
100,000	120	115	155
0	5	9	2

$\Delta\varepsilon$ is the sum of channels A and B.

TABLE C3 - LOAD CELLS #2 AND #7 - CALIBRATION

LOAD CELL #6

LOAD(N)	$\Delta\varepsilon$ (1)	$\Delta\varepsilon$ (2)	$\Delta\varepsilon$ (3)
0	0	0	0
100,000	198	229	236
200,000	350	372	424
300,000	496	534	592
400,000	654	712	764
500,000	814	890	938
600,000	980	1070	1102
700,000	1152	1259	1229
600,000	979	1078	1085
500,000	806	885	911
400,000	635	700	728
300,000	338	505	546
200,000	306	322	357
100,000	163	188	176
0	-2	-3	0

LOAD CELL #8

	$\Delta\varepsilon$		
0	0	0	0
100,000	208	245	253
200,000	334	364	384
300,000	448	481	508
400,000	567	617	641
500,000	688	775	779
600,000	810	935	915
700,000	936	1097	1017
600,000	803	925	899
500,000	672	750	746
400,000	522	583	592
300,000	394	421	438
200,000	266	274	302
100,000	152	158	165
0	-3	3	0

$\Delta\varepsilon$ is the sum of channels A and B.

TABLE C4 - LOAD CELLS #6 AND #8 - CALIBRATION

Load cell no.	Relationship	Coefficient of Determination (r^2)
1	$y=0.6236\,x - 17.8698$	.9874
2	$y=0.6039\,x - 17.3285$	.9882
3	$y=0.6013\,x - 24.0932$	.9901
4	$y=0.6091\,x + 15.0796$	.9897
5	$y=0.5922\,x - 1.3322$	.9812
6	$y=0.5804\,x - 12.7504$	.9889
7	$y=0.6225\,x - 3.3985$	.9853
8	$y=0.7053\,x - 32.1037$	.9793

where y = normal load (kN)
x = sum of micro-strains read in both strain gauges (x = AVERAGE STRAIN$\times 10^{-6} \times 2$)

TABLE C5 - EQUATIONS RELATING LOADS TO MICROSTRAIN FOR THE LOAD CELLS 1 TO 8.

ZERO READINGS:	A	B	
	-385	-293*	* tunnel
	-362	-269	
	-366	-268	
	-366	-268	

DATE (81)	TIME	DIST.F/ TAIL(m)	A	B	△A-B (zero read/ tunnel)	LOAD KN
17-02	15:00	2.2	-740	-249	-358	210
18-02	07:00	2.2	-720	-262	-351	205
18-02	11:15	4.2	----	-291	----	---
18-02	13:40	6.4	-577	-302	-248	140
19-02	14:30	6.4	-616	-295	-280	160
20-02	08:58	6.4	-632	-284	-285	160
23-02	14:05	8.4	-655	-282	-306	175
24-02	09:20	10.0	-663	-276	-308	177
25-02	14:20	16.0	-678	-269	-316	180
26-02	11:45	18.4	-685	-270	-324	187
03-03	14:25	38.8	-694	-278	-294	170
10-03	11:16	65.2	-706	-274	-302	172
17-03	11:00	88.0	-719	-273	-314	180
19-03	18:00	88.0	-717	-274	-313	179
09-04	13:30	88.0	-755	-256	-333	192
27-05	15:05	88.0	-785	-248	-355	205

TABLE C6 - LOAD CELL #1 - FIELD DATA

ZERO READINGS:	A	B	
	-691	-1015	
	----	-1016	
	----	-1026*	* tunnel
	-692	-1016	

DATE (81)	TIME	DIST. TAIL(m)	A	B	△ A+B (zero read/ lab)	LOAD kN
17-02	13:40	0.4	-850	-1137	-270	145
17-02	15:00	2.2	-861	-1083	-227	120
18-02	07:00	2.2	-878	-1093	-254	135
18-02	11:15	4.2	-883	-1065	-231	120
18-02	13:40	6.4	-834	-1080	-197	105
19-02	14:30	6.4	-868	-1098	-249	135
20-02	08:58	6.4	-888	-1097	-268	145
23-02	14:05	8.4	-897	-1095	-275	150
24-02	09:20	10.0	-933	-1097	-313	170
25-02	14:20	16.0	-911	-1114	-308	160
26-02	11:45	18.4	-937	-1115	-346	190
03-03	14:25	38.8	-931	-1123	-348	195
10-03	11:16	65.2	-923	-1136	-353	200
17-03	11:00	88.0	-926	-1145	-365	205
19-03	18:00	88.0	-922	-1147	-363	204
09-04	13:30	88.0	-953	-1142	-389	217
27-05	15:05	88.0	-981	-1141	-416	233

TABLE C7 - LOAD CELL #2 - FIELD DATA

ZERO READINGS:

A	B	
+68*	-636*	* tunnel
+87	-611	
+89	-619	
+82	-624	

DATE (81)	TIME	DIST.F/ TAIL(m)	A	B	△ A+B (zero read/ tunnel)	LOAD kN
18-02	07:0[illegible]	[illegible]	----	-659	----	---
18-02	[illegible]	[illegible]	-354	-672	-458	255
18-02	[illegible]	[illegible].2	-345	-679	-456	255
19-02	14:3[illegible]	5.2	-347	-698	-477	265
20-02	08:58	5.2	-352	-700	-484	267
23-02	14:05	7.2	-377	-710	-519	287
24-02	09:20	8.8	-354	-716	-502	275
25-02	14:20	14.8	-380	-721	-533	297
26-02	11:45	17.2	-390	-717	-539	300
03-03	14:25	37.6	-395	-723	-550	305
10-03	11:16	64.0	-395	-729	-556	310
17-03	11:00	86.8	-401	-734	-567	317
19-03	18:00	86.8	-397	-736	-565	315
09-04	13:30	86.8	-427	-723	-582	326
27-05	15:05	86.8	-452	-720	-604	336

TABLE C8 - LOAD CELL #3 - FIELD DATA

ZERO READINGS:	A	B	
	-228*	-343*	* tunnel
	-207	-323	
	-208	-326	

DATE (81)	TIME	DIST TAIL(m)	A	B	△ A+B (z. r. tunnel)	LOAD kN
18-02	07:40	1.3	-456	-376	-261	173
18-02	13:38	5.2	-488	-360	-277	185
19-02	14:30	5.2	-505	-366	-300	197
20-02	08:58	5.2	-513	-358	-300	197
23-02	14:30	7.2	-539	-365	-333	217
24-02	09:30	8.8	-543	-362	-334	217
25-02	14:20	14.8	-548	-370	-347	224
26-02	11:45	17.2	-562	-365	-356	230
03-03	14:25	37.6	-572	-370	-371	240
10-03	11:16	64.0	-574	-372	-375	243
17-03	11:00	86.8	-582	-375	-386	250
19-03	18:00	86.8	-580	-378	-387	251
09-04	13:30	86.8	-604	-377	-410	264
27-05	15:05	86.8	-624	-383	-436	277

TABLE C9 - LOAD CELL #4 - FIELD DATA

ZERO READINGS:	A	B	
	-96*	-315*	* tunnel
	-87	-300	
	-84	-300	
	-89	-307	

DATE (81)	TIME	DIST TAIL(m)	A	B	△ A+B (z. r. tunnel)	LOAD kN
18-02	07:40	1.6	-320	-324	-233	135
18-02	13:33	4.0	-322	-312	-223	130
19-02	14:30	4.0	-348	-333	-270	157
20-02	08:58	4.0	-366	-318	-273	160
23-02	14:05	6.0	-387	-331	-307	180
24-02	09:30	7.6	-383	-333	-305	180
25-02	14:20	13.6	-405	-333	-327	190
26-02	1[illegible]:45	16.0	-428	-322	-339	200
03-03	14:25	36.4	-440	-331	-360	210
10-03	11:26	62.8	-449	-334	-372	215
17-03	11:00	85.6	-460	-338	-387	230
19-03	18:00	85.6	-456	-340	-385	220
09-04	13:30	85.6	-495	-328	-412	240
27-05	15:05	85.6	-520	-333	-442	258

TABLE C10 - LOAD CELL #5 - FIELD DATA

ZERO READINGS:	A	B	
	-422*	+115*	* tunnel
	-403	+141	
	-400	+141	
	-415	+131	

DATE (81)	TIME	DIST TAIL(m)	A	B	Δ A+B (z. r. tunnel)	LOAD kN
18-02	09:53	1.6	-578	+ 59	-212	110
18-02	13:33	4.0	-613	+ 81	-225	120
19-02	14:30	4.0	-630	+ 69	-254	137
20-02	08:58	4.0	-560	+ 49	-204	107
23-02	14:30	6.0	-589	+ 67	-215	114
24-02	09:30	7.6	-645	+102	-236	125
25-02	14:20	13.6	-645	+ 94	-244	130
26-02	11:45	16.0	-650	+ 91	-252	135
03-03	14:25	36.4	-657	+ 81	-269	145
10-03	11:16	62.8	-660	+ 80	-273	147
17-03	11:00	85.6	-672	+ 79	2864	155
19-03	18:00	85.6	-668	+ 77	-284	154
09-04	13:30	85.6	-685	+ 87	-291	158
27-05	15:05	85.6	-704	+ 86	-311	170

TABLE C11 - LOAD CELL #6 - FIELD DATA

ZERO READINGS:

A	B
+314*	-316*
+386	-306
+380	-309
+372	-316
+378	-308

* tunnel

DATE (84)	TIME	DIST TAIL(m)	A	B	△ A+B (z. r. tunnel)	LOAD kN
18-02	11:06	1.6	+154	-313	-195	125
18-02	13:33	2.8	+313	-371	-58	40
19-02	14:30	2.8	+296	-383	-85	57
20-02	08:[illegible]	2.8	+329	-370	-39	30
23-02	14:30	4.8	+308	-361	-51	35
24-02	09:30	6.4	+286	-362	-74	50
25-02	14:20	12.4	+265	-355	-88	60
26-02	11:45	14.8	+267	-356	-87	60
03-03	14:25	35.2	+249	-361	-110	70
10-03	11:16	61.6	+241	-360	-117	75
17-03	11:00	84.4	+230	-358	-12[illegible]	83
19-03	18:00	84.4	+234	-360	-129	81
09-04	13:30	84.4	+207	-347	-138	90
27-05	15:05	84.4	+176	-337	-159	103

TABLE C12 - LOAD CELL #7 - FIELD DATA

ZERO READINGS:

A	B	
-883	-237	tunnel
-867	-225	
-871	-228	
-872	-227	

DATE (81)	TIME	DIST TAIL (m)	A	B	△ A+B (z. r. tunnel)	LOAD kN
18-02	11:00	1.6	-1034	-228	-142	70
18-02	13:33	2.8	-1066	-252	-198	108
19-02	14:30	2.8	-1091	-258	-229	130
20-02	08:58	2.8	- 986	-250	-116	50
23-02	14:10	4.8	-1023	-240	-143	70
24-02	09:25	6.4	-1036	-230	-146	70
25-02	14:20	12.4	-1055	-225	-160	80
26-02	11:45	14.8	-1060	-227	-167	86
03-03	14:25	35.2	-1073	-232	-185	100
10-03	11:16	61.6	-1079	-230	-189	105
17-03	11:00	84.4	-1092	-226	-198	110
19-03	18:00	84.4	-1091	-227	-198	110
09-04	13:30	84.4	-1123	-211	-214	117
27-05	15:05	84.4	-1157	-202	-239	135

TABLE C13 - LOAD CELL #8 - FIELD DATA

SL1

Load (N)	Centre Gage (Microinches/inch)	Strain ($x10^{-6}$)	Stress (lb./in.^{2})
0	+2930	0	0
4000	+3068	138	4140
8000	+3194	264	7920
12000	+3318	388	11600
16000	+3440	510	15[illegible]
20000	+3560	630	18900
24000	+3677	747	22400
28000	+3795	865	26000
32000	+3911	981	29400
36000	+4030	1100	33000
32000	+3954	1024	30700
24000	+3761	831	24900
16000	+3508	578	17300
8000	+3230	300	9000
0	+2930	0	0

SL2

Load (N)	Centre Gage (Microinches/inch)	Strain ($x10^{-6}$)	Stress (lb./in.^{2})
0	+0569	0	0
4000	+0703	134	4020
8000	+0823	254	7620
12000	+0947	378	11340
16000	+1068	499	15000
20000	+1180	611	18300
24000	+1295	[illegible]26	21800
28000	+1406	837	25100
32000	+1513	944	28300
36000	+1627	1058	31700
32000	+1538	969	29100
24000	+1338	769	23100
16000	+1121	552	16600
8000	+0860	291	8730
0	+0572	3	90

Table C.14 STEEL LAGGING CALIBRATION - SL1 & SL2

SL3

Load (N)	Centre Gage (Microinches/inch)	Strain (x10^{-6})	Stress (lb./in.^{2})
0	-2360	0	0
4000	-2225	135	4050
8000	-2110	250	7500
12000	-1995	365	11000
16000	-1880	480	14400
20000	-1767	593	17800
24000	-1657	703	21100
28000	-1547	813	24400
32000	-1440	920	27600
36000	-1330	1030	30900
32000	-1405	955	28700
24000	-1585	775	23300
16000	-1818	542	16300
8000	-2084	276	8280
0	-2367	7	210

SL4

Load (N)	Centre Gage (Microinches/inch)	Strain (x10^{-6})	Stress (lb./in.^{2})
0	+2107	0	0
4000	+2242	135	4050
8000	+2370	263	7890
12000	+2491	384	11500
16000	+2610	503	15100
20000	+2725	618	18500
24000	+2838	731	21900
28000	+2952	845	25400
32000	+3069	962	28900
36000	+3184	1077	32300
32000	+3090	983	29500
24000	+2880	773	23200
16000	+2667	560	16800
8000	+2395	288	8640
0	+2096	11	330

Table C.15 STEEL LAGGING CALIBRATION - SL3 & SL4

SL5

Load (N)	Centre Gage (Microinches/inch)	Strain ($x10^{-6}$)	Stress (lb./in.^{2})
0	-2457	0	0
4000	-2333	124	3720
8000	-2216	241	7230
12000	-2100	357	10700
16000	-1989	468	14000
20000	-1878	579	17400
24000	-1770	687	20600
28000	-1658	799	24000
32000	-1550	907	27200
36000	-1438	1019	30600
32000	-1519	938	28140
24000	-1722	735	22100
16000	-1932	525	15800
8000	-2180	277	8310
0	-2460	3	90

SL6

Load (N)	Centre Gage (Microinches/inch)	Strain ($x10^{-6}$)	Stress (lb./in.^{2})
0	-0520	0	0
4000	-0391	129	3870
8000	-0272	248	7440
12000	-0160	360	10800
16000	-0047	473	14200
20000	+0073	593	17800
24000	+0183	703	21100
28000	+0295	815	24500
32000	+0406	926	27800
36000	+0520	1040	31200
32000	+0428	948	28400
24000	+0229	749	22500
16000	+0010	530	15900
8000	+0250	270	8100
0	-0533	13	390

Table C.16 STEEL LAGGING CALIBRATION - SL5 & SL6

SL7

Load (N)	Centre Gage (Microinches/inch)	Strain ($x10^{-6}$)	Stress (lb./in.^{2})
0	-1997	0	0
4000	-1861	136	4080
8000	-1737	260	7800
12000	-1617	380	11400
16000	-1500	497	14900
20000	-1382	615	18500
24000	-1273	724	21700
28000	-1162	835	25100
32000	-1052	945	28400
36000	-0941	1056	31700
32000	-1019	978	29300
24000	-1214	783	23500
16000	-1450	547	16400
8000	-1710	287	8610
0	-2000	3	90

SL 8

Load (N)	Centre Gage (Microinches/inch)	Strain ($x10^{-6}$)	Stress (lb./in.^{2})
0	-2774	0	0
4000	-2636	138	4140
8000	-2512	262	7860
12000	-2388	386	11600
16000	-2268	506	15200
20000	-2146	628	18800
24000	-2025	749	22500
28000	-1906	868	26000
32000	-1798	976	29300
36000	-1688	1086	32600
32000	-1768	1006	30200
24000	-1970	804	24100
16000	-2212	562	16900
8000	-2487	287	8610
0	-2788	14	420

Table C.17 STEEL LAGGING CALIBRATION - SL7 & SL8

SL9

Load (N)	Centre Gage (Microinches/inch)	Strain ($x10^{-6}$)	Stress ($lb./in.^2$)
0	-2780	0	0
4000	-2655	125	3750
8000	-2535	245	7350
12000	-2412	368	11000
16000	-2295	485	14600
20000	-2180	600	18000
24000	-2065	715	21500
28000	-1953	827	24800
32000	-1840	940	28200
36000	-1724	1056	31700
32000	-1812	968	29000
24000	-2017	763	22900
16000	-2240	540	16200
8000	-2500	280	8400
0	-2791	11	330

SL10

Load (N)	Gage (Microinches/inch)			Strain ($x10^{-6}$)			Centre Stress ($lb/in.^2$)
	Quarter Point	Centre	Quarter Point	Quarter Point	Centre	Quarter Point	
0	-2953	-2960	+3847	0	0	0	0
2000	-2896	-2894	+3490	57	66	43	1980
4000	-2955	-2835	+3935	98	125	88	3750
6000	-2809	-2773	+3979	144	187	132	5610
8000	-2765	-2714	+4023	188	246	176	7380
10000	-2719	-2653	+4066	234	307	219	9210
12000	-2675	-2594	+4110	278	366	263	11000
14000	-2632	-2534	+4152	321	426	305	12800
16000	-2590	-2476	+4196	363	484	349	14500
18000	-2545	-2418	+4236	408	542	389	16300
20000	-2503	-2362	+4280	450	598	433	17900
22000	-2460	-2304	+4320	493	656	473	19700
24000	-2421	-2246	+4365	532	714	518	21400
26000	-2375	-2187	+4407	578	773	560	23200
28000	-2337	-2133	+4450	616	827	603	24800
30000	-2290	-2071	+4492	663	889	645	26700
32000	-2254	-2015	+4540	699	945	693	28400
34000	-2210	-1960	+4575	743	1000	728	30000
32000	-2232	-1996	+4557	721	964	710	28900
24000	-2376	-2195	+4418	578	765	571	23000
16000	-2536	-2420	+4256	417	540	409	16200
8000	-2735	-2678	+4064	218	282	217	8460
0	-2961	-2968	+3845	8	8	2	240

Table C.18 STEEL LAGGING CALIBRATION - SL9 & SL10

SL11

Load (N)	Centre Gage (Microinches/Inch)	Strain ($x10^{-6}$)	Stress (lb./in.^{2})
0	-2472	0	0
4000	-2347	125	3750
8000	-2234	238	7140
12000	-2120	352	10600
16000	-2005	467	14000
20000	-1896	576	17300
24000	-1784	688	20600
28000	-1636	836	25100
32000	-1560	912	27400
36000	-1450	1022	30700
32000	-1529	943	28300
24000	-1703	769	23100
16000	-1935	537	16100
8000	-2200	272	8160
0	-2467	5	150

SL12

Load (N)	Centre Gage (Microinches/Inch)	Strain ($x10^{-6}$)	Stress (lb./in.^{2})
0	+0958	0	0
4000	+1086	128	3840
8000	+1200	242	7260
12000	+1317	359	10800
16000	+1433	475	14300
20000	+1547	589	17700
24000	+1654	696	20900
28000	+1765	807	24200
32000	+1873	915	27500
36000	+1983	1025	30800
32000	+1908	950	28500
24000	+1734	776	23300
16000	+1482	524	15700
8000	+1214	256	7680
0	+0933	25	750

Table C.19 STEEL LAGGING CALIBRATION - SL11 & SL12

PIECE OF LAGGING # 1

DATE	DIST.TAIL	$\Delta\varepsilon.10^{-6}$ E	C	W	ΔM (KN.M) E	C	W
17-02	2.2	68	85	48	0.44	0.54	0.31
18-02	2.2	55	68	15	0.35	0.44	0.10
18-02	5.2	235	274	189	1.51	1.76	1.21
19-02	6.4	183	277	195	1.17	1.78	1.25
20-02	6.4	189	294	188	1.21	1.88	1.21
23-02	8.4	200	288	184	1.28	1.85	1.18
24-02	10.0	248	295	213	1.59	1.89	1.37
25-02	17.0	213	---	198	1.37	----	1.27
26-02	18.4	233	---	232	1.49	----	1.49
03-03	38.8	---	---	208	----	----	1.33
10-03	65.2	225	305	196	1.44	1.96	1.26
17-03	88.0	203	290	193	1.30	1.86	1.24
19-03	88.0	208	305	203	1.33	1.96	1.30
9-04	88.0	198	295	188	1.27	1.89	1.21

PIECE OF LAGGING # 2

DATE	DIST.TAIL	$\Delta\varepsilon.10^{-6}$ E	C	W	ΔM (KN.M) E	C	W
17-02	2.2	-20	5	0	-0.13	0.03	0
18-02	2.2	-12	22	15	-0.08	0.14	0.10
18-02	5.2	-1	43	67	-0.01	0.28	0.43
19-02	6.4	22	62	50	0.14	0.40	0.32
20-02	6.4	39	53	49	0.25	0.34	0.31
23-02	8.4	8	36	14	0.05	0.23	0.09
24-02	10.0	39	75	8	0.25	0.48	0.05
25-02	17.0	9	55	45	0.06	0.35	0.29
26-02	18.4	64	112	89	0.41	0-72	0.57
03-03	38.8	---	61	56	----	0.39	0.36
10-03	65.2	34	64	40	0.22	0.41	0.26
17-03	88.0	-1	50	20	-0.01	0.32	0.13
19-03	88.0	34	55	40	0.22	0.35	0.26
9-04	88.0	-21	50	-50	-0.13	0.32	-0.32

TABLE C20 - STEEL LAGGING SL1 AND SL2 - FIELD DATA

PIECE OF LAGGING # 3

DATE	DIST.TAIL	Δε.10⁻⁶ E	Δε.10⁻⁶ C	Δε.10⁻⁶ W	ΔM (KN.M) E	ΔM (KN.M) C	ΔM (KN.M) W
[illegible]-02	2.2	5	4	1	0.03	0.03	0.01
[illegible]-02	2.2	10	59	16	0.06	0.38	0.10
18-02	5.2	-	32	13	-	0.21	0.08
19-02	6.4	-	-	-	-	-	-
20-02	6.4	-	-	-	-	-	-
23-02	8.4	-	-	-	-	-	-
24-02	10.0	-	-	-	-	-	-
25-02	17.0	-	-	-	-	-	-
26-02	18.4	[illegible]	47	-	0.37	0-30	-
03-03	38.8	[illegible]	81	-	1.24	0.52	-
10-03	65.2	-	66	39	-	0.42	0.25
17-03	88.0	35	59	21	0.22	0.38	0.13
19-03	88.0	45	64	26	0.29	0.41	0.17
9-04	88.0	25	59	16	0.16	0.38	0.10

PIECE OF LAGGING # 4

DATE	DIST.TAIL	Δε 10⁻⁶ E	Δε 10⁻⁶ C	Δε 10⁻⁶ W	ΔM (KN.M) E	ΔM (KN.M) C	ΔM (KN.M) W
17-02	2.2	5	4	1	0.03	0.03	0.01
18-02	-	-	-	-	-	-	-
18-02	5.2	135	149	126	0.87	0.96	0.81
19-02	6.4	138	167	159	0.88	1.07	1.02
20-02	6.4	-	-	150	-	-	0.96
23-02	8.4	150	185	-215	0.96	1.19	-1.38
24-02	10.0	136	180	-841	0.87	1.15	-5.39
25-02	17.0	-	180	-291	-	1.15	-1.87
26-02	18.4	171	232	182	0.12	1.10	1.17
03-03	38.8	139	190	171	0.89	1.22	1.10
10-03	65.2	158	209	174	1.01	1.34	1.12
17-03	88.0	155	185	149	0.99	1.19	0.01
19-03	88.0	139	190	55	0.89	1.22	0.35
9-04	88.0	115	195	144	0.74	1.25	0.92

TABLE C21 - STEEL LAGGING SL3 AND SL4 - FIELD DATA

PIECE OF LAGGING # 5

DATE	DIST. TAIL	$\Delta\varepsilon\ 10^{-6}$ E	C	W	ΔM (KN.M) E	C	W
17-02	1.3	-3	4	8	-0.02	0.03	0.05
18-02	1.3	-	-	-	-	-	-
18-02	4.0	-20	-25	-	-0.13	-0.16	-
19-02	5.2	-19	-	-1	0.12	-	-0.01
20-02	5.2	-	-	-	-	-	-
23-02	7.2	-	-24	-5	-	-0.15	-0.03
24-02	8.8	-17	-7	-	-0.11	-0.04	0.03
25-02	15.8	-20	-7	-	-0.13	-0.04	0.06
26-02	17.2	-	-	-	-	-	-
03-03	37.6	-56	-	-63	-0.36	1.19	-0.40
10-03	64.0	-30	-8	-12	-0.19	-0.05	-0.08
17-03	86.8	-45	-32	-20	-0.29	-0.21	-0.13
19-03	86.8	-35	-22	-13	-0.22	-0.14	-0.08
9-04	86.8	-45	-37	-25	-0.29	-0.24	-0.16

PIECE OF LAGGING # 6

DATE	DIST. TAIL	$\Delta\varepsilon\ 10^{-6}$ E	C	W	ΔM (KN M) E	C	W
17-02	1.3	-9	-13	-9	0.06	0.08	-0.06
18-02	1.3	31	-8	-9	0.20	-0.05	-0.06
18-02	4.0	94	80	31	0.60	0.51	0.20
19-02	5.2	135	130	82	0.87	0.83	0.53
20-02	5.2	127	165	120	0.81	1.06	0.77
23-02	7.2	126	142	111	0.81	0.91	0.71
24-02	8.8	141	157	118	0.90	1.01	0.76
25-02	15.8	103	147	118	0.66	0.94	0.76
26-02	17.2	151	180	124	0.97	1.15	0.79
03-03	37.6	-	143	119	-	0.92	0.76
10-03	64.0	189	149	-	1.21	0.96	-
17-03	86.8	136	152	23	0.87	0.97	0.79
19-03	86.8	141	162	15	0.90	1.04	0.74
9-04	86.8	121	157	113	0.78	1.01	0.72

TABLE C22 - STEEL LAGGING SL5 AND SL6 - FIELD DATA

PIECE OF LAGGING # 7

DATE	DIST.TAIL	$\Delta\varepsilon.10^{6}$ E	$\Delta\varepsilon.10^{6}$ C	$\Delta\varepsilon.10^{6}$ W	ΔM(KN.M) E	ΔM(KN.M) C	ΔM(KN.M) W
17-02	1.3	0	1	-7	0	0.01	0.04
18-02	1.3	17	60	121	0.11	0.38	0.78
18-02	4.0	21	-	-	0.13	-	-
19-02	5.2	-12	-	-	-0.08	-	-
20-02	5.2	25	-	-	0.16	-	-
23-02	7.2	-	-	-	-	-	-
24-02	8.8	25	88	21	0.16	0.56	0.13
25-02	15.8	20	53	31	0.13	0-34	0.20
26-02	17.2	20	24	29	0.13	0-15	0.19
03-03	37.6	-	52	-	-	0.33	-
10-03	64.0	41	70	-	0.26	0.45	-
17-03	86.8	25	-	26	0.16	-	0.17
19-03	86.8	37	68	21	0.24	0.44	0.13
9-04	86.8	10	78	14	0.06	0.50	0.09

PIECE OF LAGGING # 8

DATE	DIST.TAIL	$\Delta\varepsilon.10^{6}$ E	$\Delta\varepsilon.10^{6}$ C	$\Delta\varepsilon.10^{6}$ W	ΔM(KN.M) E	ΔM(KN.M) C	ΔM(KN.M) W
17-02	1.3	-	31	-	-	0.20	-
18-02	1.3	-	-	-	-	-	-
18-02	4.0	119	-	48	0.76	-	0.31
19-02	5.2	132	172	50	0.85	1.10	0.32
20-02	5.2	-	-	-	-	-	-
23-02	7.2	100	149	-	0.64	0.96	-
24-02	8.8	86	159	76	0.55	1.02	0.49
25-02	15.8	106	159	66	0.68	1.02	0.42
26-02	17.2	-	171	53	-	1.10	0.34
03-03	37.6	-	151	85	-	0.97	0.54
10-03	64.0	101	141	58	0.65	0.90	0.37
17-03	86.8	106	131	61	0.68	0.84	0.39
19-03	86.8	121	131	76	0.78	0.84	0.49
9-04	86.8	101	106	61	0.65	0.68	0.39

TABLE C23 - STEEL LAGGING SL7 AND SL8 - FIELD DATA

PIECE OF LAGGING # 9

DATE	DIST.TAIL	Δε. 10⁻⁶ E	C	W	ΔM(KN.M) E	C	W
18-02	2.8	-10	-5	-7	-0.06	-0.03	-0.04
19-02	4.0	-2	8	2	-0.01	0.05	0.01
20-02	4.0	-161	-160	-215	-1.03	-1.03	-1.38
23-02	6.0	-4	-2	3	-0.03	-0.01	0.02
24-02	7.6	12	0	3	0.08	0.0	0.02
25-02	14.8	17	-5	-10	0.11	-0.03	-0.06
26-02	16.0	40	19	16	0.26	0.12	0.10
03-03	36.4	49	13	14	0.31	0.08	0.09
10-03	62.8	-	1	-5	-	0.01	-0.03
17-03	85.6	-28	-15	-25	-0.18	-0.10	-0.16
19-03	85.6	-23	-5	-	-0.15	-0.03	
9-04	85.6	-48	-30	-30	-0.31	-0.19	-0.19

PIECE OF LAGGING # 10

DATE	DIST.TAIL	Δε.10⁻⁶ E	C	W	ΔM(KN.M) E	C	W
18-02	2.8	136	194	164	0.87	1.24	1.05
19-02	4.0	139	183	164	0.89	1.17	1.05
20-02	4.0	-	-27	-64	-	-0.17	-0.41
23-02	6.0	109	169	122	0.70	1.08	0.78
24-02	7.6	110	164	139	0.71	1.05	0.89
25-02	14.8	120	164	139	0.77	1.05	0.89
26-02	16.0	-	184	-	-	1.18	-
03-03	36.4	118	190	-	0.76	1.22	-
10-03	62.8	-	183	-	-	1.17	-
17-03	85.6	95	154	139	0.61	0.99	0.89
19-03	85.6	115	149	144	0.74	0.96	0.92
9-04	85.6	80	141	139	0.51	0.90	0.89

TABLE C24 - STEEL LAGGING SL9 AND SL10 - FIELD DATA

PIECE OF LAGGING # 11

DATE	DIST. TAIL	Δε (10⁻⁶) E	C	W	ΔM (KN.M) E	C	W
18-02	2.8	32	1	31	0.21	0.01	0.20
19-02	4.0	40	54	42	0.26	0.35	0.27
20-02	4.0	30	-	-	0.19	-	-
23-02	6.0	58	-	27	0.37	-	0.17
24-02	7.6	30	-	35	0.19	-	0.22
25-02	14.8	-	-	34	-	-	0.22
26-02	16.0	37	-	55	0.24	-	0.35
03-03	36.4	4	12	33	0.03	0.08	0.21
10-03	62.8	33	-	-	0.21	-	-
17-03	85.6	25	25	20	0.16	0.16	0.13
19-03	85.6	25	31	25	0.16	0.20	0.16
9-04	85.6	25	30	15	0.16	0.19	0.10

PIECE OF LAGGING # 12

DATE	DIST. TAIL	Δε (10⁻⁶) E	C	W	ΔM (KN.M) E	C	W
18-02	2.8	45	48	2	0.29	0.31	0.01
19-02	4.0	66	57	42	0.42	0.37	0.27
20-02	4.0	58	59	-2	0.37	0.38	-0.01
23-02	6.0	73	54	-41	0.47	0.35	-0.26
24-02	7.6	110	90	61	0.71	0.58	0.39
25-02	14.8	[illegible]	-30	6	0.61	-0.19	0.04
26-02	16.0	112	120	47	0.72	0.77	0.30
03-03	36.4	88	95	34	0.57	0.61	0.22
10-03	62.8	90	84	63	0.58	0.54	0.40
17-03	85.6	85	110	66	0.54	0.71	0.42
19-03	85.6	[illegible]	100	66	0.58	0.64	0.42
9-04	85.6	90	110	76	0.58	0.71	0.49

TABLE C25 - STEEL LAGGING SL11 AND SL12 - FIELD DATA

CONVERGENCE MEASUREMENTS (UNITS mm)

DATE 25/02/81

RING	I	II	III	IV	V	VI	VII
5	4871.18	1996.36	3934.00	3748.66	2115.59	5716.90	5694.70
6	4867.37	2000.65	3987.09	3637.45	2181.02	5727.29	5692.16
7	4907.28	1951.61	3968.87	3620.11	2207.26	5774.10	5685.64
8	4961.00	1924.86	3961.18	3642.81	2173.50	5767.85	5739.08

DATE 03/03/81

RING	I	II	III	IV	V	VI	VII
5	4871.18	1996.28	3934.81	3749.80	2115.74	5717.08	5695.57
6	4867.35	1999.94	3987.54	3638.17	2179.88	5726.83	5692.77
7	4906.39	1951.76	3969.58	3619.90	2207.43	5773.82	5685.53
8	4960.24	1924.30	3962.37	3643.22	2173.22	5767.24	5737.98

DATE 04/03/81

RING	I	II	III	IV	V	VI	VII
5	4870.75	1996.16	3934.56	3749.29	2115.36	5716.90	5694.55
6	4866.99	[illegible]	3987.75	[illegible]	2179.70	5726.40	5691.70
7	4906.23	1951.33	3969.79	[illegible]	2207.13	5773.70	5684.87
8	4959.98	1924.05	3962.73	3642.58	[illegible]	5767.19	[illegible]

I to VII : [illegible] defined in Figure 4.34

TABLE C26 - LINING DISPLACEMENTS MEASUREMENTS

D. APPENDIX - SUPPORT COMPRESSIVE STIFFNESS

$$\text{COMPRESSIVE STIFFNESS} = K_s = \frac{\Delta p / p_o}{\Delta u / u_o}$$

$$\frac{\Delta p}{\Delta D / D} = \frac{E_s \cdot A_e}{(1-\nu_s^2)R}$$ (EINSTEIN AND SCHWARTZ, 1979)

FOR THE AXISYMMETRIC CASE : $\Delta D = 2\Delta u$

$$\frac{\Delta p}{\Delta u} = \frac{2 E_s A_e}{(1-\nu_s^2) R D} = K_s \cdot p_o / u_o$$

$$K_s = \frac{2 E_s A_s u_o}{s(1-\nu_s^2) R D p_o}$$

WHERE

- p = UNIFORM RADIAL PRESSURE
- p_o = IN SITU FIELD STRESS
- u = RADIAL LINING DISPLACEMENT
- u_o = WALL DISPLACEMENT OF UNLINED TUNNEL (ELASTIC SOIL)
- $E_s\ A_s\ \nu_s$ = LINER PROP. SEE TABLE 5.1
- s = RIBS SPACING
- $A_e = A_s / s$
- D = TUNNEL DIAMETER
- R = TUNNEL RADIUS

LRT TUNNELS $K_s = 2.62$

EXP. TUNNEL : $K_s = 3.3$[illegible]

Figure D.1 DERIVATION OF THE SUPPORT COMPRESSIVE STIFFNESS